FABRICATION AND CHARACTERIZATION OF POLYPHENYLSULFONE BASED ULTRAFILTRATION HOLLOW FIBER MEMBRANES FOR GROUNDWATER TREATMENT STUDIES

Thesis

Submitted in partial fulfillment of the requirements for the degree of

DOCTOR OF PHILOSOPHY

by

MITHUN KUMAR

(158015 ME15F20)

DEPARTMENT OF MECHANICAL ENGINEERING

NATIONAL INSTITUTE OF TECHNOLOGY KARNATAKA

SURATHKAL, MANGALORE -575025

SEPTEMBER, 2022

FABRICATION AND CHARACTERIZATION OF POLYPHENYLSULFONE BASED ULTRAFILTRATION HOLLOW FIBER MEMBRANES FOR GROUNDWATER TREATMENT STUDIES

Thesis

Submitted in partial fulfillment of the requirements for the degree of

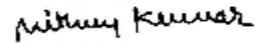## DOCTOR OF PHILOSOPHY

by

MITHUN KUMAR

(158015 ME15F20)

DEPARTMENT OF MECHANICAL ENGINEERING

NATIONAL INSTITUTE OF TECHNOLOGY KARNATAKA

SURATHKAL, MANGALORE -575025

SEPTEMBER, 2022

DECLARATION

I hereby declare that the Research Thesis entitled "**Fabrication and Characterization of Polyphenylsulfone Based Ultrafiltration Hollow Fiber Membranes for Groundwater Treatment Studies**" which is being submitted to the **National Institute of Technology Karnataka, Surathkal** in partial fulfillment of the requirements for the award of the degree of **Doctor of Philosophy in Mechanical Engineering** is a *bonafide report of the research work carried out by me*. The material contained in this Research Thesis has not been submitted to any other Universities or Institutes for the award of any degree.

Mithun Kumar
MITHUN KUMAR

Register Number: **158015/ME15F20**

Department of Mechanical Engineering

Place: NITK-Surathkal

Date: 30-09-2022

CERTIFICATE

This is to certify that the Research Thesis entitled "Fabrication and Characterization of Polyphenylsulfone Based Ultrafiltration Hollow Fiber Membranes for Groundwater Treatment Studies" submitted by Mr. MITHUN KUMAR (Register Number: 158015/ME15F20) as the record of the research work carried out by him, *is accepted as the Research Thesis submission* in partial fulfillment of the requirements for the award of the degree of **Doctor of Philosophy.**
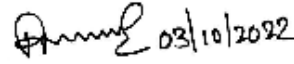
Dr. Somasekhara Rao T.

Assistant Professor

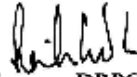Department of Mechanical Engg.

Research Guide(s)

03/10/2022

Prof. Arun M. Isloor

Professor

Department of Chemistry.

Research Guide(s)

Chairman - DRPC

Date: 3·10·2022

ACKNOWLEDGEMENTS

very thankful to Prof. Ramin Farnood, Department of chemical engineering from University of Toronto, Canada for providing opportunity me to conduct research work in his laboratory. I truthfully appreciate the support extended by my research group at NITK, including Mr. Prashanth R Kubasad, Mr. Subodh Kumar Suman, Mr. Vinay Prajapati, Mr. Rahul Nayak, Mr. Sandeep Jahns, Mr. Vamshi N, Mr. Nipahade Kiran Vishnu, Mr. Kasina Hruday and Miss Nabeela from Department of Mechanical Engineering and Dr. G. P. Syed Ibrahim, Dr. Chandrashekhara Nayak, Dr. Raghavendra S Hebbar, Dr. Shivaram B, Dr. Irfana Moideen, Mr. Satish Bhat, Mr. Sooraj, Mr. Sathyanarayana D.S, Mr. Sivaprakash R., Mr. Mrutyunjay Swamy, Miss. Panchami, Miss. Netravati Miss. Pallavi K C, Miss. Nikhila, Miss Amruta C M, Miss Vani and Miss Uma from Department of chemistry, NITK. I am thankful to my friend Mr. Mohanraj G. K. research scholar in Department of Metallurgical and Materials engineering for his guidance and support for modifying a thesis according to the institute format. I am thankful to all my friends at NITK, for making my stay during research days a fun-filled and memorable one. I am thankful to the non-teaching staff, Ms. Rashmi for her timely cooperation with laboratory and analysis work.

I am highly indebted to my beloved parents Shri. Yallappa Gouda & Smt. Sumangala, brother, sister and uncles for their cooperation, encouragement, support, love and affection. It was because of strong support of my family, that I am able to complete my Ph.D. work. Finally, I extend my gratitude to all those who have contributed directly or indirectly towards the completion of my Ph.D. work.

Thank you

MITHUN KUMAR

ABSTRACT

Groundwater is a vital resource that furnishes drinking water to human beings. Liquid and solid wastes, animal wastes, sewage plants, and septic tanks are all main sources of contamination in the groundwater. Furthermore, sewage, industrial effluents, agricultural discharge and residential waste, inorganic pollutants, fertilizer, run-off from urban areas, thermal contaminants, organic compounds, radioactive pollutants and toxic metals all cause a hazard to the groundwater quality. Drinking water is derived from groundwater, which is a valuable natural resource. Drinking water continues to be a significant source of many of the water-borne diseases and death of human beings in the world due to untreated and uncontrolled release of contaminated water to rivers and many other water collecting ponds. Drinking water purification by low-pressure ultrafiltration hollow fiber membrane has become more popular. It replaces many traditional separation technologies due to their high surface area to volume ratio, high packing density, high flux and resistance to chemical degradation. Polyphenylsulfone (PPSU) is a versatile polymer for membrane preparation with high chemical/thermal stability, increased heat resistance, hydrolysis stability and excellent mechanical properties. However, membranes prepared by PPSU as a base polymer are more prone to fouling, hydrophobic and offer less water permeability. In current research work, various inorganic hydrophilic nanoparticles are incorporated into the hydrophobic PPSU membrane matrix to improve hydrophilicity, antifouling and separation efficacy of the fabricated hollow fiber membrane.

In present study, the hydrophobic PPSU hollow fiber membranes were fabricated with different dosages of zirconium oxide (ZrO_2), zinc–magnesium oxide (ZnO-MgO), aluminum oxide (Al_2O_3) and polydopamine (PDA) along with constant dosages of cellulose derivatives (cellulose acetate and cellulose acetate phthalate) using non-solvent induced phase separation (NIPS) process. The blended membranes surface morphologies and topologies were analyzed using scanning electron microscopy (SEM) and atomic force microscopy (AFM) respectively. Also studied hydrophilicity, thermal properties and surface charge properties of the fabricated membranes. A cross-flow filtration system was used for analyzing the water permeability, antifouling properties and separation performance of arsenic-V from laboratory prepared arsenic-V solution.

The PPSU membranes with 1.5 wt% and 1 wt% of Al_2O_3 and 3 wt% of cellulose acetate showed improved arsenate oxide removal of 98.67% and 94.89% with permeabilities were 88.41 L/m^{2}h bar and 88.41 L/m^{2}h bar respectively. A 0.6 wt% of ZnO-MgO in CAP/PPSU and 1 wt% of ZnO-MgO in CA/PPSU decontaminated 81.31% and 78.48% with permeabilities of

69.58 L/m^{2}h bar and 198.47 L/m^{2}h bar respectively. Membranes prepared by 1 wt% of ZrO$_2$ in CA/PPSU exhibited arsenic (As-V) rejection of 87.24% with permeabilities of 89.94 L/m^{2}h bar. A 3 wt% of PDA in PPSU/PVP executed enhanced (As-V) removal as 87.15% with flux of 31.80 L/m^{2}h. The modified membranes exhibited enhanced hydrophilicity, antifouling and efficient arsenic-V removal properties.

CONTENT

CHAPTER 1

INTRODUCTION

CHAPTER 2

EXPERIMENTAL SECTION

CHAPTER 3

USE OF CELLULOSE ACETATE/POLYPHENYLSULFONE DERIVATIVES TO FABRICATE ULTRAFILTRATION HOLLOW FIBER MEMBRANES FOR THE REMOVAL OF ARSENIC-V FROM WATER

CHAPTER 4

REMOVAL OF TOXIC ARSENIC-V FROM AQUEOUS MEDIA USING POLYPHENYLSULFONE/CELLULOSE ACETATE AND POLYPHENYLSULFONE/CELLULOSE ACETATE PHTHALATE HOLLOW FIBER MEMBRANES CONTAINING ZIRCONIUM OXIDE

CHAPTER 5

EFFECT OF ZnO-MgO ON THE POLYPHENYLSULFONE/ CELLULOSE ACETATE DERIVATIVES HOLLOW FIBER MEMBRANES FOR THE EFFECTIVE DECONTAMINATION OF ARSENIC-V FROM ARSENIC-V CONTAMINATED WATER

CHAPTER 6

NANO-ALUMINUM OXIDE EMBEDDED CELLULOSE ACETATE/ POLYPHENYLSULFONE DERIVATIVES HOLLOW FIBER MEMBRANES: FABRICATION, CHARACTERIZATION AND ARSENIC-V REMOVAL FROM WATER

CHAPTER 7

HYDROPHILIC POLYDOPAMINE/POLYVINYLPYRROLIDONE BLENDED POLYPHENYLSULFONE HOLLOW FIBER MEMBRANES FOR THE REMOVAL OF ARSENIC (AS-V) FROM WATER

CHAPTER 8

IMPROVED SEPARATION OF DYES AND PROTEINS USING MEMBRANES MADE OF POLYPHENYLSULFONE/CELLULOSE ACETATE AND POLYPHENYLSULFONE/CELLULOSE ACETATE PHTHALATE

CHAPTER 9

SUMMARY AND CONCLUSION

LIST OF FIGURES

LIST OF TABLES

NOMENCLATURE

Symbols	Description	Unit
A	Membrane filtration area	m^2
L	Membrane length	m
V	Filtrate permeate volume	m^3
d_i	Internal diameter	m
C_f	Solute concentration in Feed	ppm
C_p	Solute concentration in Permeate	ppm
J	Flux	L/m^2h
P	Pure water permeability	L/m^2h bar
J_{w1}	Pure water permeability before Bovine serum albumin (BSA) filtration test	L/m^2h bar
J_p	BSA filtration test	L/m^2h bar
J_{w2}	Pure water permeability after BSA filtration test	L/m^2h bar
p	Filtration pressure	psi
R	Rejection	%
t	Filtration time	min or h
W_w	Wet weight of the membrane	g
W_d	The dry weight of the membrane	g
δ	The thickness of the membrane samples	cm
ρ_w	Density of water	0.998 g/cm^3
T_g	Glass transition temperature	$^\circ$C

ΔT	Change in temperature (temperature gradient)	$^{\circ}C$
ΔE	Change of energy (energy gradient)	Calorie
ΔP	Change in pressure (pressure gradient)	bar
R_r	Reversible fouling	%
R_{ir}	Irreversible fouling	%
R_t	Total fouling	%
M_w	Molecular weight	g/mol
R_a	Surface roughness	nm
R_z	Root mean Z-data	nm
R_q	The height difference of the five corresponding maximum peaks and minimum peaks	nm
n	Number of membranes	

ABBREVIATIONS

AC	Activated carbon
AFM	Atomic force microscopy
Al_2O_3	Aluminum oxide
AN	Acrylonitrile
AN-MA-SSA	Acrylonitrile-methacrylate-sodium sulfonate acrylate
As-III	Arsenite
AsO_4^{3-}	Arsenate oxide
As-V	Arsenate
ATP	Arsenic treatment plant
ATR-FTIR	Attenuated total reflectance-Fourier transform infrared spectroscopy
BER	Bore extrusion rate
BFD	Black foot disease
BSA	Bovine serum albumin
CA	Cellulose acetate
CAB	Cellulose acetate butyrate
CAP	Cellulose acetate phthalate
Cd-II	Cadmium (II)
CNT	Carbon nanotube
CTA	Cellulose triacetate
Cu-II	Copper (II)
DBS	Doppler broadening spectroscopy

DER	Dope extrusion rate
DIPS	Diffusion induced phase separation
DLS	Dynamic light scattering
DMA	Dimethylacetamide
DMF	Dimethylformamide
DSC	Differential scanning calorimeter
E.coli	Escherichia coli
EA	Egg albumin
ED	Electrodialysis
EDX	Energy-dispersive X-ray
EIPS	Evaporation induced phase separation
FDR	Flux decline ratio
FESEM	Filed emission scanning electron microscopy
FO	Forward osmosis
FRR	Flux recovery ratio
GO	Graphene oxide
GS	Gas separation
HA	Humic acid
HCl	Hydrochloric
HF	Hollow fiber
HR-TEM	High-resolution transmission electron microscopy
IEP	Isoelectric point
IPA	Isopropyl alcohol

KOH	Potassium hydroxide
MB	Methylene blue
MD	Membrane distillation
MF	Microfiltration
MWCNT	Multi-walled carbon nanotube
MWCO	Molecular weight cut off
NaCl	Sodium chloride
NF	Nanofiltration
NFs	Nanofibers
NGL	Natural gas liquids
Ni-II	Nickel (II)
NIPS	Non-solvent induced phase separation
NMP	N-methyl-2-pyrrolidone
NMR	Nuclear magnetic resonance
Np	Nanoparticle
PA	Polyamide
PALS	Positron annihilation lifetime spectroscopy
PAN	Poly(acrylonitrile)
PANI	Polyaniline
PBNPI	Polymeric (bisphenol-A-co-4-nitro-phthalic anhydride – co-1,3 – phenylenediamne
PDA	Polydopamine
PEG	Polyethylene glycol

PEI	Polyethylene imine
PES	Polyethersulfone
PEUF	Polymer enhanced ultrafiltration
PIP	Piperazine
PMMA	Poly (methyl methacrylate)
P-PPSU	Phosphonated polyphenylsulfone
PPSU	Polyphenylsulfone
PSCF	Preferentially sorption-capillary flow
PSf	Polysulfone
PU	Polyurethane
PV	Per-vaporization
PVA	Polyvinyl alcohol
PVDF	Polyvinylidene difluoride
PVP	Polyvinylpyrrolidone
PWF	Pure water flux
RB-5	Reactive black-5
RO	Reverse osmosis
RO-16	Reactive orange-16
RT	Room temperature
S. aureus	Staphylococcus aureus
SAED	A Selected area (electron) diffraction pattern
SEM	Scanning electron microscopy

sPES	sulfonated Polyethersulfone
sPPSU	sulfonated Polyphenylsulfone
sPSF	sulfonated Polysulfone
TEM	Transmission electron microscopy
TFC	Thin-film composite
TGA	Thermogravimetric analysis
TiO_2	Titanium dioxide
TIPS	Temperature-induced phase separation
TMC	Trimesoyl chloride
TMP	Transmembrane pressure
UF	Ultrafiltration
UNEP	United Nations environmental program
USEPA	United states environmental protection agency
UV	Ultraviolet
UV-Vis	Ultraviolet-Visible
VIPS	Vapor induced phase separation
WCA	Water contact angle
WHO	World health organization
XPS	X-ray photoelectron spectroscopy
XRD	X-ray diffraction
ZnO-MgO	Zinc-magnesium oxide
ZrO_2	Zirconium oxide

CHAPTER -1
INTRODUCTION

Abstract

This chapter demonstrated extensive information about ongoing research on water purification in the field of membrane science and technology. It primarily highlights the global water crisis, arsenic in the environment, hazardous health effects of arsenic on human beings, history and classifications of membrane separation, types of membranes, methods of membrane preparation and membrane technology applications. A literature review highlights the use of polyphenylsulfone, cellulose acetate as a polymeric material and the significance of nanomaterials in membranes for arsenic-V removal applications also included in this chapter.

1.1 SCARCITY OF WATER AND OTHER WATER RESOURCES

Purified drinking water is always the first and foremost medicine in the world. In the absence of fresh-water, the world is on the verge of a severe global crisis. Water shortage is more of a concern as the population continues to grow. A 70% of the earth is filled by water and it is easy to believe that, it will be abundant. Nevertheless, the availability of fresh drinking water on the earth is less than 1% and about 1.1 billion populations lack of access to clean and healthy drinking water. The remaining water is getting contaminated due to the continuous development of various industries, climate change and urbanization. Owing to the ever-increasing demand for water, access to clean drinking water is now one of the most challenging issues for humanity (Campling et al. 2021; Vörösmarty et al. 2010). Water is an essential natural resource that is important to ensure human needs. Heavy metals such as lead, cadmium, arsenic, fluoride and mercury are major toxic elements present in the water. Compared to other toxins, heavy metals classified as dangerous and hazardous to ecosystems and humans (Yurekli 2016).

As a result, there is a strong drive for efficient and cost-effective treatment methods to be developed to remove pollutants from the contaminated water. As the population in the world increases, pure water becomes a limited source. According to the World Health Organization (WHO), almost 1.1 billion people have no access to pure drinking water. Therefore, the conservation of existing freshwater supplies is becoming paramount and new water resources are to be established to meet the increasing demand for pure drinking water. The employed technologies cannot extract heavy metal ions and some dissolved inorganic/organic compounds from the contaminated water. Diseases such as typhoid fever, cholera and other water diseases (i.e., gastrointestinal disease, diarrhea) are exposed. According to the WHO, every year, 3.4 million populations mainly children die from diarrheal disease alone (Rahman

et al. 2010; Ravenscroft et al. 2011). The bar-chart of water distribution on the earth is illustrated in Figure 1.1.
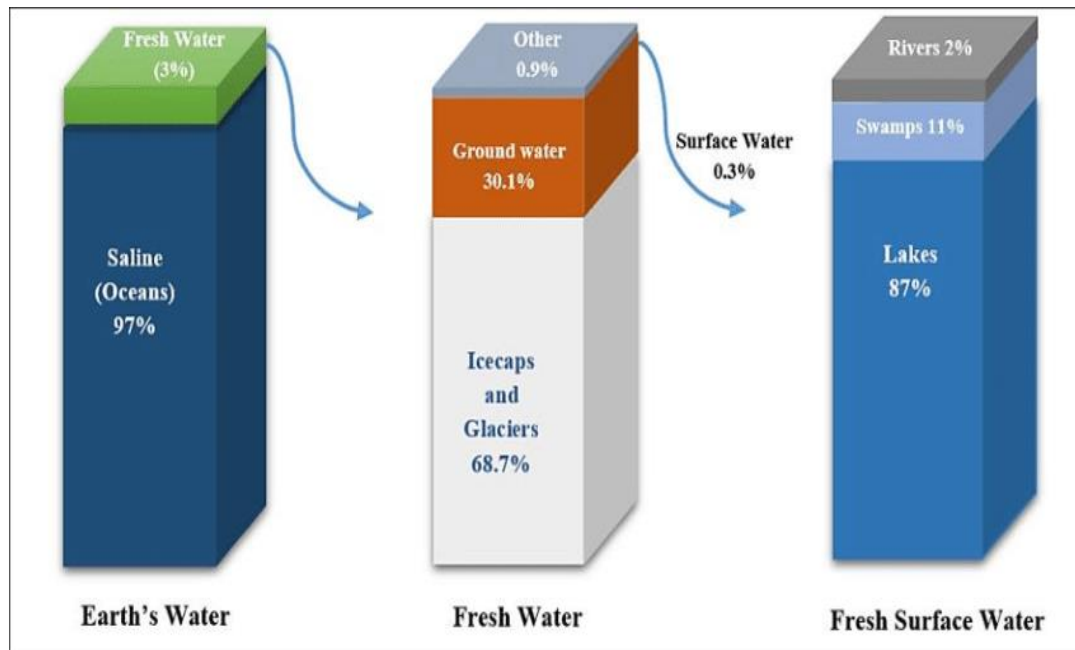
Figure 1.1 Distribution of water on the Earth (Abd Elkodous et al. 2018) (Open access).

Many of the limitations are noticed by utilizing conventional water treatment technologies, including chemical or biological treatment. The limitations are high costs, hazardous chemicals, increased pollution rate and ample space needed for equipment. Consequently, the physical treatment process using membrane technology was identified as an important solution to these problems. Membrane treatment processes have many benefits, including limited area prerequisite for installing the equipment, no chemicals contribution to the treatment process and consistent quantity of effluent. Membrane technology depends on surface pore size. Depending on the pore size, membrane processes were categorized as nanofiltration, microfiltration, reverse osmosis and ultrafiltration respectively. Figure 1.2 illustrated the global freshwater scarcity.
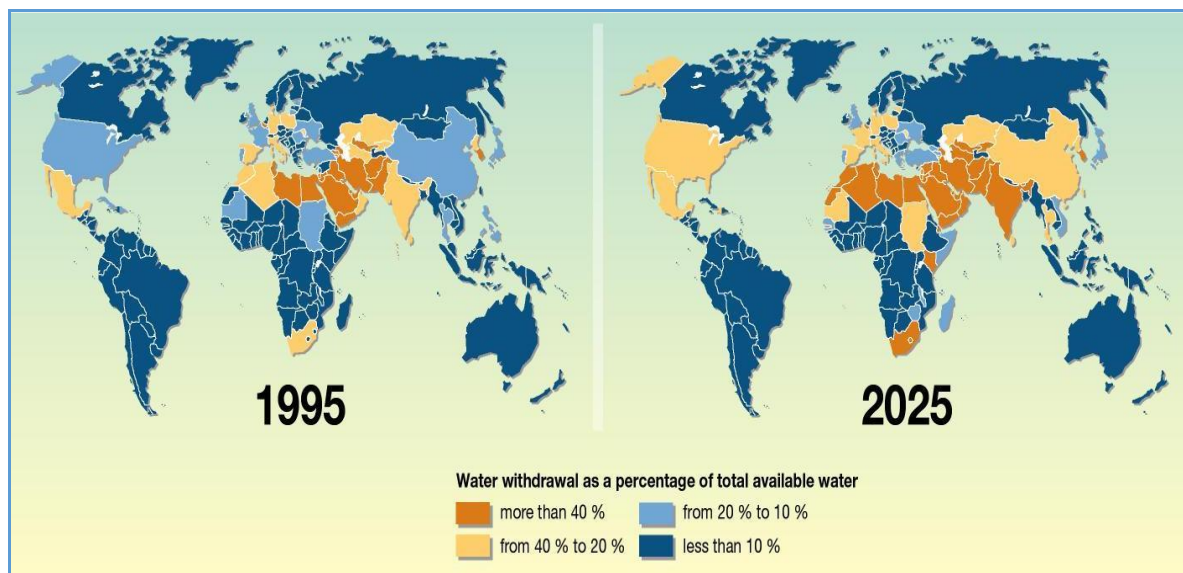
Figure 1.2 Scarcity of fresh water stress (Source: Homaeigohar and Elbahri, 2014) (Open access).

1.2 MEMBRANE HISTORY

The first reported study regarding membrane processes occurred in 1748 by the French Abbe Nollet. In the experiment, stored wine spirit in a vessel, the vessel mouth was closed and immersed in water with an animal bladder. The bladder swelled and often burst because it was more permeable to water than wine, showing semi-permeability for the first time (Böddeker 2008). In the 1820s, Dutrechet introduced the term "osmosis" to describe the spontaneous flow of liquid through a permeable barrier. Fick prepared the first synthetic membrane, made from nitrocellulose, in 1855. The first dialysis experiments with synthetic membranes were recorded in 1861 by Graham. Graham also showed that the permeability of rubber films to various gases was different (Graham 1861). Traube and Pfeffer fabricated artificial membranes for the next 30 years and their work related to osmotic phenomena contributed to the van't Hoff osmotic pressure relationship. The word ultrafiltration was invented by Bechold in 1906 and in the 1960s, Michaels pioneered modern ultrafiltration (UF). Many of these membranes could be utilized as an exceptionally fine particle or the molecular filters. In 1910, Zigmondy and co-workers developed asymmetric microporous filters containing a fine porous skin layer and open structure permeating sides. The membrane's tightest UF were prepared by cellophane along with regenerated cellulose. In 1927, the membranes filters were initially commercialized using zigmondy method by the Sartorius company in Germany (Singh 2014). Firstly, discovered reverse osmosis (RO) membranes in the 1920s. However, 30 years later, it remained unnoticed until Reid and his co-workers rediscovered it. In the 1940s, the first functional hemodialysis phenomenon was shown by Kolff (Ronco et al. 2004).

Since 1945, microporous membranes utilized to extract microorganisms from liquid and gaseous streams for diffusion studies and estimate the shape (linear or spherical) and macromolecular size (particle). Juda and McRae pioneered electrodialysis (ED) using ion-exchange membranes after the Second World war. Later, for desalination of brackish water, the electrodialysis systems were commercialized. The RO (also called "hyperfiltration") was started in the early 1950s for desalting seawater by the saline water to fulfill potential water needs, as microporous membranes were not appropriate for desalination due to the greater pore size. Raid and Berton discovered polymeric membranes in the mid-1950s and demonstrated high salt rejection, but they could not cast thin membranes without imperfections. Membranes are too thick (approximately 6 μm) and showed water fluxes, which are too low to be practical; the flux is inversely proportional to the thickness of the membrane through a semi-permeable membrane. The first breakthrough occurred in 1959 using the phase inversion process; Leob and Sourirajan discovered a method to fabricate very thin cellulose acetate (CA) membranes. This approach developed a homogeneous asymmetric (or anisotropic) membrane structure. The membranes exhibited asymmetric morphologies and high flux because of the high thinness and porosity (Strathmann et al. 1971). The total thickness of the membrane was found to be 0.1 mm, although the active surface layer's thickness was 30-100 nm. The spiral-wound module was invented by Westmoreland and later Bray in the late 1960s and is more influential than the tube-in shell module. It is possible to consider the spiral-wound membrane as a rolled-up plate-and-frame (PAF) configuration. Simultaneously, new RO membrane materials and module designs were explored by scientists and engineers at Dow and DuPont. Mahon and others at Dow fabricated cellulose triacetate (CTA) hollow fiber membranes. Henry Hoehn and George Milford developed the polyamide (PA) hollow fiber membranes at DuPont in the late 1960s (Singh 2014). This is the first non-cellulosic asymmetric membrane. The L-S type CA spiral-wound membrane turned out to be very competitive. The fiber of the PA is solution-spun into the excellent hollow fiber. The fiber's inner diameter was 42 μm and the outer diameter was 85 μm. On the shell side, the fibers had an asymmetric skin shape.

The thin-film composite (TFC) RO membrane was developed in the early 1970s by Cadotte and Rozelle from a new class of membrane materials. It was formed by depositing, by interfacial polymerization reaction, a very thin layer of a salt-rejecting PA polymer on the surface of a suitable fine porous substrate such as the polysulfone ultrafiltration membrane (Abdel-Fatah 2018). Cadotte also developed TFC membranes in 1976 that showed increased flux and high rejection of divalent ions but high permeability related to aqueous chloride solution. The nanofiltration was given to these loose RO membranes in 1984 by Petersen.

Thus, in Petersen's words, another membrane process is the fascinating extension of reverse osmosis technology. The polyamide membrane of TFC type is now the state-of-art membrane and the new RO and NF market dominate. Although they are costlier than the CA membranes, TFC membranes have higher flux and thus work at a low feed pressure than CA membranes (Freger et al. 2002). In addition, TFC membranes are not biodegradable and significant rejection of boron, silica, nitrate and other organic compounds more effectively than the CA membranes.

Without a brief discussion of the water transport mechanism by RO membranes, a historical analysis of the membrane technology will be inadequate. The primary membrane transport mechanisms are the solution diffusion model and preferentially sorption-capillary flow (PSCF). In the 1960s, Sourirajan and his team proposed the PSCF model based on the assumption that the RO membrane surface has pores, while the SD model assumes that the membrane surface was pore-free. It was subsequently shown that RO membranes have a two-size membrane (bi-modal) pores distribution on the surface of the RO membrane; predominantly small pores (about ≤ 10 A) estimated to occur in perfect or ideal membranes, and often large pores (about ≥ 100 A) that are due to the unavoidable presence of skin layer defects. The pore size and contact force control the solute separation from the solvent.

In summary, commercial membrane processes and outstanding success of the water separation processes such as reverse osmosis (RO), nanofiltration (NF), ultrafiltration (UF) and microfiltration (MF) wouldn't have been plausible without the proper invention. Ensuring improvement of high flux, thin layer CA membranes by Srinivasa Sourirajan and Sidney Loeb at UCLA, accompanied by John   production of TFC PA membranes. The work on the RO in the 1950s and 1960s motivated membrane technologies such as NF, PV and GS. This progress has contributed to the development of newer membrane processes such as forward osmosis (FO) and membrane distillation (MD).

1.3 ARSENIC IN THE ENVIRONMENT

In the earth's crust, arsenic is a natural element extensively circulated. With an average of 1.8 mg/kg, it is the 20th most abundant element. Standard concentrations of arsenic are 0.2-15 mg/kg, 15 mg/kg, and 0.02-2.8 ng/m^3 in the lithosphere, soil and atmosphere. Either natural or anthropogenic processes can release arsenic into the environment. Volcanic processes and weathering of arsenic are predominant natural processes. Numerous sources of arsenic are anthropogenic. They include arsenic pesticides on land, incineration of substances containing arsenic, discharge of industrial wastewater, tailing/landfill leaching of mines and manufacture

of arsenic different compounds. Arsenic because it is an indestructible element. It can be modified from one form to another and transmitted to another medium. Arsenic can precipitate out of the solution in water or be adsorbed to rocks and soils. Arsenic-containing rocks and soils can release arsenic into the water by dissolution or desorption. Aqueous arsenic has significant importance in the above media because the high level of arsenic that has also been detected in drinking water is known to cause severe adverse health effects in different locations around the globe (Abdul et al. 2015; Villaescusa and Bollinger 2008). The cycle of arsenic in the environment is illustrated in Figure 1.3. Table 1.1 represented more information of arsenic and Table 1.2 represented stability of arsenic species (Worou et al. 2021).
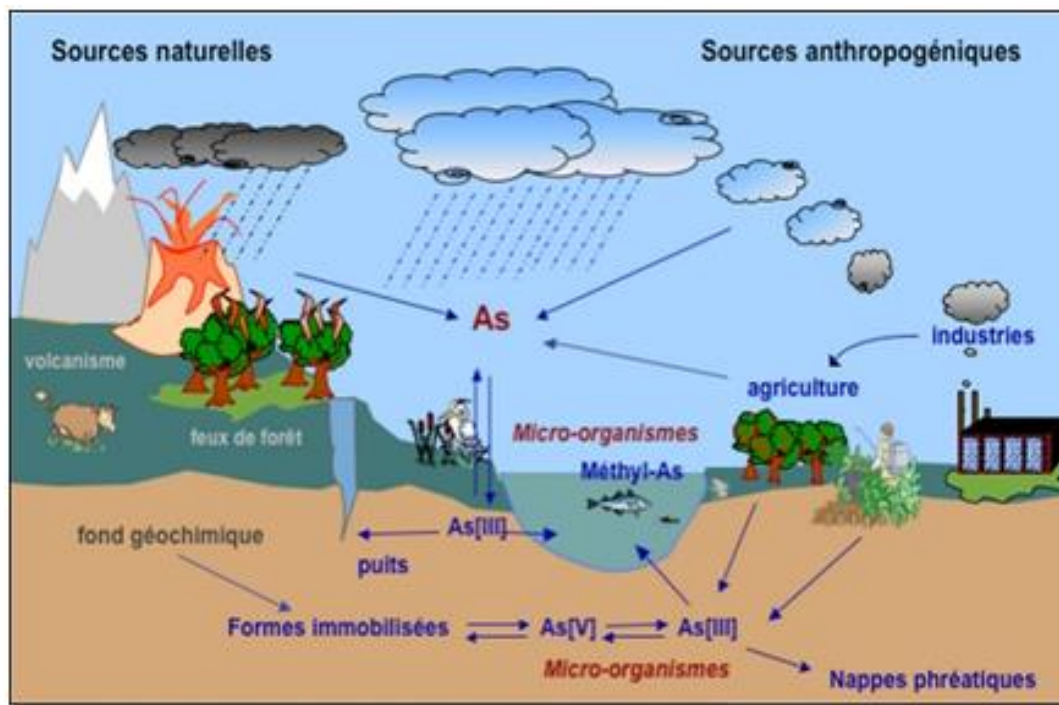
Figure 1.3 Arsenic cycle in the environment (Source:
http://nbrienvis.nic.in/Database/1_2035.aspx) (Open access)

Table 1.1 Important information of arsenic (Worou et al. 2021)

Atomic number	33
Atomic mass (g.mol^{-1})	74.9216
Sublimation point	613 $^{\circ}$C
Density	5.73
Atomic configuration	[Ar] 3d10 4s2 4p3
Valences	-3, 0, +3 and +5
Ionic radius (Å)	As (III) -- 0.58 As (V) -- 0.46
Ionic radius (Å)	($As O_4^{3-}$) -- 0.248 (Marcus, 2014)
Infinite Dilution Ionic Hydration number: From Electrostriction (Å)	($As O_4^{3-}$) -- 8.4 (Marcus, 2014)

Table 1.2 Stability of arsenic species (Worou et al. 2021)

Reducing conditions		Oxidizing conditions	
pH	As (III)	pH	As (V)
0-9	H_3AsO_3	0-2	H_3AsO_4
10-12	$H_2AsO_3^-$	3-6	$H_2AsO_4^-$
13	$HAsO_3^{2-}$	7-11	$HAsO_4^{2-}$
14	AsO_3^{3-}	12-14	AsO_4^{3-}

1.4 HEALTH EFFECTS OF ARSENIC

Arsenic has long been regarded as toxic and poisonous. Even at low concentrations, catastrophic effects on human health can occur. The toxic nature of arsenic ions depends primarily on their chemical phase. Arsine gas is most influenced by inorganic trivalent compounds, organic trivalent ions, and organic/inorganic pentavalent species. Inorganic arsenic has been categorized as a poison and carcinogen by WHO and EPA. Human arsenic exposure may occur because of ingestion, inhalation or skin problems; nevertheless, ingestion is the primary type of arsenic intake. High concentrations of arsenic result in acute toxic human effects, gastrointestinal issues (poor apatite, diarrhea and vomiting, etc.) reduced functions of the cardiovascular and nervous system (e.g. muscle cramps and heart complaints) or even death (Choong et al. 2007). The toxicity of arsenic depends on how arsenic is present. In drinking water, inorganic arsenic ions exhibited more toxicity than the organic arsenic ions found in food from the sea. The trivalent form of arsenic was more toxic than pentavalent arsenic. Toxicity is measured as the number of milligrams per kilogram of the compounds body weight that will result in the death of half those who were exposed to it in a single dose within a few days. Long-term exposure to relatively low concentrations of arsenic in the drinking water is also a health hazard. Various studies discussed the effect of the long-term exposure to arsenic on people's health. The first apparent effect of exposure to low concentrations of arsenic while drinking water is an irregular black-brown pigmentation of the skin known as melanosis and hardening keratosis of the soles and palms. If the consumption of arsenic persists, de-pigmentations of the skin result in white spots that appear as raindrops. A high amount of "raindrop" pigmentation was observed in a clinical investigation of people in West Bengal who had been exposed to high levels of arsenic in their drinking water. Palms and soles are thickened further and develop painful cracks. Symptoms of these kinds were referred to as hyperkeratosis and led to skin cancer. The disease symptoms caused by chronic ingestion of arsenic are called arsenicosis, which forms when ingested polluted arsenic water for several years.

Nonetheless, there is no universal description of the arsenic-induced disease and no way to tell which condition is caused by arsenic. Cancer cases have been caused by water affected by consuming arsenic. Long-term consumption of arsenic can cause severe damage to the kidney, liver and internal organs such as the bladder and livers. Arsenic can damage the peripheral vascular systems that contribute to black foot disease in some countries.

- **Acute arsenic health effects**

Ingestion of high dosage of arsenic generally outcomes in symptoms within 30-60 min. However, it may have been delayed if ingestion along with food. Toxic acute arsenic concentration commonly begins with metal or garlic-like flavor, burning of lips and dysphagia. Later, extreme vomiting and hematemesis can take place. Acute arsenic poisoning survivors usually incur damage to their peripheral nervous system. In the case of acute poisoning, arsenic(III) and arsenic(V) functions differently. Arsenic(III) associates and inhibits enzymes containing sulfhydryl essential for adequate physiological functions. But on the other side, by mimicking phosphate and interfering with arsenic treatment plant (ATP) production in the mitochondria, arsenic(V) generates toxicity. Acute arsenic poisoning was witnessed as 50-75% death rates and death usually in 48h. The lethal type of arsenic can differ, but 0.2-0.3g of arsenic trioxide was typically dangerous in adults (Baker et al. 2018). Arsenic As(III) is thus more harmful than arsenic As(V) in magnitude.

- **Chronic toxicity of arsenic (III) and arsenic (V)**

Chronic exposure to a lower level of arsenic concentrations has also been associated with adverse human health risks for a prolonged time. There are contradictory results about the chronic toxicity of arsenic(III) and arsenic(V). On the one hand, arsenic(III) could be more toxic than the As(V) as the extension of reports on acute toxicity. On the other hand, some assume that, as observed in most groundwater, chronic toxicity at low arsenic levels is affected only by total concentrations of arsenic, not by speciation. Long-term exposure to arsenic has proven to cause dermal, vascular and cancer effects.

- **Dermal:** Chronic exposure to arsenic initially induces changes in the skin, including keratosis and hyperpigmentation. Hyperpigmentation is a colour change that results in patches on the skin and the hardening of skin bulges, typically occurring in the palms and soles. Cancer can happen following hyperkeratosis and hyperpigmentation.
- **Vascular effect:** Arsenic exposure has been associated with different vascular disorders that affect large (cardio-vascular) and small blood vessels (peripheral vascular). Black foot disease (BFD) is one of the peripheral vascular diseases in part of the Taiwan. The feet coldness and numbness are characterized by BFD, accompanied by ulceration, black discoloration and dry gangrene of infected regions. Furthermore, all patients with BFD have a substantially higher mortality risk due to cardiovascular issues.
- **Cancer:** Exposure to a high level of arsenic leads to lung, kidney and bladder cancer occurring after 20 years or more, in addition to skin cancer. Studies have continuously proven

excessive mortality risks from lung, kidney, bladder cancer among populations exposed to arsenic through consuming water. In addition, the risk of cancer at these levels increased as the exposed level increased.

1.5 TECHNOLOGIES FOR ARSENIC REMOVAL

Arsenic contaminated water would be plentiful and arsenic-free sources or contaminated with various compounds. In such areas, removing arsenic from the arsenic-polluted water may be the most effective, at least as a minimum to be measured. Several technologies were developed for the removal of arsenic. Many of the recorded experiences would also have been for large treatment plants, although some of the same technologies can be used for limited household applications. All arsenic removal technologies rely on a few simple chemical processes that are summarized as follows,

- **Oxidation/reduction**: Under the near-neutral pH and slightly decreasing groundwater conditions, As(III), which are in the form of uncharged molecules, is primarily arsenic. However, several techniques have efficiently eliminated the negatively charged As(V). Accordingly, oxidation has been applied as a pre-remedy technique to transform As(III) to As(V) before the treatment, which includes filtration and coagulation-adsorption. Generally, redox transformation among As(III) and As(V) can be defined as follows,

$$H_3AsO_4 + 2H^+ + 2e^- \longrightarrow H_3AsO_3 + H_2O \qquad E = +0.56V$$

Arsenic is not eliminated from the solution by these reactions, but is instead used to improve other processes (Zaw and Emett 2002).

- **Precipitation:** The process of precipitation/co-precipitation can effectively treat the wide variety of increased concentrations of drinking water containing arsenic. Because of the characterization and contaminants removal properties, the efficacy of this process is less likely to be effective than other treatments. Precipitation technology is more cost-effective as the process requires skilled labour (Harper and Kingham 1992).

- **Adsorption:** Adsorption is one of the most straightforward techniques for extracting arsenic from the water. Adsorption is the mass transfer method wherein a substance is transferred from the liquid section to the surfaces of the solid and is bounded through chemical or physical forces. In the adsorption process, water purification mainly depends on the large surface area and increased surface energy of the adsorbent (Gupta and Chen 1978).

- **Ion exchange:** Ion exchange process is often a commonly implemented method of extracting arsenic from the water. Arsenic-contaminated species were substituted with another ion in the water. The ion exchange process is related to a physicochemical mechanism,

wherein ions are electrostatically retained from solid surface phase exchanged in a solution containing a similar charge. It includes the reversible displacement by a dissolved ion of an ion adsorbed onto the solid surfaces (Epsztein et al. 2019).

- **Coagulation-flocculation:** Coagulation-flocculation is the economic process for extracting arsenic and can treat large quantities of water with increased arsenic concentrations. Initially, it incorporated chemicals into the coagulation process for destabilizing the dissolved arsenic compounds. They are converted into insoluble precipitate. It is then possible to remove the solids through sedimentation and filtration. In this process, different chemicals such as aluminum coagulation, iron coagulation, enhanced coagulation by ferric ions with the coarse calcite, lime softening, co-precipitation with the manganese and iron. Furthermore, electrocoagulation can be used as a coagulant. Most commonly, aluminum coagulant salts such as ferric and aluminum sulfate are widely used because of their low cost and relative ease of use. However, the main drawback of this technology is preserving the chemicals regularly, which build more amount of sludge (Pallier et al. 2010).

- **Lime softening:** Slaked lime and soda ash were introduced to precipitate unwanted polyvalent metallic ions in the lime softening process. The removal of arsenic may be enabled by calcium carbonate, magnesium hydroxide and iron hydroxide, and magnesium hydroxide precipitates. At higher pH (10-12), the extraction rates are greatly improved by adding iron to the influent one (Fields et al. 2000).

- **Membrane filtration process:** As stated by (Mondal et al. 2006) the arsenic may be removed from the water by flowing it through a permeable barrier or membrane. The efficacy of arsenic removal in membrane filtration depends on the membrane's pore size and the particle size of the arsenic ions. The essential pressure-driven membrane processes are microfiltration, nanofiltration and reverse osmosis. In advancing water and wastewater treatment, nanotechnology has great potential to enhance the quality of the treatment and increase the availability of water through the safe use of unconventional water sources. In general, the efficacy of traditional adsorbents was regulated by the surface area or the number of active sites, the lack of selectivity and adsorption kinetics. Nano-adsorbents substantially improve their extremely high specific surface area and associated sorption sites, short intra-particle diffusion distance, tunable pore size and membrane surface chemistry. Membrane filtration systems were classified based on the applied pressure, viz. low pressure-driven membranes (5 and 100 psi) and high pressure-driven membranes 50 to 1000 psi). However, arsenic is not extracted from water by boiling.

1.6 ESSENTIAL FEATURES OF MEMBRANES

A membrane may be a semipermeable barrier that separates two vicinal stages and controls the particular transport of varieties of components before the influence of driving force over it in a specific way. One of the membrane's most valuable properties is the capacity to control the permeation rate of different species. Therefore, the membrane separation method depends on the type of membranes utilized. Figure 1.4 demonstrated the separation mechanism of the membrane, in which the feed, i.e., the solution to be handled by the membrane, passes to provide permeate, i.e., the species moving through the membrane. At the same time, retentate is the portion rejection by the membrane.
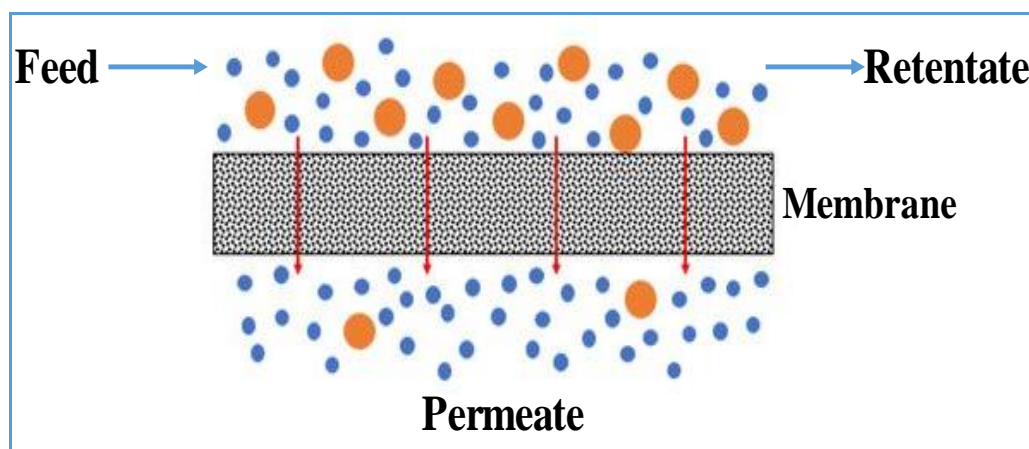
Figure 1.4 Principle of membrane separation processes (Araújo et al. 2020) (Open access).

While there is a considerable computation amongst the membrane processes and traditional approaches for wastewater treatment, membrane processes over conventional methods include significant benefits.

- It is easy to work and produces water of high quality.
- Membrane processes are more efficient and cost-effective than specific other traditional water treatment methods.
- It is an economical and energy-efficient process.
- In mild conditions, the separation was carried out.
- As no harmful chemicals are used in the process and no heat is produced, they have lower environmental effects.
- The membranes properties are diverse and can be changed depending on the requirement.
- Simple to handle and to scale up.

Since it also endures from certain disadvantages such as,

- The long-term performance of the membrane processes is not confirmed.
- Use of pre-treatment as a result of fouling and concentration polarization sensitivity.
- Low mechanical strengths of membranes can result in damage in severe conditions of operations.

1.6.1 Basic membrane process terminologies

The basic terminologies utilized in the membrane filtration process are explained as follows,

- **Membranes permeability**: Quantifies the efficiency of the membrane in terms of permeability or productivity. It is also expressed in terms of flux and is defined in unit time as the amount of water passing through the unit area of the membrane. Membrane's permeability was calculated using Equation 1.1.

$$J_w = \frac{Q}{\Delta p \times di \times n \times \pi \times L} \tag{1.1}$$

Where, $'J_w'$ is the water permeability in (L/m^{2}h bar),

$'di'$ is the inner diameter in m,

$'n'$ is the number of membranes used,

$'L'$ is the length of the membrane in m

- **Solute rejection**: The most important property of the membrane is the perm-selectivity of the membrane and is described in terms of rejection (R, %). Solute rejection was calculated using Equation 1.2.

$$R = \left(1 - \frac{C_p}{C_f} \right) \times 100 \tag{1.2}$$

Where, C_p is the solute concentration in the permeate (which can be expressed in ppb or ppm)

C_f is the solute concentration in the feed solution.

- **Swelling:** The membrane's water uptake ability was calculated using Equation 1.3.

$$\% \text{ Water Uptake} = \frac{W_w - W_d}{W_d} \times 100 \tag{1.3}$$

Where, 'W_w' wet weight of the membranes (g),

'W_d' dry weight of the membranes (g).

- **Porosity**: It is defined as the ratio of pore volume to geometric column and it is calculated using Equation 1.4.

$$\% \text{ Porosity} = \frac{W_w - W_d}{\rho_w \times A \times \delta} \times 100 \tag{1.4}$$

Where, 'W_w' wet weight of the membranes sample (g),

'W_d' dry weight of the membranes sample (g),

'A' is the area of the membrane sample (cm^2),

'δ' is the thickness of the membrane samples (cm),

ρ_w is the density of water (0.998 g/cm^3).

- **Membrane fouling and factors controlling the fouling:** Fouling is caused during filtration by the accumulation of rejected material/particle on a membrane surface or in membrane pores, which is one of the significant disadvantages of the membrane systems. Fouling results in a decrease in the efficiency of the membrane, leading to an increase in operating cost, increase in the energy needed, increase in chemical cleaning and a decline in the lifetime of the membrane. One of the essential parameters in membrane filtration is controlling fouling. Therefore, proper membrane selection, suitable pre-treatment of the process fluid and optimization of the functional design and other conditions are needed to reduce fouling. Some of the variables that minimize the fouling are described as flows.

- **Surface roughness:** As the surface roughness of the membrane increases, the flux through the membrane increases as the regions available for membrane transport increase. Simultaneously, it encourages the interaction between the rough membrane surface and colloidal particles; colloidal particles preferentially aggregate over rough membrane surface pores. Also, as result, pores are blocked and hence more fouling by decreasing surface roughness, which can be avoided.

- **Surface charge:** The repulsion interaction between some of the co-ion in feed and charge on the membrane surface is commonly known to prevent deposition of solute on membrane surfaces, thereby reducing fouling.

- **Hydrophilicity:** It is generally recognized that hydrophilic membranes show better fouling resistance because most foulants, such as proteins are hydrophobic. Chemical modifications and other methods can help to achieve the above.

1.6.2 Membrane materials and properties

With the addition of different types of nano additives, various materials such as metals, polymers, glass materials and ceramics, etc., to produce industrial synthetic membranes have been increased. Also, every membrane material has distinct mechanical strength, chemical resistance by hydrophilicity and flexibility. For a specific membrane separation application, the choice of membrane material is not arbitrary but relies on its features, which specifications the production process. During membrane material selection, the following significant properties must be taken into account,

- Excellent film forming nature
- Mechanical robustness to withstand higher pressure in the filtration process
- Thermal stability, used polymer glass transition temperature (T_g) should be greater than the processing temperature.
- Chemical stability: The polymer should resist extreme pH levels and other chemical circumstances.
- Hydrophilic/phobic properties, the polymeric material hydrophilic/phobic balance to acquire better flux, low level of fouling and overall excellent performance.

Although there are numerous membrane materials analyzed to date that exhibited few of the properties, several polymeric membrane materials are generally utilized for the membrane synthesis, such as polysulfone (PSF), polyethersulfone (PES), chitosan, poly(vinylidene fluoride) (PVDF), cellulose acetate, etc. Polymers such as PES, PAN, PVDF and PSF normally result in ultrafiltration and microfiltration membrane applications.

1.6.3 Polyphenylsulfone (PPSU) as a membrane material

Owing to its unique properties, polyphenylsulfone (PPSU) prefers a main polymeric membrane material in the present research study for fabricating asymmetric hollow fiber membranes also with the incorporation of various inorganic nanomaterials including its specific membrane properties like chemical stability, better mechanical properties, ability to solvent-resistant, hydrophilicity, resistance to a higher temperature, excellent thermal stability and better chemical resistance (pH 1-13), etc. PPSU with aromatic ring sulfone group ($-SO_2$) is considered a high-performance flexible polymer for membrane fabrication. In addition, the

glass transition temperature (T_g) of the PPSU was 220 $^\circ$C, which is appreciably higher than the polysulfone (PSf, 190 $^\circ$C) and equivalent to polyethersulfone (PES, 225 $^\circ$C). Nevertheless, the solid hydrophobic nature of the PPSU is still one of the prime drawbacks. The hydrophobic nature can affect the resistance of the PPSU towards fouling. Thus with the various dosages of hydrophilic additives and nanoparticles, the hydrophobic nature of the PPSU is being minimized. The modified PPSU membranes are frequently used in MF, UF and NF, which plays a key role in beverages, medicine, membrane fabrication and drinking water application (Darvishmanesh et al. 2011; Shukla et al. 2017).

1.6.4 Membrane fabrication

A large variety of materials can be employed to fabricate the differently configured membranes. Depending on the need for a specific separation method, the available polymers can be modified by implementing the appropriate membrane preparation methods. A few are listed below

- Sintering
- Stretching
- Track etching
- Template leaching
- Phase inversion
- Electrospinning

Due to its simplicity, the phase inversion method is very significant and widely used. It is a versatile technique resulting from various forms of morphologies of the membranes. This technique typically results in asymmetric membranes maintained on a dense porous sublayer with a relatively thin selective active layer. The polymeric solution is cast on a plate, a belt, or fabric support by dissolving it in an appropriate solvent. The various membrane preparation technique operated by phase separation was described as follows

- **Non-solvent induced phase inversion/separation process (NIPS):** Phase inversion is a technique; a polymer is safely converted from liquid to solid. In the transition from one liquid form to two liquid forms, solidification was initiated at this time. During the demixing process, one of the liquid phases can solidify so that a solid matrix is formed (high polymer dosages phase). The membrane morphology can be controlled by regulating the initial stage of the phase inversion process, which is to prepare the porous and nonporous membranes. The immersion precipitation fabricated the bulk of phase inverted membranes. A polymer solution is cast on suitable support in this system and then immersed in coagulation, i.e., the non-

solvent bath. There is the interaction of solvent and non-solvent and membrane was formed. Schematic representation of phase inversion process for the preparation of flat and hollow fiber membrane was shown in Figure 1.5. Almost every polymer would be soluble in an appropriate solvent and can be utilized to fabricate membrane. By selecting different kinds of polymer, concentration, the temperature of precipitation, the microporous phase inverted membranes can be prepared with a wide range scale from lesser than 0.1 µm to more than 20 µm.
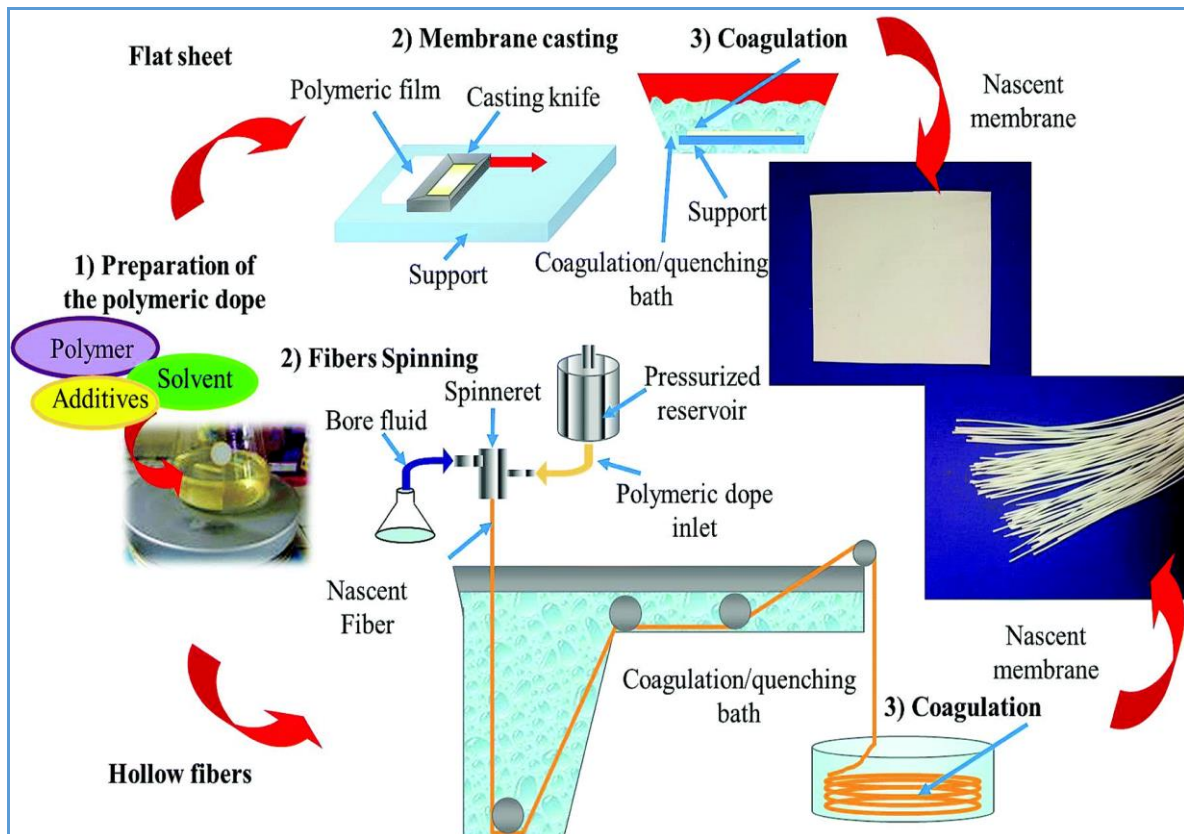
Figure 1.5 Phase inversion process for flat sheet and hollow fiber membranes preparation (Source:(Figoli et al. 2014)) (Open access).

- **Diffusion-induced phase separation process (DIPS):** A polymer solution is cast on support or extruded along with the die as a thin film in this membrane preparation process. Later it was immersed in a non-solvent (coagulation) bath. Precipitation occurs by occurrences of the phase inversion with diffusion exchange of a better solvent in a polymer solution and non-solvent in the coagulation bath (water). This process mainly consists of two steps for separation: liquid-liquid (L-L) demixing, which forms a porous morphological structure with pores the voids between the crystalline sections; the second one is a solvent-liquid form of demixing, which results in the crystalline sections.

- **Temperature-induced phase separation process (TIPS):** In the 1980s and 1990s, the usage of the TIPS process was first adopted to fabricate microporous membranes. The TIPS method can prepare most of the microfiltration membrane's cross-sectional morphological structures. First, the polymer solution is made by dissolving a polymer in a solvent at a higher temperature equal to or greater than the glass transition temperature due to the reduced solubility of the polymer by a decrease in solution temperature, the polymer precipitates. Later, by either evaporation or freeze-drying, the solvent was removed. Depending on the polymer dosage in the casting solution, the inner structures for this kind of membrane are either porous honeycomb-like or spherulitic. The TIPS process can produce membranes from polymers that are unsuitable at room temperature. In addition, the TIPS process is a binary phase without the non-solvent, which makes it simpler to control than the ternary NIPS process.

- **Vapor induced phase separation process (VIPS):** The VIPS process for membrane preparation was developed in 1918 by Zsigmondy and Bachman. The cast film consists of polymer in this process and a solvent is exposed to a vapour atmosphere of non-solvent media (generally water). The polymer's precipitation occurs because the vapour penetrates the film, which gradually forms a symmetrical porous membrane without a dense layer. The slow and uniform diffusion rate of vapours into the polymer solution, resulting in consistent polymer precipitation without a drastic change in polymer concertation, is the critical feature of the VIPS process.

- **Evaporation-induced phase separation process (EIPS):** Membrane formation occurs in the EIPS or dry cast process due to the evaporation of a volatile solvent from a polymer solution mixture containing a volatile solvent, a lesser volatile nonsolvent and a polymer. The polymer's solubility decreases with the continuous solvent evaporation and the polymer segregates into a polymer-rich phase and polymer–lean phase. Finally, a porous membrane structure was formed by removing the non-solvent from the membrane. Generally, the membrane fabricated by the EIPS method has a more porous structure. The morphologies of the membrane are greatly influenced by the initial concentration of the nonsolvent and the evaporation rate. Delayed phase separation will lead to the formation of denser membranes at the low concentration of non-solvent.

1.6.5   Important modes of filtration

In membrane technology, the two filtration process modes are dead-end filtration and cross-flow filtration.

- **Dead-end filtration:** The feed was transmitted perpendicular to the membrane surface in the membrane filtration process in the dead-end water filtration as shown in Figure 1.6(a). The method of filtration is better for the operation of batch membranes. In comparison to cross-flow, the efficiency of this model is very high; the only downside is membrane fouling; the membrane gets fouled over time and the process efficiency decreases. The membrane needs to be washed several times during the process, contributing to the cost of wear and tear. For a more extended period of use, this makes the procedure a little expensive and unsuitable. Consequently, the cross-flow filtration process was employed for more prolonged usage.

- **Cross-flow filtration:** The aqueous feed solution flows parallel or along the membrane surfaces in the cross-flow mode of filtration, as shown in Figure 1.6(b). Here, the particulate aggregation is less and thus, low fouling is induced as the concentration polarization was decreased because of the continuous feed flow. But as the feed solution is circulated at high speed, cross-flow needs high energy than the dead-end filtration. However, as the feed solution is circulated at a high velocity, cross-flow filtration requires high energy than the dead-end filtration system.
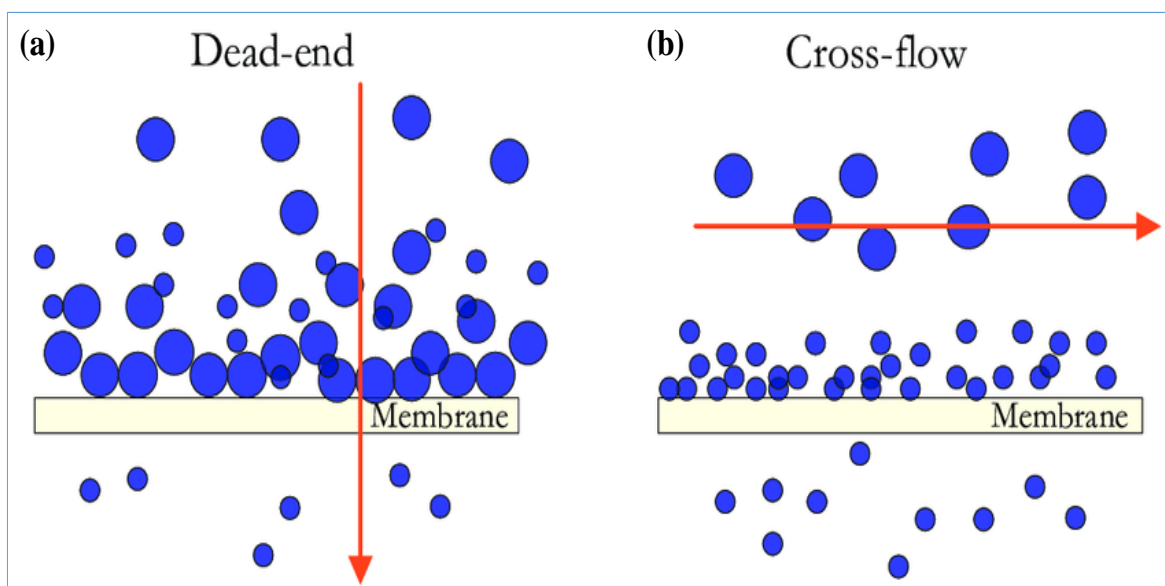
Figure 1.6 Different modes of membrane filtration system (Source: (Ketola 2016)) (Open access).

1.6.6 Membrane classification

It is very difficult to classify membranes and broadly classified on the basis of configuration, morphology, nature and applications.

Pressure-driven membranes processes

The four most common pressure-driven membrane processes are classified as follows and shown in Figure 1.7.

- **Microfiltration (MF) membrane process:** Microfiltration is the membrane separation method for the solute separation of size in the range of 0.1 to 10 μm. The separation outcome of this membrane process is generally related to the membrane's pore size and the size of the ions in the aqueous solution to be separated. As for the membrane material, polytetrafluoroethylene (PTFE), nylon, PVC, cellulose-type, and various other polymeric materials have potential membrane materials. MF is based on a different pore size sieving mechanism to preserve particles more significantly in size than the pore diameter. MF has a wide range of applications in the food, beverage, and chemical industries. In water treatment, biotechnology and many other sectors, it has high potential.

- **Nanofiltration (NF) membrane process:** Compared to RO, nanofiltration (NF) can work at moderate pressure. NF process is ideal for applications with high organic and mild inorganic removal. NF can concentrate the bivalent salts, dyes, proteins, and other heavy metals with a molecular weight larger than 1000 Da. The membranes used for NF are fabricated from cellulose acetate and aromatic polyamide, with the salt rejection characteristics ranging from 95% and 40% for bivalent salts and monovalent salts respectively.

- **Ultrafiltration (UF) membrane process:** Ultrafiltration membranes can carry organisms in the molecular weight of 300-500000 Da, with the pore size varying from 20 to 1000Å. Most of these were defined by their nominal MWCO, which means the smallest species with a molecular weight for which membranes have more than 90% rejection. The pressure differential operating at about 2 to 10 bar is the driving force for transport through the membrane. It is widely used for solutes to be clarified and fractioned. The permeate rate was controlled rather than by membrane properties, by the transport rate through the polarization layer. UF output, therefore, depends on the membrane's physical properties such as membrane layer thickness, permeability and variables of the process and system, such as feed intake, the concentration of feed, velocity system pressure and temperature. Porosity, membrane surface properties, morphology, mechanical strength, and chemical resistance are essential membrane materials. Polymeric materials are successfully used to produce UF membranes, such as polysulfone, nylon-6, polyvinyl chloride (PVC) polypropylene and acrylic copolymer. To make UF membranes, inorganic materials such as ceramics, zirconia and carbon-based membranes. UF has significant potential for various applications, such as

pharmaceutical, bioprocessing, oil and paint, separation technology, food and dairy industries proteins harvesting and separation of biological macromolecules, etc.

- **Reverse osmosis (RO) membrane process:** Suspended materials more significant than 1 µm can be removed by conventional water filtration. At the same time, RO or hyperfiltration can remove the dissolved solids, viruses, bacteria and other germs contained in raw water. For the separation of dissolved solutes, RO is essentially a pressure-driven membrane process. It is typically used for brackish water or seawater desalination to convert into potable water. It works at an ambient temperature and does not involve any phase change. Compared to conventional distillation, the reverse osmosis process is relatively a low-energy process. RO membranes are made of polymeric materials, such as aromatic polyamide and cellulose acetate. They are mainly of two main classifications (a) skinned or asymmetric membranes and (b) composite thin film (TFC) membranes. The support materials are usually polysulfone, while the thin film is made of different polyamine compounds. Generally, the RO membranes have a smaller pore structure, ranging from 3Å–5Å (0.3–0.5 nm) in pore diameter. Organic molecules and monovalent solutes do not permit to pass through the membrane pores.
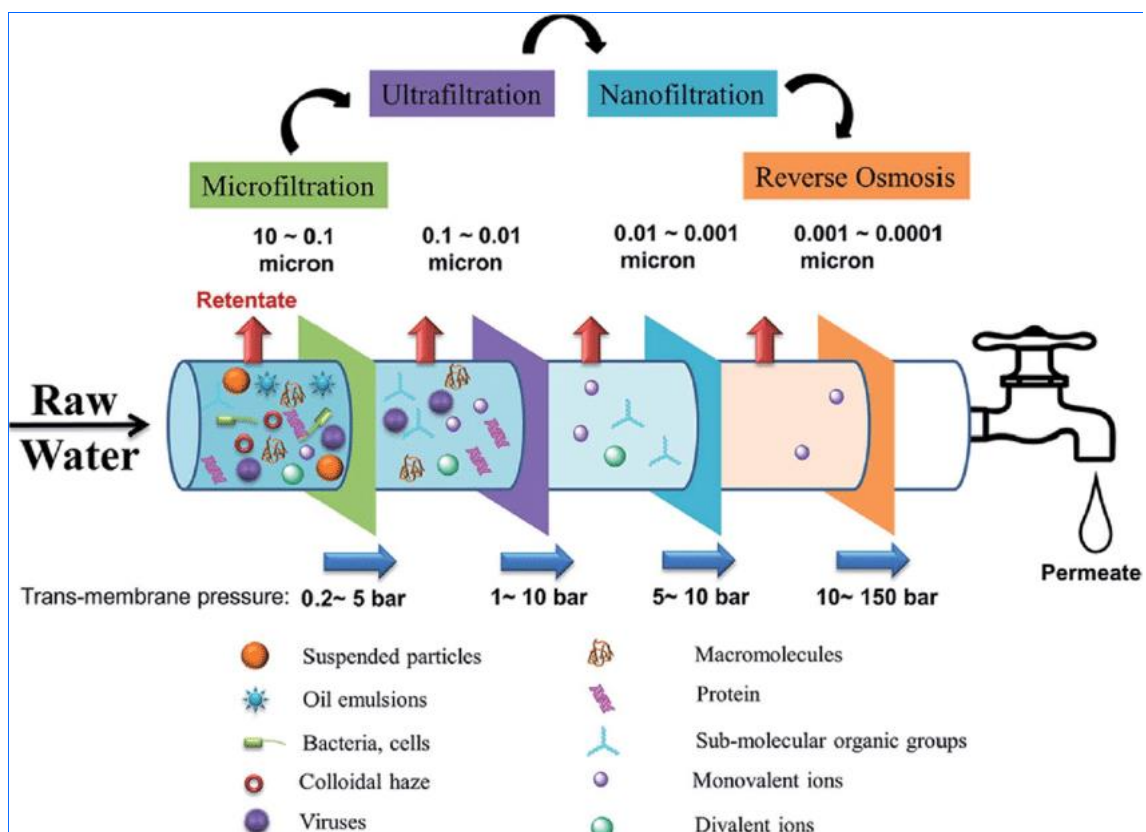
Figure 1.7 Classification of pressure driven membrane process. Reproduced with permission from ref. Liao et al. 2018. Copyright 2022, Elsevier Science Ltd (Liao et al. 2018).

Based on Membrane morphological structure

- **Symmetric membranes:** Morphological structures and transport properties are similar with a uniform pore size around the cross-sections. By sintering or tracking etching procedures, these kinds of membranes were prepared. The schematic representation of symmetric membranes is shown in Figure 1.8(a).

- **Asymmetric membranes:** Two layers of membranes of different thickness, porosity and pore size can be witnessed in asymmetric membranes morphologies. The schematic representation of symmetric membranes is shown in Figure 1.8(b). Pressure-driven filtration membranes have an integral or composite anisotropic cross-section structure with a thin, microporous, non-porous and mesoporous support layer (100-300 m) providing adequate mechanical stability (about 50 nm with a few micrometers). The selectiveness of the barrier is minimized, thus ensuring high membrane permeabilities. Anisotropic membranes can therefore have exhibited better performance than isotropic membranes.

- **Integrally skinned asymmetric membrane**: this type of membrane consists of an identical material formed during the phase inversion in its dense top active layer and the porous sublayer. The schematic representation of symmetric membranes is shown in Figure 1.8(c).

- **Thin film composites membranes**: in these membranes, two distinct compositions make up the thick active thin coating of the porous support. On the top of porous support that is physically separate, an ultra-thin polymer layer is deposited. The schematic representation of symmetric membranes is shown in Figure 1.8(d).
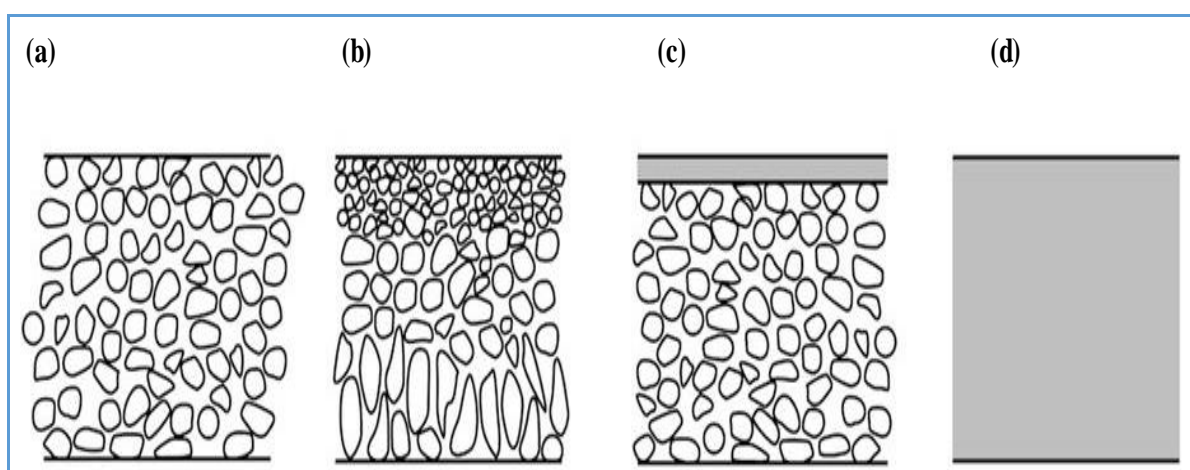
Figure 1.8 (a) Porous symmetric membranes (b) porous asymmetric membranes (c) thin-film, nonporous membrane (d) dense homogeneous, nonporous membrane (Source: (Salama et al. 2021)) (Open access).

Isotropic membranes

- **Isotropic nanoporous membranes:** Dense non-porous isotropic membranes consist of a dense film through which the diffusion mechanism transports permeants. The permeation rate of transport in the membrane was measured by diffusivity and solubility within the membrane material. These membranes are rarely used commercially because the permeation through the thicker membranes surfaces is too low. In laboratory work, they are commonly used to describe properties of membranes. This membrane was fabricated using thermal pressing and solution casting method.

- **Isotropic microporous membranes:** The isotropic microporous membrane is made from a single polymer throughout the membrane. It consists of pore size, which is significant with the standard filter in structure and functionality. It consists of a rigid, intensely voided, randomly distributed porous system. The pores in these membranes vary from conventional filters and have extremely small 0.01 µm to 10 µm in pore size. The membrane flux related to this membrane type is much higher than dense isotropic non-porous membranes and is commonly used for MF membranes. Various methods, such as track-etching and expanded film-template leaching, are mainly used to fabricate isotropic non-porous membranes.

1.6.7 Transport mechanisms of membranes

The driving forces such as temperature (ΔT), electrical potential (ΔE), pressure (ΔP) and concentration (ΔC) gradients in membrane matrix regulate the movement of species across the membrane surfaces. There are mainly two kinds of models that describe the membrane's transport mechanisms; they are models for pore flow and models for solution –diffusion.

The separation processes in the pore flow model as permeates were transported in pressure-driven natural convective flow through pores. The molecules are rejected here based on the sieving process, wherein the permeate was separated by size exclusion and pore flow. Typically, this mechanism was observed in the case of porous membranes, MF, along with UF. The pressure-controlled separation method describes the pre-flow and is expressed from Darcy's law as shown in Equation 1.5.

$$J_i = K' c_i \frac{dp}{dx}$$

$$(1.5)$$

Where, 'i' is the medium, 'K'' is coefficient describing medium's nature, 'c_i' is components concentration, 'dp/dx' is the difference of pressure present in the porous medium.

Separation is based on the solution-diffusion process in nonporous dense membranes. In the solution-diffusion model, the permeate dissolves and then diffuses through the membrane. The rejection is based on the distinction from solubility and the differences in membrane diffusion rate. The negative symbol indicated that the diffusion i.e. from the range of high concentration to low concentration is known as the concentration gradient which is shown in Equation 1.6.

$$J_i = -D_i \frac{dci}{dx} \tag{1.6}$$

Where, the flux 'J_i' in (g/cm^{2}s) related to species (i) is corresponding to the concentrations gradient (dc$_i$/dx) and is the diffusion's coefficient (Cm^{2}s^{-1}) is a measurement of the mobility of the specific molecules. The negative symbol indicated that the diffusion i.e. from the range of high concentration to low concentration is down the gradient of concentration.

The relative size and permanency of the pores are the fundamental differences between these models. The size and positions of free-volume elements (pores) are fixed in the pore-flow model. The dense membranes have no defined free-volume elements in the solution-diffusion model. In addition, the model of pore flow, which was a pressure-driven phenomenon, results in a higher flux than the model of diffusion, which operates on the concentration gradient.

1.7 APPLICATIONS OF MEMBRANE FILTRATION PROCESS

Many applications are related to membrane filtration treatments to extract impurities from contaminated water and provide clean water. Today, membrane technology has increased in various industrial processes such as mining, painting, textile, food and beverage, milk processing units, pharmaceutical industries, etc. The pressure-driven membrane processes are used in membrane technology for different separation applications. Membranes are used as a separation tool in various areas, apart from water purification and desalination, summarized below.

- **RO membrane applications:** RO membranes have been successfully used for brackish water treatments, seawater desalination processes since the 1970s. RO membranes reduce waste generation and wastewater treatment in the food process units, textiles, paint, pharmaceuticals, paper and pulp industries.

- **NF membrane applications:** the operations of NF membranes are similar to the RO membranes; such membranes can consider various separations such as separating

multivalent ions from aqueous solution, removal of colour, deletion of pesticides, extraction of amino acids and lipids from the blood in medicine, etc.

- **UF membrane applications:** UF membranes were being used in a wide range of applications ranging from removal of enzymes from cows, the separation process in the industry, the removal of suspended solids, macromolecules, turbidity from the industrial effluents, and the treatments of dialysis blood filtration.

- **MF membrane applications:** membranes have been used to extract >0.01 μm of the suspended particle from the wastewater. MF membranes are also used to treat sterile water by pharmaceutical companies and for various applications in the chemicals, food and beverages industries.

Semipermeable membranes may be applied to extract either positive or negative ions under the effect of electricity during the electrodialysis method. For the separation of casein from whey products, bacteria removal and suspended solids from milk products, membranes have been used in everyday industries for the past few years. Membrane technologies can be employed to identify several separation applications at an industrial level. Few of them are here,

- Extraction of proteins, enzymes, sugars and natural products
- Removal of biomass by UF and MF membranes
- Extracting organic solvents using NF membranes
- Various forms of recovery of metals including in mining wastewater.
- Separations of different gases such as phosphorous, hydrogen sulfate, carbon dioxide, hydrocarbon recycling, petrochemical waste from the oil and petroleum wastes from the crude oil and petroleum industry and natural gas liquids (NGL).

Due to the non-involvement of chemicals in separation processes, the membrane technology was considered a 'GREEN TECHNOLOGY'.

1.8 LITERATURE SURVEY

Over recent decades, membrane technology has become a worthy technology for separation. Research and development for improved membrane materials have made considerable progress. Due to its excellent mechanical, chemical and thermal properties, PPSU along with cellulose acetate derivative membranes have been widely used for wastewater treatment applications. To develop novel PPSU along with cellulose acetate derivative membranes, there are various literature, that is listed below,

1.8.1 Literature on cellulose acetate membranes for heavy metal removal from water

Mahendran et al. (2004) studied the various blend compositions of CA and PES by precipitation phase inversion technique. Pure water permeation, proteins rejection (EA, BSA, trypsin and pepsin) along with heavy metals (Ni(II), Cd (II) and Cu(II)) on PEI complexation have been tested with CA/PES blended membranes. Maximum protein rejection was witnessed for BSA (93%) and heavy metal for Cu(II) as 94% respectively. The proteins and heavy metal rejection were lower than the unmodified CA membranes and had high permeation properties.

Sivakumar et al. (2005, 2006) developed the cellulose acetate and polysulfone ultrafiltration membranes, polyvinylpyrrolidone (PVP) was used as pore former for heavy metal and protein removal. Increased pure water flux and water uptake were witnessed with increased PSf concentrations in the blend membranes. The high molecular weight of BSA revealed greater rejection with low flux. Because of the formation of large aggregate pores, the PWF of the membrane improved as the PVP and PSf concentrations increased. The filtration study of heavy metals such as Cu^{2+}, Zn^{2+}, Cd^{2+} and Ni^{+2} was carried out using 1 wt% of PEI. Owing to the strong PEI-Cu^{2+} complex formation Cu^{2+} exhibited higher rejection (>70%) with the low flux of 40 L/m^{2}h respectively.

Arockiasamy et al. (2009) prepared cellulose acetate and polyetherimide blended membranes. Fabricated membranes exhibited increased antifouling properties due to the amine concentrations in the blend. The higher rejection was reported because of the strong bond between the Cu^{2+} heavy metal and the PEI. Hydrophilicity and pure water flux of the membrane improved with the incorporation of PEG-600 in the blend composition.

Li et al. (2006) using immersion precipitation method, hollow fiber membranes were prepared from cellulose/ monohydrate N-methylmorpholine –N–oxide (NMMO·H_2O)/polyethylene glycol (PEG–400). The membranes demonstrated higher antifouling behavior with an operating pressure of 0.1 MPa, relatively low permeability 7.67 L/m^{2}h.

Shibutani et al. (2011) developed three various sets of hollow fiber membranes viz., cellulose acetate butyrate (CAB), cellulose acetate (CA), cellulose acetate propionate (CAP) using a thermally induced phase separation process. Although hydrophilicity varies, membrane preparation was the same; CA membrane has higher hydrophilicity than CAP. However, CA has also demonstrated increased resistance to fouling for BSA and humic acid.

Razzaghi et al. (2014) PVDF/CA blend membranes were fabricated using phase inversion process-induced immersion precipitation in various concentration ratios. The prepared membranes were examined for the fouling tendency and permeation properties. The membrane blended with a 20/80 ratio (CA/PVDF) exhibited high water permeability and excellent antifouling properties.

Terrazas-Bandala et al. (2014) fabricated composite cellulose triacetate (CTA) and activated carbon (AC) membranes using the evaporation-precipitation technique with maintaining the proper relative humidity and temperature in the synthesis process. The molecular weight of the solute was increased from 801.15 kDa to 1194.29 kDa by 1% of AC. The increased rejection of arsenic of about 45% was witnessed for a 500 ppb arsenic aqueous solution. As the concentration of the additives in the casting solution increased, the modified membranes showed increased hydrophilicity, water uptake, pure water flux, porosity and surface roughness.

Riaz et al. (2016) prepared cellulose acetate and polyurethane blended membranes for the chromium (VI) from the contaminated water. The SEM configurations confirm the enlargement of finger-like and microporous structures with the incremental dosages of hydrophilic additive. The blended membranes also exhibited improved hydrophilicity by improving water uptake and pure water permeability. The membranes showed enhanced chromium (VI) ions removal as the adsorptive dosages of cellulose acetate increased in the polyurethane dope solution.

Moradihamedani and Abdullah (2017) fabricated ultrafiltration membranes using cellulose acetate (CA) and polysulfone (PSf) with the addition of polyvinylpyrrolidone (PVP) for the removal of various heavy metals (Pb^{2+}, Ni^{2+}, Cd^{2+} and Zn^{2+}). The SEM images evidenced that the finger-like morphologies were expanded as the polymer dosages were increased. Blended membranes exhibited improved hydrophilic, water uptake and permeability properties as the dosages of CA increased in the dope solution. The CA/PSf (80:20) membrane showed excellent performance in terms of rejection 98% for Pb^{2+} with the permeability of 49 L/m^2h at 3 bar transmembrane pressure.

Durthi et al. (2018) have developed mixed matrix membranes using cellulose acetate and zinc oxide as an additive by phase inversion solvent evaporation technique. It was witnessed that the increase of 5 to 25% in the flux after dosage of ZnO nanoparticle. The existence of ZnO nanoparticles causes the membrane's hydrophilicity to increase, allowing it to be more porous. In natural waters, As(III) is present in the uncharged species H_3AsO_3, and its removal is

primarily due to steric exclusion rather than charge effects. When CA membranes were compared to CA–ZnO membranes, the CA with ZnO nanoparticle membranes had higher removal performance.

1.8.2 Literature on polyphenylsulfone (PPSU) membranes for heavy metal (arsenic) removal

Sun et al. (2002) fabricated polyphenylsulfone (PPSU) and polyethersulfone (PES), high-performance thermoplastic polymers that have been used to form polymeric micromolecular foam using the two-phase batch foaming process. SEM analyzed morphological properties to measure the foam density and size distributions in the water-displacement test. With the continuous rise in temperature and time, the experimental results showed a substantial increase in foam size.

Parcero et al. (2006) fabricated polymeric blend membranes using N-methyl-pyrrolidone (NMP) as a solvent, phosphonated polyphenylsulfone (P-PPSU) and sulfonated polyphenylsulfone (S-PPSU). The membranes were examined with 1H-NMR, thermogravimetric analysis, water uptake processes, etc. The efficiency of membranes was evaluated by permeability analysis with water and ethanol. The S-PPSU membranes exhibited improved performance than the P-PPSU membranes.

Weng et al. (2008) fabricated novel polymeric (bisphenol-A-co-4-nitro-phthalic anhydride – co-1,3 –phenylenediamine (PBNPI) and polyphenylsulfone (PPSU) blend polymeric flat sheet membranes of various concentrations. Characterization of the membrane was carried out using different methods such as SEM, TGA, XRD, FTIR and etc. With the gradual increase in the MWCNT wt%, the gas permeability capability of the membrane was increased. The outcome revealed a continuous increase in the gas permeability from 0 to 15% of the membrane was evidenced.

Darvishmanesh et al. (2011) fabricated polyphenylsulfone (PPSU) nanofiltration membranes using phase separation technique with various compositions such as (17 wt%, 21 wt% and 25 wt%) using different solvent systems such as N-methyl-2-pyrrolidone (NMP), dimethylacetamide (DMA) and dimethylformamide (DMF). The essence of solvent and polymer concentration has significantly affected the morphology and efficiency of membranes. The gradual increase in polymer concentration decreased the formation of macrovoids and rejection of rose bengal dye was increased. They also documented the fabrication of membranes based on PPSU by a dry-wet spinning technique. And also, hollow fiber membranes revealed an asymmetric structure with a thick layer of skin and porous sub-

layers. The tested membranes were favorable for retaining the Rose bengal dye. They showed that the rejection of dye increased with an increased PPSU concertation consistent with its small pore size.

Hwang et al. (2011) documented the fabrication of PPSU/polyetherimide blend membranes by blending hydrophobic PPSU and hydrophilic polyetherimide. The membrane morphologies and efficiency were evaluated to study the influence of blend composition. It was observed that with the increase in the polyetherimide concentration in the blend, there is increased hydrophilicity and pore size of the blend membranes. In addition, an increase in the hydrophilicity of the membrane led to the resistance to reversible fouling. The membranes also showed resistance to the humic acid because of the electrostatic repulsive forces between negatively charged humic acid and weak negative changes formed on the membrane.

Liu et al. (2012) fabricated TFC sulfonated membranes with the assistance of PPSU. Sulfonated diamines like benzenesulfonic acid 2,5-bis(4-amino-2-trifluoromethylphenoxy), biphenyl-4,-4-disulfonic acid and piperazine (PIP) were reacted with TMC by interfacial polymerization to form a polyamide layer. TFC membrane surfaces were treated with the attenuated total reflectance –fourier transform infrared spectroscopy (ATR-FTIR), scanning electron microscopy (SEM) and water contact angle measurements that have studied the TFC membrane surface. The Methyl Orange and Rhodamine-B dye rejection studies were carried out. Without sacrificing the dye removal performance, the inclusion of the sulfonic group by sulfonated diamine resulted in high hydrophilicity and water flux.

Zhao et al. (2012) formulated polyaniline (PANI)-PVP nanocomposite and integrated it into the PSf base polymer to prepare nanocomposite membranes using the phase inversion process. As used PANI-PVP additives played a better pore-forming and hydrophilic agent. The nanocomposite membranes have been examined for their antifouling properties using the cross-flow filtration unit as-fabricated membranes had been compared with PSf/PVP. The low flux decrease and high flux recovery on water washing, PSF/PANI-PVP membranes showed increased flux, hydrophilicity and enhanced antifouling qualities.

Díez-Pascual and Díez-Vicente (2014) developed nanocomposite membranes by solution casting method incorporating the titanium dioxide nanoparticles included in the polyphenylsulfone to examine membranes biocompatible properties. Two kinds of bacteria like Escherichia coli (Gram-negative) and Staphylococcus aureus (Gram-positive) with the assistance of UV-selected irradiation. The outcome showed a steady increase in antibacterial

activity on UV irradiation from plane membrane to the high concentrated membranes (5 wt%) because of the influence of the TiO_2 nanoparticle.

Kiani et al. (2015) novel nanofibrous membranes of polyphenylsulfone (PPSU) were fabricated by electrospinning process with the increased dosages of polyethylene glycol (PEG 400; 0, 2.5 along with 10 wt%) for studying the BSA fouling nature of membranes. In the outcome, a gradual improvement was witnessed in water flux and BSA fouling, respectively, from neat membrane to high dosage of PEG additive (10 wt%).

Thanigaivelan et al. (2015) examined the impact of nano-TiO_2 by implementing increased dosages in polyphenylsulfone (PPSU) membrane to enhance the membrane's hydrophilic behavior. In this contemporary work, 0.3% of nano-TiO_2 was demonstrated as the best-executed membrane with high flux and relatively high rejection for BSA in membrane performance.

Shukla et al. (2017) examined the antifouling properties of polyphenylsulfone membranes by various concentrations of graphene oxide (GO; 0.2, 0.5, and 1 wt%) as nanoadditive, polyvinylpyrrolidone (PVP) as a pore-forming additive and N-methyl-2-pyrrolidone (NMP) by non-solvent induced phase separation (NIPS) process. The outcome showed an enhancement of flux by a dosage of 0.5 wt% of graphene oxide. Also, the authors reported that the integration of GO considerably inhibits the relationship between the membrane surfaces and protein molecules. Consequently, increased fouling resistance potential and enhancement of mechanical and thermal properties.

Liu et al. (2016) fabricated flat sheet ultrafiltration membranes using polyphenylsulfone as a prime polymer and increased concentrations of polyvinylpyrrolidone (PVP) and polyethyleneglycol (PEG) as pore-forming agents to analyze the antifouling behavior of the membranes through the non-solvent induced phase separation method. Furthermore, the fabricated membranes were analyzed by SEM, porosity/water uptake and contact angle measurement. The PVP implemented membranes exhibited improved permeability and BSA rejection ability than the PEG incorporated membranes.

It was clear from the above-prescribed literature that PPSU and CA derivatives can be used as an excellent material for membrane preparation. Nevertheless, due to lower hydrophilicity, less porous nature related to PPSU, the low oxidation, chemical resistance and lower mechanical strength, CA membranes are not suitable for vigorous cleaning. Thus, the CA membranes modification becomes essential. Therefore, more significant research is

needed to address its disadvantages, as PPSU would make an economical membrane material than other polymers. By taking these considerations into account, subsequent work has been proposed.

1.9 PROBLEM STATEMENT

Almost four billion populations in the globe will live without the proper supply of fresh drinking water by 2025 according to (Kolbasov et al. 2017). The continuous pollution of water bodies such as lakes and rivers with the heavy metals by industrial activities such as alloy and steel production, mining, electronics, chemicals, electrospinning and so on are the main reasons for the contamination of the freshwater. Because heavy metals are non-degradable, they will remain in the environment for a long time. Therefore, to address this problem, remediation steps must be carried out. Different wastewater decontamination methods had been proposed and used in the past; they are adsorption, ozonation, chemical reduction/oxidation, electrodialysis, ion exchange, biological treatment and membrane technology have also been proposed and utilized. Nowadays, the membrane filtration approach via nano-adsorbents has been focused, because it is an economical and efficient approach to extract heavy metals from the contaminated aqueous solution. And the usage of binary oxide nanoparticles (ZnO-MgO) has also resulted in the improved separation and agglomerated-free membranes. This investigation describes the extraction of arsenic (As-V) using polyphenylsulfone (PPSU)/ cellulose acetate derivatives in the presence of zirconium oxide (ZrO_2), zinc-magnesium oxide (ZnO-MgO) and nano-aluminum oxide (nano-Al_2O_3) nanoparticles using a membrane filtration approach.

1.10 SCOPE AND OBJECTIVES OF THE PRESENT WORK

Consumption of arsenic can pose a severe health risk to humankind. Minute concentrations of arsenic in drinking water and the atmosphere causes severe health problems. It was also considered that arsenic was poisonous and dangerous to human health. Therefore, a clear need exits to efficiently decontaminate arsenic from drinking water. From recent studies, membrane filtration is an effective method to extract arsenic from drinking water. Many researchers employed various polymers such as polysulfone (PSf), polyethersulfone (PES), cellulose acetate (CA), polyvinylidene fluoride (PVDF) and etc to enhance the membrane properties and separation performance. Nevertheless, because of the increased hydrophobicity, the used polymers exhibited some downsides, such as PSf membranes being less capable of penetration along with severe fouling. PES membranes suffer from a lower limit of transmembrane pressure, toxicity and are more susceptible to foul. Chitosan is

insoluble in organic solvents. However, less scientific work has been reported to extract arsenic from drinking water using polyphenylsulfone (PPSU) as a prime polymer to incorporate hydrophilic additives and nanoparticles. Research is ongoing to solve this problem by containing various suitable nanoparticles (inorganic) and pore-forming agents to fabricate the membrane and enhance different membrane properties. So, the scope of this work is limited to experimentally investigate arsenic-V rejection using fabricated polyphenylsulfone hollow fiber membranes.

Objectives of the present work

The main aim of this proposed research work is to fabricate and characterize a novel polyphenylsulfone with cellulose acetate and cellulose acetate phthalate as additives ultrafiltration hollow fiber membranes containing different concentrations of nanoparticles (ZrO_2, ZnO-MgO and Al_2O_3) and polydopamine (PDA) for arsenic-V removal from drinking water.

- ❖ To study the effect of different additives such as cellulose acetate (CA) and cellulose acetate phthalate (CAP), Zirconium oxide (ZrO_2) nanoparticle, Zinc-magnesium oxide (ZnO-MgO) nanoparticle, aluminum oxide (Al_2O_3) nanoparticle and polydopamine (PDA) in polyphenylsulfone (PPSU) ultrafiltration hollow fiber membranes.

- ❖ To characterize the prepared ultrafiltration hollow fiber membranes in terms of morphological structure and topography by SEM and AFM, the surface potential of the membrane was analyzed by zeta potential measurement, hydrophilicity by contact angle measurement, pure water permeability, porosity/ water uptake, the functional groups by FTIR, XPS and thermal properties by TGA. Fouling resistant nature of the prepared hollow fiber membranes was evaluated by bovine serum albumin (BSA) and molecular weight cut-off was investigated using polyethylene glycol (PEG). Also as used nanoparticles were characterized by TEM, XRD and particle size distribution.

- ❖ To study the Arsenic-V (As-V) removal from all prepared hollow fiber membranes from drinking water.

- ❖ And also an attempt was made for analyzing the dyes/proteins removal from as-fabricated polyphenylsulfone/cellulose acetate and polyphenylsulfone/cellulose acetate phthalate hollow fiber membranes.

CHAPTER -2
EXPERIMENTAL SECTION

2.1 Materials and Methods

2.2 Materials

Polyphenylsulfone (PPSU, Radel~5000, M_w ~ 50,000 g/mol) was furnished from Solvay polymer company (Belgium). Cellulose acetate and cellulose acetate phthalate of molecular weight of 50000 and 2534.12 g/mol respectively, zirconium oxide (ZrO_2) nanoparticle with the molecular weight of 123.22 g/mol, nano-aluminum oxide (nano-Al_2O_3 size <50 nm) of molecular weight (M_w) of 101.96 g/mol, bovine serum albumin (BSA) (M_w ~66,463 g/mol), egg albumin (M_w ~18,400 g/mol), pepsin (M_w ~34,500 g/mol), N-methyl-2-pyroledone (NMP) and polyethylene glycol (PEG) of different molecular weight 6000, 10000 and 20000 g/mol, polyvinylpyrrolidone (M_w ~ 360000 g/mol) were purchased from Sigma–Aldrich, India. Zinc-magnesium oxide (ZnO-MgO, M_w ~ 103.909 g/mol) was purchased from the American elements; Japan. The arsenic standard solution was furnished from Merck, India. All polymers were dried at 50 °C using a vacuum oven to get rid of the moisture present on the surfaces of the polymer.

2.3 Hollow fiber membrane preparation

2.3.1 Preparation of dope solutions for neat and modified membranes

The procedure for preparation of dope solutions by neat and nanoparticles (ZrO_2, ZnO-MgO, nano-Al_2O_3 blended with polyphenylsufone (PPSU)/ cellulose derivative (cellulose acetate and cellulose acetate phthalate) and PDA in PPSU/(polyvinylpyrrolidone) PVP by non-solvent induced phase separation process (NIPS) process is explained as follows. Individually, various dosages of the ZrO_2, ZnO-MgO and nano-Al_2O_3 nanoparticle (0.6, 1 and 1.5 wt%) and polydopamine (PDA; 1, 2, 3 and 5 wt%) were allowed for proper sonication of about 60 min in NMP using a high-resolution probe sonicator (CY-500 LAS ROZAS, deMadrid) at 240W and 55 Hz for complete dispersion. Later, 3 wt% of hydrophilic additives (CA and CAP) were allowed to disperse in NMP for PPSU/CA and PPSU/CAP dope solutions and polyvinylpyrrolidone (3 wt%; PVP) was also allowed to disperse in NMP for PPSU/PDA dope solutions by sonication process for about 60 min.

The constant proportions of (17 wt%) of polyphenylsufone (PPSU) was allowed to dissolve in NMP by a mechanical stirrer at 50 °C for about 350 RPM to procure homogeneous dope solutions (Kumar et al. 2020a). The detailed structure of the chemical composition for the preparation of the hollow fiber membrane's dope solution was described in Table. 2.1, 2.2 and 2.3.

2.3.2 Spinning of the dope solution for preparing hollow fiber membranes

Polyphenylsulfone (PPSU) ultrafiltration hollow fiber membranes have been fabricated using non-solvent induced phase separation (NIPS) technique by overviewing the literature (Nayak et al. 2018). With the aid of nitrogen gas pressure, the prepared dope solutions were allowed to flow through the annular zone of the spinneret. Reverse osmosis (RO) water was used as bore fluid and permitted to flow through the adjacent sides of the spinneret. The spinneret was placed 4 cm away from the coagulation bath. The distance is known as the air gap distance. The dope solution was pumped at the top and bore fluid through the spinneret on the adjacent sides. The structure for spinning the dope solution has been demonstrated in Table 2.4. The fabricated hollow fiber membranes were coiled onto a rotating drum. The membranes were soaked in distilled water for about 24h and again in the 10 wt% of the glycerol solution for another 24h to avoid hollow fiber membranes pore shrinkage. Eventually, the wet hollow fiber membranes were dried at room temperature.

Table 2.1 Composition of prepared dope solutions

Membrane code	Dope solution preparation composition			NMP (g)
	PPSU (g)	**CA (g)**	**CAP (g)**	
Neat membrane (NM)	14	0	0	86
CA-1/PCA-1	14	0.1	0	85.9
CA-3/PCA-3	14	0.3	0	85.7
CA-5/PCA-5	14	0.5	0	85.5
CAP-1/PCAP-1	14	0	0.1	85.9
CAP-3/PCAP-3	14	0	0.3	85.7
CAP-5/PCAP-5	14	0	0.5	85.9

Table 2.2 Chemical compositions of prepared dope solution

Membranes code	NMP (g)	PPSU (g)	CA (g)	CAP (g)	ZrO_2/ZnO-MgO/nano-Al_2O_3 (wt%)	ZrO_2/ZnO-MgO/nano-Al_2O_3 (g)
PZCA-0/ ZMCA-0/ ALCA-0	82.85	17	0.3	0	0	0
PZCA-0.6/ ZMCA-0.6/ ALCA-0.6	82.79	17	0.3	0	0.6	0.102
PZCA-1/ ZMCA-1/ ALCA-1	82.76	17	0.3	0	1	0.170
PZCA-1.5/ ZMCA-1.5/ ALCA-1.5	82.72	17	0.3	0	1.5	0.255
PZCAP-0/ ZMCAP-0/ ALCAP-0	82.85	17	0	0.3	0	0
PZCAP-0.6/ ZMCAP-0.6/ ALCAP-0.6	82.79	17	0	0.3	0.6	0.102
PZCAP-1/ ZMCAP-1/ ALCAP-1	82.76	17	0	0.3	1	0.170
PZCAP-1.5/ ZMCAP-1.5/ ALCAP-1.5	82.72	17	0	0.3	1.5	0.255

Table 2.3 PPSU/ PVP/polydopamine (PDA) hollow fiber membranes dope compositions

Membrane Code	PPSU (Wt. %)	NMP (Wt. %)	PVP (Wt. %)	PDA (Wt. %)	PDA (g)
PDA-0	17	80	3.0	0	0
PDA -1	17	79.83	3.0	1.0	0.17
PDA -2	17	79.66	3.0	2.0	0.34
PDA -3	17	79.49	3.0	3.0	0.51
PDA -5	17	79.15	3.0	5.0	0.85

2.4 Characterization of the prepared hollow fiber membranes

2.4.1 High resolution- Transmission electron microscopy (HR-TEM) analysis of the nanoparticles

The morphological characteristics of the nanoparticles (ZrO_2, ZnO-MgO and Al_2O_3) have been analyzed using JOEL-JEM-2100 PLUS, high resolution-transmission electron microscopy (HR-TEM) analyzer. A calculated amount of nanoparticles was distributed and sonicated in the ethanol solution for about 30 min to acquire a relatively homogenous blended solution (Ibrahim et al. 2017a). The homogenous solution was appropriately placed on a copper grid and was dried under the incandescent lamp. The completely dried sample was used for the TEM characterization.

2.4.2 X-ray diffraction (XRD) analysis of the nanoparticles

The XRD measurement of used nanoparticles (ZrO_2, ZnO-MgO, Al_2O_3) and polydopamine (polymer)) was performed using Rigaku XRD Miniflex 600 powder supplied graphite monochromated Cu-Ka with the radiation of $\lambda=0.1540$ nm collected at 50 mA from the 2θ parameter of 10° to 80° (Ibrahim et al. 2017b).

Table 2.4 Spinning specifications for fabrication of hollow fiber membranes

Specification	Condition
Dope solutions	NMP/PPSU/CA and NMP/PPSU/CAP
	NMP/PPSU/CA/ZrO$_2$ and NMP/PPSU/CAP/ZrO$_2$
	NMP/PPSU/CA/ZnO-MgO and NMP/PPSU/CAP/ZnO-MgO
	NMP/PPSU/CA/Al$_2$O$_3$ and NMP/PPSU/CAP/Al$_2$O$_3$
	NMP/PPSU/PVP/PDA
OD/ID of Spinneret (mm)	1.1/0.55
Bore fluid	RO water
Air gap (cm)	4
Coagulation bath temperature ($^\circ$C)	26
Bore fluid flow rate (ml/min)	2.5
Dope extrusion rate (ml/min)	3.5
Nitrogen gas pressure (bar)	1.5
Fiber drawing velocity (cm/s)	15
Temperature bath	Water
Speed of gear pump (RPM)	10
Speed of drum (RPM)	13

2.4.3 Particle size distribution of nanoparticles

Nanotrack wave, microtrack, USA was employed for the particle size distribution of the used nanoparticles. The nanoparticle analysis was carried out by two primary techniques, i.e., the dynamic light scattering and the zeta potential analysis (Dos Santos et al. 2014).

2.4.4 Morphologies of prepared hollow fiber membranes

The dried hollow fiber membrane was analyzed for the scanning electron microscopy (SEM) cross-sectional and surface morphological studies using Hitachi TM -3000, scanning electron microscope. The prepared membranes were immersed for about 3 min in methanol to prevent membrane surface charge and freeze-fractured in a liquid nitrogen bath. With the aid of the EMITECH K575 sputter coater, the membrane surfaces were coated with a thin layer of platinum (Ibrahim et al. 2017a).

2.4.5 Hydrophilicity/hydrophobicity of the prepared membranes

Hydrophobic and hydrophilic responses of the surfaces of blended membranes were analyzed using the sessile droplet method, dynamic FTA-200 contact angle measurement. Properly dried and the defect-free membrane was placed on the fixture. The droplet of DI water was collected on the membrane surfaces and allowed for uniform dispersion for about 30 sec. A similar approach was engaged for determining contact angle for various places on membrane surfaces and an average of readings were noted (Kumar et al. 2020b).

2.4.6 Water uptake and porosity of the hollow fiber membranes

The dry-wet weigh principle was used to assess the membrane's porosity/water uptake assessment. The fine hollow fiber membrane was selected from the fiber bundle and cut into a length of 2 cm each. On either side of the hollow fiber membranes were properly closed using epoxy/hardener in the ratio of 2:1 and membranes were immersed in de-ionized water for about 24h. After complete wiping the membrane surfaces using blotting paper, membrane wet weight (W_w) was recorded. Later, membranes were heated at 50 $^{\circ}$C for about 12h, then membrane's dry weight (W_d) was also noted (Kolangare et al. 2019). By substituting the membrane's dry weight and wet weight values in Equation 2.1, the water uptake can be calculated.

Porosity measurement of the fabricated hollow fiber membranes was carried out using the dry-wet weigh technique. The hollow fiber membranes were dipped in de-ionized water for 24h and wiped with blotting paper; thereby, the membranes wet weight (W_w) was calculated. Furthermore, wet membranes were dried in a vacuum oven at 50 $^{\circ}$C for about 12h and dry weight (W_d) of the membranes was also noted (Nayak et al. 2018). By substituting the 'W_w' and 'W_d' in Equation 2.2 to determine the porosity of the membranes.

$$\text{Percentage water uptake} = \frac{W_w - W_d}{W_w} \times 100 \qquad (2.1)$$

$$\text{Percentage porosity} = \frac{W_{w-}W_d}{\rho_w \times A \times \delta} \times 100 \qquad (2.2)$$

Where, $'\rho_w'$ is the density of water (0.998 g/cm^3), 'A' is area of the membrane (wet), 'δ' is the thickness of the membrane.

2.4.7 Pure water permeability analysis of fabricated hollow fiber membranes

A cross-flow filtration unit was used to assess pure water permeability (PWP) for properly dried PPSU/CA and PPSU/CAP along with nanoparticles incorporated hollow fiber membranes. Five defect-free good performed membranes were selected from fabricated membrane bundles and cut into an appropriate length of 15 cm. The stainless steel adaptor was employed to hold fabricated hollow fiber membranes firmly with EA E-30CL epoxy/hardener of 2:1 as adhesive and allowed to dry for 24h. The fabricated hollow fiber membranes were inserted in the cylinder of the cross-flow filtration setup. The centrifugal pump was employed for continuous water flow within the permeation cell to ensure the desired pressure in the system. The setup was also fitted with a pressure indicator to accurately control the excessive pressure in the system. The membranes were subjected to compaction for 20 min at the beginning of the process with an initial pressure (compaction) of 0.15 MPa at room temperature. The permeate was collected by reducing the filtration transmembrane pressure (TMP) by 0.1 MPa and noted for every 4 min and PWP was tabulated for about 60 min (Hebbar et al. 2017b). The de-mineralized water was used to investigate pure water permeability in the experiment. The PWP of the hollow fiber membranes was measured using Equation 2.3.

$$J_{w1} = \frac{Q}{\Delta p \times di \times n \times \pi \times L} \qquad (2.3)$$

Where, 'Q' is the volumetric flow rate in (mL/min), 'L' is the length of the membranes (m), 'D_i' is the inner diameter of the membrane (m), 'ΔP' is the difference in transmembrane pressure (bar), 'n' is the total number of membranes, 'J_{w1}' is pure water permeability (L/m^{2}h bar) (Hebbar et al. 2017c).

2.4.8 Antifouling properties of the prepared membranes

The antifouling behavior of the fabricated hollow fiber membranes was characterized by overviewing the literature (Ibrahim et al. 2017a). The membranes were initially subjected to compaction pressure of 0.15 MPa for about 20 min in a cross-flow filtration system. To determine the pure water permeability (J_{w1}, in L/m^{2}h bar), the pressure in the system was

reduced to a TMP of 0.1 MPa. Again washed membranes were subjected to laboratory prepared 0.8 g/L of bovine serum albumin (BSA) in an aqueous solution. The permeability of the BSA (J_p, in L/m^{2}h bar) was reported from each membrane at 0.1 MPa TMP. Then, hollow fiber membranes were cleaned two to three times with distilled water and blotting paper. The membrane's water permeability (J_{w2}, in L/m^{2}h bar) was recorded using the same hollow fiber membrane. The antifouling nature of the membrane was confirmed by calculating the total recovery ratio (R_t), flux recovery ratio (FRR), reversible fouling (R_r) and irreversible fouling (R_{ir}). The antifouling features of the membrane were established using Equations 2.4-2.7.

$$\text{FRR} = \frac{J_{w2}}{J_{w1}} \times 100 \tag{2.4}$$

$$R_r\,(\%) = \frac{J_{w2} - J_p}{J_{w1}} \times 100 \tag{2.5}$$

$$R_{ir}\,(\%) = \frac{J_{w1} - J_{w2}}{J_{w1}} \times 100 \tag{2.6}$$

$$R_t\,(\%) = \frac{J_{w1} - J_p}{J_{w1}} \times 100 \tag{2.7}$$

2.4.9 Study of molecular weight cut off

To determine the molecular weight of the best performing membranes, a 1 wt% of polyethylene glycol (PEG) of 20000, 10000 and 6000 g/mol was employed. The PEG rejection was performed using a cross-flow filtration system of 0.1 MPa TMP. The same working procedure was introduced with different molecular weight PEG rejection. Initially, each PEG aqueous solution prepared at 100 ppm was permitted to flow via hollow fiber membranes for PEG filtration. The dosages of PEG in the feed (C_f) and permeate (C_p) sample was measured using the Shimadzu 5050A apparatus of total organic carbon (TOC). Subsequently, PEG rejection was measured in percentage using the following Equation 2.8 (Ibrahim et al. 2017a).

$$\text{Percentage rejection} = R = (1 - \frac{C_p}{C_f}) \times 100 \tag{2.8}$$

2.4.10 Attenuated total reflectance - Fourier transforms infrared spectroscopy (ATR-FTIR) spectroscopy

Using Perkin-Elmer, Attenuated fourier transform infrared spectroscopy (ATR-FTIR) was employed to identify the various functional groups on the membrane surface. The fabricated membranes were effectively dried using a vacuum oven at 60 $^\circ$C to extract water molecules present on the membrane surfaces. Within the scan range of 600 to 4000 cm^{-1} and

24 scans per cm, functional groups were reported by compressing the membrane sample in-between the crystal plate (Kumar et al. 2019).

2.4.11 X-ray photoelectron spectroscopy (XPS) of the prepared membranes

The chemical composition of the surface of the fabricated best performing membrane was carried out by overviewing the literature (Ibrahim et al. 2018). The investigation was carried out using K-alpha (Thermo scientific, USA) x-ray photoelectron spectroscopy (XPS) using monochromatic x-ray source Al-Kα at pass energy of 93.9 eV at a voltage of 15 kV and current 10 mA. The XPS spectrum of the membrane sample was reported with the binding energy in the range of 0-1200 eV. The calibration was conducted by carbon contained C1s at 284.6 eV and at base pressure was maintained as 10^{-7} Pa.

2.4.12 Thermogravimetric analysis (TGA) of the prepared membranes

The study of TGA was carried out by Thermoanalyzer GmbH, BAHR, thermogravimetric analyzer, Germany. The percentage weight loss of the prepared neat membranes and best-performing membranes was analyzed by overviewing the literature (Golpour and Pakizeh 2018). Each 10 mg sample of hollow fiber membranes were dispersed uniformly in the platinum crucible and heated from room temperature to 800 $^{\circ}$C with a heat rate of 10 $^{\circ}$C/min and an air-flow rate of 20 cm^3/min.

2.4.13 Topographical structure of the prepared membranes

The atomic force microscopy (AFM) demonstrated an essential tool for interpreting the surface topological structures of the prepared hollow fiber membranes. The surface topological images of the prepared membranes were analyzed by tapping tool fastened on cantilever beam of Brucker –Alpha, atomic force microscopy. The prepared hollow fiber membranes were cut at a length of 2 cm and attached to a glass plate of cross-sectional size 2 cm×1 cm with the help of two-sided tape. The topological characterization was evaluated in the scan range of 3 µm ×3 µm (Golpour and Pakizeh 2018). At least two to three pictures were acquired and the membrane surface roughness was tabulated.

2.4.14 Surface potential of the prepared hollow fiber membrane

An electrokinetic surpass (Anton Paar GmbH, Austria) analyzer was used to analyze the zeta potential of the best-performing membrane. The specimen holder in the zeta potential apparatus is 3 cm × 1 cm. Fabricated membranes were cut open into 2 cm length on both sides and placed side by side on the specimen holder. The solution 0.001 M KCl was circulated on the measuring cell that comprises samples to be tested. A manual titration was performed

using a solution of 0.1 M HCl and 0.1 M NaOH, respectively to evaluate the pH-dependent zeta potential nature of the membrane sample (Ibrahim et al. 2017a; Jung et al. 2015). Furthermore, the zeta potential parameter has been evaluated to analyze the surface potential and at what pH the zeta potential of the best-performed membrane was zero (Ibrahim et al. 2017b).

2.4.15 Study of arsenic-V removal from the fabricated membrane

Atomic absorption spectroscopy (AAS; Shimadzu Japan) graphite furnace was employed to determine the concentration of arsenic-V in feed and permeate solutions. The contaminated arsenic-V solution was prepared with 1 ppm (1 mg/L) from standard arsenic solution within the pH range of 6.8 ± 0.2. The solution was contaminated with arsenic-V, known as feed (C_f). For filtration, the toxic arsenic-V aqueous solution was allowed to flow through the hollow fiber membrane surface in a cross-flow filtration unit with initial compaction pressure of 0.15 MPa for about 20 min and later compaction pressure was reduced to 0.1 MPa as TMP for about 60 min and permeate was collected at room temperature. The collected permeate was noted as C_p. By substituting the parameters of AAS concentrations of permeate (C_p) and feed (C_f) in the following Equation 2.8, the arsenic-V removal efficiency was calculated (Durthi et al. 2018).

2.4.16 Positron annihilation lifetime spectroscopy (PALS) study of the membranes

Positron annihilation studies were done on the two samples (neat membrane (PZCA-0) and ZrO_2 modified membrane (PZCA-1)) using sodium (^{22}Na) radioactive isotope as the source of positrons. The source is prepared in the form of sodium chloride (NaCl) dissolved in an aqueous solution of hydrochloric (HCl) acid and depositing it drop by drop on a thin (thickness ~2 mm) foil of pure and well annealed Ni till the required strength of about 5 μCi is obtained. The non-deposited part of the foil is then folded to cover the deposition. The source in this form is used to get sandwiched between specimens of the samples on either side in which the emitted positrons are stopped and annihilated. The ^{22}Na emits positrons of all possible energies from a few meV to 545 keV. The range of positrons of the end-point-energy 545 keV is calculated using the formula $R(mm) = 1.86/density$ in g/cm^3 (Evans 1955). In this case, the thickness of the membrane sample was much lesser than the maximum positron range. Therefore, to ensure that all the positrons are stopped within the samples, the membrane had to be folded to give enough layers so that the total thickness is larger than the maximum positron range. The details are represented in Table 2.5.

Two types of measurements were carried out – Positron annihilation lifetime spectroscopy (PALS) and Doppler broadening spectroscopy (DBS). In PALS, the time interval between the emissions of a 1.276 MeV gamma-ray, which is emitted simultaneously with the positron, and that of the two 0.511 MeV gamma rays, which are emitted at the time of annihilation, is measured using a gamma-gamma coincidence setup. The setup consisted of BaF2 scintillators as gamma-ray detectors coupled with the XP2020Q photomultipliers tubes and chains of nuclear electron module to process the signals. About 0.8 million counts were collected in PALS with a peak-to-background ratio of about 8000:1. The data were analyzed using PALS fit (Evans 1955).

Table 2.5 Positron properties of the membranes

Sample	Mass (g)	Area of the membrane (cm^2)	Thickness (cm)	Density (g/cm^{-3})	Range of positrons (mm)	No. of foils needed to stop positrons	No. of foils used in the experiment
Neat membrane (PZCA-0)	0.7788	283.34	0.008	0.3436	5.41	67.62	80
Modified membrane (PZCA-1)	0.1658	74.61	0.007	0.3167	5.85	83.50	80

2.4.17 Study of leachability of the prepared membranes

Hollow fiber membranes containing ZrO_2 are tested with reverse osmosis water for leachability with different pH values (4.3, 7.1 and 9.1). The finely prepared membranes were initially selected and broken into 15 cm from the hollow fiber membrane bundle. The hollow fiber membranes were assembled using sufficient proportions (2:1) of epoxy/hardener on the stainless steel adaptors. In the cross-flow filtration device, the membranes were subjected to pure water permeability (RO water) for 2h at a transmembrane pressure of 0.1 MPa and the permeate was collected. Later, using inductively coupled plasma mass spectroscopy (ICP-MS), the concentration of ZrO_2 in the permeate solution was evaluated (Peretyazhko et al. 2014).

2.4.18 Mean pore diameter and concentration polarization of the membrane

Mean pore radius of the membrane

Mean pore radius of the membrane was calculated using Equation 2.9. (Karimipour et al. (2021)

$$\text{Mean pore radius (r}_m) = \sqrt{\frac{(2.9-1.75\varepsilon)\times 8\eta lQ}{(\varepsilon\times A\times \Delta P)}} \tag{2.9}$$

Where, 'η' is the viscosity of water (8.9×10^{-4} Pa s at 25 $^{\circ}$C), 'Q' is the volume of permeate water per-unit time, and 'ΔP' is the operational membrane pressure (0.1 MPa), 'ε' is porosity, 'r_m' is mean pore radius, 'A' is effective area of membrane (m^2).

Concentration polarization of the membrane was evaluated using Equation 2.10.

$$\frac{C_m}{C_b} = \frac{\exp(\frac{J_w}{K})}{R+(1-R)\,\exp(\frac{J_w}{K})} \tag{2.10}$$

Where, '$\frac{Cm}{Cb}$' is concentration polarization ratio at the membrane surface, 'C_b' is bulk concentration, 'J_w' is permeability, 'K' mass transfer co-efficient, 'R' is rejection (Mulder & Mulder, 1996).

Mass transfer co-efficient (K)

Mass transfer co-efficient of the membrane was calculated using simplified Leveque's correlation as illustrated in Equation 2.11.

From Sherwood number,

$$\text{Sh} = 1.62 \times \sqrt[3]{\left(\text{Re Sc}\left(\frac{d}{l}\right)\right)} \tag{2.11}$$

$$K = 1.62 \times \sqrt[3]{\frac{vD^2}{dL}}$$

$$V = \frac{Q}{A_s}$$

Where, '*d*' is diameter of hollow fiber membrane, '*V*' is velocity of flow (m/s), '*Q*' is flow rate (m^3/s), '*D*' is diffusivity, '*L*' is length of the membrane (m), '*A$_s$*' is cross sectional area (*m^2*) of the membrane (Estay et al. 2018; Mondal et al. 2020).

Reynolds number,

$$R_e = \frac{\rho v d}{\mu}$$

Where, '*ρ*' is density of water (1000 kg/m^3), 'V' is velocity of flow and 'μ' is viscosity of water.

CHAPTER -3

USE OF CELLULOSE ACETATE/POLYPHENYLSULFONE DERIVATIVES TO FABRICATE ULTRAFILTRATION HOLLOW FIBER MEMBRANES FOR THE REMOVAL OF ARSENIC-V FROM WATER

Abstract

Polyphenylsulfone (PPSU)/ cellulose acetate (CA) and polyphenylsulfone (PPSU)/ cellulose acetate phthalate (CAP) ultrafiltration hollow fiber membranes were fabricated using a non-solvent induced phase separation (NIPS) process. Fabricated membranes were characterized using scanning electron microscopy (SEM) and atomic force microscopy (AFM) to interpret the effect of incremental dosages (1, 3 and 5 wt%) of the additives on PPSU hollow fiber membranes. Hydrophilic properties were also confirmed by analyzing the contact angle measurement, porosity, water uptake and pure water permeability. The antifouling nature of prepared membranes was evaluated using bovine serum albumin (BSA) as a model protein. The principle objective of the current research work is to assess and compare the Arsenic-V removal properties from prepared hollow fiber membranes. The increased percentage of arsenic-V removal was revealed from 5 wt% of CA in PPSU (CA-5) and 5 wt% of CAP in PPSU (CAP-5) were 34% and 41% with corresponding permeabilities of 44.42 L/m^{2}h bar and 40.11 L/m^{2}h bar respectively.

3.1 INTRODUCTION

At present, the drinking water is polluted with varieties of heavy metals and metalloids due to the continuous growth of population and development of various industries are the leading causes of water pollution. Arsenic comes from both natural and geological sources. Arsenic in groundwater is also produced via the desorption and reductive dissolution of surface reactive mineral phases in aquifer sediments, such as hydrous ferric, aluminum, as well as manganese oxides, which are present as coatings (disperse phase). In this aspect, the toxic arsenic influences a drastic health effect on human beings (Ghosh et al. 2021). Acute arsenic toxicity leads to nausea, vomiting, sore throat, tingling of the hands and feet and severe headaches. Chronic exposure to arsenic leads to significant health hazards such as numbness, cardiovascular diseases, bladder-related cancer, kidney failure, darkening of skin and even death (Yadav et al. 2021). The rejection of arsenic ions from water is challenging because of the toxicity and neutrality in drinking water. Recently, several researchers used a variety of conventional treatment methods to extract arsenic from the drinking water such as ion-exchange (Ghurye et al. 1999), lime softening (Khandaker et al. 2004), co-angulation (Balasubramanian et al. 2009), flocculation (Pallier et al. 2010), adsorption (Zhou et al. 2017), oxidation (Garcia-Costa et al. 2021) and membrane-based filtration technology by ultrafiltration (Terrazas-Bandala et al. 2014), reverse osmosis (Abejón et al. 2015; Jarma et al. 2021) and nanofiltration (Siddique et al. 2020).

The essential benefits of membrane-based filtration processes are no phase change during separation, easy operation, low energy requirements, higher quality and good filtration capability. Related to membranes filtration, reverse osmosis and nanofiltration are used for the separation of arsenic from an aqueous solution. Nevertheless, these processes have demonstrated limited degrees of achievement in arsenic removal because they have constraints in the separation process of arsenic-contaminated drinking water. Therefore, ultrafiltration is a modern filtration process to provide efficient rejection with increased permeability, cost-effectiveness and less tendency towards fouling (Ibrahim et al. 2017a). However, these processes have demonstrated a limited level of achievement in the elimination of arsenic and suffering from few drawbacks in the extraction process of arsenic-contaminated drinking water. The ultrafiltration membrane process has benefits in terms of improved rejection with increased permeability, cost-effectiveness and lower tendency for fouling.

Polyphenylsulfone (PPSU) is a stable polymer. It plays a vital role in membrane fabrication due to its superior properties such as high thermal and chemical stabilities, increased thermal tolerance, hydrolysis stability and ease of handling. However, membranes prepared using PPSU as a base polymer suffers from extreme hydrophobicity, which is a powerful tendency of fouling and brittle (Darvishmanesh et al. 2011). In order to overcome issues concerned with PPSU, the surfaces of the pristine PPSU membrane must be modified. The additive dosages influence on neat membrane improves outcomes in terms of hydrophilicity and high adsorption properties. In the current work, bio-sorbent additives such as cellulose acetate and cellulose acetate phthalate were selected to modify the surfaces of pristine PPSU membranes. The cellulose acetate membranes are simple, easy to prepare, oxidant-resistant and mechanically robust (Rahimpour and Madaeni 2007; Terrazas-Bandala et al. 2014).

Ferjani et al. (2002) fabricated an asymmetric cellulose acetate membrane with polymethyl-hydrosiloxane (PMHS) for surface modification with increased additive (CA) by phase inversion process. The modified membranes demonstrated expanded structures associated with the micropores and finger-like projections along with sponge-like structures from SEM morphological studies. Membranes have also been tested for the pure water flux and NaCl rejection properties. Increased dosages of hydrophilic cellulose acetate in the hydrophobic PMHS have led to a decline in NaCl solution preservations.

Rahimpour and Madaeni (2007) prepared membranes using polyethersulfone (PES) as a base polymer, cellulose acetate phthalate (CAP) as an inorganic additive along with the polyvinylpyrrolidone (PVP) act as pore former by NIPS process. The fabricated membranes have been tested for pure water and liquid permeation. In addition, SEM and AFM of the membrane surfaces have been studied to analyze the membrane's surface properties. Improved dosages of the CAP in the PES membranes enhance the membrane hydrophilicity, porosity, water uptake and improved antifouling properties.

Rajesh et al. (2011) prepared membranes using cellulose acetate and polyamide-imide by NIPS process. The membranes were studied for SEM, AFM, water content, porosity, pure water permeability and antifouling properties. The hydrophilicity of the blended membranes has been demonstrated by improved porosity, water uptake, hydrophilicity and pure water permeability. The modified membranes have significantly increased flux recovery ratio (FRR), indicating excellent antifouling properties. SEM and AFM showed improved surface roughness as the dosages of the additive were increased in the polymer matrix. The membranes reportedly demonstrated improved porosity, pure water permeability, water uptake and antifouling with intensified dosages of the additives.

Sun and Chen (2016) fabricated polyethersulfone (PES)/cellulose acetate (CA) mixed matrix membranes. With the gradual dosages of CA, membranes demonstrated improved hydrophilicity, permeability and antifouling properties. SEM and TGA further characterized the prepared membranes to analyze the membrane morphologies and thermal stability. Morphological studies have shown expanded finger-like projections and microvoids. Improved thermal equilibrium has been witnessed from the modified membranes with the variation of cellulose acetate dosage in PES.

In overviewing the above literature, membranes prepared using polyphenylsulfone /cellulose acetate and polyphenylsulfone /cellulose acetate phthalate to remove arsenic-V using arsenic-V-contaminated drinking water efficiently is still not yet been reported. To meet the aforementioned research gap, it was proposed that hollow fiber membranes be fabricated using polyphenylsulfone /cellulose acetate derivatives for arsenic-V removal. This research work aims to fabricate, characterize and evaluate the efficiency of arsenic-V removal from blended hollow fiber membranes.

3.2 RESULTS AND DISCUSSION

3.2.1 Scanning electron microscopy (SEM) morphological studies

Figure 3.1 shows the fabricated hollow fiber membrane's cross-sectional and surface morphological properties. All fabricated neat and blended membranes demonstrated asymmetric structure. The water interaction in the coagulation bath and polymer dope solution, the neat membranes contain microvoids structural configuration and the narrow finger-like structure sandwiched by spongy layer (Ibrahim et al. 2017a). There is a considerable change in the morphologies, with incremental dosages (1 wt%, 3 wt% and 5 wt%) of cellulose acetate and cellulose acetate phthalate to the neat membrane. The steep finger-like structures are expanded. Figures 3.1(e) – (g), the CAP contained hollow fiber membranes revealed more porous-like structure than CA, containing hollow fiber membranes, because the CAP itself acts as a better pore former. This in turn promoted the CAP hollow fiber membranes enhancement of porosity, hydrophilicity and pure water permeability as compared to CA membranes (Mukherjee and De 2014; Rahimpour and Madaeni 2007). The detailed SEM cross sectional (complete view) was illustrated in Figure 3.2. From Figure 3.3, the hollow fiber membranes surface morphologies of 5 wt% of CAP in the PPSU (CAP-5) membrane produce increased porous-like morphologies compared with other membranes. Beyond this additive dosage, the membrane exhibited an improved agglomerated structure and is not suitable for any other separation process (Durthi et al. 2018). The outer and inner dimeter along with mean pore radius of the hollow fiber membranes were incorporated in Table 3.1.
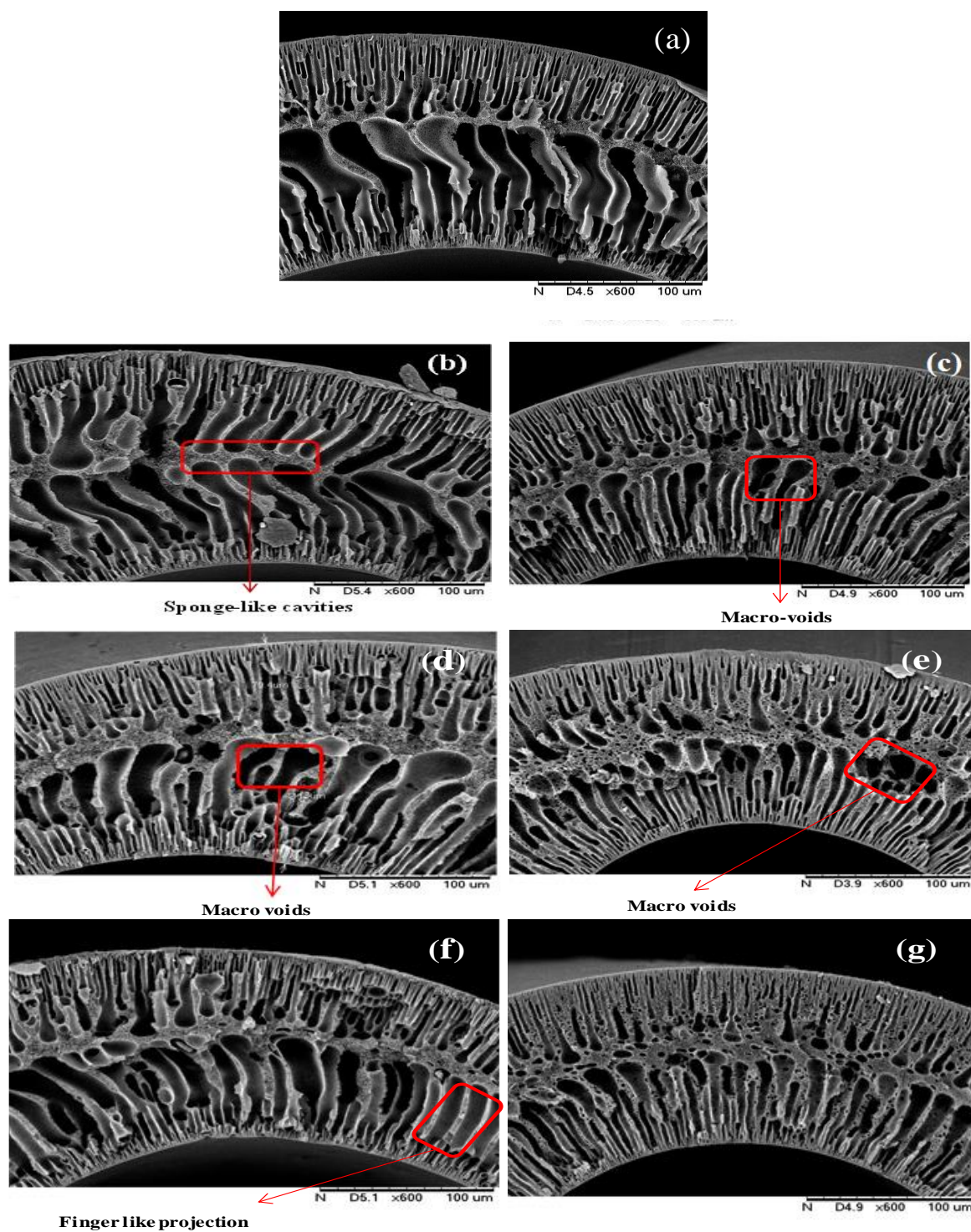
Figure 3.1 Cross-sectional scanning electron microscopy (SEM) images of the neat membrane (a), and cellulose acetate (1, 3 and 5 wt %) incorporated PPSU membrane (b, d, and f) and cellulose acetate phthalate (1, 3 and 5 wt %) incorporated PPSU membrane (c, f, and g).
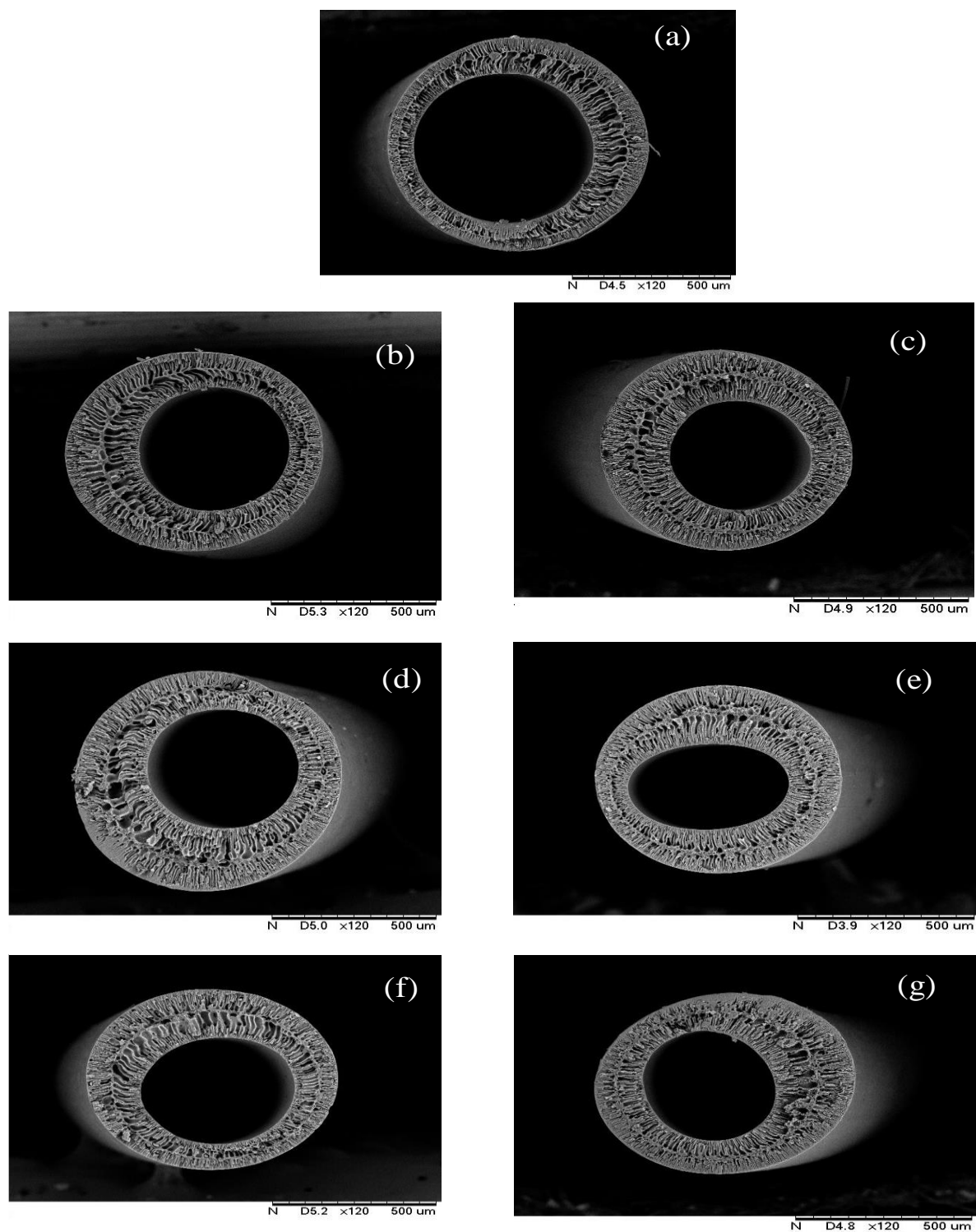
Figure 3.2 Cross-sectional (complete view) scanning electron microscopy (SEM) images of the neat membrane (a), and cellulose acetate (1, 3 and 5 wt %) incorporated PPSU membrane (b, d, and f) and cellulose acetate phthalate (1, 3 and 5 wt %) incorporated PPSU membrane (c, f, and g).
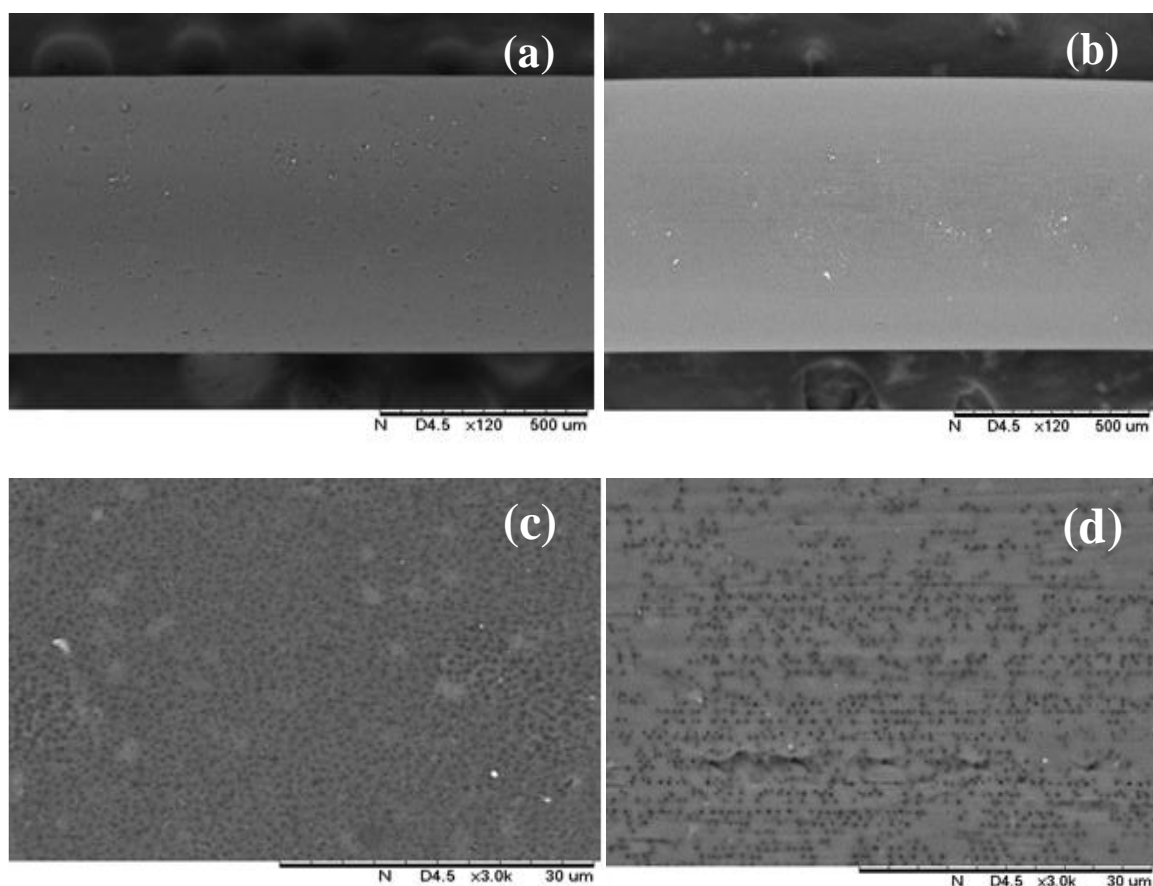
Figure 3.3 Surface SEM images of CA-5 (a and c) and CAP-5 (b and d) hollow fiber membranes.

3.2.2 Hydrophilicity/phobicity of the hollow fiber membrane

Figure 3.4 illustrated the hydrophilicity/phobicity of the pristine and CA/CAP contained hollow fiber membranes. High hydrophobic and less porous structures of the pristine hollow fiber membrane showed an increased parameter of the contact angle 80.48°. Implementing incremental hydrophilic additives (CA and CAP) into the PPSU dope solution significantly reduces the contact angle parameters (Nevárez et al. 2011). From Table 3.3, for CA-5 and CAP-5 membranes, the contact angle parameters were recorded as 60.83° and 43.40° respectively. Since, the carboxyl and hydroxyl, functional groups on the CAP membrane surfaces demonstrated the increased hydrophilicity from the modified membranes enhances the absorption of the water molecules (Shenvi et al. 2014). The decreased contact angle parameters for the CA and CAP hollow fiber membranes were represented as CA-0 > CA-1 >CA-3 > CA-5 and CAP-0 > CAP-1 > CAP-3 > CAP-5.
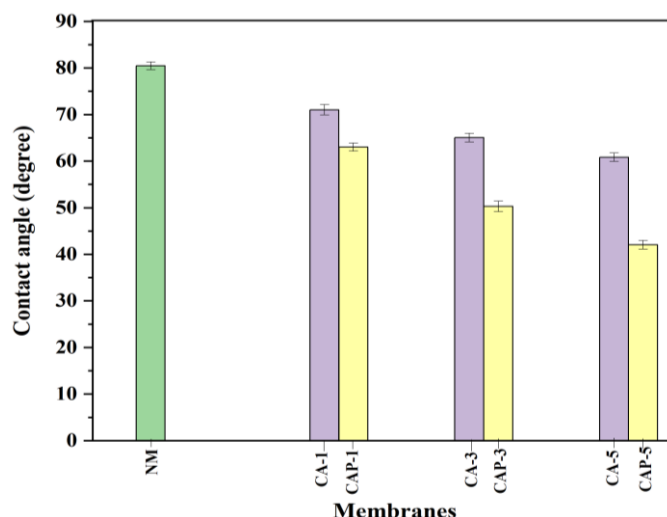
Figure 3.4 Hydrophilic/phobic measurement of prepared neat and cellulose acetate (CA) and cellulose acetate phthalate (CAP) contained PPSU membranes.

3.2.3 Water uptake and porosity of the membranes

Figure 3.5(a) – (b) demonstrated the pristine membrane and CA/CAP modified membrane in PPSU dope solution. The pristine membrane with high hydrophobic nature exhibited smaller water uptake and porosity parameters as 37.50% and 5.48% respectively, as witnessed from Table 3.3. The concentrations of CA and CAP in the neat dope solution to enhance the porosity parameter for CA-5 and CAP-5 as 26.97% and 27.96% respectively. The enhanced value of the porosity is because of the leaching of additives in the membrane fabrication. Another reason for increased porosity as intensified dosages of additives resulted in thermal instability, which further causes the rapid demixing of additives in the water coagulation bath (Qin et al. 2005). The improved porosities on the membrane surface also enhance the water uptake from the modified membrane. As such, from Table 3.3 the water uptake parameters for modified membrane as CA-5 and CAP-5 are 69.01% and 77.01%, respectively, compared to neat membrane 37.50%. The existence of a polar functional group and increased hydrophilicity due to the uniform distribution of additives in the dope solution facilitates the increased water-holding capability of the modified membranes (Han et al. 2013).
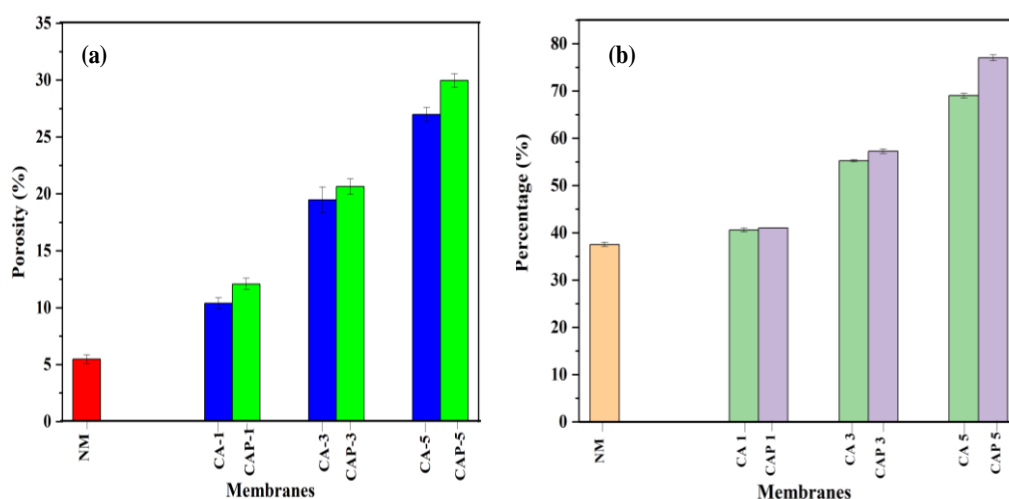
Figure 3.5 (a) Porosity and (b) water uptake parameter of fabricated neat and modified hollow fiber membranes.

3.2.4 Pure water permeability of the membranes

Figure 3.6(a) – (b) show the pure water permeability of fabricated hollow fiber membranes. The smaller value of pure water permeability was observed from neat membrane (37.93 L/m^{2}h bar) compared to the modified blend hollow fiber membranes because of the hydrophobic and less porous nature of PPSU in the casting solution (Moideen K et al. 2016). Furthermore, there is a gradual improvement in the value of pure water permeability as the incremental dosage of hydrophilic cellulose acetate (CA) and cellulose acetate phthalate (CAP) additives into hydrophobic PPSU dope solution. For the fabrication of membranes, the additives CA and CAP were leached out, which increases the porosity of the membrane. Since the incremental dosages of the CA-5 and CAP-5 enhances the porosity on surfaces of the hollow fiber membranes. The membrane water permeability also depends on hydrophilicity and water uptake. As porosity on the surfaces of the hollow fiber membranes increases, the water-holding capability of the membranes also increases as more pores are present. Furthermore, the hydrophilicity of the hollow fiber membranes was increased as an increase in additive dosage (CA-5 and CAP-5) into the PPSU casting solution due to the presence of an enormous amount of polar functional groups (–OH, –CH and –CO) on the surfaces of the hollow fiber membranes (Han et al. 2013; Rahimpour and Madaeni 2007).

From Table 3.1, the pure water permeability of the CAP /PPSU (CAP-5 as 77.01 L/m^{2}h bar) hollow fiber membrane is higher as compared to CA /PPSU (CA-5 as 69.01 L/m^{2}h bar) and neat membrane because of two reasons. Primarily, carboxylic functional sites (–CO$_2$H) on the surfaces of the CAP/PPSU membranes. The carboxylic group reduces fouling behavior by

improving hydrophilicity. Secondly, as a result, the CAP additive itself serves as a stronger pore former, more to be seen by incremental dosages of CAP in the hydrophobic PPSU dope solution (Rahimpour and Madaeni 2007). This is also evidenced by the SEM micrograph.

Table 3.1 Properties of the fabricated membranes

Membrane code	Contact Angle (°)	Standard deviation (Std. Dev.)	Porosity (%)	Std. Dev.	Water Uptake (%)	Std. Dev.	Pure water permeability (L/m²h bar)	Std. Dev.	Outer diameter (OD in m) ×10⁻⁶	Inner diameter (ID in m) ×10⁻⁶	Mean pore radius (m) ×10⁻⁷
NM	80.48	1.6	5.4	0.6	37.5	0.7	37.9	1.5	855	598	1.93
CA-1	71.02	2.1	11.3	0.8	40.5	0.7	41.4	1.7	761	450	1.85
CA-3	65.04	1.8	19.4	1.9	55.2	0.3	48.6	1.3	855	465	1.41
CA-5	60.83	1.7	26.9	1.0	69.0	0.8	61.4	1.6	773	458	1.16
CAP-1	63.01	1.7	12.0	0.8	41.0	0.01	45.7	1.3	723	397	1.81
CAP-3	50.27	2.2	20.6	1.2	57.2	0.8	55.5	1.4	733	431	1.20
CAP-5	43.40	1.8	27.9	1.0	77.0	1.0	69.6	1.2	755	417	1.08
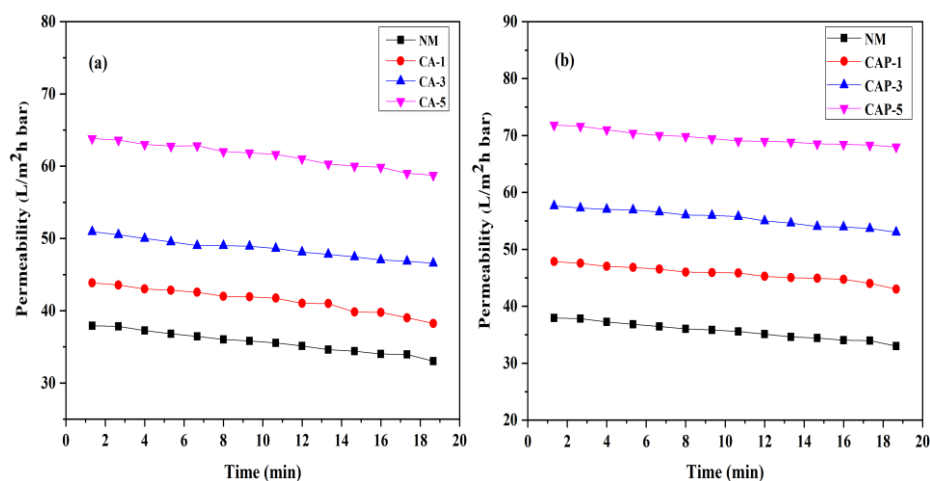
Figure 3.6 Pure water permeability of the prepared (a) CA /PPSU hollow fiber membranes (b) CAP /PPSU hollow fiber membranes.

3.2.5 Study of antifouling properties of the membrane

Figure 3.7(a) – (b) shows the time-dependent antifouling study for three stages i.e., permeability measurement with pure water, BSA permeability and pure water permeability after washing the membrane with water. There is an increased antifouling permeability with the intensified concentrations of additives (CA and CAP) due to the high adsorptiveness of the surfaces of the membrane. Table 3.2 and Figure 3.7(c) – (d), the neat membrane with less flux recovery ratio (FRR) 73.64% revealed more fouling tendency of the prepared membrane. The FRR value was considerably increased as the dosages of additives were increased in the PPSU dope solution. As such membrane CA-5 and CAP-5 exhibited the improved value of FRR as 88.67% and 91.95% respectively. The increased FRR parameter proved the enhancement of antifouling properties of the modified membranes (Huisman et al. 2000). The increased FRR is due to the hydroxyl and amine functional groups on membranes surfaces. It is also noted that the decreased parameter of BSA permeability as compared to the other two water permeability. The deposition or adsorption of BSA protein molecules on pores of membrane surfaces results in pore blockage, which further reduces BSA permeability (Vetrivel et al. 2018a). The increased parameters of reversible fouling (R_r), total fouling ratio (R_t) and decreased parameter of irreversible fouling (R_{ir}) from pristine membrane to modified membrane revealed better filtration life.

Table 3.2 Antifouling properties of hollow fiber membranes

Membrane sample	J_{w1} (L/m²h bar)	Std. dev.	J_{w2} (L/m²h bar)	Std. dev.	J_p (L/m²h bar)	Std. dev.	FRR (%)	Std. dev.	R_r (%)	Std. dev.	R_{ir} (%)	Std. dev.	R_t (%)	Std. dev.
NM	48.5	0.9	35.7	1.0	13.3	1.0	73.6	1.1	46.1	0.07	26.3	0.1	72.5	0.1
CA-1	50.7	1.2	39.8	1.0	16.1	0.8	78.5	0.7	46.7	0.1	21.4	0.2	67.1	0.1
CA-3	56.2	1.4	49.8	0.9	22.3	1.0	88.7	0.7	49.0	0.09	11.3	0.2	60.3	0.3
CA-5	64.6	1.3	57.3	0.9	26.3	1.2	88.6	0.8	47.8	0.1	11.3	0.1	59.1	0.2
CAP-1	54.2	1.1	45.2	0.1	20.1	0.6	88.3	0.6	46.2	0.4	16.6	0.38	62.1	0.1
CAP-3	61.3	1.1	53.9	0.9	24.5	0.9	87.9	0.8	47.8	0.02	12.0	0.1	59.1	0.1
CAP-5	71.2	0.9	65.5	0.8	28.4	0.8	91.9	0.8	52.0	0.06	8.0	0.1	60.1	0.09
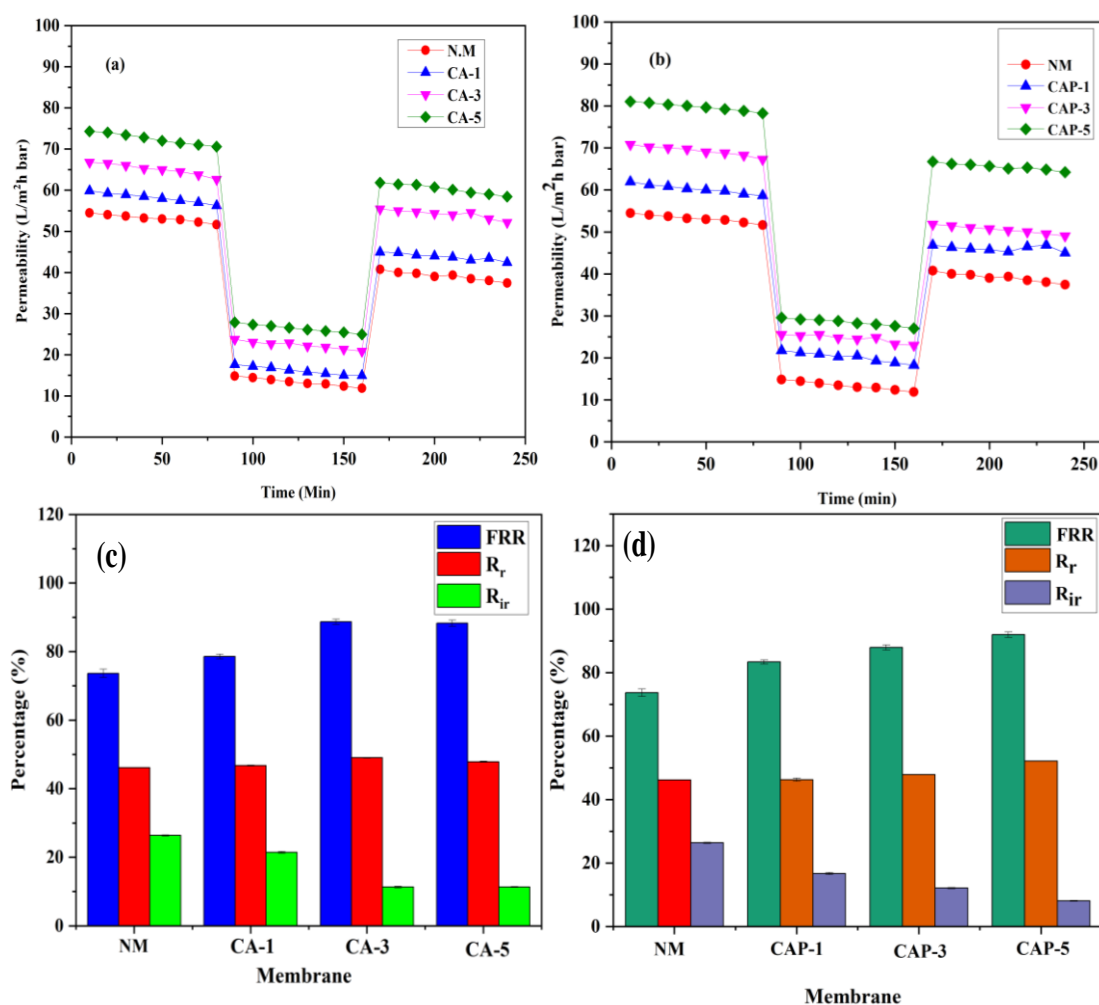
Figure 3.7 (a) Time dependant antifouling behavior of the (a) CA/PPSU hollow fiber membranes and (b) CAP/PPSU hollow fiber membranes. Comparison of antifouling properties (flux recovery ratio, reversible fouling and irreversible fouling) of the prepared (c) CA/PPSU hollow fiber membrane and (d) CAP/PPSU hollow fiber membranes.

3.2.6 Molecular weight cut off (MWCO) study

Figure 3.8 illustrated the best performing (CAP-5) membrane's molecular weight cut-off found to be 14489 Da. The MWCO corresponds to the lowest molecular weight of solute (preferably PEG) in Daltons, in which the membrane decontaminates 90% of the solute (Ortega-Requena and Rebouillat 2015). The MWCO outcome of the CAP-5 membranes was also revealed that the fabricated membrane was an ultrafiltration membrane. The polyethylene glycol (PEG) 6000, 10,000 and 20,000 Da increased rejection properties of 63.22%, 65.78% and 92.69% respectively. As the molecular weight of the PEG increases, there is an improved rejection performance from the measured membrane (Dorra et al. 2018).
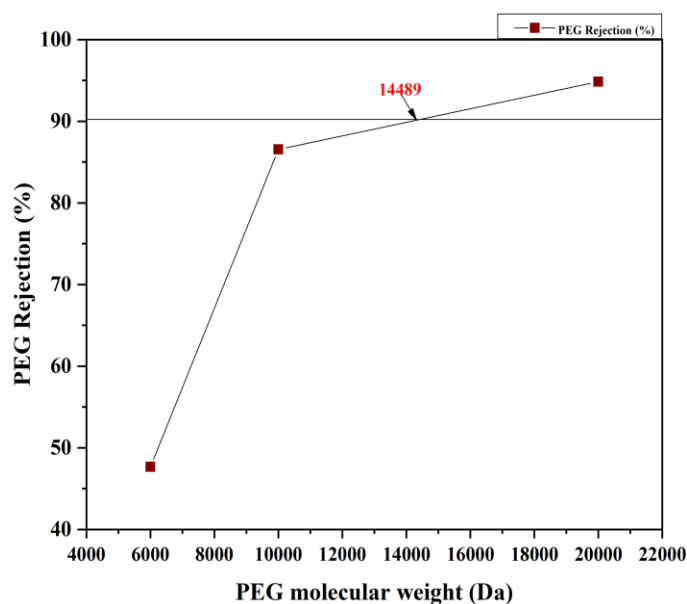
Figure 3.8 Molecular weight cut-off (MWCO) of CAP-5 hollow fiber membrane with the transmembrane pressure of 1 bar.

3.2.7 Atomic force microscopy (AFM) of the membranes

Figure 3.9 represents topographical 3-D AFM images of neat and CA/CAP-contained PPSU hollow fiber membranes. The surface roughness depends primarily on the mean arithmetic surface roughness deviation (R_a), the height of significant difference of the five corresponding maximum peaks and minimum peaks (R_q) and root mean Z-data (R_z). In general, the deviation of arithmetic mean surface roughness (R_a) was considered to analyze the roughness nature of the membrane (Ramos et al. 2016). From Table 3.3, the pristine membrane revealed the R_a parameter as 8.05 nm, which was increased with the CA/CAP concentration in the PPSU dope solution. The intensified values of R_a for CA-5 and CAP-5 were 39.8 nm and 47.4 nm respectively. From Figure 3.8, CAP membranes with the increased surface roughness exhibited enhanced hydrophilic and water holding capability.

Table 3.3 Surface roughness properties of the hollow fiber membranes

Membranes	R_a (nm)	R_q (nm)	R_z (nm)	R_{max} (nm)
NM	8.05	12.0	3.72	108
CA-1	9.5	13.5	4.24	160
CA-3	22.05	29.6	8.26	203
CA-5	39.8	49.9	10.30	386
CAP-1	20.1	30.6	5.14	242
CAP-3	26.3	39.3	12.53	365
CAP-5	47.4	61.4	28.35	442
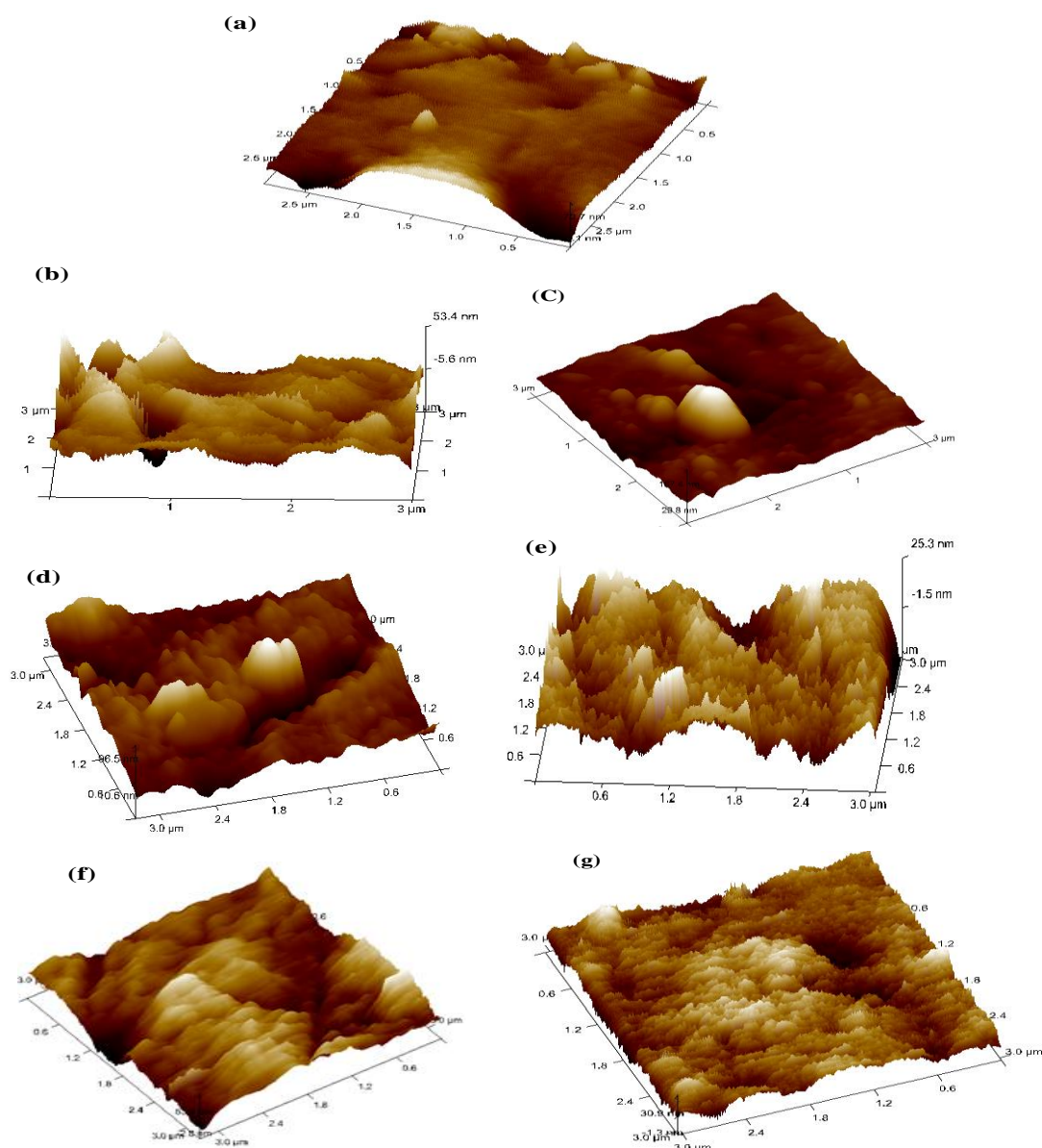
Figure 3.9 Atomic force microscopy (AFM) topographical structure of the prepared neat and CA/PPSU and CAP/PPSU hollow fiber membranes.

3.2.8 ATR-FTIR study of the hollow fiber membrane

Figure 3.10 represents the Attenuated total reflectance– Fourier transform infrared spectroscopy (ATR-FTIR) study of the fabricated neat and modified hollow fiber membranes. FTIR confirmed the occurrence of the used CA and CAP additives in modified membranes than the neat membrane, as shown in Figure 3.10(b) – (c). The details of different functional groups regarding peak value were represented as follows in Figure 3.10(a) – (c). From ATR-FTIR graph of CA membrane attributed the stretching vibration of –OH functional sites at peak 3316 cm^{-1}. The –CH$_2$ (methyl group) was attributed stretching vibrations at peak 2924-2871 cm^{-1}, the alkyl group was attributed to 1486 cm^{-1}, the peak at 1231 cm^{-1} represents

stretching vibration bond corresponding to the ether group of cellulose acetate. Moreover, the peak of 1107 cm^{-1} was allocated as the –C–O–C– stretching frequency and 870 cm^{-1} peaks corresponds to the functional sites of –CH (Greish et al. 2010). In the case of CAP membrane, owing to the presence of the hydroxyl functional groups, a small change occurs in the –OH group of CAP-modified membranes as illustrated in Figure 3.10(c). At peak 3360-2938 cm^{-1} assigned to –C–H– sites, 1056 cm^{-1} stretching vibration, 1252 cm^{-1} referring –C–O–C– functional sites. The peak 1600 cm^{-1} identified the aromatic vinyl conjugated ring, the peak 1732 cm^{-1} belongs to the carboxylic group (–C=C–) (Manjunath and Sailaja 2014). The carboxylic peak 1732 cm^{-1} sites did not exist in the CA modified hollow fiber membrane (Ravikumar et al. 2017). The existence of the numerous functional sites from the FTIR data supports the additive CA and CAP in the polymeric membrane matrix of PPSU.
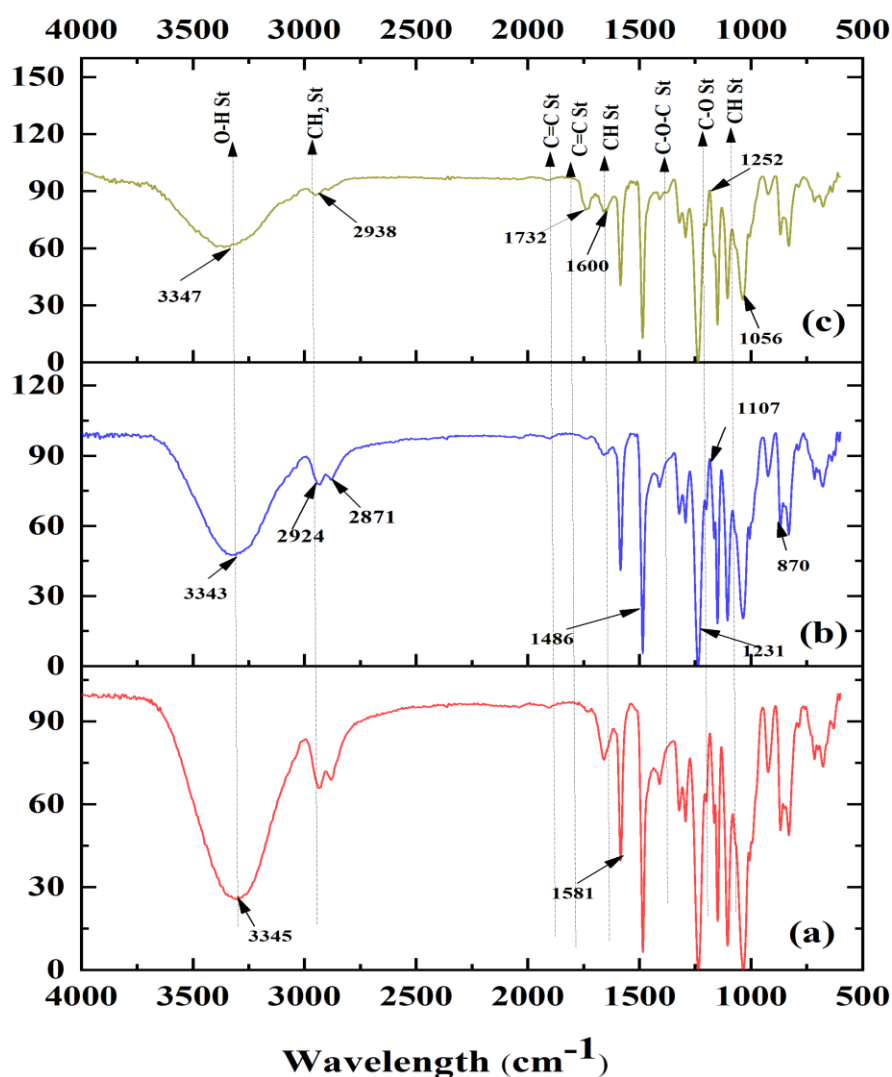
Figure 3.10 ATR- FTIR spectra of the fabricated (a) neat membrane (NM), (b) CA-5 and (c) CAP-5 hollow fiber membranes.

3.2.9 Surface potential measurement of the membrane

In Figure 3.11 x-axis represents different pH and Y-axis stands for zeta potential (in millivolts) of the best-performed membrane (CAP-5). The pH of the zeta potential measurement was adjusted as 1.5 to 9.7 with 0.1N hydrochloric (HCl) and potassium hydroxide (KOH). The results described as membrane surfaces were positively charged over pH in the range of 1.53 and negatively charged over 9.7. The increased zeta potential parameter for the tested membrane was noted as -18.75 mV, which corresponds to the pH value of 9.7. Also, arsenic-V ion species were repelled back from the negatively charged membrane surfaces at this pH level. Furthermore, the isoelectric point (IEP) from CAP-5 membrane surfaces was recorded at pH 1.9. The surface charge at IEP was recorded as zero, and surfaces of the membrane are not exhibited any membrane surface potential (Shukla et al. 2017).
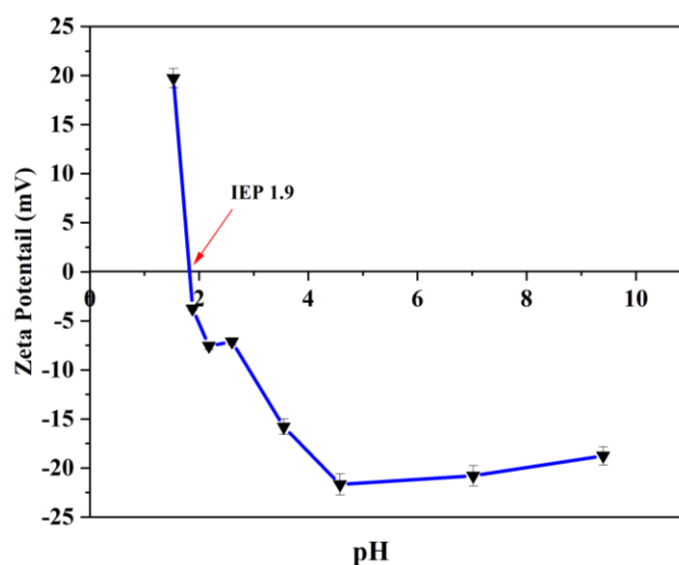
Figure 3.11 Surface potential measurement of the CAP-5 membrane.

3.2.10 Rejection of arsenic-V from prepared hollow fiber membranes

Figure 3.12(a) demonstrated arsenic-V rejection in percentage from fabricated pristine and CA/CAP modified PPSU membranes. A 1 ppm lab-prepared arsenic-V aqueous solution was exposed to filtration study using the same cross-flow filtration system. Initially, the arsenic-V solution (H_3AsO_4) was ionized with water (H_2O) to form arsenate oxide (AsO_4^{3-}) aqueous solution and illustrated in Equation 3.1. Furthermore, as used arsenic is from the stock, which is arsenate (As-V) as mentioned in the left side i.e. (H_3AsO_4) which forms a arsenate oxide (AsO_4^{3-}) after ionizing with water (shown in right side). On both sides (left and right side) of the Equation 3.1 was arsenate (As-V), the left side presented protonated and

acidic form of arsenate and right side was deprotonated and ionized form of arsenate. Due to the increased negative charge of the CAP, the membrane exhibited enhanced arsenate oxide (AsO_4^{3-}) repulsion (CAP-5, as 41%) than neat membrane (NM, as 22%) and CA modified membrane (CA-5, as 34%). Additionally, arsenic-V rejection also depends on the molecular weight cut off of the polymers used for membrane preparation. As compared to CA membranes, the CAP membranes with an increased molecular weight cut-off influences increased arsenic-V removal from CAP blended membrane (Chatterjee and De 2014). Figure 3.12(b) illustrated the arsenic-V membrane permeability for the neat membrane, CA/PPSU and CAP/PPSU modified membrane. The arsenic-V membrane permeability for nascent membrane was 40.11 L/m^{2}h bar, for CA-5 membrane as 44.42 L/m^{2}h bar and CAP-5 membrane as 47.61 L/m^{2}h bar. The hollow fiber membranes incorporated with cellulose acetate phthalate exhibited the negative potential on membrane surfaces at neutral pH, which in turn helps in the repulsion of negatively charged AsO_4^{3-}. During arsenic-V repulsion, increased permeability was observed and decreased as time increased considerably. The decline in the permeability is because of concentration polarization on the membrane surfaces. Also, after some time, the active sites are saturated and the membrane needs to be regenerated. The concentration polarization for arsenic-V removal of fabricated hollow fiber membranes was illustrated in Table 3.4.

$$\text{(acidic arsenate)} + 3\,H_2O \longrightarrow \text{(ionized arsenate)} + 3\,H_3O^+ \qquad\qquad 3.1$$
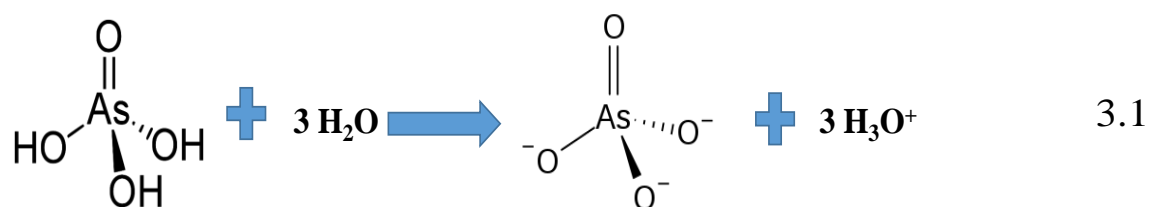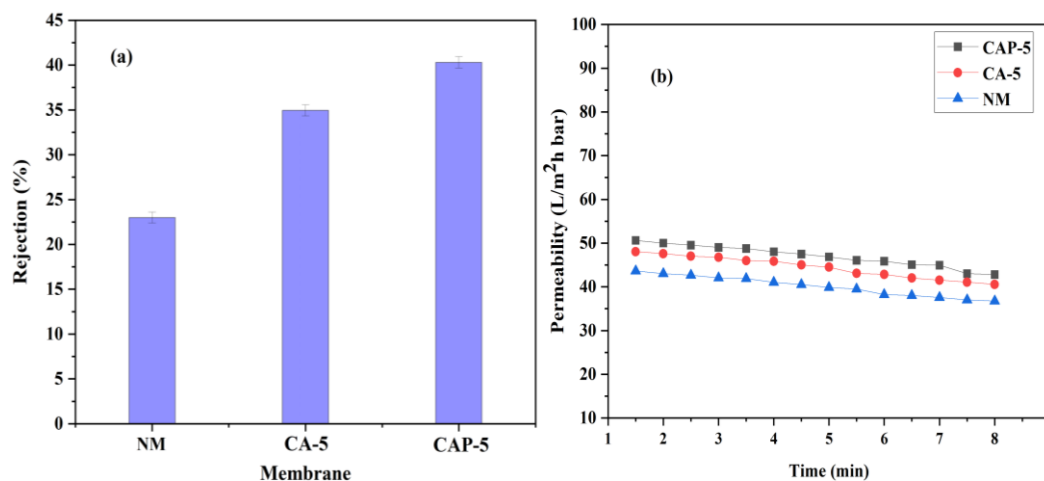
Figure 3.12 (a) Study of the percentage of arsenic-V removal from neat membrane (NM), CA-5 (5 wt% of cellulose acetate in polyphenylsufone), CAP-5 (5 wt% of cellulose acetate phthalate in polyphenylsufone) and (b) time dependent membrane permeability for arsenic-V removal from fabricated neat membrane (NM), modified membranes (CA-5 and CAP-5).

Table 3.4 Concentration polarization for arsenic-V removal of the fabricated hollow fiber membranes.

Membrane codes	Velocity (v) (m/s)	Mass transfer coefficient (K) (m/s)	Concentration polarization ($\frac{Cm}{Cb}$)
NM	0.0615	3.401×10^{-5}	1.07
CA-5	0.0538	3.039×10^{-5}	1.12
CAP-5	0.0433	2.75×10^{-5}	1.36

3.3 SUMMARY OF THE PRESENT WORK

The hollow fiber membranes of polyphenylsulfone /cellulose acetate and polyphenylsulfone /cellulose acetate phthalate were fabricated using the non-solvent induced phase separation (NIPS) method. By SEM and AFM, the morphological structure was clearly interpreted. FTIR and zeta potential measurements confirmed the presence of additives and surface potential behavior of the blended membranes. Increased pure water permeability and percentage of arsenic-V removal was witnessed from CAP membranes due to the increased hydrophilicity and repulsion between negatively charged membrane surface and negatively charged AsO_4^{3-}. The presence of polar functional groups from additives influenced the increased hydrophilicity, water uptake, water permeability and antifouling properties. The arsenic-V removal from hollow fiber membranes fabricated with 5 wt% of CAP in PPSU (CAP-5) and 5 wt% of CA in PPSU (CA-5) decontaminated 34% and 41% corresponding arsenic-V membrane permeabilities were 60.92 L/m^2h bar and 54.01 L/m^2h bar respectively. Due to the limited removal of arsenic-V, the fabricated ultrafiltration membranes are moderate for arsenic-V removal.

CHAPTER -4

REMOVAL OF TOXIC ARSENIC-V FROM AQUEOUS MEDIA USING POLYPHENYLSULFONE/CELLULOSE ACETATE AND POLYPHENYLSULFONE/CELLULOSE ACETATE PHTHALATE HOLLOW FIBER MEMBRANES CONTAINING ZIRCONIUM OXIDE

Abstract

Novel ultrafiltration hollow fiber membranes were prepared using polyphenylsulfone (PPSU) /cellulose acetate (CA) and polyphenylsulfone (PPSU) /cellulose acetate phthalate (CAP), including enhanced dosages of zirconium oxide (ZrO_2; 0.6, 1 and 1.5 wt %) by non-solvent induced phase separation (NIPS) process. Scanning electron microscopy (SEM) and atomic force microscopy (AFM) were employed to analyze the neat and ZrO_2 contained membrane's cross-section along with surface morphologies and topological structures. Transmission electron microscopy (TEM) and X-ray diffraction (XRD) were employed to determine the morphologies and crystalline structures of the nanoparticle. Membrane hydrophilicity was confirmed by determining contact angle, porosity, water uptake and pure water permeation studies. Bovine serum albumin (BSA) has been employed to assess each of the membrane's antifouling properties. Measurement of the Fourier transform infrared (FTIR) and X-ray photoelectron spectroscopy (XPS) confirmed the presence of the integrated additives (CA and CAP) and nanoparticle (ZrO_2) in the blended membranes. Using zeta potential analysis, measurement of surface potential of the best-performed membrane was carried out. The improved concentrations of ZrO_2 in the blended membranes resulted in improved arsenic-V removal. The efficient properties of arsenic-V rejection can be observed from the membranes prepared by 1 wt % of ZrO_2 in PPSU/CA (PZCA-1) and 0.6 wt % of ZrO_2 in PPSU/CAP (PZCAP-0.6) were proven to be effective for arsenic-V removal (i.e. PZCA-1 as 87.24 % and PZCAP-0.6 as 70.48 % and arsenic-V permeability of 89.94 L/m^2h bar and 70.59 L/m^2h bar respectively) using 1 ppm of standard arsenic-V solution in a pH range of 6.8±0.2. Moreover, arsenic-V rejection tendency was observed to be decreased with excess dosages of ZrO_2 due to agglomerations of nanoparticles on membrane surfaces.

4.1 INTRODUCTION

In recent decades, the world's ever-growing population has generated tremendous demand for pure drinking water. Nevertheless, the fundamental contemplations for pollution of drinking water in the ecosystem are rapid industrialization and urbanization. The untreated and uncontrolled release of wastewater from industries includes different metalloids and heavy metals such as arsenic (Li et al. 2018; Sadeghfam et al. 2021). Arsenic poisoning of groundwater, as well as its consumption through the food chain, results in social disorders, health risks, and socioeconomic disintegration. Arsenic contamination is considered to be geogenic, with arsenic being released from soil under conditions that allow it to dissolve from the solid phase on soil grains to the liquid phase in water, with fertilizer residues perhaps

playing a moderating effect in its further amplification. Exposure to drinking water containing arsenic results in severe health-related issues. Acute or short-term exposure to arsenic may cause extreme throat dryness, diarrhea, severe headache, nausea, tingling of foot and hand, jaundice, weakens of the nervous system and erythema. In addition, long-term or chronic arsenic toxicity also leads to significant human health cancer-related risks such as lung, bladder, kidney, darkening of the skin, abdominal pain, diabetes, numbness, cardiovascular diseases and so on (Sharma et al. 2021; Wan et al. 2020). In its review of these safety-related issues, the World health organization (WHO) has mentioned that, arsenic is a Class-I carcinogenic to human health. Despite the huge advances made in decreasing arsenic exposure to human health, WHO concluded that among 70 countries, more than 200 million populations are suffering from arsenic-related health problems. Among countries affected by arsenic issues, Bangladesh and Bengal basin in West Bengal, India have suffered increased arsenic-connected symptoms. Hence, the United states environmental protection agency (USEPA) has set 10 µg/l as a higher level of arsenic contamination in the drinking water (Ociński et al. 2016; Sheikhi et al. 2021).

Many industries worldwide are still facing a problem for effective arsenic removal due to no significant improvements in conventional methods such as coagulation, flocculation, ion exchange, precipitation and adsorption. Nevertheless, these methods are costly, high production of sludge, ionic competition and the used adsorbents need regeneration. The membrane filtration method is an innovative, versatile technique for removing low molecular weight compounds such as heavy metal ions or compounds (Wang et al. 2014; Zeng et al. 2020). The key benefits of the membrane-based filtration systems are no phase transitions during the separation of ions, less energy consumption, increased efficiency, simple operation and high filtration performances. Generally, in membrane filtration, reverse osmosis, ultrafiltration and nanofiltration were used for the rejection of arsenic from aqueous arsenic solution (Mondal et al. 2017; Worou et al. 2021). Nonetheless, these methods have demonstrated less removal of arsenic, as they have their constraints in the arsenic- separation from arsenic-contaminated drinking water. Ultrafiltration is, a modern filtration process to provide efficient filtration performance in terms of increased permeability with efficient arsenic rejection, less tendency towards fouling and inexpensive (Kumar et al. 2019).

Polyphenylsulfone (PPSU) is a versatile polymer for membrane fabrication due to its high chemical and thermal stability, increased resistance to heat, stability of hydrolysis, excellent mechanical properties, and easy handling. Unfavorably, neat PPSU based

membranes are more vulnerable to fouling due to their hydrophobic nature and it offers less water permeability (Darvishmanesh et al. 2011). Fouling is one of the crucial issues related to membrane filtration. Generally, the accumulation or adsorption of the foulants on the membrane pores leads to a decrease in water permeability, an improvement in the reversible fouling that greatly restricts membrane filtration efficacy and lifetime of the membrane. Subsequently, the hollow fiber membranes were washed by chemicals or backwashing processes for a daily period, which reduces operational costs and the membrane lifespan (Ibrahim et al. 2018). Additionally, the PPSU ultrafiltration membrane pore size is larger than the arsenic ions. For modifications of the membrane surfaces, metal complexing functional groups such as $-CO_2H$ and $-NH_2$ are to be introduced.

Many researchers have exhibited surface modifying adsorbents such as alumina, zirconium oxide, clay-like compounds, zeolite and manganese-based sorbents to modify the membrane surfaces and enhance hydrophilic and rejection properties of the prepared membranes. The zirconium-based sorbent (ZrO_2) has gained more interest among the adsorbents listed above due to its advantages over other adsorbents such as non-toxic, cost-effective, more hydrated, and highly hydrated soluble. ZrO_2 is more stable than titanium oxide and aluminum oxide and has a strong affinity to the arsenic species (Fausey et al. 2019; Yu et al. 2019).

Genne et al. (1996) fabricated mixed matrix ultrafiltration membranes by polysulfone and incremental concentrations of the ZrO_2 by non-solvent induced phase separation (NIPS) process. The effect of enhanced dosages of the nanoparticle on the PSf membranes has been well described. The membranes revealed enhanced hydrophilicity and improved porosity as well as pure water permeability parameters. The improved dextran rejection properties were attributed to the intensified dosages of ZrO_2 to PSf dope solution.

Bottino et al. (2002) fabricated n-methyl-2 pyrrolidone (NMP) and triethyl phosphate (TEP) composite membranes with polyvinylidene fluoride (PVDF) as a base polymer and ZrO_2 as nano additive. Compared to PVDF/ZrO_2/TEP, the membranes prepared using PVDF/ZrO_2/NMP demonstrated increased porosity. The PVDF/ZrO_2/NMP membranes demonstrated the increased flux with the decreased rejection properties.

Zhang et al. (2006) used acrylonitrile-methacrylate-sodium sulfonate acrylate (AN-MA-SSA) as a copolymer and ZrO_2 as an inorganic additive by phase inversion technique. The objective of the present analysis was to develop acrylonitrile (AN) based copolymer

membranes by gradual dosages of the ZrO_2 nanoparticle. The ZrO_2 concentrations in the PAN membranes intensified overall porosity, pure water flux, hydrophilicity and improved bovine serum albumin (BSA) removal.

Aerts et al. (2006) developed the polysulfone and sintered zirconium oxide (ZrO_2) mixed matrix membranes by immersion precipitation method. The migration of the used nanoparticle on the blended membrane surfaces was confirmed using XPS, SEM and porosity measurement. The increased ZrO_2 nanoparticle dosages enhanced the porosity on the membrane surfaces. From SEM images, intensified dosages of ZrO_2 revealed enhancement of macrovoids in the sublayer.

Zheng et al. (2011) fabricated flat sheet membranes by polyvinylidene fluoride (PVDF) and ZrO_2 using the NIPS process. The membranes have been characterized by studying SEM, AFM, water uptake and arsenic rejection properties. The ZrO_2 blended membranes exhibited drastic improvement in surface roughness and expanded finger-like projections. The FTIR and XPS studies revealed the presence of nanoparticles in the blended membranes. The improved arsenic adsorption was noticed with the intensified dosages of ZrO_2.

He et al. (2014) developed polysulfone (PSf) hollow fiber membranes with incremental dosages of ZrO_2 nanoparticles by the non-solvent induced phase separation (NIPS) method. The main objective of the present work was to improve the hydrophilicity, pure water flux and arsenic uptake capacity of the PSf membrane by improved concentrations of ZrO_2. The modified membranes exhibited the expanded finger-like structure and the spongy structure from SEM images. There is an improved flux along with arsenic rejection properties as the content of ZrO_2 increases in the PSf dope solution.

Zhao et al. (2016) prepared the flat sheet membranes using PVDF as base polymer and the improved concentration of novel ZrO_2/polyvinyl alcohol (PVA) to remove organic arsenic from drinking water. The adsorption of the arsenic was observed to be improved with the increased pH of an aqueous solution. Furthermore, the hydrophilic ZrO_2/PVA content in the PVDF improved hydrophilicity and pure water permeability. Also, the increased nanoparticle dosages improved adsorptive properties, resulting in enhanced arsenic uptake from the arsenic-contaminated aqueous solution.

Sigwadi et al. (2019) fabricated Nafion membranes by intensifying ZrO_2-carbon nanotube (CNT) nanoparticle concentrations. The objectives of the study were to interpret the influence

of nanoparticles on the membrane in terms of the surface hydrophilic properties, morphology, AFM, thermal and mechanical properties. The ZrO_2-CNT contained membranes exhibited improved properties and porous membrane structure. Increased dosages improved the surface roughness of the membrane.

Obaid et al. (2020) developed nanocomposite membranes using PSf- ZrO_2 nanofibers (NFs) by the non-solvent induced phase separation process as-fabricated ZrO_2 modified nanocomposite membranes exhibited superior mechanical strength, a high degree of hydrophilicity, a large pore size and high pure water permeability without compromising the selectivity. The morphology of nanocomposite membranes was altered by ZrO_2 NFs, which modified the finger-like morphology of the pristine membrane to more finger-like macrovoids morphology. With the enhancement of the flux recovery ratio (FRR) and decreased irreversible fouling (R_{ir}) the ZrO_2 contained PSf membranes exhibited increased antifouling properties.

However, neat ZrO_2 membranes are susceptible to the absence of various functional groups such as amine ($-NH_2$) and carboxylic ($-COOH$), which are extremely important for arsenic ions rejection (He et al. 2014; Shih 2005). Different dosages of hydrophilic additives prepared hollow fiber membranes to manage the above needful. Versatile hydrophilic bio-sorbents were chosen in the present research, such as cellulose acetate derivatives (cellulose acetate and cellulose acetate phthalate), rich in hydroxyl, amine and carboxylic functional groups.

Liu et al. (2017) developed mixed matrix membranes by zwitterion and cellulose acetate by the NIPS method. In the current experimental results, cellulose acetate derivatives provide enhanced features than other additives in terms of their high hydrophilicity, less tendency towards fouling, cost-effectiveness and bio-compatibility.

In overviewing the literature, no any research work was documented related to ZrO_2 incorporated polyphenylsulfone and cellulose acetate derivatives hollow fiber membranes for the decontamination of arsenic-V from aqueous solution. To satisfy as mentioned research gap, it was planned to prepare hollow fiber membranes using incremental dosages of ZrO_2 along with cellulose acetate /polyphenylsulfone and cellulose acetate phthalate /polyphenylsulfone by non-solvent induced phase separation method (NIPS) (Ibrahim et al. 2017; Nayak et al. 2017). The impact of polymer blending ratio on morphologies and membrane performance was thoroughly investigated. The blended pristine and ZrO_2

membranes surface and cross-section structural morphologies were analyzed using SEM and topographical configuration by AFM analysis. TGA investigated the thermal stability of the membranes. FTIR and XPS studies confirmed the presence of the nanoparticle (ZrO_2), CA and CAP in the blended membranes. The zeta potential analysis was carried out to measure the surface charge of the membranes. In addition, water uptake, pure water permeability, contact angle measurement and fouling analysis were investigated for the performance of the hollow fiber membranes. Additionally, the removal of AsO_4^{3-} from prepared hollow fiber membranes was also performed. Finally, TEM and XRD characterization was carried out for ZrO_2 nanoparticles.

4.2 RESULTS AND DISCUSSION

4.2.1 Morphological studies of prepared hollow fiber membranes

Figure 4.1 and Figure 4.2 demonstrated the cross-section and surface morphologies of scanning electron microscopy (SEM) images of the fabricated neat and ZrO_2 contained hollow fiber membranes. From Figure 4.1, as fabricated, hollow fiber membranes revealed asymmetric structure with the finger-like projection on either side, which is sandwiched by a thin layer of the sponge-like structure. The neat membrane contains the less dense top layer and the porous-like sublayer (Shukla et al. 2017). Also, the neat membranes have less porous structure i.e., micropores on the surfaces of the membranes. The microporous structure in the neat membrane in turn expanded as the incremental dosages (0.6, 1 and 1.5 wt %) of ZrO_2 to the PPSU neat dope solution. The steep finger-like projections of neat membranes become bulged as the nanoparticle (ZrO_2) concentrations were increased in the neat dope solution.

Furthermore, from Figure 4.3(e) − (h), the migration of the increased dosages of nanoparticles (ZrO_2) onto the membrane surfaces results in the enhancement of surface roughness of the membrane. However, from Figure 4.3(a) − (d), the homogeneous dispersion of the used additives (CA and CAP) and nanoparticle (ZrO_2) resulted in less agglomerated membrane surfaces. From Figure 4.3, the surfaces of the CAP hollow fiber membranes contain a more porous structure because CAP behaves as a better pore former than CA membranes (Kumar et al. 2019). The improved porous structure of the CAP further facilitated the improvement in membrane overall porosity, water uptake, pure water permeabilities and increased arsenic-V removal properties (Kumar et al. 2020). The outer/inner diameter and mean pore radius of the hollow fiber membranes were illustrated in Table 4.1. The detailed SEM complete view of fabricated hollow fiber membranes was illustrated Figure 4.2.
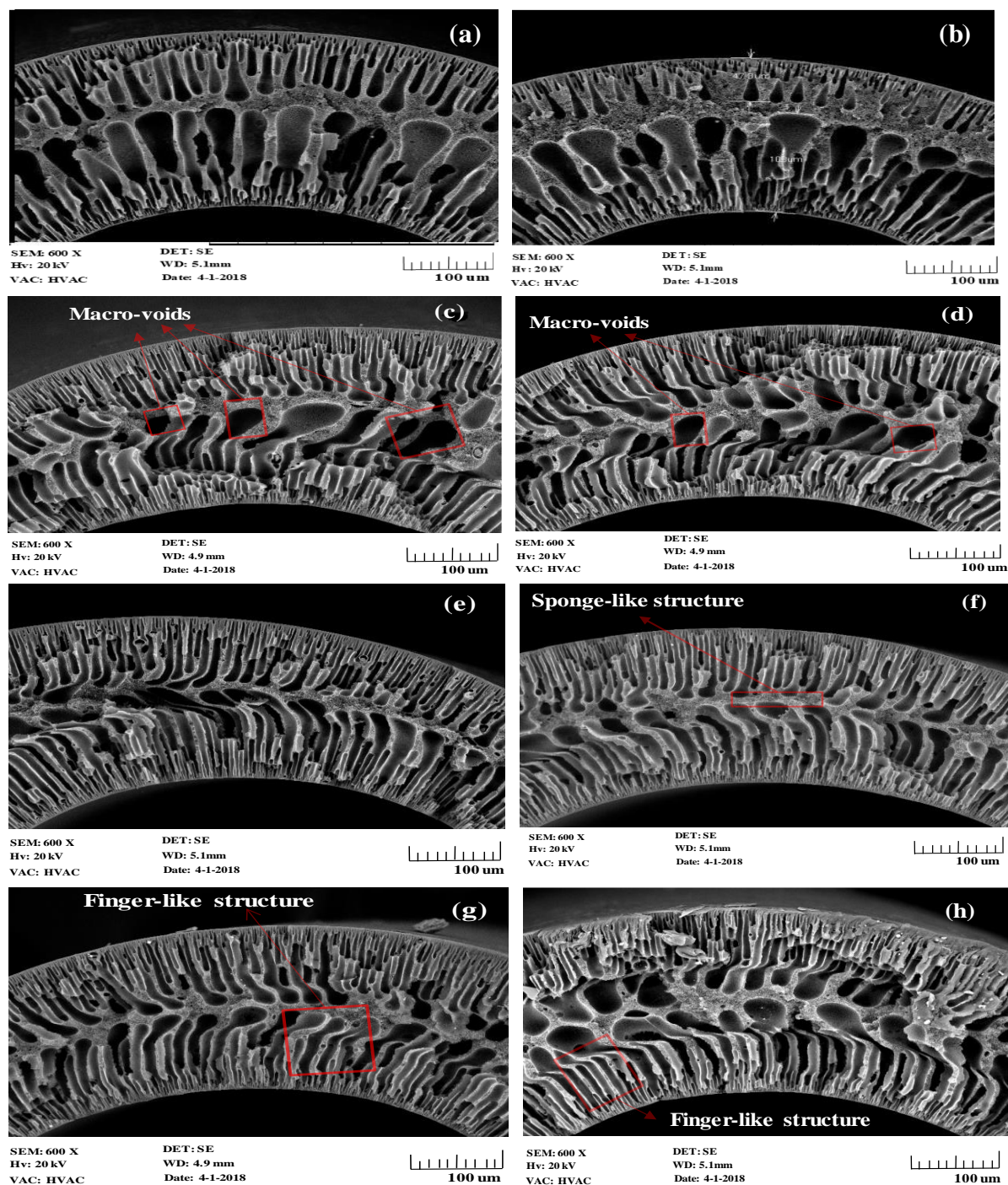
Figure 4.1 Cross-sectional scanning electron microscope (SEM) images of neat membranes PZCA-0 and PZCAP-0 as (a and b). Followed by the enhanced dosages (0.6, 1 and 1.5 wt %) of ZrO_2 in PZCA-0 as PZCA-0.6, PZCA-1 and PZCA-1.5 as (c, e, and g). ZrO_2 dosages in the PZCAP-0 as PZCAP-0.6, PZCAP-1 and PZCAP-1.5 as (d, f and h) respectively.
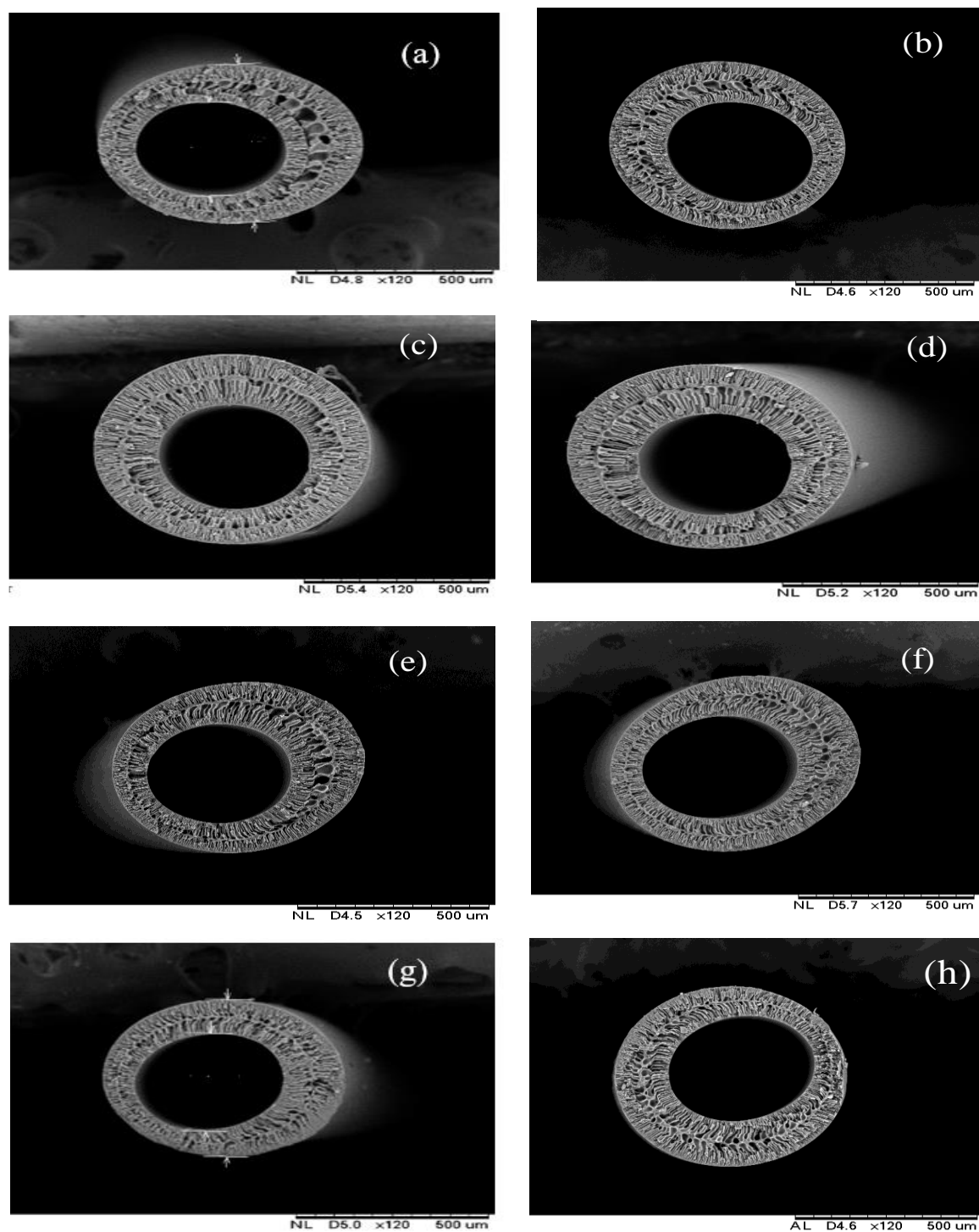
Figure 4.2 Cross-sectional (complete view) SEM images of the neat membranes PZCA-0 and PZCAP-0 as (a and b). Followed by the enhanced dosages (0.6, 1 and 1.5 wt %) of ZrO_2 in PZCA-0 as PZCA-0.6, PZCA-1 and PZCA-1.5 as (c, e, and g). ZrO_2 dosages in the PZCAP-0 as PZCAP-0.6, PZCAP-1 and PZCAP-1.5 as (d, f and h) respectively.
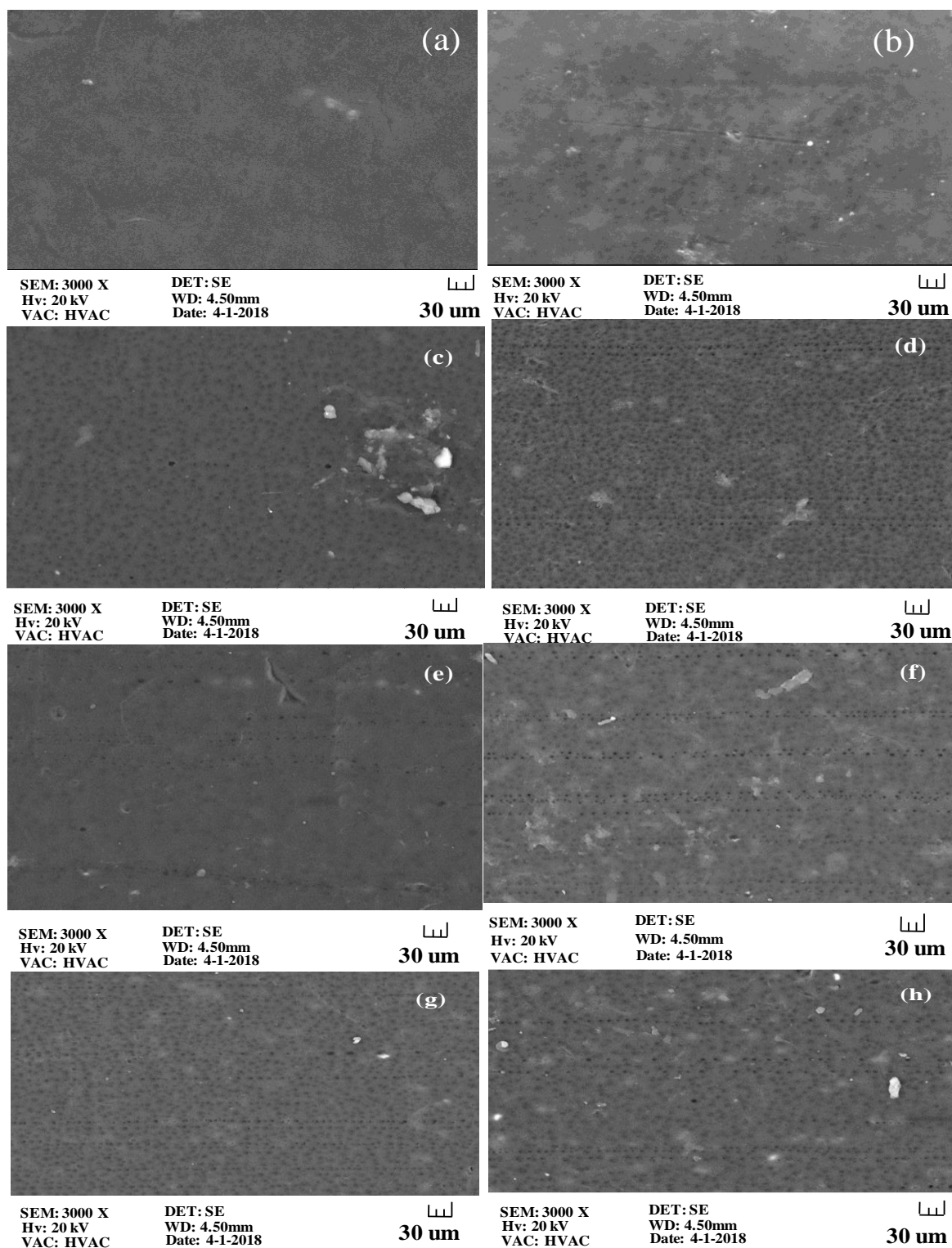
Figure 4.3 SEM surface images of the prepared neat membranes PZCA-0 and PZCAP-0 as (a and b) and ZrO$_2$ modified membranes as PZCA-0.6, PZCA-1, PZCA-1.5 as (c, e, g) and PZCAP-0.6, PZCAP-1, PZCAP-1.5 as (d, f, h) respectively.

Table 4.1 Outer/ inner (OD/ID) diameter and mean pore radius of the hollow fiber membranes

Hollow fiber membranes	Outer diameter (OD in µm)	Inner diameter (ID in µm)	Mean pore radius (m)
PZCA-0	815	486	1.315×10^{-7}
PZCA-0.6	652	385	8.322×10^{-8}
PZCA-1	649	381	8.616×10^{-8}
PZCA-1.5	615	383	8.242×10^{-8}
PZCAP-0	710	405	1.349×10^{-7}
PZCAP-0.6	651	382	2.319×10^{-8}
PZCAP-1	686	396	6.699×10^{-8}
PZCAP-1.5	693	398	6.009×10^{-8}
Spinneret dimension, inner diameter: 550 µm, outer diameter:1100 µm			

4.2.2 Contact angle measurement

Figure 4.4 illustrates the hydrophobic/hydrophilic performances of the fabricated neat and ZrO_2 contained hollow fiber membranes. From the figure, the neat membrane with less porous and hydrophobic nature exhibited higher parameters of contact angle. The neat membranes revealed the increased parameters of contact angle for PZCA-0 and PZCAP-0 as 83.86° and 77.12° respectively. The gradually increased concentrations of ZrO_2 in the neat dope solution decrease parameters of contact angle. Increased ZrO_2 concentrated membranes PZCA-1.5 and PZCAP-1.5 revealed the contact angle parameters as 50.18° and 48.95° respectively. The intensified ZrO_2 concentrations (0.6, 1.0 and 1.5 wt%) in the neat PPSU/CA and PPSU/CAP dope solution improve the hydrophilicity of the membranes. Also, various hydrophilic functional groups such as –O, –OH and –CH on the membranes surfaces facilitate the enhanced affinity for water to the metal adsorbent (Sivakumar et al. 2005).
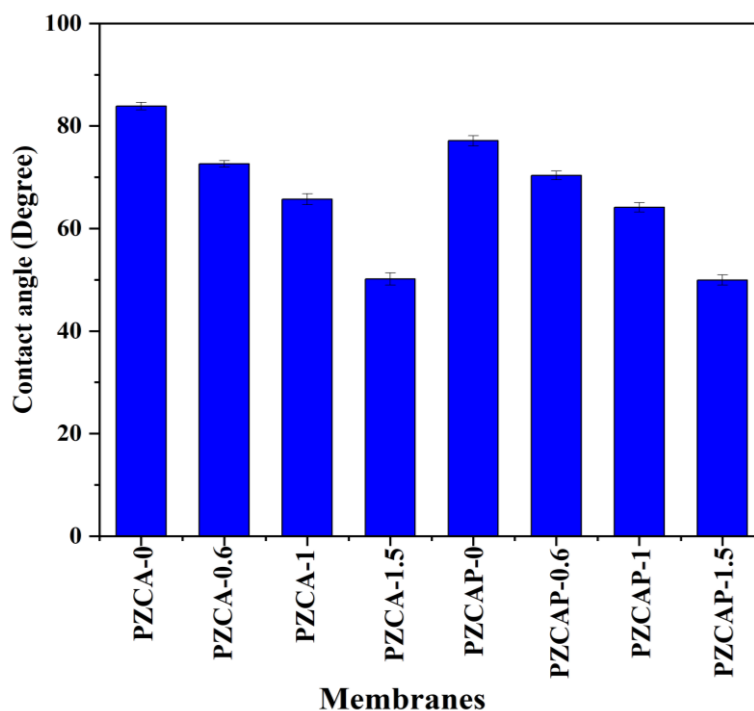
Figure 4.4 Contact angle measurement of the fabricated hollow fiber membranes.

4.2.3 Study of percentage porosity and water uptake measurement

Figure 4.5 demonstrated the porosity and water uptake outcome from the fabricated membranes. Hydrophilic membrane functional groups on membrane surfaces affect the properties of the prepared membranes in terms of water uptake and porosity respectively. From Figure 4.5 the porosity for the neat membrane PZCA-0 was 22.41% and PZCAP-0 was 25.20% respectively. The intensified dosages of the ZrO_2 in the neat dope solution, PZCA-1.5 and PZCAP-1.5 were 71.24% and 51.23% respectively. The improved percentage porosity of the membrane was due to the following reasons. Firstly, the thermal instability on the membrane surfaces is due to the intensified dosages, leading to a rapid demixing of the solvent in the coagulation bath (Sajitha and Mohan 2005). Secondly, the small amount of leaching of the ZrO_2 in rapid demixing of the solvent in the non-solvent coagulation bath leads to the porosity on the membranes surfaces (Genne et al. 1996). From Figure 4.5, the water uptake parameter for neat membrane PZCA-0 was 54.21% and PZCAP-0 was 54.60% respectively. The enhanced dosages of ZrO_2 contained membranes PZCA-1.5 was 72.26% and PZCAP-1.5 was 82.42% respectively. The enhancement of porosity and water uptake parameters further indicated increased membrane's hydrophilic property. Finally, amine and carboxylic functional groups on the CAP membranes exhibited the increased water uptake and porosity of the hollow fiber membranes (Kumar et al. 2019).
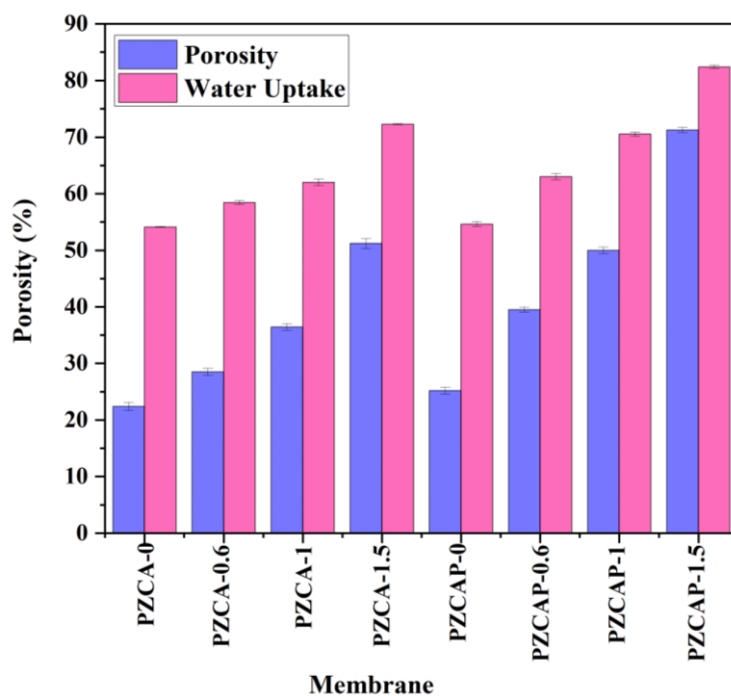
Figure 4.5 Porosity and water uptake of the prepared neat and ZrO_2 incorporated PPSU/CA and PPSU/CAP modified hollow fiber membranes.

4.2.4 Pure water permeability (PWP) of fabricated membranes

Figure 4.6(a)–(b) illustrated the water permeability of the prepared pristine and zirconium oxide immobilized PPSU/CA and PPSU/CAP hollow fiber membranes. Due to more hydrophobic and less porous structures, the neat membrane exhibited the least parameter of water permeability for PZCA-0 was 48.36 L/m^{2}h bar and PZCAP-0 was 61.28 L/m^{2}h bar. The increased parameter of the water permeability was evidenced from membranes PZCA-0.6 was 84.05 L/m^{2}h bar and PZCAP-0.6 was 100.96 L/m^{2}h bar. The enhanced permeability parameter was evidenced due to the presence of a huge amount of oxygen (–O–) from ZrO_2 nanoparticles in the PPSU/CA and PPSU/CAP dope solution that creates an affinity for hydrogen bonding in the PPSU casting solution (Thuyavan et al. 2014). The pure water permeability property of the membrane also depends on the parameter of hydrophilicity and porosity. From the figure, the increased dosages of nanoparticle influence increased the hydrophilicity by enhancing the membrane porosity and water uptake. Fabricated CAP membranes exhibited improved water permeability as it acts as better pore former (Rahimpour and Madaeni 2007). It was evidenced from SEM images; cellulose acetate membranes have less porosity.
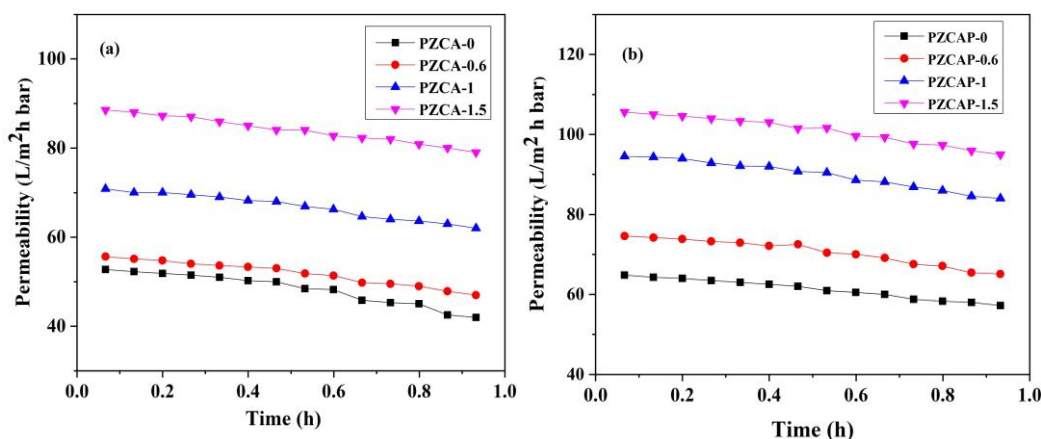
Figure 4.6 Pure water permeability of the prepared (a) PPSU/ZrO$_2$/CA and (b) PPSU/ZrO$_2$/CAP hollow fiber membranes.

4.2.5 Antifouling properties of the fabricated hollow fiber membranes

Figure 4.7 shows the antifouling study of the fabricated hollow fiber membranes, which includes three stages: pure water permeability, BSA permeability and water permeability, later washing with the water. The behavior of fouling from the prepared hollow fiber membranes hinders the durability performance of the membrane and finally reduces the efficiency (Liu et al. 2017; Lv et al. 2017). From the figures, the neat membrane exhibited the decreased parameter of pure water permeability in all the three stages due to its high hydrophobicity and less porous structural features. There is an improved BSA permeability parameters exhibited from modified hollow fiber membrane due to increased adsorption and hydrophilicity of the membrane surface (Arockiasamy et al. 2017; Lv et al. 2017). The augmented FRR parameter for the membranes PZCA-1.5 and PZCAP-1.5 were 79.01% and 81.94% respectively, due to the polar functional groups such as carboxylic, hydroxyl and oxygen functional groups from the nanoparticle and additives on the membrane surfaces. The enhancement of the FRR value further indicated better hydraulic cleaning from the membrane (Hebbar et al. 2014; Rahimpour and Madaeni 2007). Furthermore, from figure 4.8(a) and 4.8(b) the other parameter, such as reversible fouling (R_r) and total fouling (R_t) for neat membranes PZCA-0 and PZCAP-0 were 42.20% and 74.71% respectively. The modified membranes increased 'R_r' and 'R_t' parameter to 55.07% and 76.99% respectively for PZCA-1.5. In addition, the decreased 'R_{ir}' parameter of modified membranes were 20.98% and 18.08% for PZCA-1.5 and PZCAP-1.5 respectively, compared to neat membrane R_{ir} value of 32.50%. In conclusion, the increased parameter of the R_r and R_t and reduced parameter of R_{ir} exhibited good antifouling behavior of the membrane. The lesser parameter of the R_{ir}

exhibited the improved reversible cleaning of the modified membrane (Kumar et al. 2019; Pereira et al. 2014).
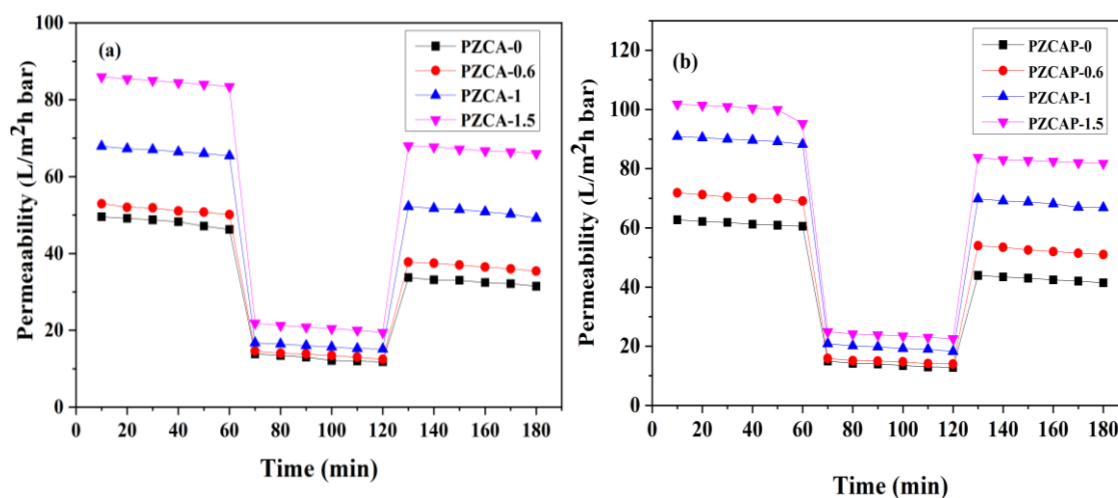
Figure 4.7 Antifouling permeability properties of fabricated neat and ZrO_2 contained PPSU membranes for (a) the cellulose acetate (b) the cellulose acetate phthalate hollow fiber membranes.
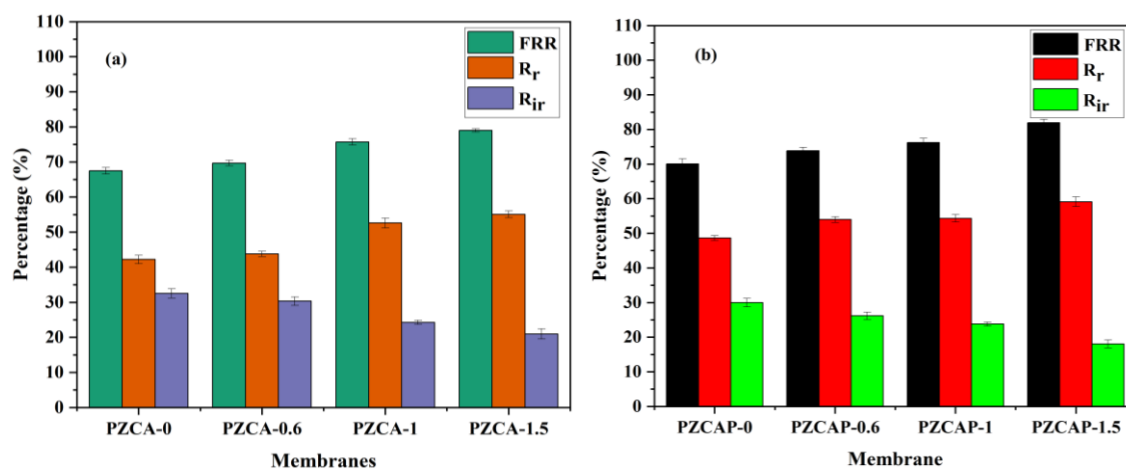
Figure 4.8 Antifouling properties such as flux recovery ratio (FRR), reversible fouling (R_r) and irreversible fouling (R_{ir}) of the neat membrane, along with (a) ZrO_2 modified CA/PPSU membranes and (b) ZrO_2 contained CAP/PPSU hollow fiber membranes.

4.2.6 Topography images of the membranes

Figure 4.9 demonstrated 3-dimensional topological surface roughness pictures of the fabricated pristine and modified hollow fiber membranes. The tapping mode of the atomic force microscopy for analyzing the surface topology was explained in the literature (Hebbar et al. 2018a). Generally, the surface roughness parameter (R_a) was considered to study the

88

membrane surfaces roughness (Kumar et al. 2019b). In this analysis, the value 'R$_a$' for neat membrane was found to be 22.51 nm and 27.26 nm for PZCA-0 and PZCAP-0 respectively. As ZrO$_2$ concentration increased in the dope solution, the membrane surface roughness parameter was improved (Zheng et al. 2011). From Table 4.2, the 'R$_a$' value for PZCA-1.5 and PZCAP-1.5 was 49.75 nm and 53.62 nm respectively. The SEM pictures also promise the enhancement of the porosity from the modified blended membranes. Also, from Figure 4.9(g)–(h) the nodular configuration was evidenced as the enhanced ZrO$_2$ concentrations in neat dope solutions.

Table 4.2 Surface roughness properties of fabricated hollow fiber membranes

Membranes code	R$_{max}$	R$_z$ (nm)	R$_a$ (nm)	R$_q$ (nm)
PZCA-0	203	8.26	22.51	29.62
PZCA-0.6	264	11.42	27.26	35.01
PZCA-1	324	19.52	39.48	49.54
PZCA-1.5	456	26.02	49.75	63.16
PZCAP-0	252	12.53	26.35	39.31
PZCAP-0.6	310	15.20	37.01	46.35
PZCAP-1	372	27.78	45.20	58.40
PZCAP-1.5	508	34.56	53.62	65.21
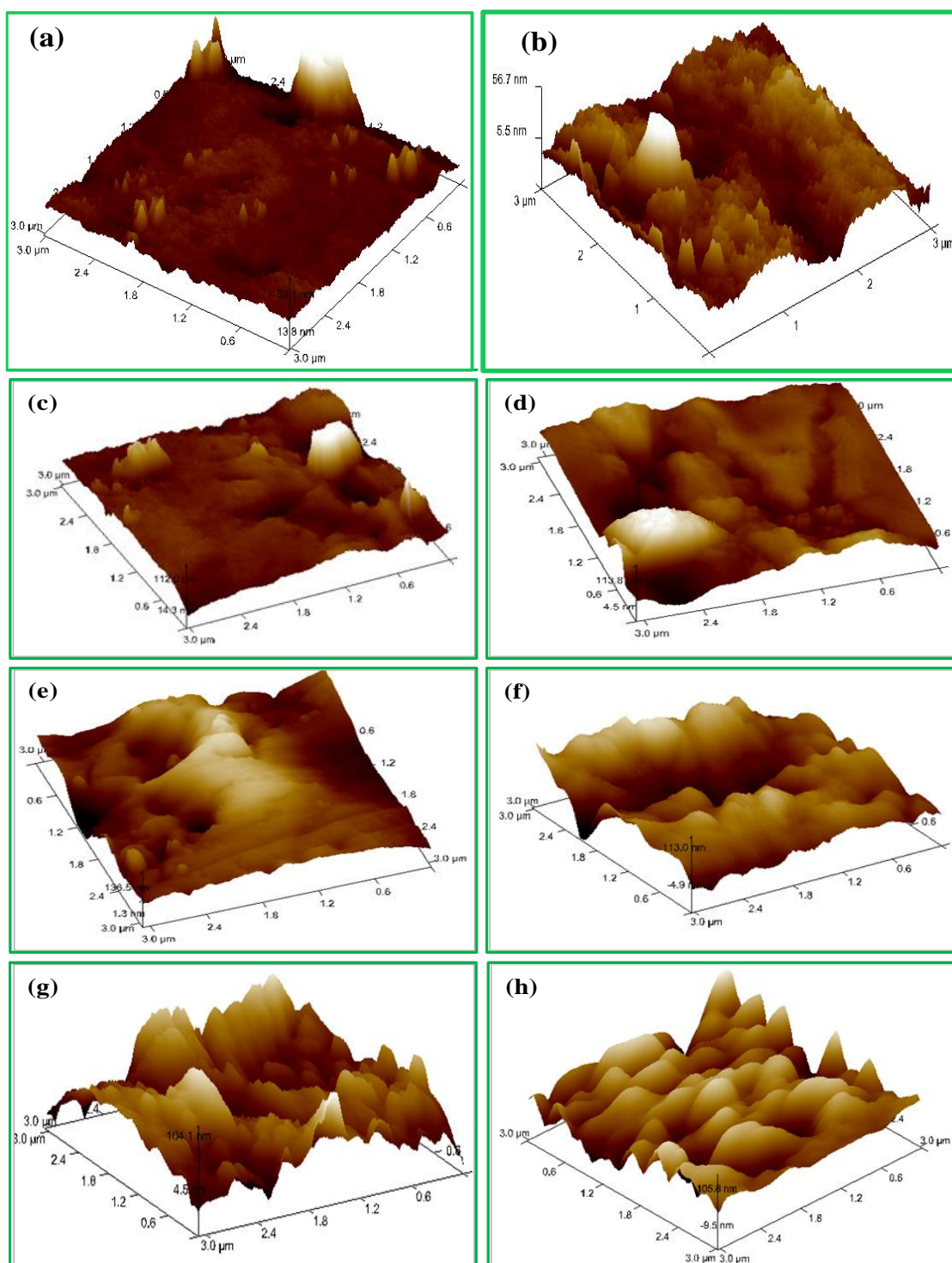
Figure 4.9 3- dimensional membranes topological images of the neat membrane PZCA-0 and PZCAP-0 (a and b) and increased dosages of ZrO_2 in cellulose acetate membranes (0.6 wt% of ZrO_2 in PPSU/CA) PZCA-0.6, PZCA-1 and PZCA-1.5 as (c, e and g) and cellulose acetate phthalate (0.6 wt% of ZrO_2 in PPSU/CAP) PZCAP-0.6 membranes, PZCAP-1 and PZCAP-1.5 as (d, f and f) respectively.

4.2.7 Attenuated total reflectance-Fourier transform infrared spectroscopy (ATR-FTIR)

Figure 4.10 illustrated the ATR-FTIR spectra for prepared neat hollow fiber membranes (PZCA-0 and PZCAP-0) and ZrO_2 contained membranes (PZCA-1 and PZCAP-0.6). From Figure 4.10(a) PZCA-0 membrane mainly attributed to the following functional groups as –CH_2 (alkane group), –OH (stretching), –C=O (carbonyl), O=C–OR (alkyl), and –C–O– (cyclic ether functional group), attributed to the peaks related to 2833.25-2932.12 cm^{-1}, 3324.32 cm^{-1}, 1584.1653.23 cm^{-1}, 1484.25 cm^{-1} and 1233.40 cm^{-1} respectively. The peak at 1103.12 cm^{-1} attributed to the –C–O–C– functional group of stretching vibration. The –C–H stretching vibration was assigned at the peak of 870 cm^{-1}. From the membrane PZCAP-0, Figure 4.10(b) the peak 2835.42 –2937.12 cm^{-1} assigned to CH_2 group which is methyl symmetric stretching functional group –C–H. The peak 3360 cm^{-1} attributed to –OH vibrational stretching. The carbonyl functional group (–C=O) was attributed to the peak at 1740 cm^{-1}. The cyclic ether group of CAP was assigned at the peak of 1237 cm^{-1}. The –C–H– vibrational stretching at the peak of 868 cm^{-1}, in addition the vinyl aromatic conjugated group was assigned at the peak of 1600 cm^{-1} respectively (Kumar et al. 2019b; Manjunath and Sailaja 2014b).

In a similar way from the Figure 4.10(c) the functional group of membrane PZCA-1, the peak of 3419.33 cm^{-1} was assigned to –OH stretching cellulose vibration, 2918.76 cm^{-1} attributed to the CH_2 functional group. The group of –Zr–O–C– was assigned at the peak of 1579.13 cm^{-1}. The stretching vibrational methyl functional group (CH_3) at peak appeared at 1485.85 cm^{-1}. The –C–O–C functional group was assigned to the peak of 1104.48-1147.48 cm^{-1} respectively. From the Figure 4.10(d), membrane PZCAP-0.6 functional groups are, –CH_2 group at a peak of 2926.66 cm^{-1}. The peak at 1582.92 cm^{-1} ascribed to –Zr–O–C which was coupled to the –C–O–. The peak at 1640.88 cm^{-1} is attributed to the –OH bending vibration. The peak at 1104.06-1149.86 cm^{-1} was assigned to the –C–O–C–, stretching vibration. Therefore, the existence of the –Zr–O–C– groups attributed on to the ZrO_2 containing membranes as PZCA-1 and PZCAP-0.6 confirmed the proper blending mixture of ZrO_2 along with CA and CAP in the PPSU dope solution (Maximous et al. 2010; Zheng et al. 2011).
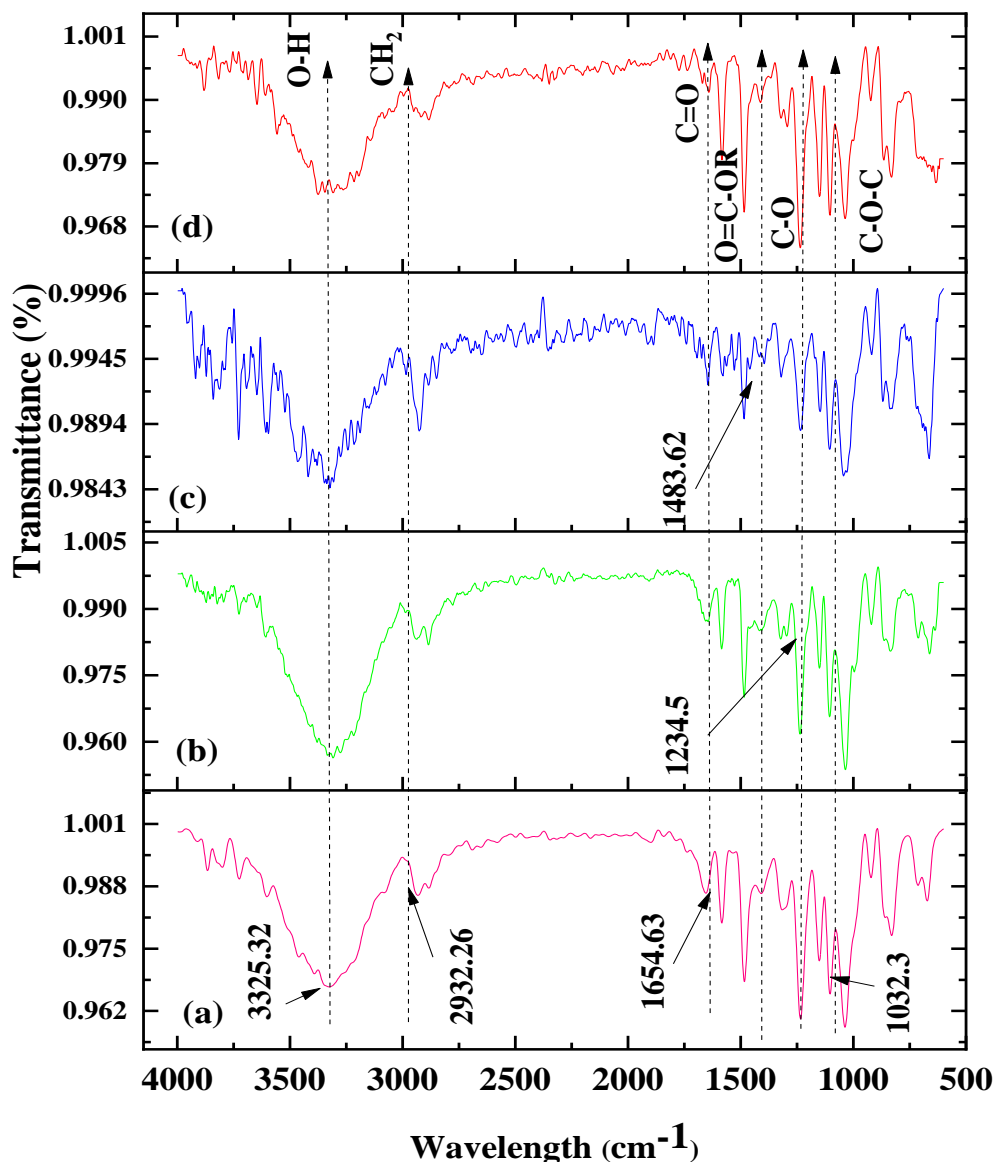
Figure 4.10 Fourier transform infrared spectra of the neat membrane (a) PZCA-0 (b) PZCAP-0 (c) PZCA-1.0 and (d) PZCAP-0.6 hollow fiber membranes.

4.2.8 Zeta potential of the membrane

The best performing membrane PZCA-1 surface potential measurement was performed by illustrating pH and surface potential on the X- and Y- axis, respectively, as shown in Figure 4.11. From pH 2.5 to 8.0, the membrane surface was negatively charged. The increased zeta potential -28.13 mV was recorded at neutral pH (pH 7). The other pH parameter, at pH 8.09, the surface potential recorded as -28.19 mV. In addition, the reduced zeta potential of -14.49 mV was noted at pH 4.88. The negative parameter of the surface potential was also observed at pH 3.58 as -8.06. The higher positive surface potential of 0.43 mV was recorded at pH 2.46. The membrane surfaces became more negatively charged with

increased pH value and hence the negatively charged arsenate oxide (AsO_4^{3-}) was repelled (Lohokare et al. 2008). Due to the de-protonation of cellulose acetate, the hydrophilic functional group as $-CO_2H$ and $-OH$ imposes a negative charge to the ZrO_2 contained membrane surface. The membrane isoelectric point was noted at pH 2.53. At this pH, no surface potential was observed. The negative membrane surface potential enables the enhancement of the hydrophilicity and repulsion properties (Gupta et al. 2013; Luo et al. 2013).
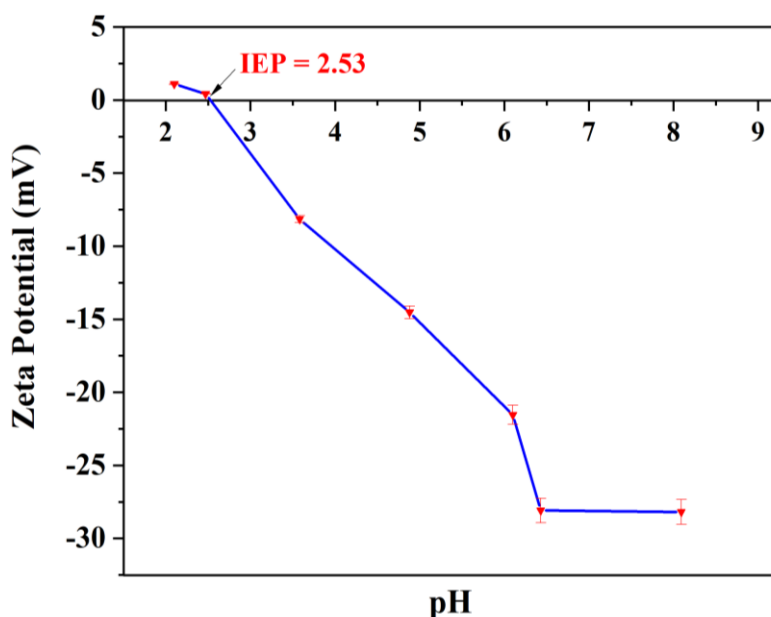
Figure 4.11 Surface potential (Zeta potential) measurement of the membrane PZCA-1.

4.2.9 TEM images of the nanoparticle

High-resolution transmission electron microscopy (HR-TEM) pictures of the nanoparticle (ZrO_2) are shown in Figure 4.12(a)–(d) along with the ZrO_2 selected area diffraction pattern (SAED) was illustrated in Figure 4.12(e). Agglomerated ZrO_2 particles were observed from Figure 4.12. The nanoparticles were not dissolved evenly in the ethanol solution because of the agglomeration of ZrO_2 in the solvent. The counter-ions electrostatic attraction between the nanoparticle leads to agglomeration in the ethanol solution. Furthermore, ZrO_2 revealed the uniform shape and size in the 3-5 nm diameter range. The lattice finger-like projection was evidenced. The distance between the finger-like projections was maintained as 0.254 nm. The lattice structures were observed in HR-TEM microstructural images because of the edge dislocation (Ibrahim et al. 2018a). Owing to the occurrence of the tiny spots and particles in the rings, ZrO_2 exhibited polycrystalline behavior (Doyen et al. 1991).
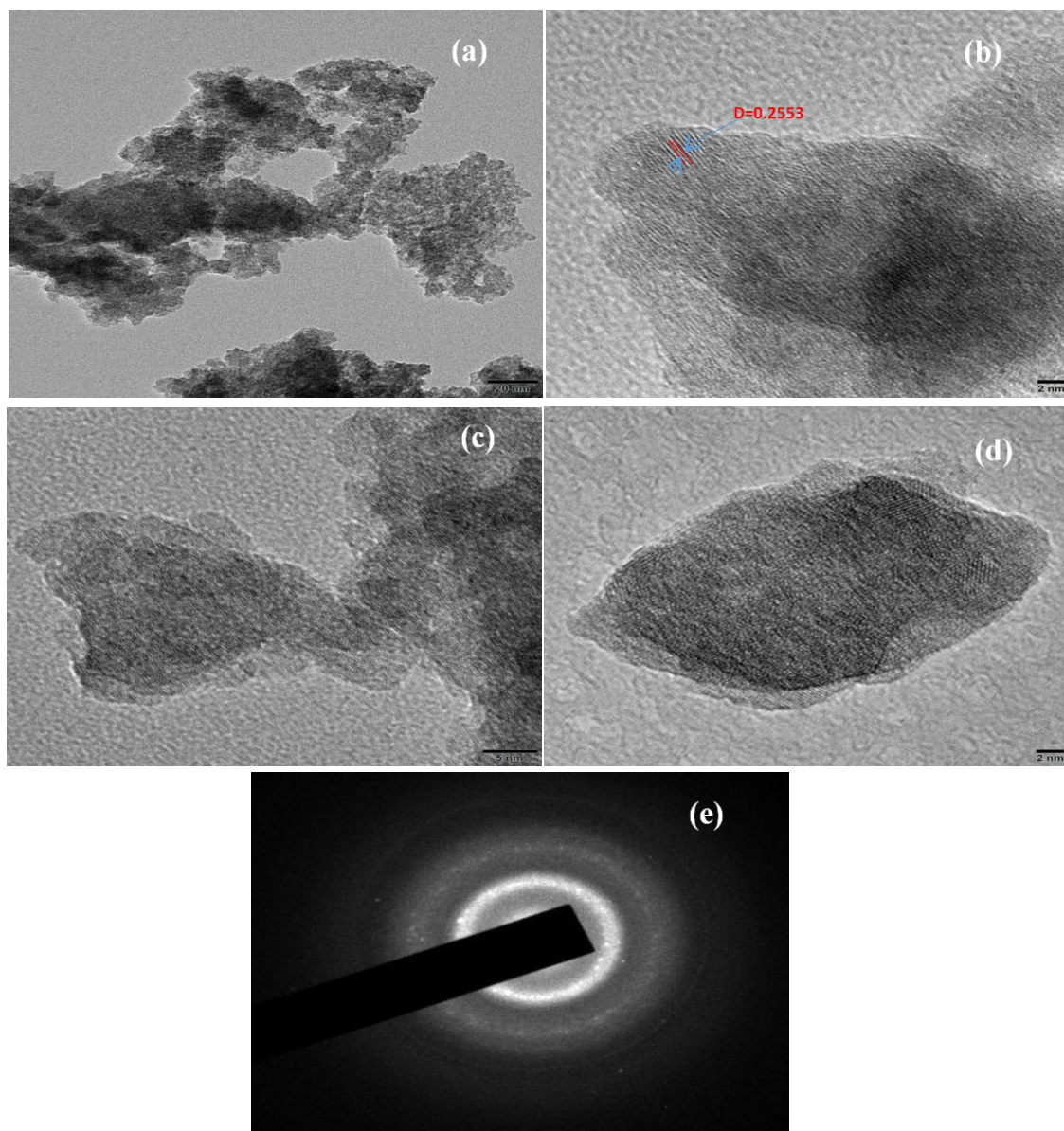
Figure 4.12 TEM images of ZrO$_2$ nanoparticles with different magnifications (a-d) and SAED pattern (e).

4.2.10 XRD of nanoparticle

The intensity of the peaks concerning the diffraction angle is represented in Figure 4.13. The crystalline behavior of the ZrO$_2$ nanoparticle was analyzed in detail using X-ray diffraction (XRD). The behavior of the nanoparticle was amorphous and polycrystalline with corresponding angle peaks at 27.78°, 29.81°, 31.26° and 31.90° with respect to the plane of (1 1 1), (1 0 1), (1 0 1) and (1 1 1) respectively. From the two theta values of XRD, there is no such differences concerning with the diffracted angle in comparison to a reference pattern (Ren et al. 2011).
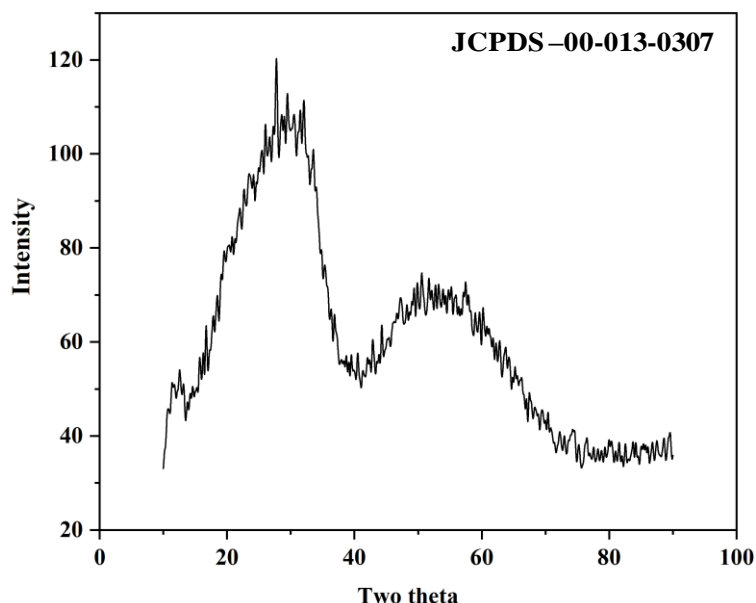
Figure 4.13 X-ray diffraction image of zirconium oxide nanoparticle.

4.2.11 Particle size distribution of the nanoparticle

The ZrO_2 nanoparticle's dynamic light scattering (DLS) and zeta potential have been illustrated in Figures 4.14(a)–(b). The measured 20 wt% of ZrO_2 nanoparticle was homogeneously blended by probe sonicator in the water for about 15 min. From Figure 4.14(a), the average particle size is specified as 1638 nm in the diameter from the DLS process. From Figure 4.13(b), the zeta potential measurement of the nanoparticle has negative polarity along with the zeta potential of -142.9 mV and zeta charge of the nanoparticle 1.56449 Coloumb (Dos Santos et al. 2014).
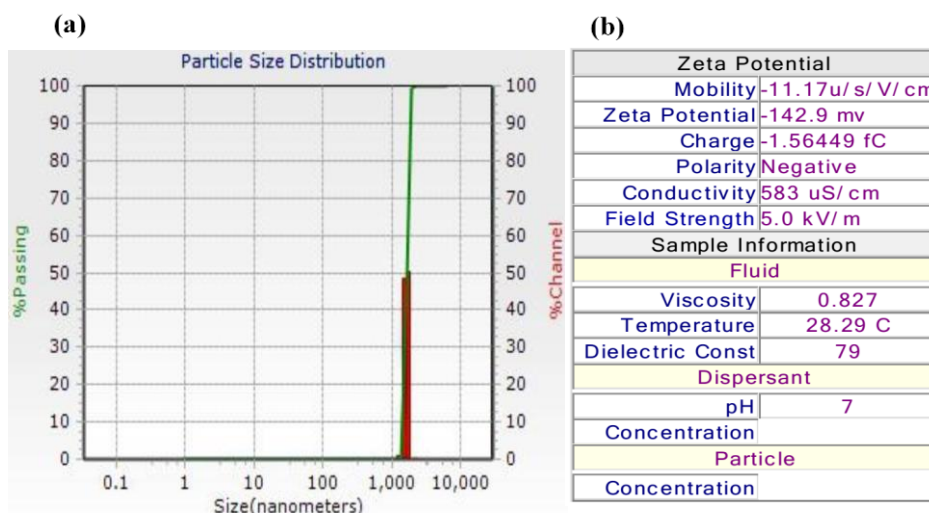
Figure 4.14 (a) Particle size analysis by dynamic light scattering (DLS) method and (b) zeta potential parameter of the zirconium oxide nanoparticle.

4.2.12 Thermogravimetric analysis (TGA) of the membrane

The percentage weight loss of the membrane represented on the Y-axis and with respect to temperature (°C) on the X-axis of neat (PZCA-0 and PZCAP-0) and ZrO_2 containing membranes (PZCA-1 and PZCAP-0.6) are shown in Figure 4.15. From the figure, the decomposition temperature of the neat membrane was higher than the ZrO_2 incorporated membranes. The primary stage of degradation starts from temperature 25 °C to 205 °C. This stage was related to the volatilization of the volatile matter and the adsorbed water evaporation. Due to the decomposition of the sulphuric acid chains present in the membrane, the most important second stage of degradation happens from 210 °C to 555 °C. The final stage of decomposition occurs from 560 °C to 850 °C. The polymeric blended chains were absolutely broken into ash at this temperature range.

In addition, the initial stage of thermal degradation for PZCA-1 and PZCAP-0.6 was from room temperature to 190°C. This is due to the vaporization of the adsorbed water. The next stage of thermal degradation was from 195 °C –590 °C due to the decomposition of the nanoparticle (ZrO_2) and additives (CA and CAP). Lastly, the chains of polymers decompose to form ash above 600 °C. Due to the incorporation of the hydrophilic additives and nanoparticle (ZrO_2) into the PPSU polymer matrix, there is a notable thermal miscibility. The ZrO_2 contained membranes have superior thermal stability from TGA analysis (Gupta et al. 2013; Shukla et al. 2017c).
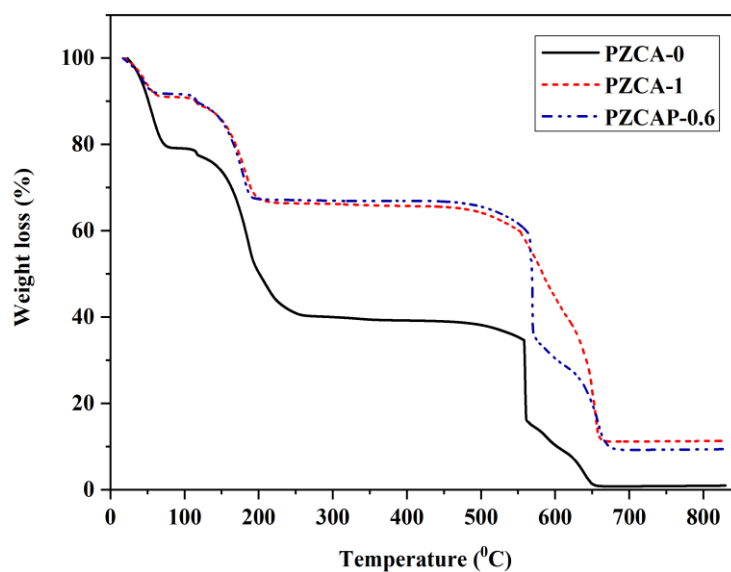
Figure 4.15 Thermogravimetric analysis (TGA) of the prepared membrane.

4.2.13 Molecular weight cut off study of prepared hollow fiber membrane

The molecular weight cut off (MWCO) analysis of the fabricated best performing membrane (PZCA-1) was illustrated in Figure 4.16. The MWCO of the best-performing membrane was analyzed using different molecular weights of PEG. The measured MWCO of the beast performing membrane (PZCA-1) was 17745 Da, confirming that the prepared membrane was an ultrafiltration membrane. The PZCA-1, PEG rejection was 62.98%, 67.97% and 94.24% corresponding PEG molecular weights of 4,000, 6,000 and 20,000 Da respectively. It was observed that when the molecular weight of the PEG improved, the proportion of membrane rejection increased as well.
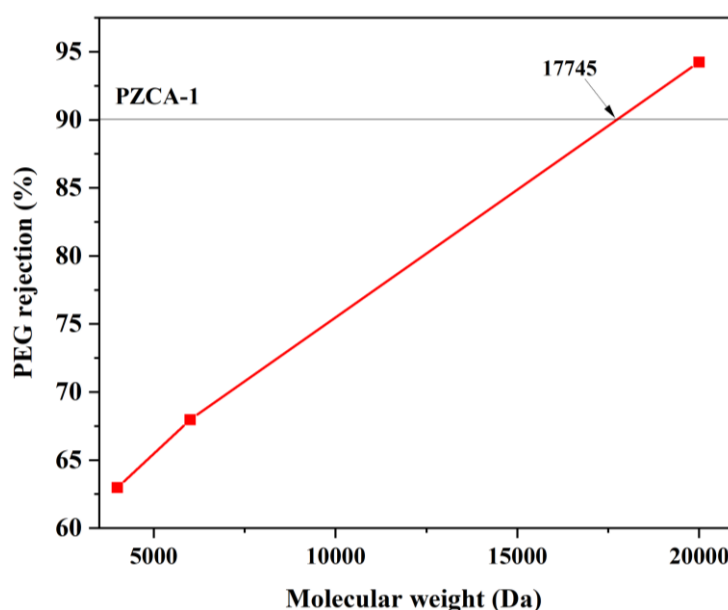
Figure 4.16 Molecular weight cut off study of the prepared membrane.

4.2.14 XPS images of the membrane sample

The chemical bonds such as 532.11 eV, 284.78 eV and 167.91 eV were attributed to the O1s, C1s and S2p respectively were illustrated in Figure 4.17(a). The exertion peaks at 284.79 eV, 532.10 eV and 167.90 eV were attributed to the presence of deconvoluted elements of C1s, O1s and S2p respectively. In addition, the deconvolution of O1s, C1s and S2p outcomes are shown in Figure 4.17(b) – (d). The binding energies 531.90 eV and 533.10 eV were attributed to the functional group –C=O and –C–O–H functional groups corresponding to the O1s group. From Figure 4.17(c) the binding energies 287.97 eV, 286.10 eV and 284.97 eV were related to –C–O–, –C=O and –C–C– for C1s bonds respectively (Rodrigues-Filho et al. 1996). From Figure 4.17(d), the 167.86 eV, sulphur binding energy S2p were attributed to

S2p($\frac{3}{2}$) as SO$_4^{(2-)}$ (sulphate) and 168.94 eV attributed to S2p($\frac{1}{2}$) as the SO$_2$-C (sulphone) respectively (Castner et al. 1996). From Figure 4.17(e), the Zr3d binding energy peaks attributed to 183.6 eV as Zr3d($\frac{3}{2}$) and 181.71 eV attributed to Zr3d($\frac{5}{2}$) respectively. Therefore, the XPS outcomes also confirmed the existence of the blended additives and nanoparticles on the PPSU ultrafiltration hollow fiber membranes.
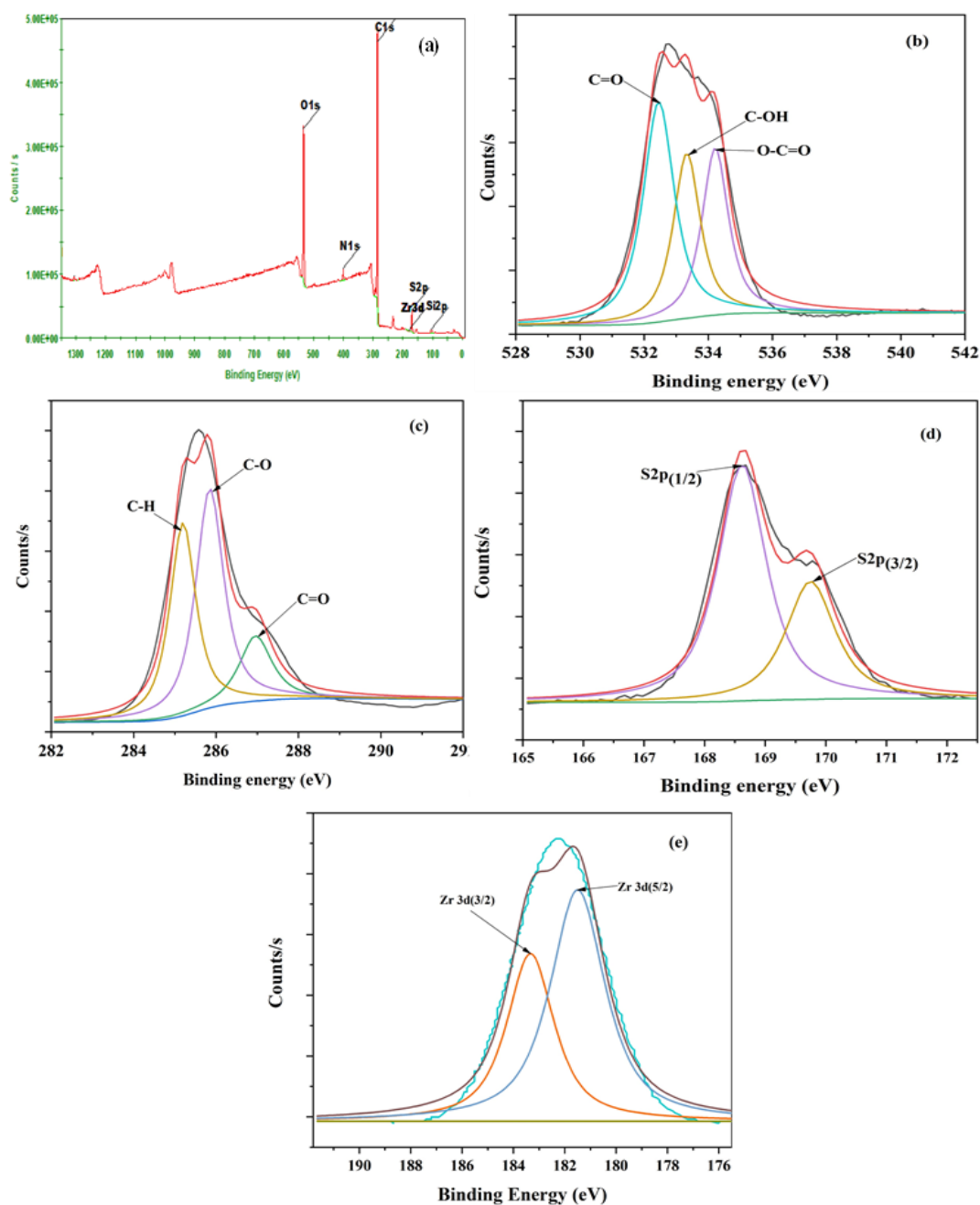
Figure 4.17 (a) XPS wide angle spectra, (b), (c), (d) and (e) deconvoluted narrow spectra of the bonding element of O 1s, C 1s, S 2p and Zr-3d respectively of the PZCA-1 membrane.

4.2.15 Arsenic-V removal from prepared membranes

The arsenic-V rejection efficiency of as-fabricated neat and zirconium oxide incorporated PPSU/CA and PPSU/CAP hollow fiber membranes was demonstrated in Figure 4.18. Prepared membranes were subjected to a laboratory-made 1 ppm arsenic-V aqueous solution with transmembrane pressure of 0.1 MPa. After ionization of H_3AsO_4 in water (H_2O), it was converted to arsenate oxide (AsO_4^{3-}) solution as represented in Equation 3.1. $HAsO_4^-$, $HAsO_4^{2-}$ and AsO_4^{3-} are the various forms of arsenate (Hao et al. 2018a). From Figure 4.18, membranes PZCA-1 and PZCAP-0.6 demonstrated improved arsenate oxide removal than the other membranes. From Figure 4.18 and Figure 4.19, less arsenic-V removal properties can be observed as 18.89% and 28.53% with corresponding permeability of 41.54 L/m^2h bar and 58.19 L/m^2h bar respectively for neat PZCA-0 and PZCAP-0 membranes. The lesser removal behavior of arsenic-V from neat membranes is because of the hydrophobicity and the absence of the amine and carboxylic functional group (Shukla et al. 2018). Therefore, to improve the various functional groups and hydrophilicity on the membrane surfaces, zirconium oxide (ZrO_2) as a nanoparticle was selected. The incremental dosages of ZrO_2 (0.6, 1 and 1.5 wt%) to the pristine membrane PZCA-0 and PZCAP-0 resulted in a dramatic increase of arsenic-V removal. Membranes PZCA-1 and PZCAP-0.6 showed enhanced arsenic-V rejection of 87.24% and 70.48% with arsenic-V membrane permeability of 89.94 L/m^2h bar and 70.59 L/m^2h bar respectively. This is due to the improved repulsive ability and the homogeneous blend of the additives (CA and CAP) and ZrO_2 nanoparticle in the PPSU dope solution, which further helps to increase arsenic-V removal efficiency. Also, because of the presence of the –COOH and –NH_2 functional group on the membrane surfaces, increased rejection of arsenate oxide from the membranes was witnessed, which provides more electrostatic-repulsive force between negatively charged membrane surface and negatively charged arsenate oxide (AsO_4^{3-}) (Pérez-Sicairos et al. 2009a). However, PZCA-0.6 demonstrated 13.53% arsenate oxide rejection without the influence of ZrO_2 dosages in the PPSU/CA membranes. Increased nanoparticle dosage in the PPSU dope solution showed arsenic-V removal as 41.28, 10.35 and 31.14% for membranes PZCA-1.5, PZCAP-1 and PZCAP-1.5 respectively. The decrease in arsenic-V rejection properties is because of the increased concentration polarization on the surfaces of the membranes (Hao et al. 2018b; Pessoa-Lopes et al. 2016). Figure 4.19(a)-(b) lowered arsenic-V permeability 84.18 L/m^2h bar and 105.52 L/m^2h bar for PZCAP-1.5 and PZCAP-1 membranes respectively. The reduced permeability for arsenic-V removal of PZCAP-1.5 is attributed to the increased zirconium oxide concentration (1.5 wt%), leading to

nanoparticle agglomeration, that blocks the membrane surface pores. The concentration polarization for arsenic-V removal of the fabricated hollow fiber membranes were illustrated in Table 4.3.
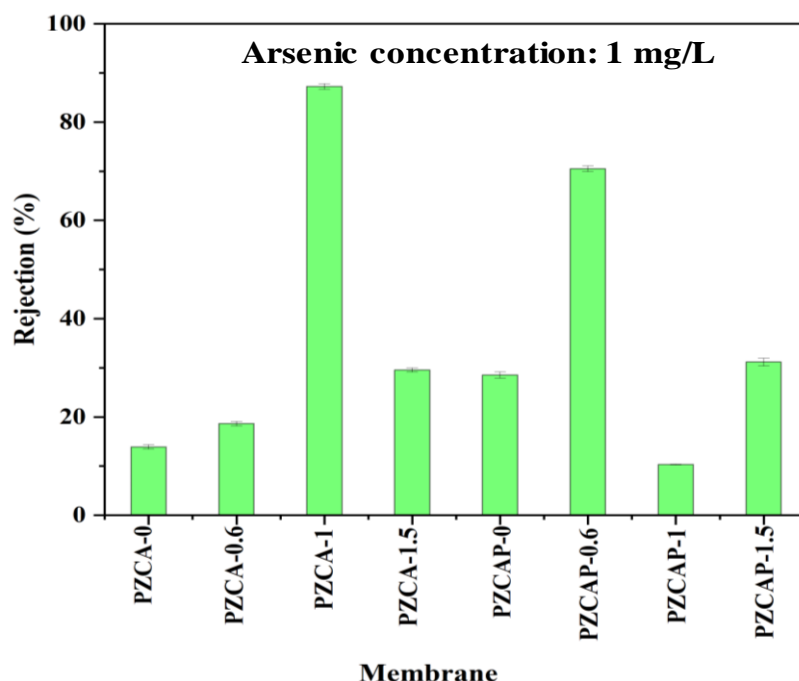
Figure 4.18 Comparison of the arsenic-V removal properties of the neat membrane (PZCA-0 and PZCAP-0) and ZrO$_2$ in PPSU/CA membrane as (PZCA-0.6, PZCA-1 and PZCA-1.5) and ZrO$_2$ in PPSU/CAP membranes as (PZCAP-0.6, PZCAP-1 and PZCAP-1.5).
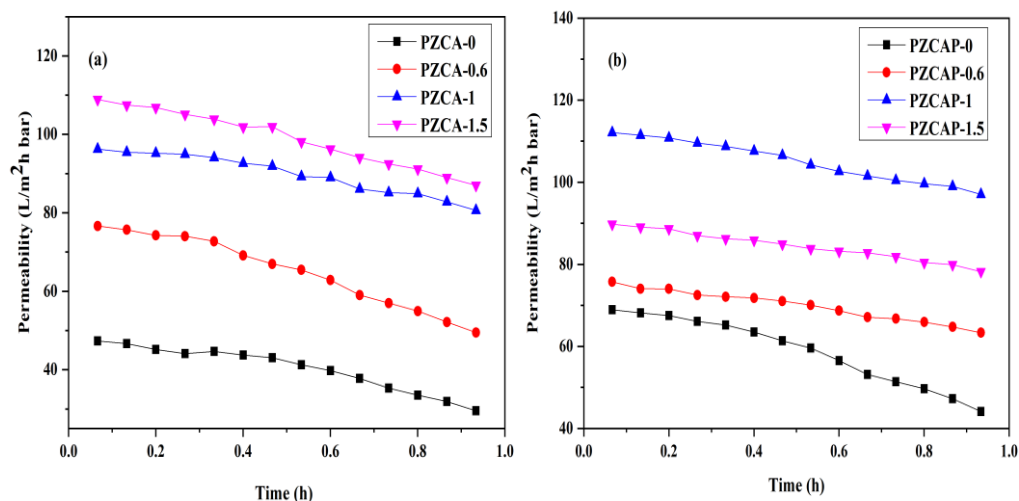
Figure 4.19 Arsenic-V permeability of the (a) neat membrane (PZCA-0) and ZrO$_2$ modified CA membranes as (PZCA-0.6, PZCA-1, and PZCA-1.5), (b) neat membrane (PZCA-0) ZrO$_2$ modified CAP membranes as (PZCAP-0.6, PZCAP-1, and PZCAP-1.5).

Table 4.3 Concentration polarization for arsenic-V removal of the fabricated membranes

Membrane codes	Velocity (v) (m/s)	Mass transfer coefficient (K) (m/s)	Concentration polarization ($\frac{Cm}{Cb}$)
PZCA-0	0.00256	1.085×10^{-5}	1.110
PZCA-0.6	0.00482	1.44×10^{-5}	1.153
PZCA-1	0.0784	3.696×10^{-5}	1.780
PZCA-1.5	0.1330	4.55×10^{-5}	1.197
PZCAP-0	0.0697	3.339×10^{-5}	1.122
PZCAP-0.6	0.02132	2.374×10^{-5}	1.655
PZCAP-1	0.0689	3.403×10^{-5}	1.077
PZCAP-1.5	0.0957	3.786×10^{-5}	1.139

4.2.16 Positron annihilation lifetime spectroscopy (PALS) analysis of the membranes

The neat (PZCA-0) and ZrO_2 contained (PZCA-1) membranes positron annihilation was carried out using radioactive isotope sodium (^{22}Na) as a source of positrons. The sodium chloride (NaCl) was dissolved in hydrochloric acid (HCl) solution and deposited drop by drop on HCl solution. The foil of pure and well-annealed Ni (thickness of 2 mm) until the necessary strength of around 5 Ci was obtained. The non-deposited component of the foil was then folded to protect deposition. In this form, the source used on either side to get sandwiched between specimens of the samples where the positrons were released are stopped and annihilated. From a few meV to 545 keV. ^{22}Na emits positrons of all possible energies. The formula R measured the positron spectrum of 545 keV endpoint energy (mm)=1.86/density. In this instance, the membrane sample thickness was much smaller than the maximum range of the positron. To ensure that all positrons were stopped inside the samples, a membrane had to be folded to create enough layers. The total thickness was more significant than the maximum range of positrons. The positron properties were illustrated in Table 4.4.

Table 4.4 Positron properties of the membranes

Sample	Mass (g)	Area of the membrane (cm^2)	Thickness (cm)	Density (gcm^{-3})	Range of positrons (mm)	No. of foils needed to stop positrons	No. of foils used in the experiment
Neat membrane (PZCA-0)	0.7788	283.34	0.008	0.3436	5.41	67.62	80
Modified membrane (PZCA-1)	0.1658	74.61	0.007	0.3167	5.85	83.50	80

Two tests have been performed: Positron annihilation lifetime spectroscopy (PALS) and Doppler broadening spectroscopy (DBS). In PALS measurement, the time of interval between the 1.26 MeV emissions emitted at the same time as the positron and the time of interval between the two 0.511 MeV gamma rays emitted at the time of annihilation were calculated using a gamma-gamma coincidence method. As gamma rays detectors paired with the XP2020Q photomultiplier tubes and nuclear electron module chain to process the signals, the setup consisted of BaF$_2$ scintillators. In PALS, with a peak to background ratio of about 8000:1, approximately 0.8 million counts were obtained. Using PALSfit, the data collected were analyzed.

The PALS findings are given in Table 4.5. As shown in Figure 4.20, the predicted multi-exponential decay nature of the spectra for the two samples is more or less overlapping, suggesting very little or no change between them. In terms of four lifetimes and intensities, each spectrum was analyzed. The first and second lifetimes, τ_1 and τ_2 are those positrons that are annihilated in the free state and then caught in defects and eventually annihilated. The third and fourth lifetimes τ_3 and τ_4 are those of orthopositronium (o-Ps) atoms that are formed within the samples in free volume cavities of two different size regimes and annihilated by surrounding electrons.
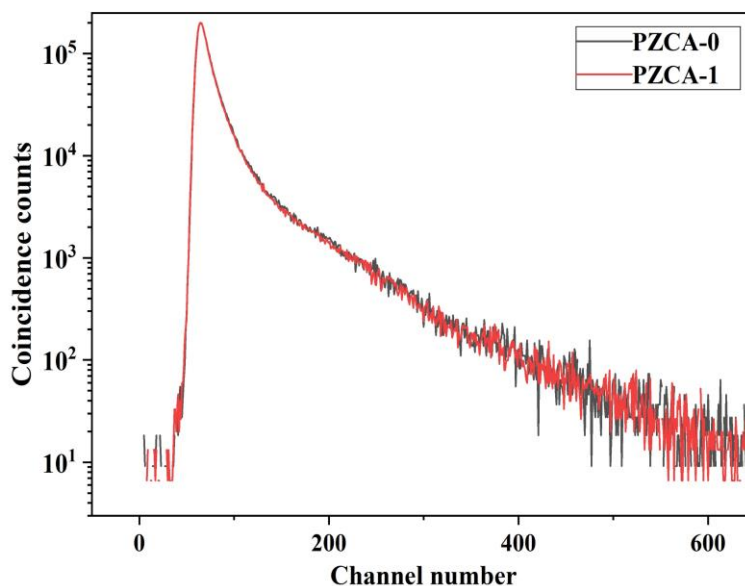
Figure 4.20 PALS lifetime spectrum for neat membrane (PZCA-0) and zirconium oxide contained membrane (PZCA-1) samples.

In terms of four lifetimes and strength, each spectrum was analyzed. The first and second lifetimes of τ_1 and τ_2 are those positrons annihilated in the free state and stuck in defects and eventually annihilated. The third and fourth lifetimes τ_3 and τ_4 are those of orthopositronium (o-Ps) formed inside the samples in free volume cavities of two different size regimes and annihilated by electrons from the atmosphere. The outcome was summarized in Table 4.5.

As already mentioned, the changes are too small to attribute any real significance. But still, we observe a small increase in all the positron/o-Ps lifetimes. This shows that the open volume defects have slightly grown in size. The Tao-Eldrup equation connects the measured o-Ps lifetime τ_3 (ns) or τ_4 (ns) with the respective radii R_3 or R_4 of the free volume defects in which o-Ps are formed by the relation using Equation 4.1.

$$\tau_{3/4} = \frac{1}{2}\left(1 - \frac{R_{3/4}}{R_0} + \frac{1}{2\pi}\sin\frac{2\pi R_{3/4}}{R_0}\right)^{-1} \tag{4.1}$$

Where, $\tau_{3/4}$ is expressed in ns (nanosecond), $R_{3/4}$ is the free volume cavity radius represented in Å and R_0 is $R_{3/4} + \Delta R$ where, Å is the parameter of the empirical electron layer thickness, taken in 1.66 Å, across the cavity. The free volume fraction f_v was also reported using Equation 4.2.

$$f_{v3/4} = AV_{f3/4}I_{3/4} \tag{4.2}$$

where $V_{f\,3/4} = (4/3)\pi R_{3/4}^3$ is the size of the free volumes and $A = 0.0016$ Å^{-3} is a constant.

Table 4.5 Positron lifetime and intensity properties from the prepared membranes

Sample	τ_1 (ns)	τ_2 (ns)	τ_3 (ns)	τ_4 (ns)	I_1 (%)	I_2 (%)	I_3 (%)	I_4 (%)	τ_m (ns)
Neat membrane (PZCA-0)	0.1109 ± 0.0055	0.3532 ± 0.0099	1.5362 ± 0.0851	2.9786 ± 0.3343	25.70 ± 1.54	48.95 ± 1.18	21.21 ± 1.35	4.14 ± 0.80	0.6505 ± 0.0200
Modified membrane (PZCA-1)	0.1223 ± 0.0071	0.3694 ± 0.0115	1.6322 ± 0.0549	4.1221 ± 0.5131	25.30 ± 1.91	49.12 ± 1.55	23.47 ± 0.49	2.11 ± 0.69	0.6825 ± 0.0230

Table 4.6 The results of these calculations are given below

Sample	R_3 (Å)	R_4 (Å)	f_{v3} (%)	f_{v4} (%)	S parameter
Neat membrane (PZCA-0)	2.38	3.62	1.92	1.32	0.4209±0.0008
Modified membrane (PZCA-1)	2.49	4.31	2.42	1.13	0.4215±0.0008

Results have indeed shown from Table 4.6 that the free volume cavities have increased in size. The fractional free volumes (f_v) values indicated that, although the smaller free volumes increase the concentration marginally, the more significant one decreases, likely suggesting a kind of free volume agglomeration.

Also, a DBS experiment was performed, and spectra have been presented in Figure 4.21. The S parameter is derived from each spectrum as the ratio of counts under 0.511±0.00058 MeV to the total counts under the full spectrum. The energy interval chosen around 0.511 MeV corresponds to the magnitude of the doppler shift that can affect the annihilation gamma-ray energy (0.511 MeV) by the momentum of the low momentum (valence and free)

electrons in the material. The S parameter is proportional to the total defect volume within the sample. The values are shown in the last column of the above table. The observed change is within the error bars; hence, little can be derived from this result. A tiny increase of the 'f' parameter, the 'S' parameter in the case of the modified membrane has slightly more defect volume than the neat membrane (PZCA-0). This is consistent with the positron lifetimes results, which show the overall defect volume fv3 + fv4 as 1.92+1.32 = 3.24% in the neat sample, whereas 2.42+1.13 = 3.55% in the modified sample.
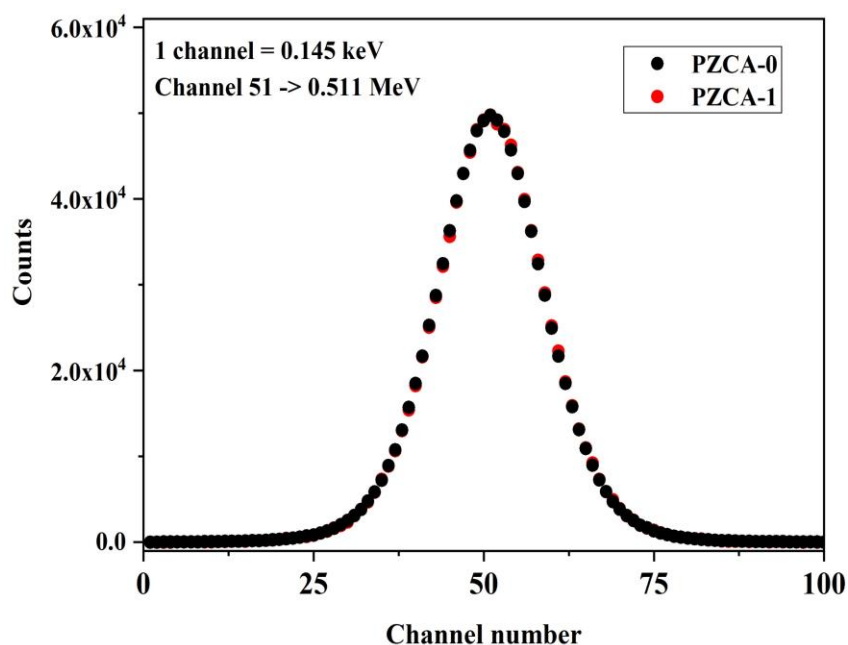
Figure 4.21 Doppler broadening spectroscopy (DBS) spectra for neat membrane (PZCA-0) and zirconium oxide modified membrane (PZCA-1) samples.

4.2.17 Leachability study of the neat and ZrO_2 contained membranes

The leachability nature of the Zr from the hollow fiber membrane with different pH values (4.3, 7.1 and 9.1) was illustrated in Table 4.7. It was witnessed from the table that there was much less leaching (<0.08 ppb) of Zr from modified hollow fiber membranes. This is due to the reason that, in presence of water, the surface of the ZrO_2 is protonated by a surface hydroxyl group, which undergoes acidic pH protonation. The protonation tended to weaken and break the surfaces of the Zr-O bonds, resulting in greater release of the Zr in the acidic permeate pH solution than the neutral pH solution. The pH of the water increases, the leachability from the prepared membranes decreases. There is no considerable leakage of the nanoparticle (Zr), because of the homogeneous solubility of the zirconium oxide in the PPSU

dope solution. Due to the increased solubility and reduced leakage of the zirconium implies increased stability of the modified membranes.

Table 4.7 Leachability of zirconium oxide with different pH

Membranes code	pH-4.3	pH-7.1	pH-9.1
PZCA-0.6	0.055 ppb	0.03 ppb	<0.01 ppt
PZCA-1	0.026 ppb	<0.01 ppt	<0.01 ppt
PZCA-1.5	0.094 ppb	0.015 ppb	0.011 ppb
PZCAP-0.6	0.026 ppb	0.015 ppb	0.008 ppb
PZCAP-1	0.038 ppb	0.024 ppb	0.024 ppb
PZCAP-1.5	0.066 ppb	0.005 ppb	<0.01 ppt

4.3 SUMMARY OF THE PRESENT WORK

The zirconium oxide incorporated cellulose acetate derivatives in polyphenylsulfone novel ultrafiltration hollow fiber membranes were fabricated. The fabricated membranes have successfully removed arsenic-V from arsenic-V-contaminated aqueous solution. The effect of different dosages of ZrO_2 on CA/PPSU and CAP/PPSU polymeric matrix was well understood. FTIR and XPS analysis confirmed the implementation of additives and nanoparticle (ZrO_2) into the PPSU matrix in terms of their different functional groups and chemical bonds. Incorporating ZrO_2 into the neat membranes causes expansion of the finger-like projections and improves overall porosity on the membrane surfaces. The membrane surface hydrophilicity was improved with intensified dosages of ZrO_2, which enhanced the pure water permeability and water uptake.

The ZrO$_2$ containing membranes revealed enhanced antifouling behavior compared to the pristine membranes. Because of the increased antifouling behavior, the hollow fiber membranes exhibited the improved flux recovery ratio (FRR), as noticed from membranes PZCA-1.5 as 67.49% and PZCAP-0 as 70.02% respectively. The increased repulsion of arsenate oxide from negatively charged ZrO$_2$ containing membranes influences the increased percentage of arsenic-V removal from arsenic-V aqueous solution. As such, 87.23% and 70.48% with permeability of arsenic-V as 89.94 L/m^{2}h bar and 70.59 L/m^{2}h bar was observed for PZCA-1 and PZCAP-0.6 respectively. There is an improved removal of arsenic-V in the pH range of 2.1-8 from fabricated membranes. Increased ZrO$_2$ nanoparticle concentration has also shown decreased arsenic-V removal behavior. This is due to the ZrO$_2$ agglomeration on the membrane surfaces. Therefore, the modified membranes can be used for efficient removal of arsenic-V from aqueous solution, as the membranes exhibited improved arsenic-V rejection properties.

CHAPTER -5

EFFECT OF ZnO-MgO ON THE POLYPHENYLSULFONE/ CELLULOSE ACETATE DERIVATIVES HOLLOW FIBER MEMBRANES FOR THE EFFICIENT DECONTAMINATION OF ARSENIC-V FROM ARSENIC CONTAMINATED WATER

Abstract

In many parts of the world, arsenic contamination continually threatens the safety of drinking water. Ingestion of drinking water contaminated with chronic arsenic can cause serious health concerns. The synthesis of novel efficient materials plays a vital role in the systematic rejection of arsenic-V from the aqueous solution. The effect of incremental dosages (0.6, 1 and 1.5 wt%) of zinc-magnesium oxide (ZnO-MgO) to cellulose acetate (CA)/polyphenylsulfone (PPSU) and cellulose acetate phthalate (CAP)/polyphenylsulfone (PPSU) hollow fiber membranes for arsenic-V removal from aqueous solution was performed. As used ZnO-MgO was characterized using x-ray diffraction (XRD), transmission electron microscopy (TEM) and particle size distribution analysis. The properties of the fabricated hollow fiber membranes were analyzed in detail using scanning electron microscopy (SEM), x-ray photoelectron Spectroscopy (XPS), atomic force microscopy (AFM), fourier transform infrared spectroscopy (FTIR), zeta potential, antifouling studies and thermogravimetric analysis (TGA). The outcome revealed that the overall efficiency and lifetime of the membrane were significantly enhanced. An improvement in the arsenic-V removal properties was demonstrated in 0.6 wt % of ZnO-MgO in CAP/PPSU (ZMCAP-0.6) membrane as 81.31% with an arsenic-V permeability of 69.58 L/m^{2}h bar respectively. Similarly, by 1 wt% of ZnO-MgO in CA/PPSU (ZMCA-1) membrane removed 78.48% of arsenic-V with the permeability of 198.47 L/m^{2}h bar respectively with a prepared arsenic-V aqueous solution (pH 6.8$\pm$0.2) at 0.1 MPa transmembrane pressure (TMP). Furthermore, improved antifouling properties were observed related to increased flux recovery ratio (FRR) and enhanced thermal stability of the membranes for incremental dosages of ZnO-MgO in PPSU membrane matrix. Thus the ZnO-MgO containing membranes improved arsenic-V removal tendency without compromising the permeability.

5.1 INTRODUCTION

Freshwater contributes for about 2.5% of the world's total water. Only 0.3% of this is available on the surface, with the remainder being groundwater. As a result, the majority of living things rely on groundwater. However, different natural and manmade sources have contaminated groundwater in many places (Karmakar et al. 2018). The primary source of drinking water is groundwater. The toxic arsenic contamination in the drinking water has created a global issue and a great disaster to the health of millions of population and the environment. The arsenic content in the environment is usually low. Still, it rises as the

contributions from different sources such as volcanic activities, fossil fuel consumption, industrial activities and smelting are the sources for arsenic (He et al. 2017; Meharg and Meharg 2021). Ingestion of low level of arsenic-contaminated water results in harmful health diseases such as nausea, jaundice, erythema, diarrhea, vomiting, throat dryness and headache. Chronic arsenic consumption causes health-hazardous severe problems such as cancer, disease related to cardiovascular, abdominal pain, diabetes, stomach pain and even death (Shan et al. 2019; Yadav et al. 2021b). These health issues revealed how unsafe drinking water in the human body accumulated with arsenic. Arsenic is therefore considered hazardous, toxic and carcinogenic to human health. According to a World health organization (WHO) report, Bangladesh and the Bengal basin in West Bengal of India are significant regions impacted by the possibility of drinking water polluted with arsenic. The united state environmental protection agency (USEPA) sets 10 ppb as the maximum permissible level of arsenic pollution in drinking water. More than 200 million population have reportedly been suffering from arsenic-related health-hazardous issues (Kumar et al. 2019c). Therefore, developing a cost-effective system for efficiently removing arsenic from arsenic-contaminated water is very much essential.

Many of the technologies have been reported for treating the arsenic-contaminated water such as ion exchange (Epsztein et al. 2019b), phytoremediation (Delgado-González et al. 2021; Li et al. 2018a), coagulation-flocculation (Ma et al. 2019) and membrane-based filtration process like nanofiltration (He et al. 2018; Rajendran et al. 2021) and reverse osmosis (Abejón et al. 2015b; Jarma et al. 2020). Nevertheless, the processes demonstrated their demerits for the removal of arsenic from the drinking water (Crini and Lichtfouse 2019). The ultrafiltration membrane process is versatile in membrane technology to remove arsenic (Kumar et al. 2019c; 2020a). The key benefits of using the ultrafiltration process are the high throughput of the filtered products with low-pressure intake and less maintenance requirement. Moreover, the high surface area to volume ratio associated with hollow fiber membranes was more dominant than flat sheet membranes. The increased surface area improved permeability and increased fouling resistance and high filtration performance (Kumar et al. 2020a; Mukherjee et al. 2019).

Many of the researchers used varieties of organic polymers to fabricate membranes and enhance the membranes efficiency. Researchers were attracted by polyphenylsulfone (PPSU) because of well-known properties such as high thermal stability (T_g-220 $^{\circ}$C) higher than

polysulfone (T_g-190 $^\circ$C) most equivalent to polyethersulfone (T_g-210 $^\circ$C) and better chemical stability (Golpour and Pakizeh 2018a).

Sani et al. (2014) fabricated membranes with varieties of properties using the phase inversion process. The results unveiled that with increasing concentrations of polymer in the dope, the enhanced solute rejection was witnessed because of the reduced pore size on the membrane surface, which was more effective at preventing solutes from passing through the membrane. The sponge-like morphological structures were enhanced with the increased concentrations of the PPSU in the dope from SEM images. The high contact angle and reduced methanol flux were evidenced with enhanced dosages of PPSU.

Shukla et al. (2018) developed nanofiltration PPSU membranes using carboxylated graphene oxide as nanoparticles for various heavy metal rejection from an aqueous solution. The modified PPSU membranes exhibited enhanced thermal stability.

Golpour and pakizeh (2018) reported polyamide/ metal-organic framework graphene oxide incorporated PPSU based mixed matrix membranes. Membranes produced were exhibited enhanced properties. However, the pristine PPSU membranes were less porous, hydrophobic, and vulnerable to fouling and less water permeability. In addition, the inclusion of inorganic nanoparticles in the polymer matrix enhances the hydrophilicity, porosity, fouling resistance, pure water permeability, arsenate rejection properties and membrane mechanical properties.

Moreover, in the current application, ZnO nanoparticle has raised concerns due to their excellent thermal and chemical stability, antimicrobial and antibacterial properties, and high surface area to volume ratio. Hence, magnesium oxide (MgO) was introduced as a preferred nanoparticle for preparing and improving membrane properties through homogeneous dispersion of the nanoparticles and additives in the dope solution preparation (Durthi et al. 2018c). MgO nanoparticle is well known to have contributed to a wide bandgap and high surface area, which improves membrane filtration performance and selectivity (Han et al. 2016). The literature demonstrated that, incorporating inorganic binary oxide nanoparticles into organic polymers would increase the overall efficiency of the membrane (Chung et al. 2017; Tan et al. 2017).

Hong and He (2012) developed PVDF microfiltration membranes with the increased dosages of the nano-ZnO nanoparticles. From SEM and AFM analysis, the surface roughness increased with an incremental nanoparticle dosage. Also, finger-like projections and

microporous structures were expanded with nanoparticle concentrations. The enhanced peaks and valleys were witnessed from modified membranes compared to neat membranes. The improved hydrophilicity of the membranes was promised with ZnO dosage in PVDF membranes, which was established from porosity/water uptake and contact angle measurement.

Rajabi and co-workers (2015) modified PES hydrophobic membranes with various ZnO nanomaterials such as ZnO nanoparticles and ZnO nanorods. The performance of each membrane was evaluated and compared. The nano-fillers incorporated membranes showed enhanced morphologies and hydrophilicity. The increased reusability and durability were witnessed with the ZnO nano-rods than the ZnO nanoparticle. The ZnO nanorods were outperformed with PES membranes in enhancing antifouling and improved surface roughness than the ZnO nanoparticle with PES membranes.

Wu et al. (2016) have reported polysulfone (PSf) ultrafiltration membranes by including polydopamine/ zinc complex coating on flat sheet membranes. This contributed to higher water flux and antifouling properties of Zn–PDA/PSf composite membranes than neat (PSf/PDA) membranes. More importantly, the Zn–PDA/PSf membranes exhibited considerably improved stability in the both basic and acidic solutions, because the complexity of the zinc species and PDA helps to cross-link the self-assembled PDA oligomers. The zinc complex coating can thus resist electrostatic repulsion force between the charged PDA oligomers and under harsh conditions, maintain the integrity of the thin PDA coatings.

Han and group members (2016) developed hybrid membranes of polyethersulfone (PES)/magnesium hydroxide $Mg(OH_2)$ by phase inversion process. The dosage of $MgOH_2$ on the PES membrane matrix has a significant outcome in terms of increased hydrophilicity, porosity and pure water permeability. The enhanced antifouling behavior exhibited a 73.8% of flux recovery ratio (FRR) for the prepared membrane for egg albumin as a model protein with increased $Mg(OH_2)$ dosages in the PES membrane matrix.

Tan and group members (2017) fabricated ultrafiltration membranes by non-solvent induced phase separation process using polyvinylidene fluoride (PVDF) and zinc-iron oxide (ZiO) nanoparticles. The ZiO contained membranes showed enhanced membrane properties interms of their high surface area, increased hydrophilicity and enhanced antifouling properties with negative surface charge.

Chung et al. (2017) have reported mixed matrix membranes prepared using binary oxide nanoparticles ZnO-graphene oxide (ZnO-GO). The best performing membrane output was shown from membranes containing 2 wt% ZnO and 0.6 wt% ZnO-GO. These two membranes had significantly better hydrophilicity, water permeability, porosity, higher humic acid rejection rate and antibacterial control. The modified ZnO-containing membranes showed enhanced antifouling behavior with the increased flux recovery ratio. To an extent, these nano-hybrid membranes have excellent antimicrobial potential proved to be a suitable candidate for resolving biofouling problems.

Ekambaram and co-workers (2017) have reported nanocomposite membranes using PVDF as base polymer and ZnO-carboxymethyl chitosan (ZnO-CMC) as binary oxide nanoparticles by NIPS process. The modified membranes exhibited increased membrane properties. From the literature, MgO as a binary oxide nanoparticle for membrane preparation is limited. Because of the absence of several functional groups, incorporating the ZnO-MgO binary oxide in the PPSU polymer matrix may present inadequate arsenic rejection from the prepared ultrafiltration hollow fiber membranes. To overcome the above issue, hydrophilic cellulose acetate and cellulose acetate phthalate was introduced to improve functional groups such as hydroxyl (–OH), carboxyl (–CO_2H) and carbonyl (–C=O) on the membrane surface. The –$OCOCH_3$ group implanted the cellulose acetate membrane, which facilitated the excellent rejection of the arsenic species from the aqueous solution through the surface complexation process.

Ayyaru et al. (2020) have developed PVDF membranes with graphene oxide /zinc oxide (GO/ZnO) as additives. The additive dosage membranes exhibited 48% increased pure water flux than the pristine membrane. The increased FRR values suggested the modified membranes have increased antifouling properties. The decreased irreversible fouling (R_{ir}) was observed from 15.09% for the pristine membrane to 7.21% for modified membranes. This further indicated the enhanced lifetime of the membranes. In addition, the Go-ZnO membranes exhibited enhanced porosity, hydrophilicity and surface roughness properties compared to neat PVDF membranes.

Also, cellulose acetate bio-sorbents derivatives consist of glycosidic linkages β-1-4, which assist in amplifying hydroxyl functional group and superior properties in reported membranes (Kumar et al. 2019c, 2020a; Shenvi et al. 2014b). In addition, the cellulose acetate as an adsorbent exhibited the following benefits: moderate permeability, non-toxic,

renewable source and low cost (Durthi et al. 2018c). Previously hollow fiber membranes had different dosages of ZrO_2 (0.6, 1 and 1.5 wt%) of PPSU/CA derivatives for enhanced uptake of the arsenic-V along with increased hydrophilic properties. Membranes prepared by 1 wt% of ZrO_2 in CA/PPSU and 0.6 wt% of ZnO-MgO in CAP/PPSU revealed improved arsenic-V rejection of 87.27% and 70.48% corresponding permeabilities were 89.94 L/m^{2}h bar and 70.59 L/m^{2}h bar respectively. However, the neat membrane 0.3 wt% of CA in PPSU and 0.3 wt% of CAP in PPSU as 18.89% and 28.53% corresponding permeability for arsenic-V were 41.54 L/m^{2}h bar and 58.19 L/m^{2}h bar respectively (Kumar et al. 2020a). The enhanced amine and carboxylic functional groups on the membrane surface enable membrane surfaces to be negatively charged. The increased arsenic-V rejection properties from ZrO_2 contained membranes were reported. Furthermore, the negatively charged membrane surfaces tend to improve the repulsion of negatively charged arsenate oxide (AsO_4^{3-}). Still, no any analysis described the advantages of ZnO-MgO in membrane filtration processes. However, binary ZnO-MgO nanoparticle has been used in nanocomposites and thin-film development applications. The key benefits of ZnO-MgO nanoparticles are high thermal stability, high antimicrobial and antibacterial properties and enhanced photocatalytic properties.

Nonetheless, no scientific research on the use of ZnO-MgO as a binary oxide nanoparticle for the fabrication of polyphenylsulfone based hollow fiber membranes has been reported from the literature. The main objective of this work is to fabricate and characterize the ultrafiltration hollow fiber membranes containing different dosages of ZnO-MgO integrated into the CA/PPSU and CAP/PPSU polymer matrix (Kumar et al. 2019c). The influence of the ZnO-MgO on the morphologies and topographies of the CA/PPSU and CAP/PPSU membranes, thermal properties and antifouling properties were studied. In addition, prepared hollow fiber membranes were subjected to the transmembrane pressure of 1 bar for arsenate oxide (AsO_4^{3-}) using laboratory prepared 1 ppm standard arsenic-V solution at pH 6.8$\pm$0.2.

5.2 RESULTS AND DISCUSSION

5.2.1 High-resolution transmission electron microscopy

The high resolution-transmission electron microscopy (HR-TEM) images of the ZnO-MgO are shown in Figure 5.1(a) – (e). Figure 5.1(f) demonstrated the selected area electron diffraction (SAED) configuration of used ZnO-MgO. The nano-sized and aggregated ZnO-MgO particle was observed from the images. A noticeable agglomeration resulted and was

noticed in Figure 5.1 due to ZnO-MgO improper sonication in the ethanol solution. The agglomeration was due to the electrostatic attraction between the counter-ions. The sheet-like thin film from the MgO nanoparticle was deposited on the ZnO nanoparticle sphere-like structure. The behavior was similar to the GO-ZnO nanoparticle literature (Mahlangu et al. 2017).

Figure 5.1(e) shows lattice predictions with the distance between the lattices were maintained as 0.281 nm from each other. The finger-like lattice structures were noticed because of the nanoparticle dislocations related to the edge of the grains. As utilized, ZnO-MgO nanoparticles demonstrated the improved surface area to volume ratio by illustrating ZnO-MgO crystalline and ferromagnetic features (Rao et al. 2018). The importance of magnetism behavior has been explained (Hu et al. 2005; Lops et al. 2019; Watson et al. 2000). This process further measures the removal of arsenate oxide (AsO_4^{3-}) from prepared membranes. Figure 5.1(e) is categorized as crystalline form owing to several light rings and spots of ZnO-MgO nanoparticle's (Fakhri and Behrouz 2015).
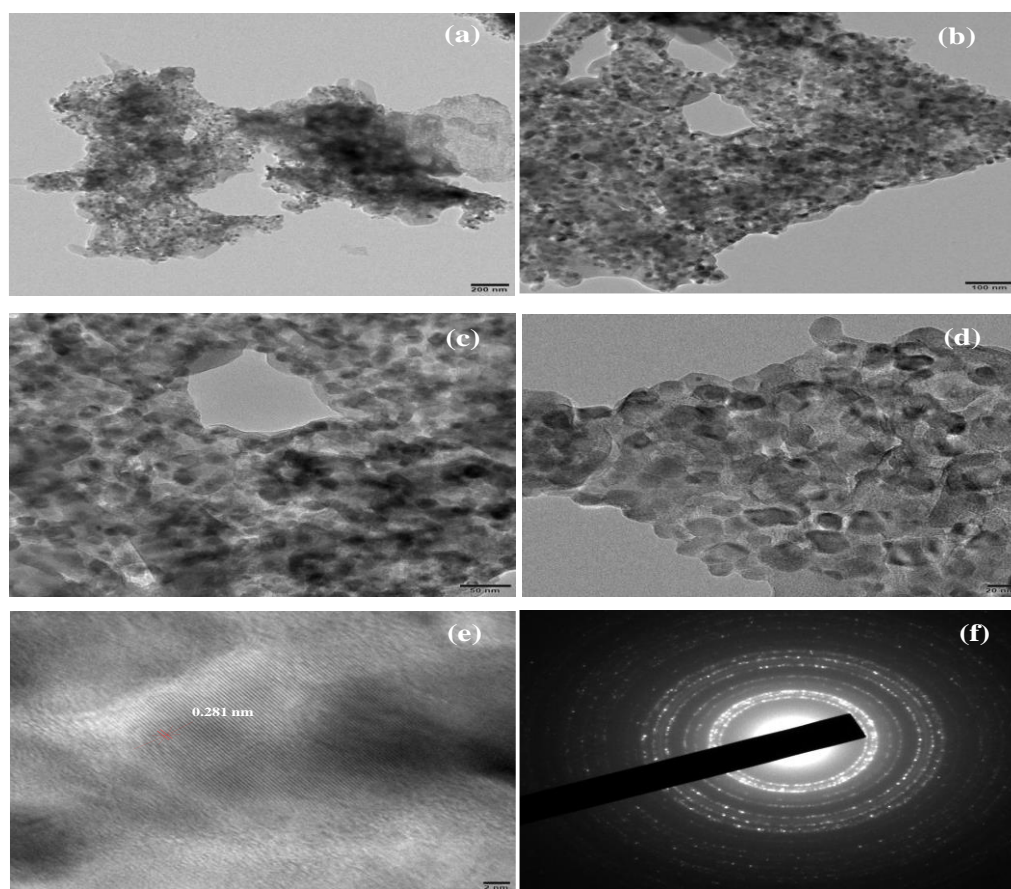
Figure 5.1 (a-e) High-resolution TEM images and (f) SAED pattern of ZnO-MgO nanoparticle.

5.2.2 X-ray diffraction analysis of the ZnO-MgO

The XRD graph of ZnO-MgO shows the peak intensities in the X-axis and the Y-axis diffraction angle (2θ) are shown in Figure 5.2. The crystalline behavior of the used ZnO-MgO nanoparticle was demonstrated from the diffraction angles from ZnO as 31.80°, 34.51°, 36.26°, 47.49°, 56.61°, 62.99°, 66.55°, 67.84° and 77.53° related to the diffraction planes 1 0 0, 0 0 2, 1 0 1, 1 0 2, 1 1 0, 1 0 3, 2 0 0, 1 1 2 and 2 0 2 respectively with the JCPDS –code as 36-1451 for hexagonal phase along with wurtzite structure (Chung et al. 2017). The diffraction angles for MgO are 42.90°, 62.30° and 78.61° related to the 2 0 0, 2 2 0 and 2 2 2 diffraction planes from JCPDS-code 45-0946 respectively containing a hexagonal cubic MgO structure (Noori and Kareem 2019). The adequate blending of ZnO-MgO nanoparticles demonstrated the occurrence of different diffraction peaks with subsequent planes.
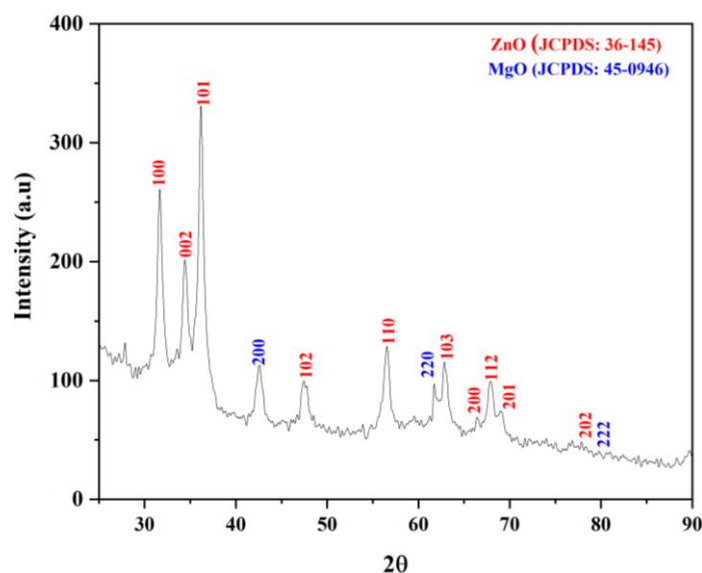
Figure 5.2 X-ray diffraction analysis (XRD) of ZnO-MgO.

5.2.3 Particle size distribution of the ZnO-MgO

The dynamic light scattering (DLS) and zeta potential characteristics of the ZnO-MgO nanoparticle are shown in Figures 5.3(a) – (b). The known quantity of ZnO-MgO was dispersed homogeneously using a probe sonicator for about 20 min. From Figure 5.3(a), the hydrodynamic particle size of the nanoparticle from the histogram is 1483 nm in diameter. From Figure 5.3(b) the nanoparticle was negatively polarized as -1 mV with a zeta charge was -0.00099 coulomb from zeta-potential analysis (Raliya and Tarafdar 2014).

(a)

Particle Size Distribution

(b)

Zeta Potential	
Mobility	-0.01u/s/V/cm
Zeta Potential	-0.1 mv
Charge	-0.00099 fC
Polarity	Negative
Conductivity	421 uS/cm
Field Strength	5.0 kV/m
Sample Information	
Fluid	
Viscosity	0.835
Temperature	27.85 C
Dielectric Const	79
Dispersant	
pH	7
Concentration	
Particle	
Concentration	
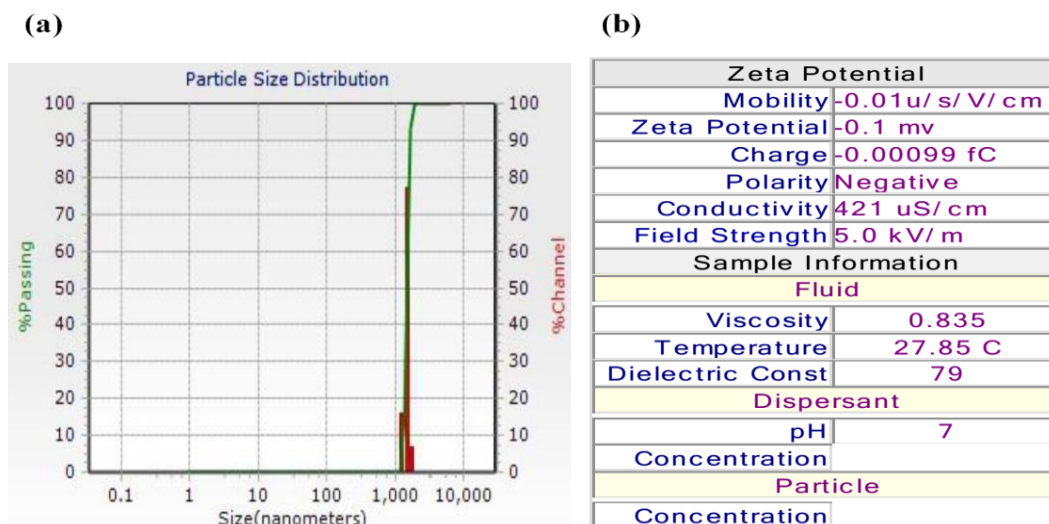
Figure 5.3 Particle size distribution data from (a) Dynamic light scattering (DLS) and (b) Zeta potential measurement.

5.2.4 Morphological study of the fabricated membranes

The cross-section and surface scanning electron microscopy (SEM) pictures of the ZnO-MgO contained membranes were illustrated in Figures 5.4 and 5.6. The asymmetric configuration morphological structure was witnessed from all prepared hollow fiber membranes. The top layer of the membrane morphology shows a dense layer and porous structure on the sublayer. There are considerable changes in the membrane cross-sectional configuration, with the dosages of hydrophilic ZnO-MgO to the PPSU dope solution. The pristine hollow fiber membranes (ZMCA-0 and ZMCAP-0) showed more extended finger-like and macro-void structures. The sponge-like structure in between the outer and inner sublayer was also evidenced, as shown in Figure 5.4(a). The incremental dosages of the ZnO-MgO (0.6, 1 and 1.5 wt%) into the PPSU dope solutions contributed to the considerable morphological modifications. The long finger-like structure was tiny and bulged in shape with increased concentrations of nanoparticles as shown in Figure 5.4(c) – (h). The possible reason behind such an outcome is the difference in dope solution viscosity. Viscosity played an essential role in establishing the specific morphological structure of the prepared membranes and the selectivity. The viscosity of the polymer dope solution is enhanced as the concentrations of the polymers increase from a neat membrane to an increased dosage of ZnO-MgO incorporated membranes. Higher viscosity hinders the non-solvent molecule by reducing the diffusion mechanism, resulting in a delayed phase inversion process. Also, the

delayed demixing was the fundamental cause for the increase in length of the finger-like morphological structures witnessed from Figures 5.4(g) and (h).

Increased dosages of nanoparticles also influenced the macrovoids morphological structure. The macrovoids are enlarged pear like structures shown in Figures 5.4(c) – (f), which cannot be identified in the neat membrane. The membrane morphological configuration with tear-drop structure is illustrated in the literature (Chong et al. 2017, 2018; Mondal and De 2015). In addition, in ZnO-MgO contained membrane, the vertical finger-like elongated structure was observed, leading to increased pure water permeability. Figure 5.6 showed the surface morphologies of the virgin and ZnO-MgO contained PPSU/CA and PPSU/CAP hollow fiber membranes. As illustrated in Figures 5.6(c) – (d), with lower dosages of nanoparticles, the membrane surface-displayed uniform and homogeneous dispersion of the nanoparticle. As demonstrated in figures 5.6(g) – (h), incremental nanoparticle dosage (1.5 wt%) causes agglomerations, which reduces the rejection performance of the fabricated hollow fiber membranes. The detailed SEM cross sectional (complete view) images were illustrated in Figure 5.5. Inner/outer diameter (ID and OD) and mean pore radius of the fabricated hollow fiber membranes were illustrated in Table 5.1.
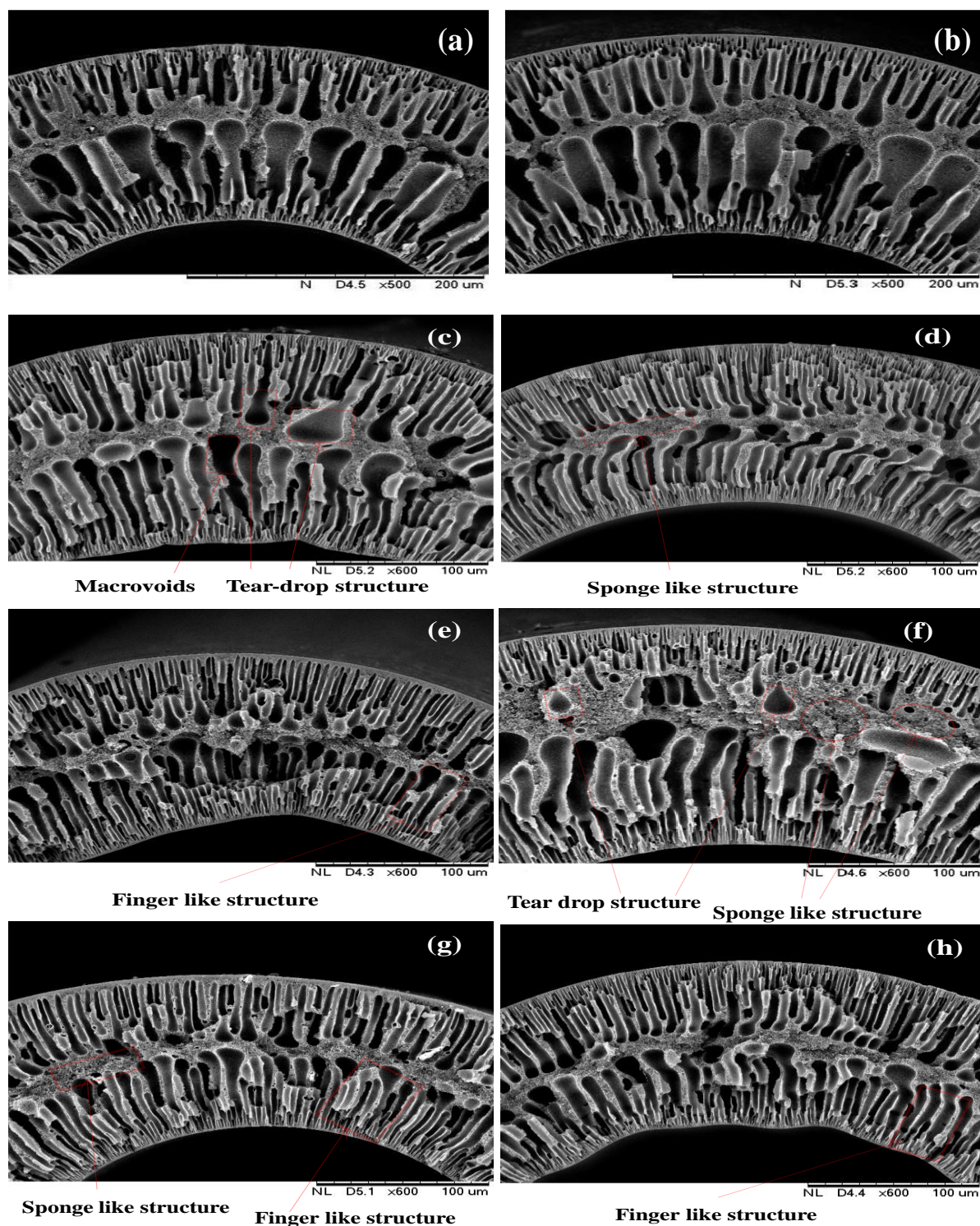
Figure 5.4 Scanning electron microscopic (SEM) cross sectional images of 'a' and 'b' neat membrane (ZMCA-0 and ZMCAP-0), 'c' cellulose acetate/polyphenylsulfone/ZnO-MgO-0.6 wt % (ZMCA-0.6), 'e' ZMCA-1 and 'g' ZMCA-1.5, 'd' cellulose acetate phthalate/polyphenylsulfone/ZnO-MgO-0.6 wt% (ZMCAP-0.6), 'f' ZMCAP-1 and 'h' ZMCAP-1.5 respectively.
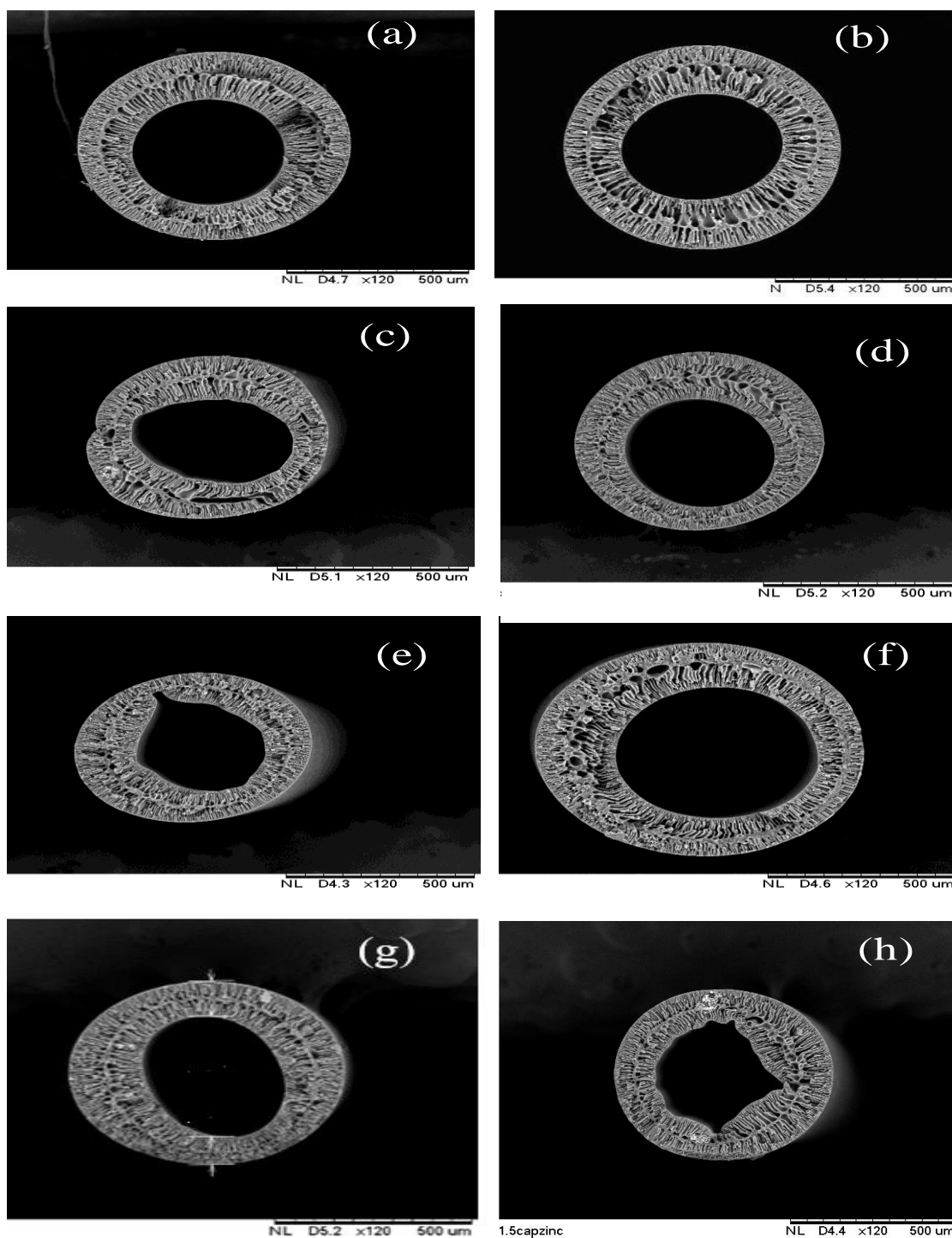
Figure 5.5 Scanning electron microscopic (SEM) cross sectional (complete view) images of 'a' and 'b' neat membrane (ZMCA-0 and ZMCAP-0), 'c' cellulose acetate/polyphenylsulfone/ZnO-MgO-0.6 wt % (ZMCA-0.6), 'e' ZMCA-1 and 'g' ZMCA-1.5, 'd' cellulose acetate phthalate/polyphenylsulfone/ZnO-MgO-0.6 wt% (ZMCAP-0.6), 'f' ZMCAP-1 and 'h' ZMCAP-1.5 respectively.
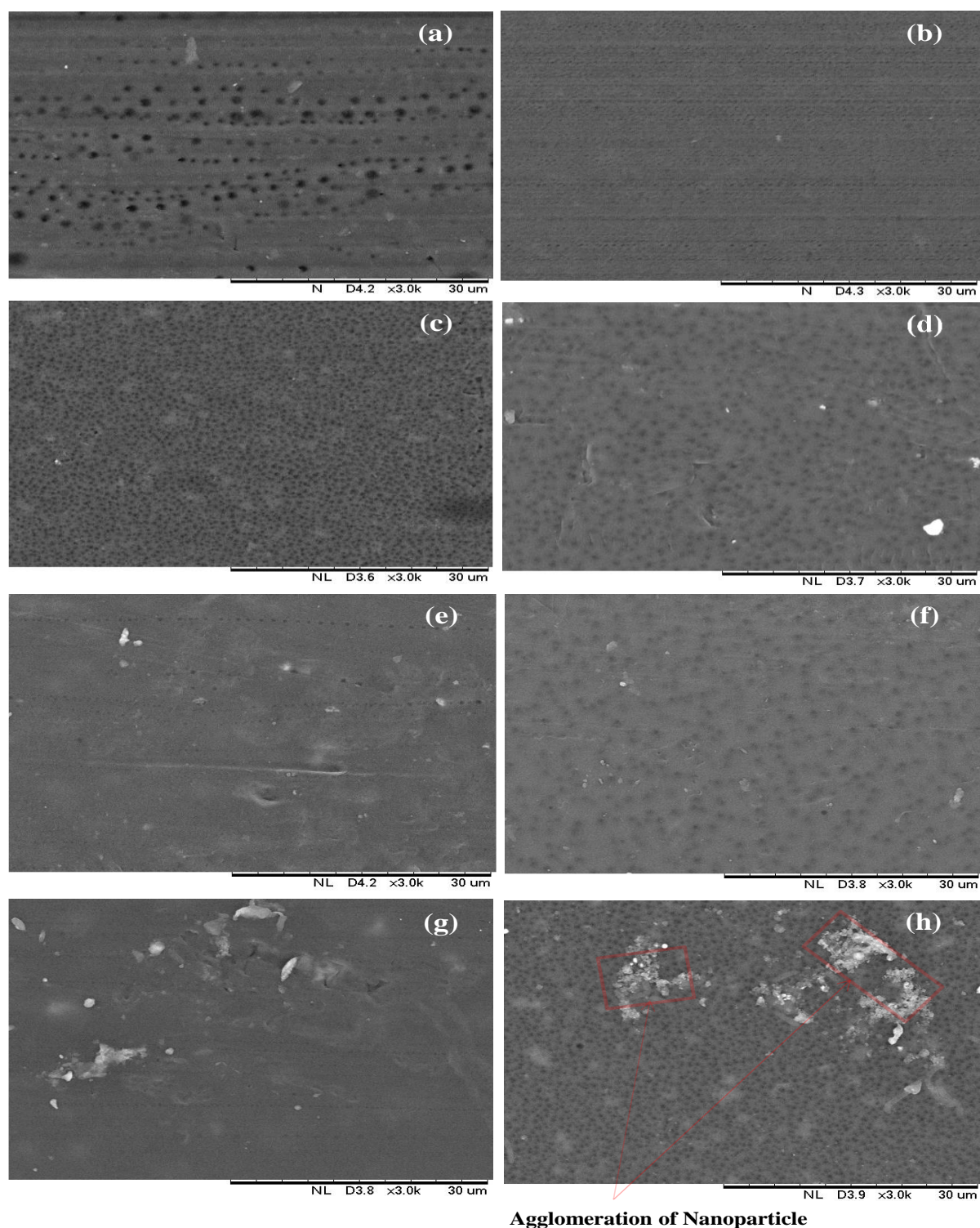
Figure 5.6 Scanning Electron Microscopy (SEM) surface images of 'a' and 'b' neat membrane (ZMCA-0 and ZMCAP-0), 'c' cellulose acetate/ polyphenylsulfone/ZnO-MgO-0.6 wt% (ZMCA-0.6), 'e' ZMCA-1 and 'g' ZMCA-1.5, 'd' cellulose acetate phthalate/polyphenylsulfone/ ZnO-MgO-0.6 wt % (ZMCAP-0.6), 'f' ZMCAP-1 and 'h' ZMCAP-1.5 respectively.

Table 5.1 Outer/ inner (OD/ID) diameter and mean pore radius of the fabricated hollow fiber membranes

Hollow fiber membranes	Outer diameter (OD in μm)	Inner diameter (ID in μm)	Mean pore radius (m)
ZMCA-0	658	354	1.365×10^{-7}
ZMCA-0.6	657	376	2.308×10^{-8}
ZMCA-1	618	357	2.473×10^{-8}
ZMCA-1.5	649	416	2.403×10^{-8}
ZMCAP-0	675	356	1.293×10^{-7}
ZMCAP-0.6	686	412	1.840×10^{-8}
ZMCAP-1	879	541	1.796×10^{-8}
ZMCAP-1.5	633	354	1.899×10^{-8}
<u>Spinneret dimension,</u> inner diameter: 550 μm, outer diameter:1100 μm			

5.2.5 Hydrophobicity/hydrophilicity of the hollow fiber membranes

The hydrophobic and hydrophilic characteristics of the prepared pristine and ZnO-MgO contained hollow fiber membranes are shown in Figure 5.7. The sessile droplet technique was used to determine the hydrophilic/phobic properties of the hollow fiber membranes. From the literature, as the hydrophilicity of the membrane surface increased, the contact angle reduced and vice versa (Hebbar et al. 2018b). From Figure 5.7, the contact angle for neat ZMCA-0 and ZMCAP-0 were 71.56° and 68.85° respectively. The incremental dosage of ZnO-MgO to the neat membrane resulted in increased hydrophilicity and reduced parameter of the contact angle. For the increased dosage of membranes ZMCA-1 and ZMCAP-1, the contact angle parameters were 60.81° and 57.32° respectively. The reduced contact angle behavior is due to the migration of the additives and nanoparticles on the surfaces of the hollow fiber membranes (Rabiee et al. 2015). The contact angle for higher dosage ZMCA-1.5 and ZMCAP-1.5 membranes were 63.85° and 60.77° respectively. The slight increase in the contact angle with the inclusion of the nanoparticle is due to the aggregation of ZnO-MgO on the surfaces of the membrane.
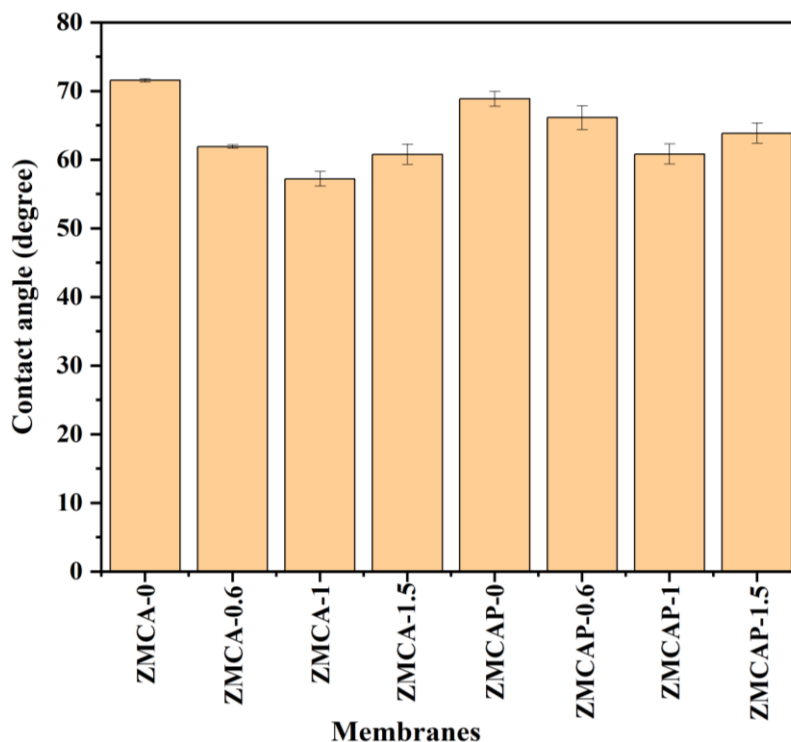
Figure 5.7 Contact angle measurement of the fabricated pristine and ZnO-MgO contained membranes.

5.2.6 Water uptake and porosity measurement studies of fabricated membranes

The percentage water uptake and porosity of the fabricated pristine and ZnO-MgO contained membranes are shown in Figure 5.8. The water absorption parameters for pristine membranes ZMCA-0 and ZMCAP-0 were 42.32% and 44.52% respectively. Due to the less porous structure and more surface hydrophobic nature, the lower the water uptake behavior (Ibrahim et al. 2018b) was observed. Incremental dosages of ZnO-MgO to the neat dope solution resulted in the increased water uptake parameters. The membrane's ZMCA-1 and ZMCAP-1 enhanced water uptake was 72.81% and 63.12% respectively. With increased concentrations of the ZnO-MgO to the pristine membrane, higher the water absorption parameters, which implies enhanced hydrophilicity by uniform dispersion of the nanoparticles provided to the hollow fiber membranes surfaces. However, nanoparticle aggregation contributes to the agglomeration on the surfaces of the membranes with a higher concentration of ZnO-MgO. It was evidenced from SEM images Figure 5.6(g) −(h) respectively. The parameters of water uptake for ZMCA-1.5 and ZMCAP-1.5 were 70.12% and 59.63% respectively. The neat ZMCA-0 and ZMCAP-0 membranes exhibited porosity parameters as 21.26% and 24.49% respectively. Thereafter, there is an enhancement in the porosity parameters as the incremental dosages of ZnO-MgO to the neat dope solution.

Membrane ZMCA-1 and ZMCAP-1 exhibited 59.73% and 55.52%, respectively. The main factors for the enhancement of the porosity are as follows. At first, the dense-like morphological structures improved due to the increased dope solution viscosity. The increased viscosity often caused delayed demixing of the phase inversion process (Kasi and Seo 2019). Secondly, the improved dosages of nanoparticles leading to thermodynamic instability causing an enhancement of the porosity on the membrane surfaces. Due to the agglomerations of further dosages of nanoparticles to PPSU dope solution, there was decrease in the porosity. It was evidenced from membranes the parameters of porosities for ZMCA-1.5 and ZMCAP-1.5 as 50.52 % and 41.38 % respectively.
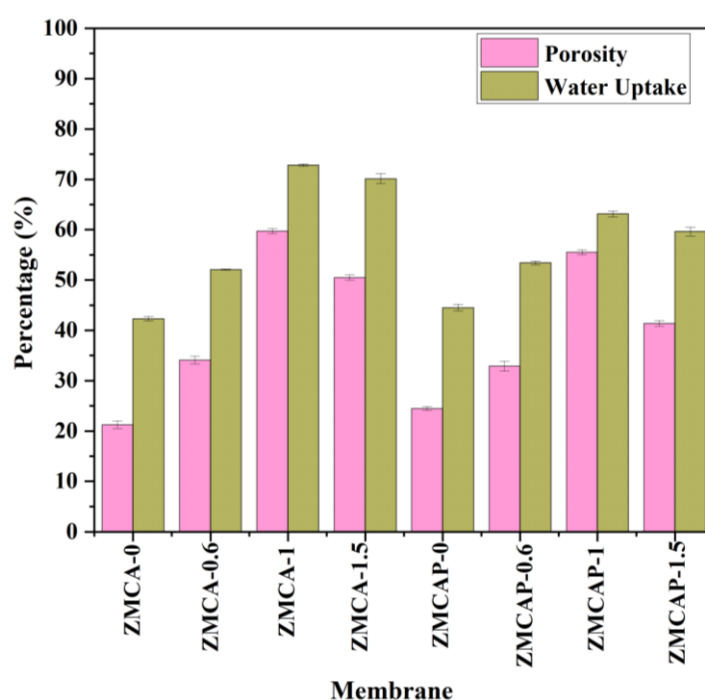
Figure 5.8 Percentage (a) porosity and (b) water uptake of fabricated neat along with increased dosages (0.6, 1 and 1.5 wt%) of ZnO-MgO incorporated membranes.

5.2.7 Pure water permeability analysis of fabricated membranes

The effect of incremental dosages of ZnO-MgO on the neat membrane (PPSU/CA and PPSU/CAP) was investigated by pure water permeability. It was illustrated in Figure 5.9(a) and (b) respectively. The pure water permeability for neat membranes ZMCA-0 and ZMCAP-0 were 49.89 and 61.34 L/m^{2}h bar respectively. From Figure 5.9(a) pure water permeabilities for the incremental dosages of the ZnO-MgO on the PPSU/CA membranes ZMCA-0.6, ZMCA-1 and ZMCA-1.5 were 94.66, 221.51 and 181.82 L/m^{2}h bar respectively. Also, from Figure 5.9(b), the pure water permeability for PPSU/CAP membranes with increased dosages

ZMCAP-0.6, ZMCAP-1 and ZMCAP-1.5 were 75.10, 86.44 and 77.38 L/m^{2}h bar respectively. The incorporation of 1.5 wt % of ZnO-MgO to the neat dope solution decreases water permeability because of the agglomeration of the nanoparticle on the membrane surfaces. It was evidenced from the SEM Figure 5.6(g) – (h). The increased nanoparticle dosages further enhanced the dense morphologies on the top surface of the membrane, which resulted in decreased water permeability (Muhamad et al. 2015).

It was proved that increased hydrophilicity from contact angle measurement also confirmed the enhancement of the pure water permeability of modified membranes. However, the water permeability has decreased because of the less porous and hydrophobic behavior. Moreover, the increase in water permeability depends on two important factors. Firstly, the incorporation of the polar functional groups (–OH and –CO) and carboxylic (–COOH) functional group on the membrane surfaces (Rabiee et al. 2015). Secondly, leaching of the ZnO-MgO and cellulose acetate derivatives in the phase inversion process improves porosities for the modified membrane. The enhanced porosity and water holding capability of the modified membranes in turn helps to improve the pure water permeability. The water permeability has reduced as the filtration time was increased, as can be observed from the membrane due to the fouling nature (Hebbar et al. 2018b; Ibrahim et al. 2017a).
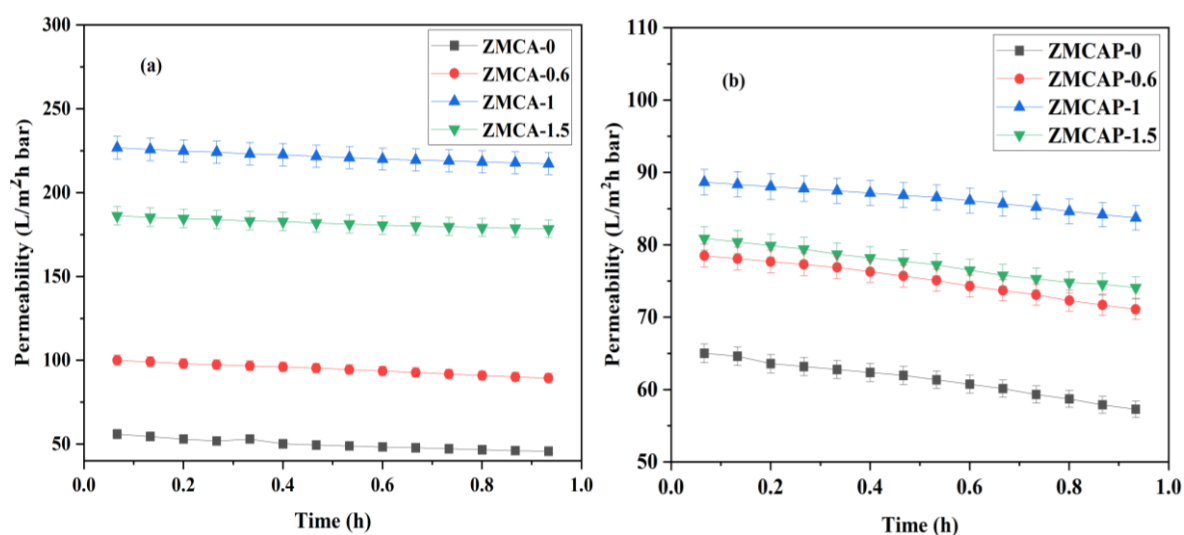
Figure 5.9 (a) Pure water permeabilities of the prepared (a) pristine membrane ZMCA-0, 0.6 wt% of the ZnO-MgO in CA/PPSU (ZMCA-0.6), ZMCA-1, ZMCA-1.5 and (b) pristine membrane ZMCAP-0, 0.6 wt% of the ZnO-MgO in CAP/PPSU (ZMCAP-0.6), ZMCAP-1, ZMCAP-1.5 respectively.

5.2.8 Antifouling properties of the membranes

The fabricated hollow fiber membrane's antifouling properties were demonstrated in Figures 5.10(a) – (b). There is a considerable fouling issue on the membrane surfaces, which reduces the hydrophilicity and pure water permeability of the membrane. With two principal classifications, membrane fouling can be reversible and irreversible fouling (Ibrahim et al. 2018b). In reversible fouling, the foulants adhered to the membrane surfaces were wiped by simple backwashing. The adhered foulants were wiped off using various chemical methods in the irreversible fouling process (Hebbar et al. 2018b). Figures 5.10(a) – (b) shows considerable decrease in water permeability from the neat membranes ZMCA-0 and ZMCAP-0 respectively. This outcome is due to the more hydrophobic and highly vulnerable nature of the membrane fouling. The improved pure water permeability of the modified membranes which is due to the incorporation of the incremental dosages of ZnO-MgO and cellulose acetate derivatives to PPSU dope solution (Chung et al. 2017; Muhamad et al. 2015). Furthermore, from Figures 5.11(c) – (d), the flux recovery ratio of the neat membranes ZMCA-0 and ZMCAP-0 was 65.42% and 69.45% respectively. The enhanced FRR of the modified membrane ZMCA-1.5 and ZMCAP-1.5 were 91.08% and 90.11% respectively. According to the role, the intensified FRR parameters suggested that the membranes have outstanding antifouling properties (Hebbar et al. 2018b).
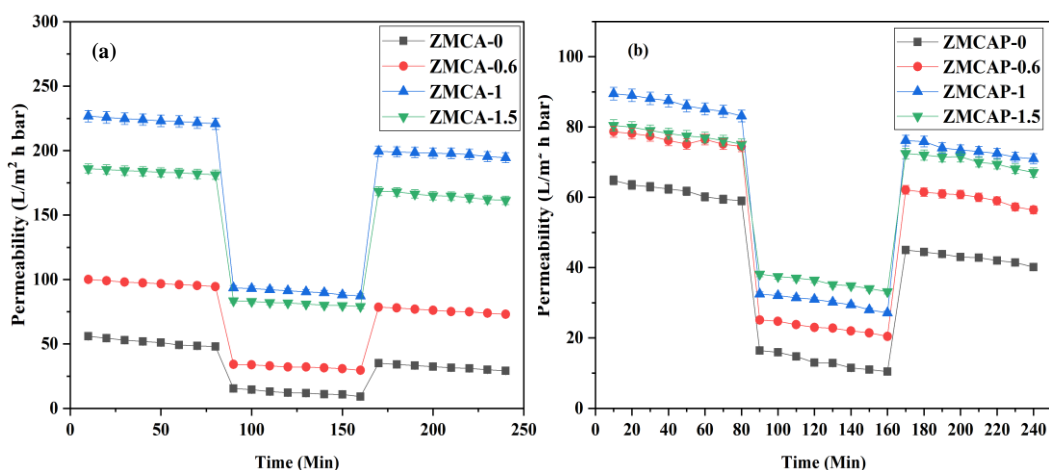
Figure 5.10 Antifouling permeability properties of the prepared (a) neat membrane ZMCA-0, 0.6 wt% of the ZnO-MgO in CA/PPSU (ZMCA-0.6), ZMCA-1, ZMCA-1.5 and (b) neat membrane ZMCAP-0, 0.6 wt% of the ZnO-MgO in CAP/PPSU (ZMCAP-0.6), ZMCAP-1, ZMCAP-1.5 respectively.

Figure 5.11 Antifouling properties (FRR - flux recovery ratio, R_r - reversible fouling and R_{ir} - irreversible fouling) of the prepared (a) pristine membrane ZMCA-0, 0.6 wt% of the ZnO-MgO in CA/PPSU (ZMCA-0.6), ZMCA-1, ZMCA-1.5 and (b) pristine membrane ZMCAP-0, 0.6 wt% of the ZnO-MgO in CAP/PPSU (ZMCAP-0.6), ZMCAP-1, ZMCAP-1.5 respectively.

5.2.9 Attenuated total reflectance–Fourier transform infrared spectroscopy (ATR-FTIR) of the fabricated membranes

ATR-FTIR studies of the fabricated neat membranes (ZMCA-0 and ZMCAP-0) along with ZnO-MgO contained membranes (ZMCA-1 and ZMCAP-0.6) illustrated in Figure 5.12. From Figure 5.12(a), ZMCA-0 membrane, the peaks at $2834.41 - 2933.51$ cm^{-1} assigned to –CH$_2$ (alkane group) vibrational stretching, 3325.41 cm^{-1} assigned to hydroxyl (–OH) group, peaks $1585.12 - 1654.21$ cm^{-1} were due to carboxyl group (–C=O). The peak observed at 1482.12 cm^{-1} was assigned as O=C−OR group, –C–O– group due to the cyclic ether peak appeared at 1234.10 cm^{-1} and –C–H functional group appeared at 869.81 cm^{-1} due to the vibration stretching respectively. From Figure 5.12(b), the membrane ZMCAP-0 demonstrated the peak at $2834.12 - 2936.21$ cm^{-1} allocated to the –CH$_2$ group as associated to –C–H methyl group in symmetric stretching. The 3359.52 cm^{-1} attributed to a stretching group of –OH, carbonyl C=O group at the peak of 1739.39 cm^{-1} respectively. Additionally, 1236.5 cm^{-1} functional group was assigned to the ether-cyclic group (–C–O–). The C−O−C group was assigned to the peak of $1036 - 1105$ cm^{-1} for vibrational stretching. The peak 1600.98 cm^{-1} functional group attributed to aromatic ring related to conjugated vinyl –C=C– group (Kumar et al. 2019c).

Furthermore, from Figure 5.12(c), the membrane ZMCA-1 showed the peak at 3538.02 − 3605.79 cm⁻¹ attributed to the –OH strong stretching vibration, –CH$_2$ stretching vibration attributed to the peak 2851.82 − 2927.11 cm⁻¹, the –C–O– stretching vibration was attributed to the peak 1103.37 − 1148.99 cm⁻¹ respectively. The peak at 1031.99 − 1103.37 cm⁻¹ ascribed to –C−O−C stretching vibration and 1234.35 cm⁻¹ associated with cyclic ether group. The peak 664.21 cm⁻¹ represents the ZnO stretching vibration. From Figure 5.12(d), membrane ZMCAP-0.6 demonstrated the following peaks at 3423.83 − 3550.60 cm⁻¹ considered to –OH stretching vibration, 2853.39 − 2927.51 cm⁻¹ was ascribed to –CH$_2$ vibration stretching (alkane), peak at 1140.94−1150.43 cm⁻¹ attributed to C−O−C vibrational stretching, the peak 1643.98 cm⁻¹ assigned to the carbonyl functional groups. The peak 664.22 cm⁻¹ is due to the ZnO stretching vibration (Gurunathan et al. 2019).
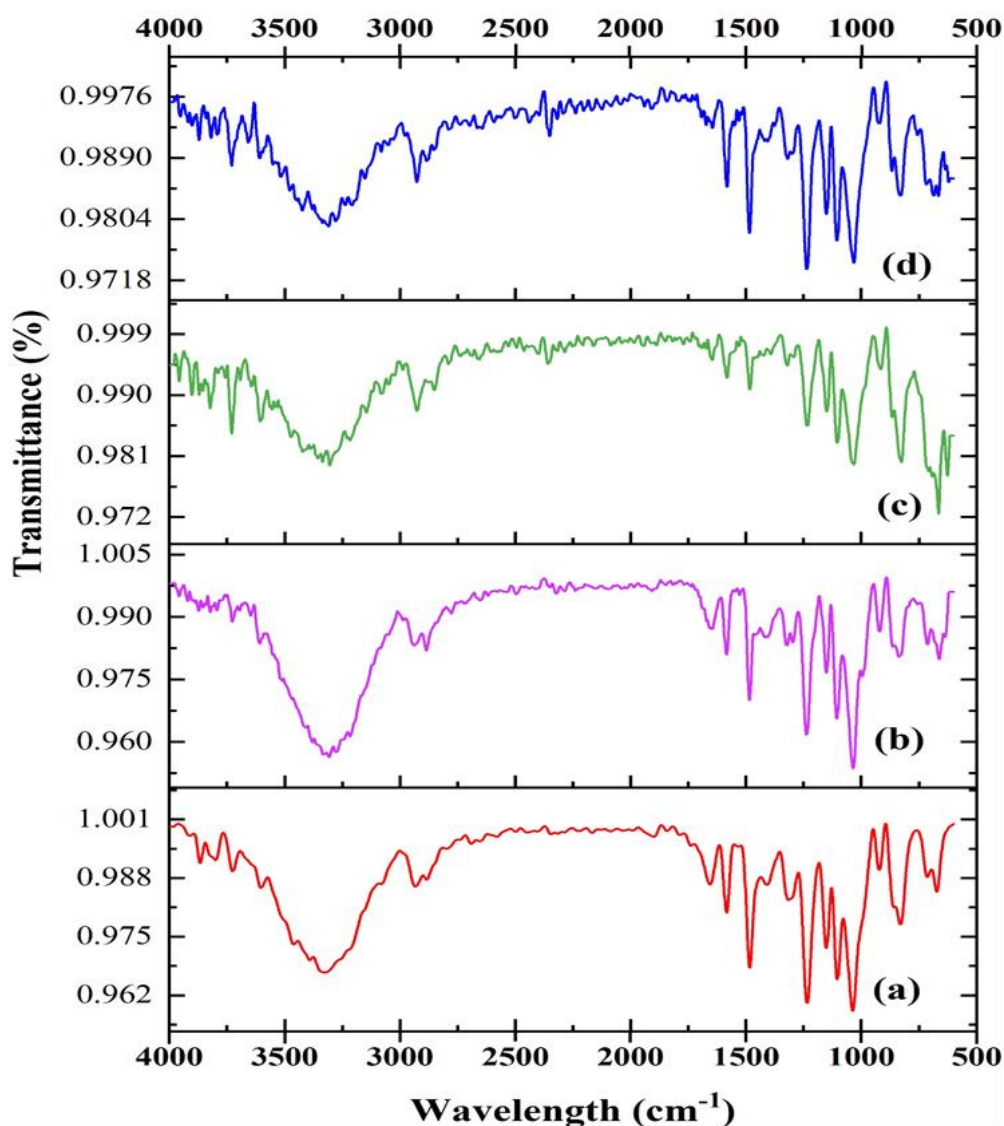
Figure 5.12 ATR-FTIR of fabricated neat membranes (a) ZMCA-0 (b) ZMCAP-0 and best-performed membranes (c) ZMCA-1 and (d) ZMCAP-0.6.

5.2.10 X-ray photoelectron spectroscopy (XPS) studies of the fabricated membrane

The XPS wide and narrow spectra of the best performing membrane (ZMCAP-0.6) was illustrated in the Figure 5.13. The important three binding exertion peaks were at 531.92 eV, 284.90 eV and 168.10 eV assigned to oxygen (O1s), carbon (C1s) and sulfur (S2p) respectively. Figure 5.13(a2) – (d) exhibited deconvolution of the O1s, C1s and S2p elements respectively. From Figure 5.13(b), the energies 534.7 eV, 534.1 eV, 533.3 eV, 532.6 eV, 531.9 eV and 530.9 eV were attributed to $-O_2/H_2O$, $-C-O-C$, $-C-O$, $-O=C-O$, $-C-OH$ and $-COOH$ respectively for O1s element (Sotoma et al. 2015; Yu et al. 2018). The binding energy 530.9 eV is also attributed to the sulfonyl functional group (O=S=O) (Muleja and Mamba 2018). From Figure 5.13(c), the energy peaks 287.7 eV, 286.6 eV, 286 eV, 285 eV and 284.2 eV assigned to $-C=O$, $-C-OH$, $-C-N$, $-C-C$ and $-C=C$ groups respectively for C1s element (Thirukumaran et al. 2019). From Figure 5.13(d), binding energies 170.6 eV, 169.2 eV, 168.1 eV and 167.3 eV were attributed for oxidized sulphur ($-Sox^-$), sulphate (SO_4^{2-}), C-$SO^{2-}.Na^{(+)}$ group, sulphite (SO_3^{2-}) group respectively. The important energy peaks 168.1 eV and 169.2 eV attributed to $S2p_{(3/2)}$ and $S2p_{(1/2)}$ respectively (Siow et al. 2018; Wang et al. 2019). The binding energy 1045.1 eV was assigned $Zn2p_{(1/2)}$ and the peaks at 1023.04 eV attributed to $Zn2p_{(3/2)}$ respectively (Ray et al. 2019). The magnesium oxide peaks Mg1s occurred at 1023.04 eV respectively (Hu et al. 2019). Therefore, the occurrence of incorporated nanoparticle and additives on the hollow fiber membrane surfaces were shown from XPS analysis.
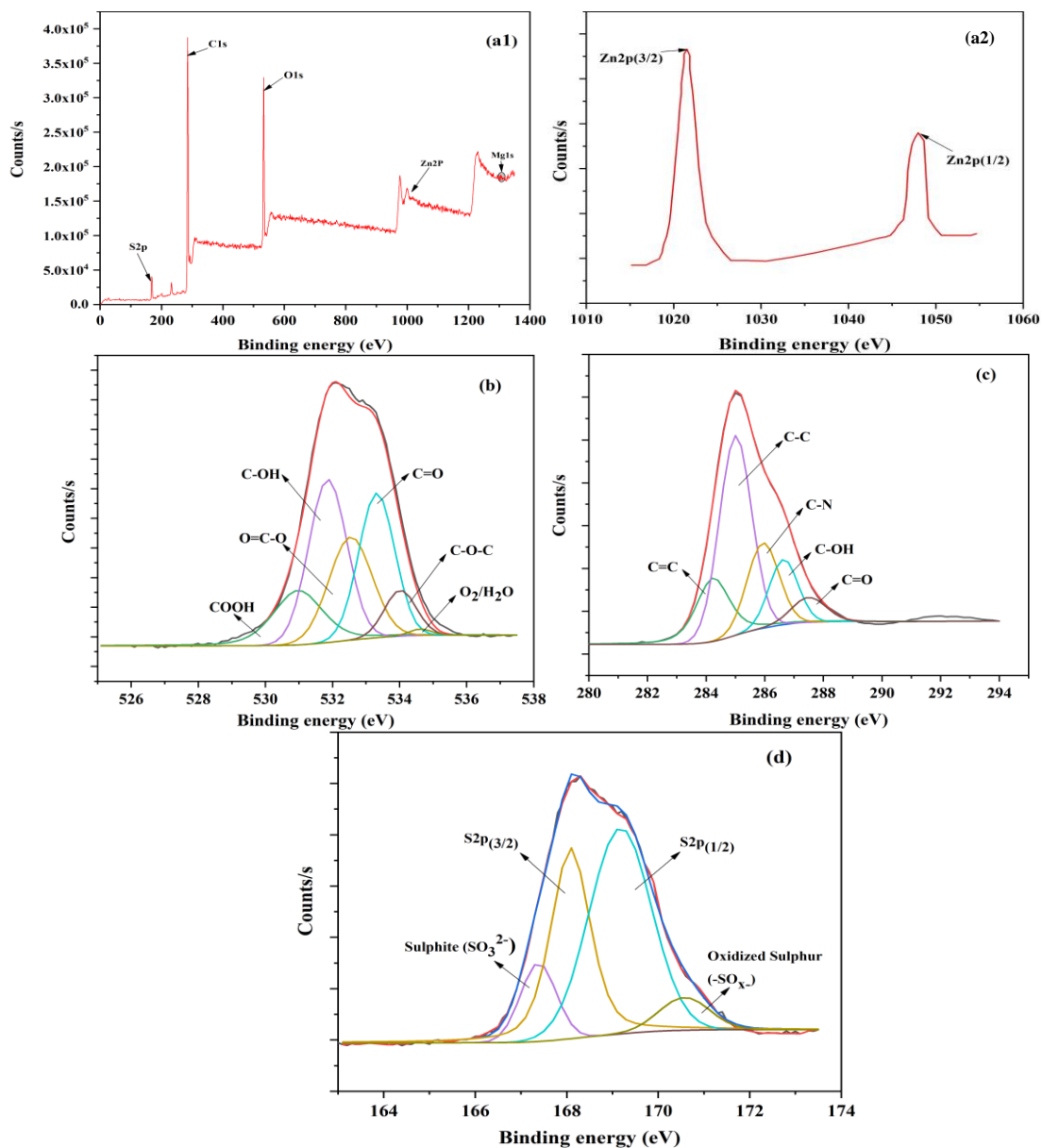
Figure 5.13 (a1) X-ray photoelectron spectroscopy (XPS) wide spectrum of the ZMCAP-0.6 membrane, (a2) narrow spectrum of zirconium (Zn2p) and (b), (c) and (d) are narrow spectrum of O1s, C1s and S2p respectively.

5.2.11 Thermogravimetric analysis (TGA) of the fabricated membranes

The thermal decomposition of the neat and ZnO-MgO blended hollow fiber membranes is illustrated in Figure 5.14, which illustrates the degradation in respective three stages with different concentrations of the ZnO-MgO to neat membranes. The initial deterioration begins from room temperature to 185 °C because of the evaporation of the volatile matters on the membrane surfaces. The next degradation level was from 190 °C to 570 °C showing remarkable thermal degradation of the cellulose acetate derivatives polymeric chains. The

degradation was above 600 °C in the third step is due to the carbonization of the used polymers, which degraded into ash. This illustration was equivalent to literature (Dehkordi et al. 2015a). Additionally, the temperature decomposition in the case of ZnO-MgO contained membranes ZMCA-1 and ZMCAP-0.6 was more or less similar and illustrated as follows. During the initial stage of the process, the volatilizing of the moisture content was initiated from room temperature to 190 °C. The following process of degradation step revealed substantial temperature degradation of the polymer chains from 200 °C to 600 °C. The polymeric chains completely degraded and resulted into ash in the final level above 610 °C (Pandas and Fazli 2018). It is also noted that weight loss was reduced as the nanoparticle concentration increased in the PPSU dope solution. This in turn helped for the enhancement of the thermal stability of the modified membranes.
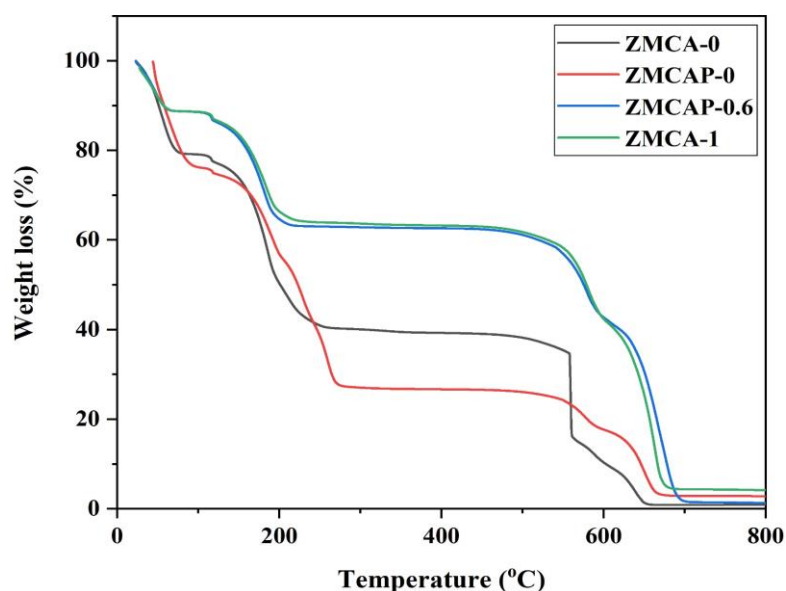
Figure 5.14 Thermogravimetric analysis (TGA) of the neat membranes (ZMCA-0 and ZMCAP-0) and 1 wt % of ZnO-MgO contained CA/PPSU membrane (ZMCA-1), 0.6 wt % of ZnO-MgO contained CAP/PPSU (ZMCAP-0.6) respectively.

5.2.12 Molecular weight cut off study

The molecular weight cut off of the good performing membrane (ZMCAP-0.6) was demonstrated in Figure 5.15. The membrane molecular weight cut off was determined to be 17089 Da. The PEG rejection percentage from ZMCAP-0.6 was found to be 67.86%, 80.14% and 92.66% for PEG-4000, PEG-6000 and PEG-20000 respectively. From the molecular weight cut off study it is demonstrated that, as fabricated membrane was ultrafiltration membrane.
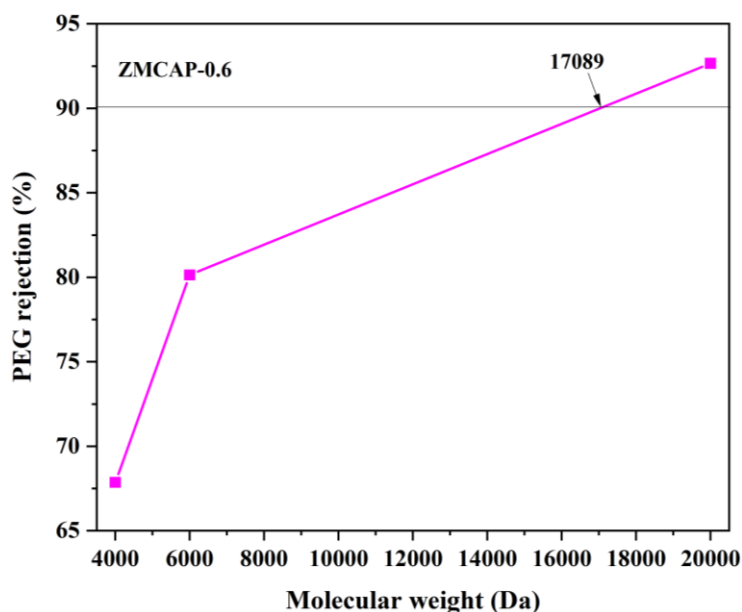
Figure 5.15 Molecular weight cut off study of the membrane (ZMCAP-0.6).

5.2.13 Atomic force microscopy (AFM) of fabricated membranes

Three-dimensional photographs containing pristine and ZnO-MgO incorporated membranes were illustrated in Figure 5.16. It showed reasonably high surface roughness properties for incremental concentrations of ZnO-MgO in PPSU neat membranes. From Table 5.2, the surface roughness (R_a) parameters for pristine membranes ZMCA-0 and ZMCAP-0 were 14.51 nm and 21.35 nm respectively. In addition, the pristine membranes represented more valleys and peaks like structures on the membrane's surfaces. ZMCA-1 and ZMCAP-1 membranes exhibited R_a parameters as 49.75 nm and 53.62 nm respectively. The incremental concentrations of the ZnO-MgO in neat (CA/PPSU and CAP/PPSU) dope solutions revealed the enhancement of the agglomerations of the nanoparticle on the membrane. From Figure 5.6, the increased surface roughness of the membrane was also confirmed by SEM surface morphologies. The incremental dosages of ZnO-MgO resulted in the enhancement of the peaks and valleys on the membranes surface, which also exhibited the enhanced surface roughness. It intends to increase the filtration area and the pore size on the membrane surface (Verliefde et al. 2008a). The increased surface area was also verified by enhanced surface roughness properties such as root mean square (R_q) and the average of the five highest peaks and valleys (R_z).

Table 5.2 Roughness properties of fabricated membranes surfaces

Hollow fiber membranes Code	R_{max} (%)	R_z (nm)	R_a (nm)	R_q (nm)
ZMCA-0	203	8.26	14.51	29.62
ZMCA-0.6	264	11.42	27.26	35.01
ZMCA-1	324	19.52	39.48	49.54
ZMCA-1.5	456	26.02	49.75	63.16
ZMCAP-0	252	12.53	21.35	39.31
ZMCAP-0.6	310	15.20	37.01	46.35
ZMCAP-1	372	27.78	45.20	58.40
ZMCAP-1.5	508	34.56	53.62	65.21
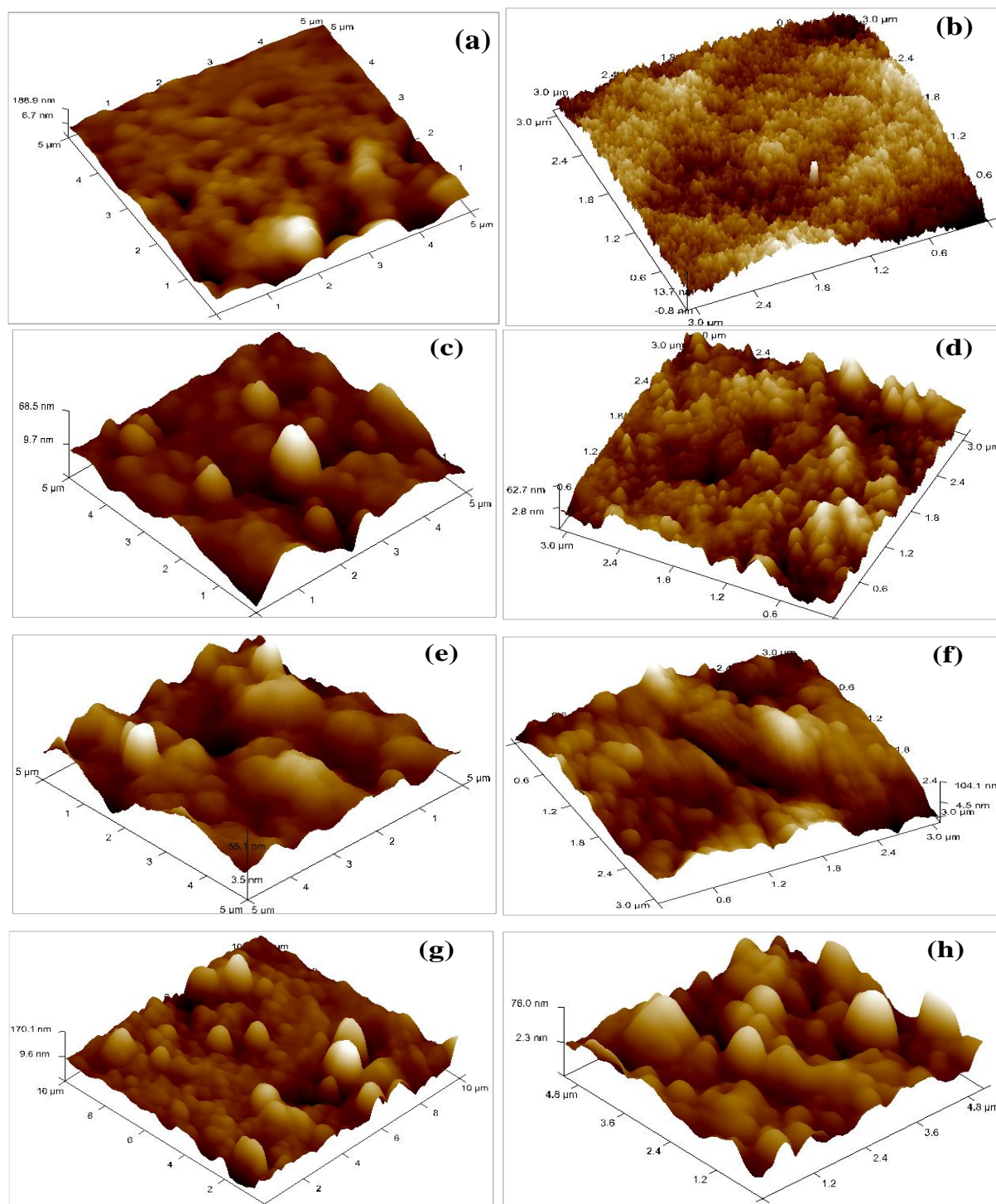
Figure 5.16 3-Dimensional surface roughness of the prepared 'a' neat membrane ZMCA-0, 'c' 0.6 wt% of the ZnO-MgO in CA/PPSU (ZMCA-0.6), 'e' ZMCA-1, 'g' ZMCA-1.5 and 'b' neat membrane ZMCAP-0, 'd' 0.6 wt% of the ZnO-MgO in CAP/PPSU (ZMCAP-0.6), 'f' ZMCAP-1, 'h' ZMCAP-1.5 respectively.

5.2.14 Surface potential analysis of the fabricated membrane

The good-performing membrane (ZMCAP-0.6) surface potential measurement was carried out, illustrating the zeta potential and different pH ranges on the X-axis and y-axis respectively, represented in Figure 5.17. The presence of intensity of surface potential with respect to different pH was measured using zeta potential analysis (Ibrahim et al. 2017a). The ZMCAP-0.6 membrane surface was negatively charged in the pH range of 2.5 to 9.45. From Figure 5.17, the surface potential (zeta potential) was subjected to an acidic level as the pH was intensified. The ZMCAP-0.6 best performing membrane experienced the isoelectric point (IEP) at pH 2.4. At this pH level, no surface potential was noticed on the membrane. The surface of the membrane was positively charged at pH 1.9 with the surface potential of 11.20 mV and negatively charged with the surface potential of -51.19 mV at pH 9.46 respectively. The negatively charged surfaces repelled more negatively charged arsenate oxide (AsO_4^{3-}). The existence of the carboxyl acid group and hydroxyl groups from the used nanoparticle and additives is the main cause for the negative charge of the membrane (Hebbar et al. 2018b; Kumar et al. 2020a).
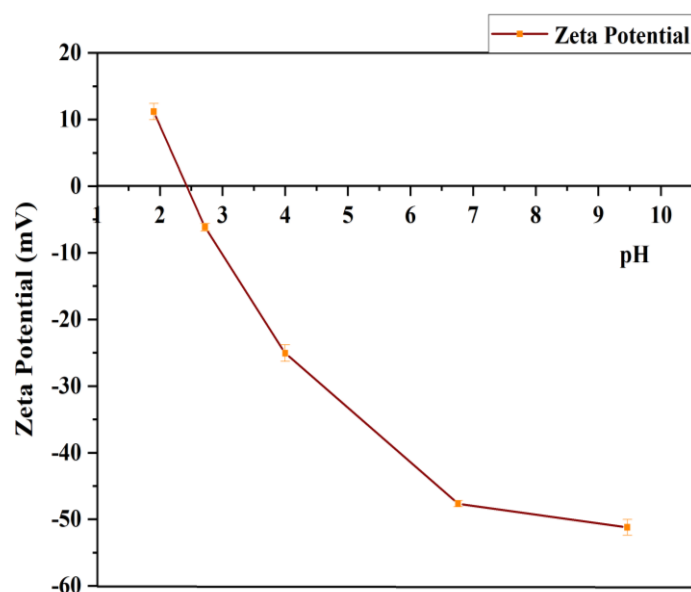
Figure 5.17 Surface potential measurement of ZMCAP-0.6 membrane with respect to pH.

5.2.15 Studies of arsenate oxide rejection from fabricated hollow fiber membranes

The removal of arsenate oxide (AsO_4^{3-}) from fabricated hollow fiber membranes were represented in Figure 5.18(a) – (b). The arsenic-V removal from membranes was analyzed with 1 ppm laboratory prepared arsenic-V aqueous solution (pH~6.8±0.2) from standard arsenic solution (H_3AsO_4) at 1 bar transmembrane pressure. The H_3AsO_4 solution was

converted to AsO_4^{3-} after ionizing with water (H_2O) which was demonstrated in Equation 3.1. The arsenate oxide rejection for the neat membranes ZMCA-0 and ZMCAP-0 was 19.89% and 27.53%, with the permeability of 40.01 and 54.75 L/m^2h bar respectively. The decreased AsO_4^{3-} rejection parameter was observed from neat membranes is due to the increased hydrophobic and less negative charge sites on the membrane (Kumar et al. 2019c). Intensified ZnO-MgO concentrations (0.6, 1 and 1.5 wt%) in the neat dope solution offer a significant enhancement in arsenate rejection properties. The efficient decontamination of the arsenate oxide was witnessed with increased dosage membranes ZMCA-1 and ZMCAP-0.6 as 78.48% and 81.31% with the permeability of 198.47 L/m^2h bar and 69.58 L/m^2h bar respectively. The hollow fiber membranes incorporated with ZnO-MgO exhibited negatively charged surfaces, which in turn helps in the electrostatic repulsion of negatively charged AsO_4^{3-} of the synthetic solution of arsenic (Verliefde et al. 2008a). The mechanism for the arsenate oxide removal from the membrane surfaces is demonstrated in Figure 5.20. Also due to the homogeneous blend of additives (CA and CAP) along with nanoparticles (ZnO-MgO) in the dope solution helps in efficient rejection of arsenic-V from the membrane surfaces (Durthi et al. 2018c). As such, the possible interaction between polyphenylsulfone/cellulose acetate and polyphenylsulfone/cellulose acetate phthalate was illustrated in Figures 5.21(a) and (b). The rejection of arsenate oxide from ZMCA-0.6 was 16.86%. It was lesser than the arsenate removal properties from neat membrane ZMCA-0, which doesn't indicate the influence of the ZnO-MgO dosage on the membrane surfaces. With the highest dosage of ZnO-MgO (1.5 wt%) membranes, ZMCA-1.5 and ZMCAP-1.5 were 6.34% and 41.28%, with permeability of 61.02 L/m^2h bar and 142.30 L/m^2h bar respectively. The decreased rejection parameter for arsenic-V is due to the concentration polarization on the membrane surfaces and less availability of negatively charged sites on the membrane (Kumar et al. 2020a). The blocking of the membrane surface pores due to the agglomeration, influences the reduced permeability with increased nanoparticle dosage membranes was observed from Figures 5.19(a) and (b). In previous studies, we fabricated hollow fiber membranes for the enhanced rejection of arsenic-V. Membranes prepared by 1 wt% of ZrO_2 in PPSU/CA (PZCA-1) and 0.6 wt% of ZrO_2 in PPSU/CAP (PZCAP-0.6) membranes removes 87.27% and 70.48% with permeability of 89.94 L/m^2h bar and 70.59 L/m^2h bar respectively (Kumar et al. 2020a). The improved rejection of arsenate from the ZMCA-1 membrane was 78.48% with the rejection permeability of 198.47 L/m^2h bar at 1 bar transmembrane pressure. Therefore, CA/PPSU and CAP/PPSU immobilized with incremental dosages of ZnO-MgO hollow fiber membranes were desirable for the enhanced arsenate rejection without compromising the permeability of

arsenate oxide rejection. The concentration polarization for arsenic-V removal of the fabricated hollow fiber membranes was illustrated in Table 5.3.

Arsenic concentration: 1 mg/L
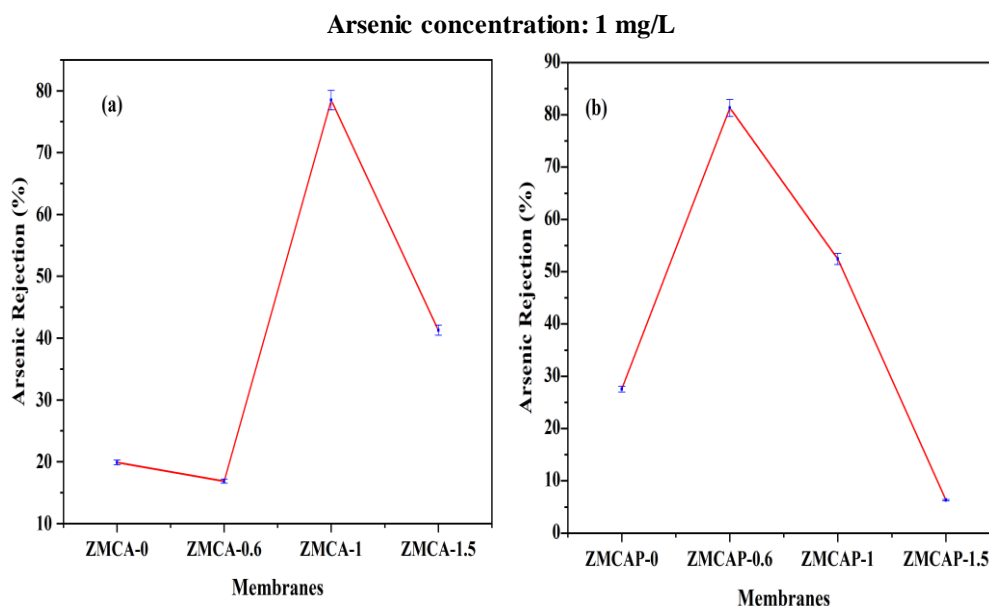
Figure 5.18 Comparison of arsenate oxide (AsO_4^{3-}) removal studies from fabricated (a) neat membrane ZMCA-0, 0.6 wt% of the ZnO-MgO in CA/PPSU (ZMCA-0.6), ZMCA-1, ZMCA-1.5 and (b) neat membrane ZMCAP-0, 0.6 wt% of the ZnO-MgO in CAP/PPSU (ZMCAP-0.6), ZMCAP-1 and ZMCAP-1.5 respectively.
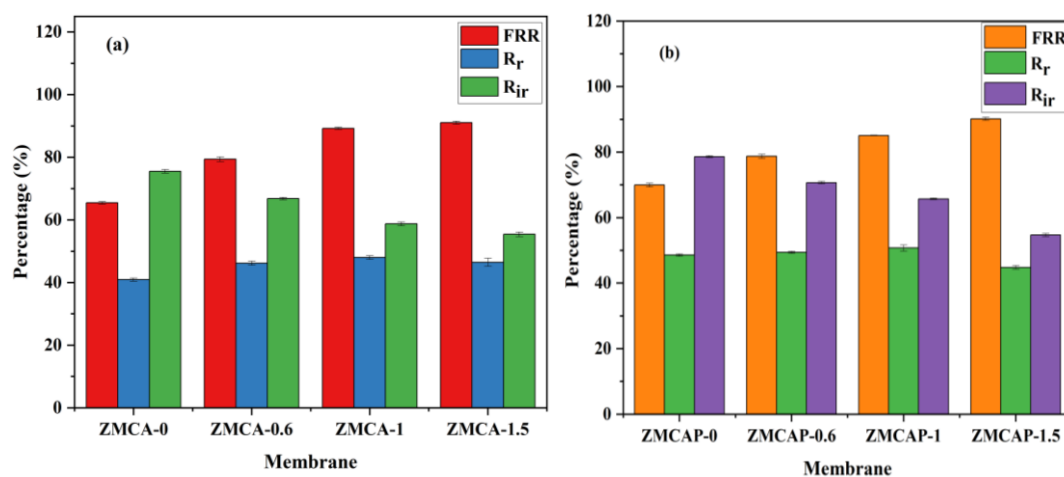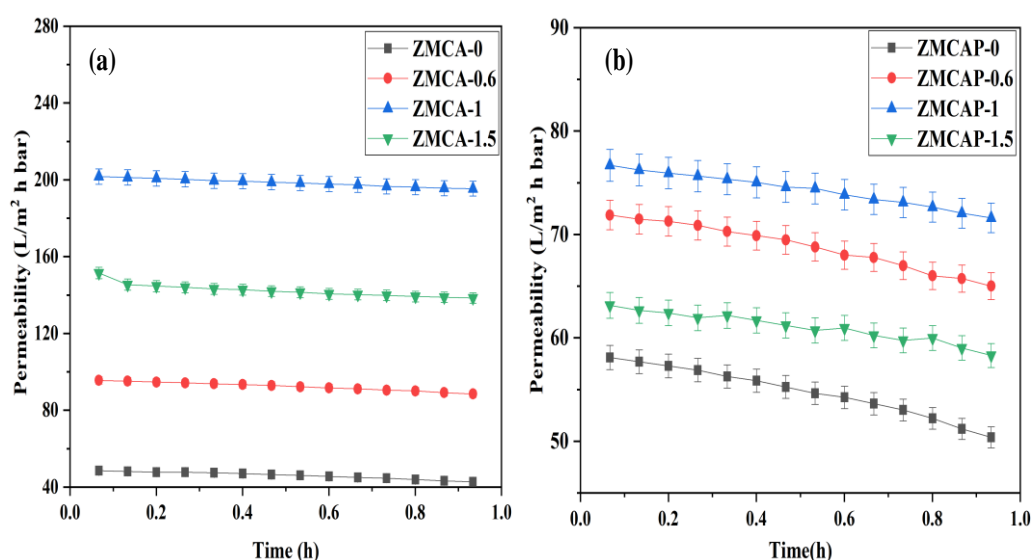

Figure 5.19 Arsenate oxide (AsO_4^{3-}) permeability of the prepared (a) neat membrane ZMCA-0, 0.6 wt% of the ZnO-MgO in CA/PPSU (ZMCA-0.6), ZMCA- 1, ZMCA-1.5 and (b) neat membrane ZMCAP-0, 0.6 wt% of the ZnO-MgO in CAP/PPSU (ZMCAP-0.6), ZMCAP-1 and ZMCAP-1.5 respectively.
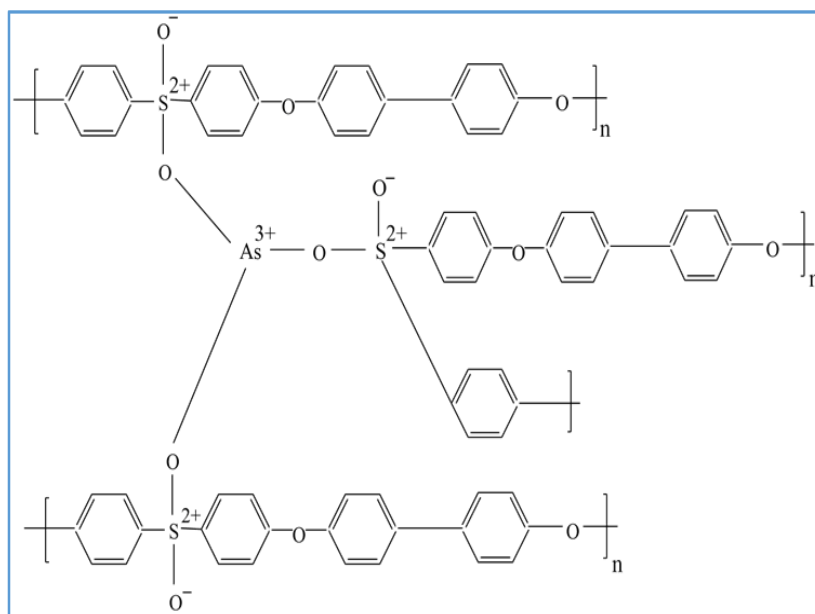
Figure 5.20 Proposed arsenic (AsO$_4^{3-}$) removal mechanism from membranes.

(a)
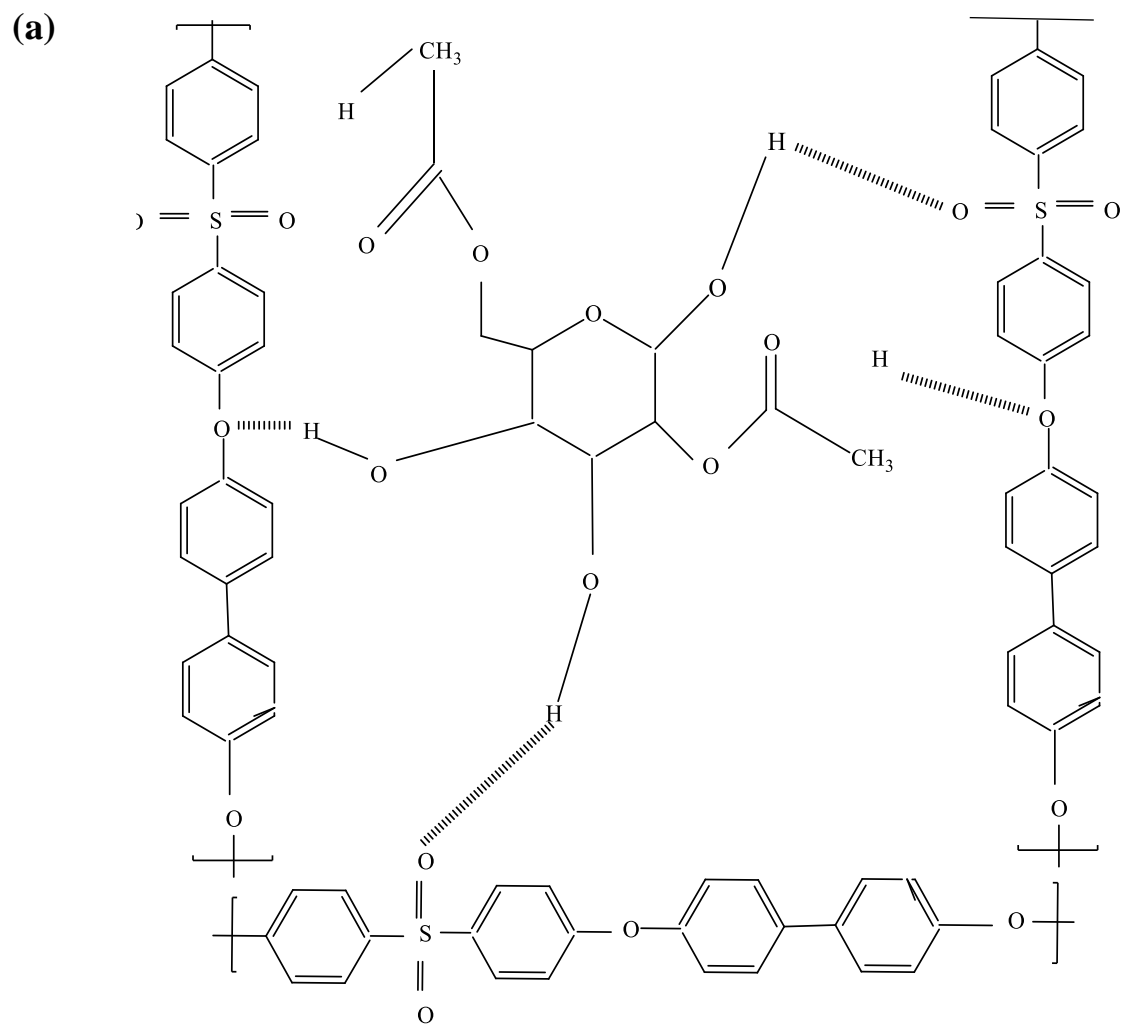
(b)
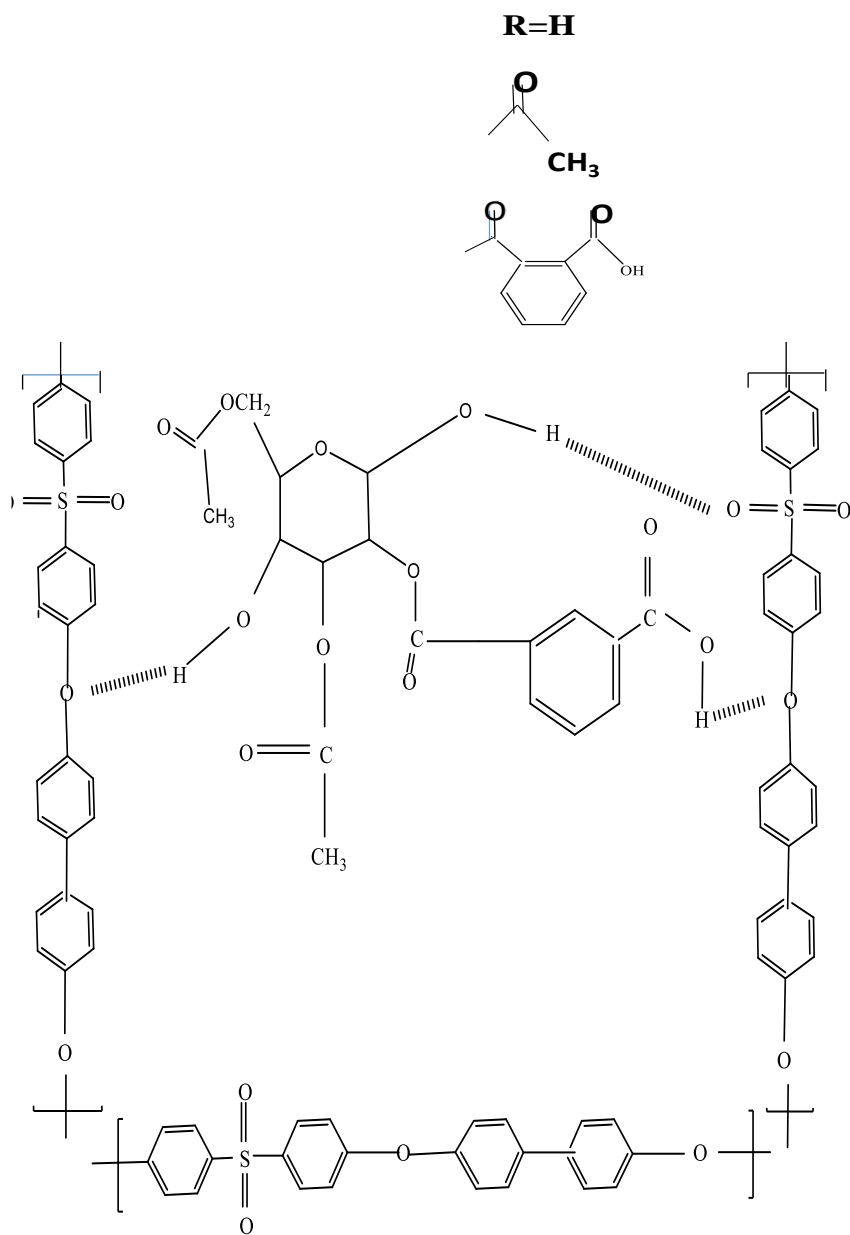
Figure 5.21 (a) Possible interactions between polyphenylsulfone and cellulose acetate and (b) Possible interactions between polyphenylsulfone and cellulose acetate phthalate.

Table 5.3 Concentration polarization for arsenic-V removal of the fabricated hollow fiber membranes.

Membrane codes	Velocity (v) (m/s)	Mass transfer coefficient (K) $\times 10^{-5}$ (m/s)	Concentration polarization ($\frac{Cm}{Cb}$)
ZMCA-0	0.06671	2.057	1.1008
ZMCA-0.6	0.00521	1.441	1.1079
ZMCA-1	0.01296	2.019	3.74
ZMCA-1.5	0.01328	2.127	3.54
ZMCAP-0	0.07938	3.55	1.1059
ZMCAP-0.6	0.00502	1.444	1.626
ZMCAP-1	0.00443	1.272	1.727
ZMCAP-1.5	0.00403	1.296	1.0483

Possible interactions of polyphenylsulfone and zinc-magnesium oxide

Polyphenylsulfone-zinc –magnesium oxide (ZnO-MgO) interaction. For interpretation of PPSU-ZnO-MgO, it was noted that there is no hydrogen bonding interaction between the polymers. However, there is a 'Van der Waals' interaction and ion-dipole interaction between Zn-PPSU and Mg-PPSU polymer.

5.3 SUMMARY OF THE PRESENT WORK

Hollow fiber membranes from polyphenylsufone/cellulose acetate derivatives and increased dosages of ZnO-MgO ultrafiltration were fabricated using the non-solvent induced phase separation (NIPS) process. The crystalline nature of the ZnO-MgO nanoparticle was confirmed from TEM and XRD analysis. The FITR and XPS analysis confirmed the blending of additives and nanoparticles on the membrane surfaces with different exertion peaks and binding energies. The extended finger-like projections and macrovoids with increased nanoparticle concentrations on the neat membranes were confirmed using SEM analysis. From AFM topographical analysis, surface roughness (R_a) from neat membranes ZMCA-0

and ZMCAP-0 were 14.15 nm and 21.35 nm respectively. The roughness was increased with increased dosages of nanoparticle for ZMCA-1.5 and ZMCAP-1.5 was 63.16 nm and 65.21 nm respectively. Additionally, the increased concentrations of the ZnO-MgO also enhances the hydrophilicity, water uptake and pure water permeability. The gradual enhancement in the FRR parameter for pristine membrane ZMCA-0 and ZMCAP-0 was 65.42% and 69.95% to increased dosage membranes ZMCA-1.5 and ZMCAP-1.5 were 91.08% and 90.11% respectively. Furthermore, the increased FRR parameters from pristine membranes to the highest additive dosage membranes imply significant improvement of antifouling behavior. The zeta potential study showed that the surface of the membrane was negatively charged from pH 2.4 to pH 9.46, with an increased surface potential of -51.59 mV. The rejection properties of arsenate oxide from the pristine membranes were ZMCAP-0.6 and ZMCA-1 was 81.31% and 78.48% corresponding permeabilities were 69.58 L/m^2h bar and 198.47 L/m^2h bar respectively. The enhanced removal of the arsenate from the ZnO-MgO modified membranes was due to the oxidation of arsenic (H_3AsO_4) to arsenate oxide (AsO_4^{3-}) and increased electrostatic repulsion from negatively charged membrane surfaces. In addition, arsenate oxide rejection from the aqueous solution is often due to amine and carboxylic functional sites on the membrane surfaces. However, there is a decreased arsenate rejection with the increased concentrations of ZnO-MgO to the neat dope solution. The reduced arsenate oxide is due to the concentration polarization on the hollow fiber membrane surfaces. This consequence revealed that prepared membranes were suitable for enhanced arsenate removal from arsenic-V contaminated aqueous solution.

CHAPTER -6

NANO-ALUMINUM OXIDE BLENDED CELLULOSE ACETATE/ POLYPHENYLSULFONE DERIVATIVES HOLLOW FIBER MEMBRANES: FABRICATION, CHARACTERIZATION AND ARSENIC-V REMOVAL FROM WATER

Abstract

Hollow fiber ultrafiltration membranes were prepared using intensified concentrations of nano-aluminum oxide (0.6, 1 and 1.5 wt%) in cellulose acetate /polyphenylsulfone and cellulose acetate phthalate /polyphenylsulfone by a non-solvent induced phase separation process. The crystalline structure and morphology of the used nano-aluminum oxide (nano-Al_2O_3) were analyzed using X-ray diffraction (XRD) and transmission electron microscopy (TEM) respectively. The effect on membrane morphology and topographical structures of different dosages of nano-aluminum oxide, cellulose acetate and cellulose acetate phthalate was studied using scanning electron microscopy (SEM) and atomic force microscopy (AFM). Fourier transform infrared spectroscopy (FTIR) and x-ray photoelectron spectroscopy (XPS) studies have been evaluated the presence of nano-aluminum oxide, cellulose acetate and cellulose acetate phthalate on membranes surfaces. Thermogravimetric analysis (TGA) revealed the thermal stability of hollow fiber membranes. The 1.5 wt% of nano-aluminum oxide in cellulose acetate /polyphenylsulfone (ALCA-1.5) membranes surface potential was analyzed using zeta potential analysis. In addition, the incremental dosages of nano-aluminum oxide also contributed to increased arsenic-V removal from membranes. As such ALCA-1.5 and 1 wt% of nano-aluminum oxide in cellulose acetate /polyphenylsulfone (ALCA-1), hollow fiber membranes decontaminated 98.67% and 94.89% with permeabilities were 88.41 L/m^{2}h bar and 53.53 L/m^{2}h bar respectively with 1 ppm of arsenic-V aqueous solution (pH 6.8±0.2) at 1 bar transmembrane pressure. Reduced arsenic-V removal properties from nano-aluminum oxide /cellulose acetate phthalate /polyphenylsulfone hollow fiber membranes have also been established with increased concentrations of nano-aluminum oxide. Antifouling investigation of the fabricated membranes was also carried out by bovine serum albumin (BSA).

6.1 INTRODUCTION

Nowadays, for better employment opportunities and a professional lifestyle, the citizens migrating to urban cities lead to urbanization and progressive growth of various industrial sectors. The groundwater in the environment is continually poisoned as a result of numerous effluents, heavy metals, and metalloids emitted by a variety of industrial resources. Arsenic mobilization in groundwater is aided by natural causes such as geochemical weathering of soil as well as biological activity (Chatterjee and De 2017). The poor quality and insufficient supply of pure drinking water are critical issues worldwide. The water is getting polluted from

one of the harmful heavy metalloids like arsenic. Arsenic can be mobilized under both acidic and basic conditions amongst other heavy metals. The anthropogenic sources include smelting of iron ores, wood preservative medium and arsenic-contained pesticides (Li et al. 2020b). In addition, forest fires, minerals, erosion of rocks and volcanic activities are the significant natural resources of arsenic polluted drinking water (Zaid et al. 2020). Over a long period, drinking water containing toxic arsenic poses life-threatening severe health-related issues to millions of population (Saha and Rahman 2020). Arsenic, therefore, has been classified by the International Agency for research on cancer (IARC) as a class-A poisonous and carcinogenic to human health. There is also a limitation for maximum arsenic concentration in drinking water as 10 µg/l by the United states environmental protection agency (USEPA) (Kumar et al. 2020b). This noticeably encouraged the researchers and scientists to identify the innovative methods and procedures for retreat and reuse of arsenic-contaminated water for various applications that can be implemented.

Many of the different methods for treating arsenic-contaminated water have been used. The performance of the various treatment techniques for arsenic depends on the arsenic chemical and physical properties. In water, arsenic is usually present in an inorganic form depending on the redox potential and pH levels. The two main species of arsenic in water are arsenite ($As^{\pm3}$) and arsenate (As^{+5}) respectively (Kumar et al. 2019a). Due to its high solubility and more volatility arsenite is not easier to decontaminate from water (Qiu et al. 2020). As a result, several researchers have demonstrated several methods for the decontamination of arsenic, such as coagulation (Song et al. 2017), flocculation (Pallier et al. 2010c), oxidation (Li et al. 2020a), adsorption (Wu et al. 2018) along with membrane filtration using reverse osmosis (Jarma et al. 2020) along with nanofiltration (Song et al. 2015). Many processes have certain disadvantages, such as precipitation, which can generate a considerable amount of toxic sludge, posing serious environmental issues (Boddu et al. 2008). For the rejection of arsenic, the ion exchange process was well described. However, the weak selectivity for (As^{+5}) was influenced by extreme competition from some co-existing anions and prohibitively discouraged the process of ion exchange. Therefore, the ultrafiltration membrane process is gaining significant importance for the filtration of varieties of heavy metals, including toxic arsenic ions. The ultrafiltration process provides high permeability, cost-effective and efficiency with a minimal fouling effect (Kumar et al. 2019a).

Many research studies have shown that arsenate-containing solution (As^{+5}) can be recycled as pure water according to the allowable contaminant water quality condition of EPA (Qiu et al. 2020; Sánchez and Rivas 2010). However, the arsenite ($As^{\pm3}$) must be processed with pre-oxidation before passing through the membrane surfaces for the reduction to arsenate species (As^{+5}) (Liu et al. 2019). The electrostatic repulsion depends on the properties of surface charge and hydrophilicity of the membrane surface (Trzaskus et al. 2015; Verliefde et al. 2008b). From our previous work, membrane 1 wt% of ZrO_2 in CA/PPSU and 0.6 wt% of ZrO_2 in CAP/PPSU exhibited 87.27% and 70.48% with the permeabilities of 89.94 and 70.59 L/m^2h bar respectively (Kumar et al. 2020b). Membranes prepared by adding 1 wt% zinc-magnesium oxide (ZnO-MgO) in CA/PPSU (ZMCA-1) and 0.6 wt% of ZnO-MgO in CAP/PPSU (ZMCAP-0.6) removes 78.48 and 81.31% of arsenic-V with the permeability of 198.47 and 69.58 L/m^2h bar respectively (Kumar et al. 2020c). With 41.01 L/m^2h bar as permeability, the neat membrane removes 22% of arsenic-V (Kumar et al. 2019a). An aqueous solution interacts with the membrane's feed sides and one of the aqueous solutions has been removed (Eftekhari et al. 2020). The concentration polarization is the liability in the membrane filtration process, which occurred due to the accumulation of the rejected arsenic-V species on the membrane surfaces. In addition, the dimensional size of the arsenic-V species is less than the surface pores of the membranes (Guha et al. 2017). Many of the researchers employed varieties of the polymers to modify the membranes surfaces and provide better membrane performances by improving its hydrophilicity, surface charge density and minimizing the concentration polarization.

Polyphenylsulfone (PPSU) has drawn significant attention in membrane fabrication and enhanced various membrane properties. High chemical resistance and thermal stability are vital properties due to the presence of the biphenyl functional group from the PPSU membrane surfaces (Dai et al. 2019). Additionally, many of the researchers introduced several inorganic additives and nanoparticles in the neat polymer matrix to provide enhanced PPSU membrane properties and rejection of different heavy metals (Nayak et al. 2020; Shukla et al. 2017d). A reliable, versatile inorganic nanomaterial, nano-Al_2O_3, was used to increase the performance of the blended membranes. Furthermore, nano-Al_2O_3 is an impressive material for membrane fabrication with low cost, chemically stable, high abrasive and high surface area to volume ratio (Kumar et al. 2011).

Youngran et al. (2007) studied the arsenic (V) removal by iron oxide and aluminum oxide adsorbents from arsenic polluted wastewater. The rejection of arsenic (V) was efficient for

aluminum oxide than the iron oxide due to the higher affinity of arsenic ions with aluminum oxide adsorbent.

Maximous et al. (2009) fabricated polyethersulfone (PES) ultrafiltration membranes with increased dosages of Al_2O_3 for wastewater treatment. The fabricated membranes including Al_2O_3, showed lower flux parameters and improved antifouling tendency properties than neat membranes.

Garcia-Ivars et al. (2014a) prepared polymeric ultrafiltration membranes using PES as an organic additive and Al_2O_3 as an inorganic additive. The increase in hydrophilic and antifouling behavior has resulted from the gradual additive dosages in the PES dope solution.

Ghaemi and Daraei (2016) fabricated intensified concentrations of polypyrrole (PPy)@Al_2O_3 in PES mixed matrix membranes. However, virgin Al_2O_3 membranes suffer from functional sites such as amine (–NH_2) and carboxylic (–COOH).

Dilshad et al. (2019) prepared membranes using cross-linking of the incremental concentrations of the Al_2O_3, polyvinyl alcohol (PVA) and polyethylene glycol (PEG). With the improved concentrations of Al_2O_3, the fabricated membranes exhibited enhanced thermal stability and hydrophilic properties.

Sherugar et al. (2021) fabricated mixed matrix membranes by zinc doped aluminum oxide (ZnO- Al_2O_3) in polysulfone as a base polymer. The ZnO-Al_2O_3 dosage membranes exhibited enhanced hydrophilic properties in terms of enhanced porosity, water uptake and pure water permeation studies. The antifouling properties of modified membranes also increased with the enhanced flux recovery ratio. From scanning electron microscopy, the improved finger-like and porous structures were evidenced. The modified mixed matrix membranes exhibited enhanced arsenic and lead removal from laboratory-prepared aqueous solution.

Additionally, cellulose acetate (CA) and cellulose acetate phthalate (CAP) hydrophilic functional sites make effective hydrophilic membrane surfaces. Furthermore, owing to the combination of the polar functional along with β-1-4 glycosidic linkages, cellulose acetate bio-sorbents are more hydrophilic and adsorptive (Shenvi et al. 2014c). The implementation of cellulose derivatives to the hydrophobic polymer matrix to enhance membrane properties has been documented in many research studies (Kumar et al. 2019a, 2020b; d).

Gholami et al. (2014) prepared a polyvinylchloride (PVC) nanocomposite nanofiltration membrane blended with cellulose acetate/iron oxide as nanoparticles. Improved

hydrophilicity, water absorption and pure water permeation were demonstrated from the modified membranes. Aluminum is used extensively in the automotive, aerospace, construction, electric industries and alloys. It is also used in food packaging and cooking utensils. Also utilized in water treatment to lower bacteria, organic matter, color and turbidity levels. In the water treatment process, it acts as a suitable adsorbent. It is widely used in the pharmaceutical industry, for example, in the production of antacids. Antiperspirants and food additives also contain nano-Al_2O_3 (DeFriend et al. 2003; Huang et al. 2020). No research work was documented from the literature on implementation of appropriate dosages of nano-aluminum oxide and cellulose acetate derivatives to the PPSU for membrane fabrication and enhancing the rejection of arsenic-V. The main objective of this research work is to prepare hollow fiber membranes for arsenic-V rejection from contaminated arsenic-V solutions to access the above-specified research gap.

In current contemporary work, polyphenylsulfone and the constant dosages of cellulose derivatives as additives and intensified concentrations of nano-aluminum oxide (nano-Al_2O_3) as nanoparticle were implemented to prepare ultrafiltration hollow fiber membranes by non-solvent induced phase separation process (Ibrahim et al. 2017d). The effect of increased concentrations of the nano-Al_2O_3 on the CA/PPSU and CAP/PPSU membrane matrix was thoroughly analyzed. The used nano-Al_2O_3 nanoparticle was tested for the XRD and TEM analysis. The prepared membrane surfaces were well characterized using various analyses such as SEM, AFM, TGA, zeta potential, FTIR and XPS, to study the membrane surface morphologies/topologies, thermal properties, surface potential and existence of various functional groups. The influence of the hydrophilic nanomaterials on membrane surfaces was confirmed by contact angle analysis, porosity/water uptake and pure water permeability measurement. In addition, the prepared membranes were further tested for the extraction of arsenic-V from arsenic-V contaminated water.

6.2 RESULTS AND DISCUSSIONS

6.2.1 Transmission electron microscopy (TEM) of the nanoparticle (nano-Al_2O_3)

High resolution- transmission electron microscopy (HR-TEM) pictures and selected area electron diffraction (SAED) pattern have been demonstrated in Figure 6.1(a) – (d) respectively. The morphologies represented the nanopowder rod-like agglomerated structure. In addition, particles were aggregated due to the nanoparticles high surface energy, and eventually nanoparticle agglomeration was observed in the ethanol solvent. In addition, with

dimensions of 20-25 nm in length, the nanoparticle contains tiny nanorods. From Figure 6.1(e) SAED pattern, the presence of many white rings and patches, which represented the polycrystalline structure of the nano-Al_2O_3.
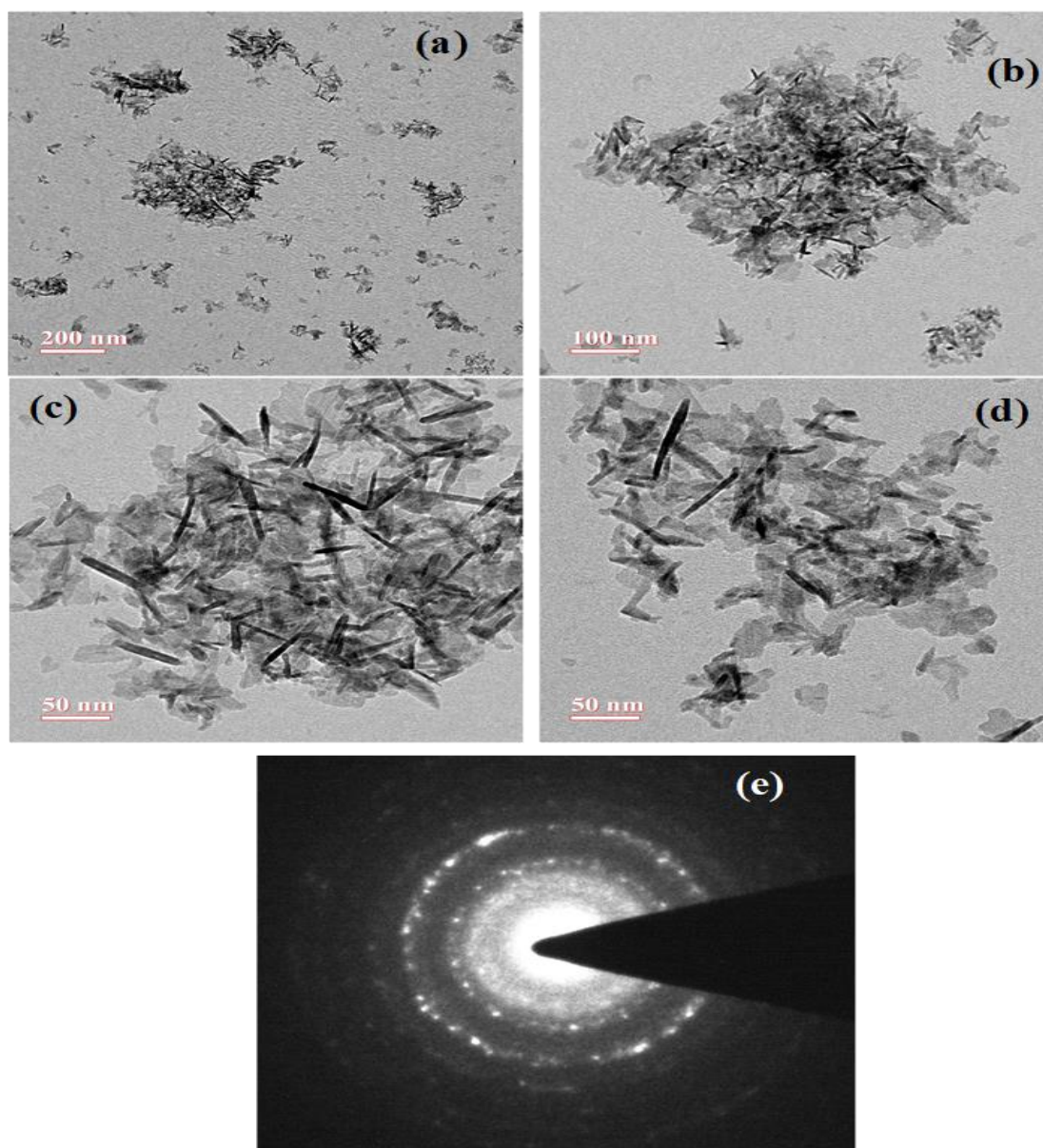
Figure 6.1 (a–d) High resolution-Transmission electron microscopy (HR-TEM) and (e) selected area electron diffraction (SAED) pattern of the used nano-aluminum oxide nanoparticle.

6.2.2 X-ray diffraction (XRD) analysis of the nanoparticle (Al₂O₃)

As used nanoparticle (nano-Al_2O_3), 2-theta diffraction peaks were demonstrated in Figure 6.2. The presence of diffraction pattern crystallinity for nano-Al_2O_3 was described in detail. It was notable that with the reference plane 1 1 1, 2 0 0, 2 2 0, 3 1 1 and 2 2 2 corresponding

diffraction angles 39.48°, 45.91°, 66.95°, 80.59° and 84.99° respectively from the JCPDS file number 01-075-0921. From the data as used nanoparticle was amorphous. No noticeable difference was observed in the peaks as a reference pattern as mentioned in the literature (Pakrashi et al. 2012).
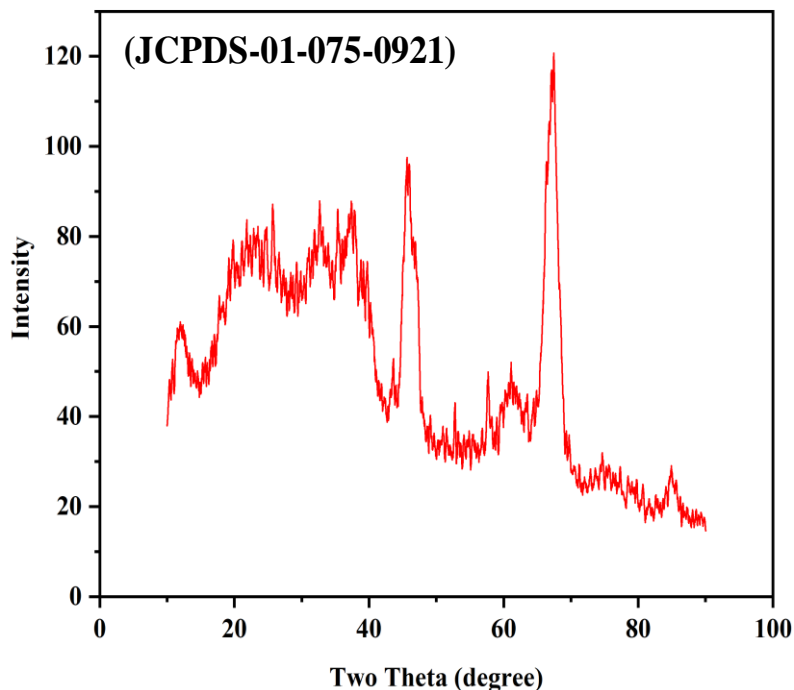
Figure 6.2 Nano-aluminum oxide nanoparticle's X-ray diffraction (XRD) analysis.

6.2.3 Particle size distribution analysis of the nanoparticle (Al_2O_3)

The size of the nano-Al_2O_3 was determined by dynamic light scattering (DLS) along with zeta potential analysis was shown in Figures 6.3(a) and (b) respectively. By the sonication process of about 30 min, a 20 wt% of nano-Al_2O_3 in water was allowed to dissolve homogeneously with the viscosity of 0.8859 cP. A homogeneous solution was tested in the Nano-track particle size analyzer for particle size distribution analysis. From Figure 6.3(a), from the DLS process histogram, the particle size in terms with a diameter of 199.2 nm. From Figure 6.3(b), the zeta potential showed that the particles were polarized with -10.7 mV and a charge -0.00180 fColumb on the particle surface. In addition, the homogeneous solution was procured by sonicating the prepared solution for about 3h (Krause et al. 2018).
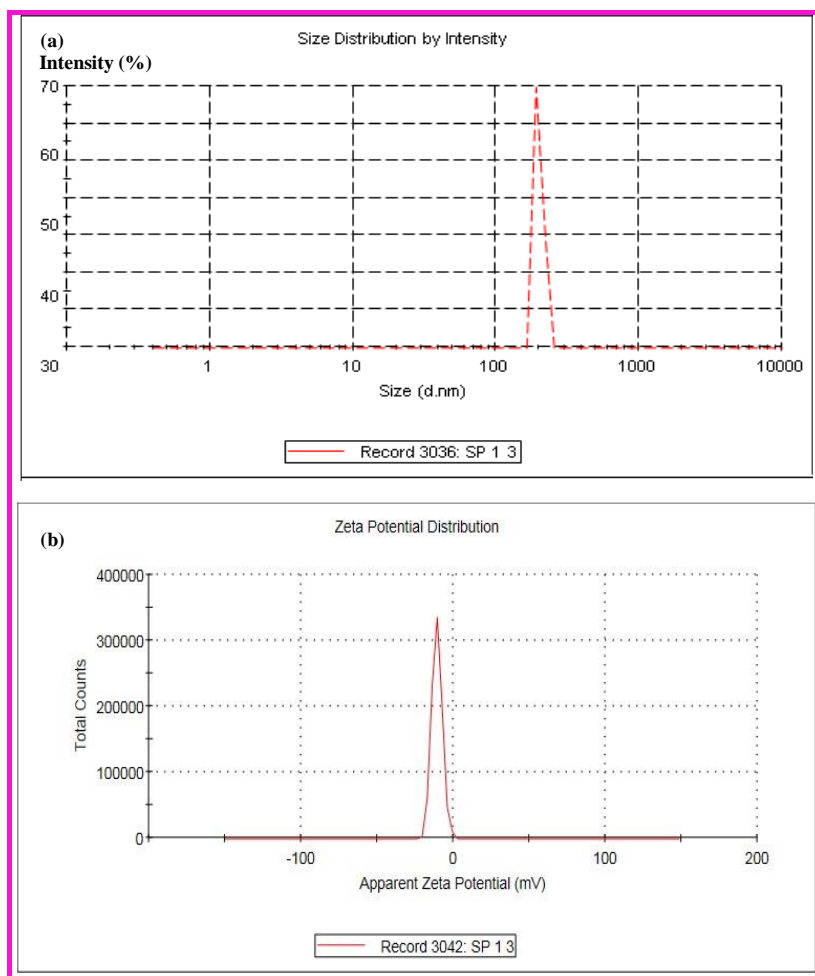
Figure 6.3 Aluminum oxide nanoparticle size distribution analysis by (a) dynamic light scattering (DLS) method and (b) zeta potential analysis of nano-Al_2O_3 nanoparticle.

6.2.4 Scanning electron microscopy (SEM) analysis of fabricated hollow fiber membranes

Morphological images of the prepared pristine and nano-Al_2O_3 incorporated membranes cross-sectional and surface images were illustrated in Figure 6.4. The cross-sectional asymmetric morphological images were witnessed from fabricated hollow fiber membranes. In the coagulation bath, the strong interaction between water and NMP was responsible for forming a thin selective layer on the surfaces of the hollow fiber membrane's inner and outer layers. The morphological structure consisted of a finger-like structure, thin top layer, thick middle layer (sponge layer) and supporting layer. As-fabricated hollow fiber membranes SEM morphologies are the direct evidence for determining the characteristics of the membrane, i.e., the top layer governs the selectivity, the middle layer affects efficiency and base layer or supporting layer responsible for the mechanical strength (Shukla et al. 2017d).

Hollow fiber membranes absence of nanoparticles (neat membranes; ALCA-0 and ALCAP-0) contains macrovoids and closed-end narrow finger-like structures as shown in Figure 6.4. Moreover, due to the difference in thermodynamic properties and kinetics of the dope solution in phase inversion, a significant improvement was observed in the SEM morphological configurations with the influence of nano-Al_2O_3. In addition, a broadened structure becomes macrovoids and small finger-like morphologies. The expansion of the sponge-like morphologies between finger-like structures has also been seen as a result of increased nanoparticle concentrations due to the delayed solvent-nonsolvent demixing, as shown in Figure 6.4. Improving the morphological structure of the membrane have an essential effect on permeability and is selectively related to the membrane (Nayak et al. 2018b). The detailed cross sectional (complete view) scanning electron microscopy (SEM) images was represented in Figure 6.5.

The membrane surface morphology and energy dispersive x-ray (EDX) observation with -3000x magnification for neat membranes (ALCA-0 and ALCAP-0) and nano-Al_2O_3 contained membranes (ALCA-1.5 and ALCAP-1.5) were illustrated in Figure 6.6. The neat membrane revealed less porous and evenly distributed membrane surfaces. The porous structures were expanded with the increased dosages of nano-Al_2O_3, promising the incorporation of the nanoparticle on the surfaces as shown in Figures 6.6(c) – (b) respectively. From Figure 6.6, EDX analysis revealed the blending and presence of nano-Al_2O_3 nanoparticle on modified membranes surfaces AlCA-1.5 and ALCAP-1.5 respectively. The absence of aluminum oxide on the membrane surfaces in pristine membranes ALCA-0 and ALCAP-0 respectively from Figure 6.6. Inner/outer diameter (ID and OD) and mean pore radius of the fabricated hollow fiber membranes were illustrated in Table 6.1.
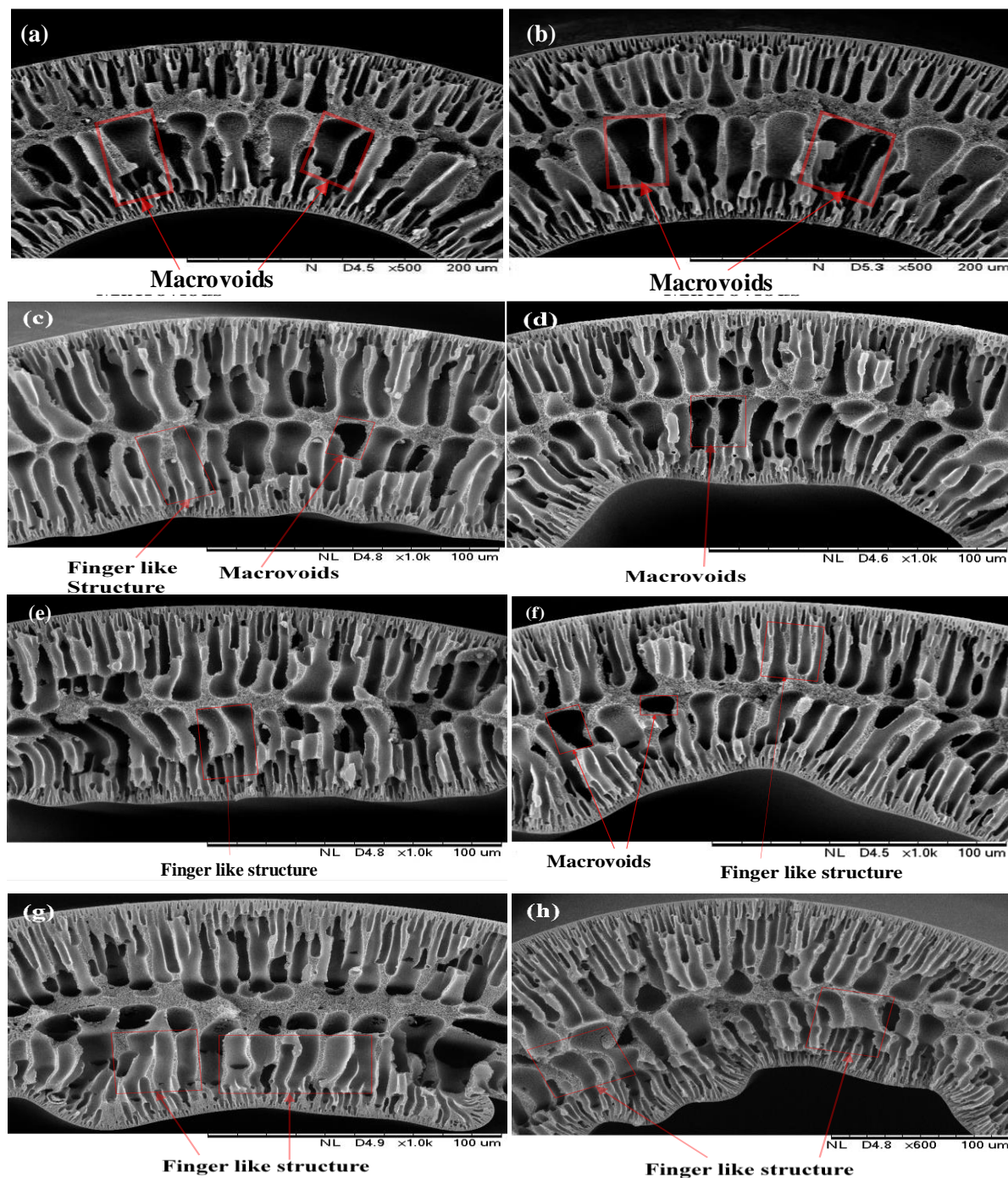
Figure 6.4 Cross-sectional scanning electron microscopy (SEM) images of neat membrane (a and b) as ALCA-0 and ALCAP-0 followed by incremental dosage (0.6, 1 and 1.5 wt%) of Al_2O_3 in CA/PPSU membranes as ALCA-0.6, ALCA-1 and ALCA-1.5 as 'c', 'e' and 'g' respectively and Al_2O_3 in CAP/PPSU membranes as ALCAP-0.6, ALCAP-1 and ALCAP-1.5 as 'd', 'f' and 'h' respectively.
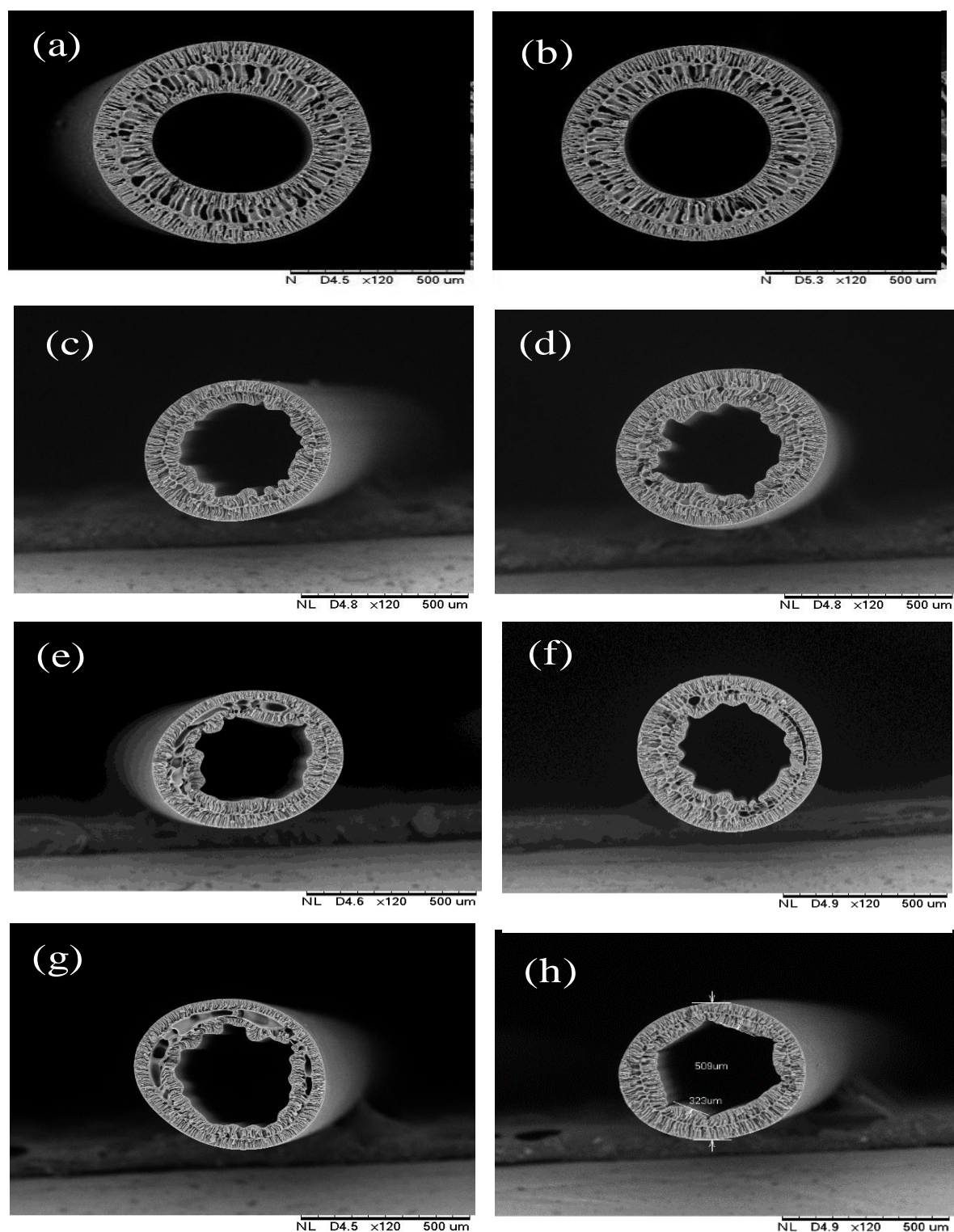
Figure 6.5 Cross sectional (complete view) scanning electron microscopy (SEM) pictures of neat membrane (a and b) as ALCA-0 and ALCAP-0 followed by incremental dosage (0.6, 1 and 1.5 wt%) of Al_2O_3 in CA/PPSU membranes as ALCA-0.6, ALCA-1 and ALCA-1.5 as 'c', 'e' and 'g' respectively and Al_2O_3 in CAP/PPSU membranes as ALCAP-0.6, ALCAP-1 and ALCAP-1.5 as 'd', 'f' and 'h' respectively.
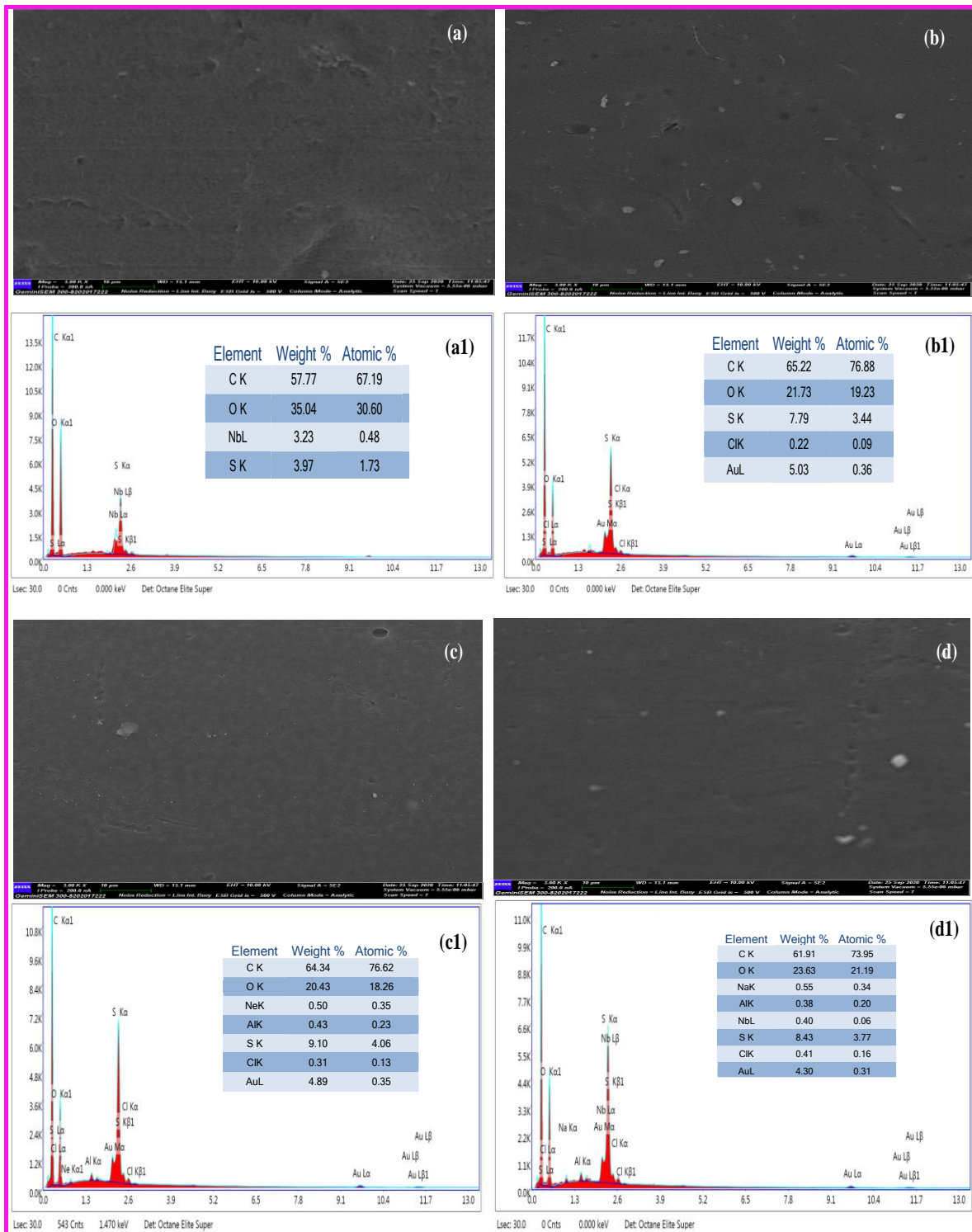
Figure 6.6 Surface morphologies field emission-scanning electron microscopy (FE-SEM) images (with the magnification of -3000x) of the neat hollow fiber membranes (ALCA-0 and ALCAP-0) was 'a' and 'b' respectively, nano-Al_2O_3 contained CA/PPSU and CAP/PPSU (ALCA-1.5 and ALCAP-1.5) was 'c' and 'd' respectively. Energy-dispersive X-ray spectroscopy (EDX) images of the neat membranes (ALCA-0 and ALCAP-0) was 'a1' and 'b1' along with (ALCA-1.5 and ALCAP-1.5) was 'c1' and 'd1' respectively.

Table 6.1 Outer/ inner (OD/ID) diameter and mean pore radius of the fabricated hollow fiber membranes

Hollow fiber membranes	Outer diameter (OD in μm)	Inner diameter (ID in μm)	Mean pore radius (m)
ALCA-0	579	394	1.543×10^{-8}
ALCA-0.6	561	369	1.501×10^{-8}
ALCA-1	509	323	8.93×10^{-9}
ALCA-1.5	615	353	1.396×10^{-8}
ALCAP-0	520	341	6.620×10^{-8}
ALCAP-0.6	547	321	1.420×10^{-8}
ALCAP-1	545	362	9.241×10^{-9}
ALCAP-1.5	589	384	1.571×10^{-7}
Spinneret dimension, inner diameter: 550 μm, outer diameter:1100 μm			

6.2.5 Porosity/water uptake studies of the fabricated hollow fiber membranes

The fabricated pristine and nano-Al_2O_3 contained membrane's porosity and the water uptake of the hollow fiber membranes were illustrated in Figure 6.7(a) and (b). The outcome of porosity and water uptake of the fabricated membranes were revealed that the pristine membranes were dominated by nano-Al_2O_3 blended membranes. From Figure 6.7(a) and (b), the neat membranes without the influence of nanoparticle exhibited the porosities as ALCA-0 and ALCAP-0 showed 22.01% and 25.08% respectively. The water uptake parameters for pristine membranes ALCA-0 and ALCAP-0 were 48.72% and 51.32% respectively. With the less porous and hydrophobic membrane surfaces, the pristine membrane surface demonstrated less porosity in the morphologies. Incremental dosages of the nano-Al_2O_3 into the dope solution of CA/PPSU and CAP/PPSU were shown to improve porosity parameters. As such, ALCA-1.5 and ALCAP-1.5 were 71.28% and 76.91% respectively. The water uptake for the increased concentrated membranes ALCA-1.5 and ALCAP-1.5 were 69.67% and 84.26% respectively. The higher percentage of hydrophilic additives contributes to thermal instability, resulting in rapid demixing in the co-angulation bath further enhancement in the porosity on the membrane surfaces (Hebbar et al. 2018c). During the phase inversion process, the leaching of used additives and nanoparticles helps to increase the surface porosity of the membrane (Kumar et al. 2019a).
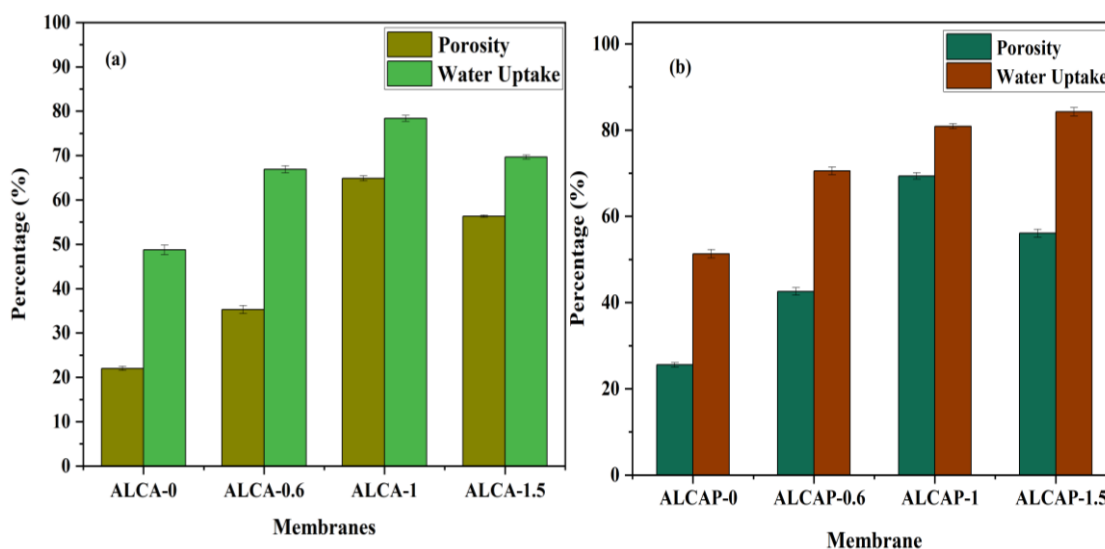
Figure 6.7 The prepared neat and nano-aluminum oxide incorporated hollow fiber membranes porosity and water uptake measurement.

6.2.6 Hydrophilicity/phobicity of the fabricated hollow fiber membranes

The hydrophobicity and hydrophilicity of the fabricated neat and nano-Al_2O_3 contained hollow fiber membranes was illustrated in Figure 6.8. The neat membrane with a less porous structure and hydrophobicity exhibited the higher contact angle parameter for ALCA-0 and ALCAP-0 were 87.74° and 82.12° respectively. The hydrophilicity and hydrophobicity natures of the prepared pristine and nano-Al_2O_3 contained hollow fiber membrane. With the influence of increased dosages (0.6, 1 and 1.5 wt% of nano-Al_2O_3) into the pristine membrane dope solution, considerably decreasing parameter of contact angle can be observed. The membranes showed 70.14° and 68.47° respectively, with the increased concentrated hollow fiber membranes ALCA-1.5 and ALCAP-1.5 respectively. The migration of these functional groups from nanoparticles and additives further leads to pore interconnectivity. In addition, in the sulphuric acids group, the hydroxyl group has a strong affinity for water. It forms H-bonds with water molecules, increasing surface wettability and membrane hydrophilicity (Tavangar et al. 2020). The water rejection capacity of the membrane was also increased as the affinity for water absorption was increased. Additionally, with the additive concentration of 1.5 wt% of nano-Al_2O_3 in CA/PPSU and CAP/PPSU dope solution, the hollow fiber membranes hydrophilicity was improved due to the presence of the enormous number of functional groups (–OH, –CH and –CO) on the surfaces of the membrane (Kumar et al. 2020c).
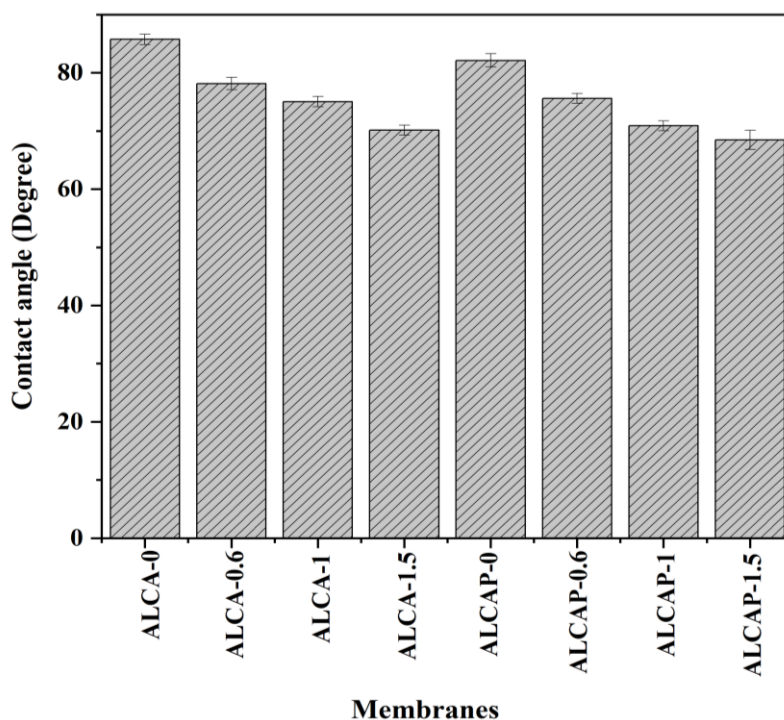
Figure 6.8 Contact angle measurement of the fabricated hollow fiber membranes.

6.2.7 Pure water permeability (PWP) of the prepared hollow fiber membranes

The fabricated pristine and nano-Al_2O_3 modified membranes pure water permeability was illustrated in Figure 6.9(a) – (b). The neat (ALCA-0 and ALCAP-0) membranes showed 26.45 L/m^2h bar and 41.43 L/m^2h bar respectively. Pure water permeability was revealed as 88.87 L/m^2h bar and 102.13 L/m^2h bar respectively for ALCA-1.5 and ALCAP-1.5 membranes with more hydrophilic functional sites. Due to the hydrophobic and decreased porous behavior of the PPSU, decrease in PWP parameters were observed for the pristine membranes rather than the membranes containing nano-Al_2O_3. In addition, with incremental concentrations (0.6, 1 and 1.5 wt%) of the nano-Al_2O_3 along with additives in the PPSU dope solutions, PWP parameters were substantially improved. Due to the leaching of the nanoparticle and the additive content in the membrane fabrication, increased porosity was observed on the hollow fiber membranes. As porosity increases on the hollow fiber membranes, the membrane water holding capacity also increases as more pores were present.

The two main factors, the permeability of the nano-Al_2O_3/CAP/PPSU hollow fiber membrane is greater than that of nano-Al_2O_3/CA/PPSU and pristine hollow fiber membranes. Firstly, the occurrence of the carboxylate group on the nano-Al_2O_3/CAP/PPSU membrane surfaces, the presence of the carboxylated group reduces the concentration polarization and improved membrane hydrophilicity and pure water permeability. Secondly, the CAP additive

itself acts as a pore former. Consequently, the incremental dosages of nano-Al_2O_3 in the hydrophobic PPSU dope solution will render enhanced pore visibility. This can be evidenced by SEM morphological structure.
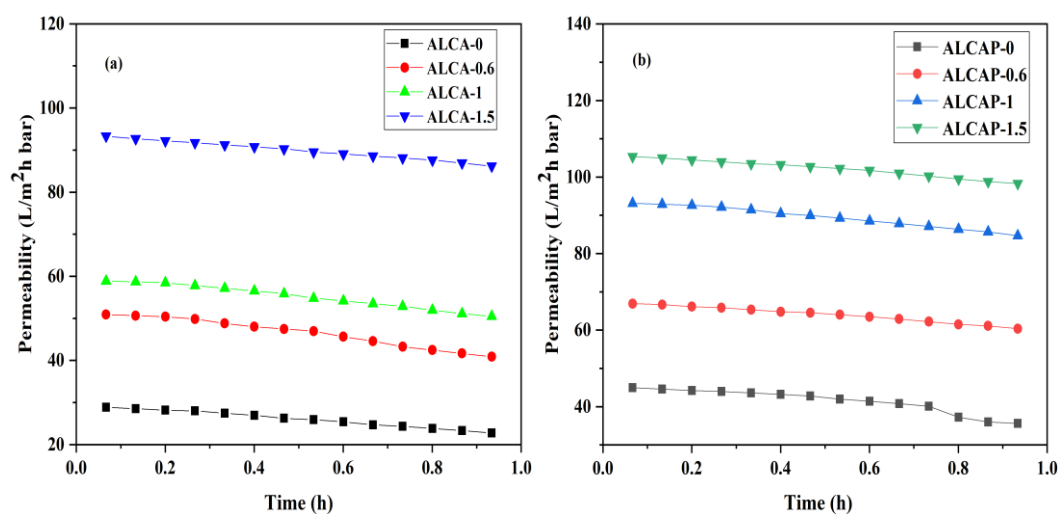
Figure 6.9 Pure water permeability of the fabricated (a) CA/PPSU with incremental dosages of nano-aluminum oxide membranes and (b) CAP/PPSU with incremental concentrations aluminum oxide membranes.

6.2.8 Antifouling analysis of the fabricated hollow fiber membranes

The antifouling efficacy of the fabricated hollow fiber membranes is shown in Figure 6.10. Generally, the primary cause of membrane fouling is the deposition or adsorption of the BSA protein molecules on the hollow fiber membranes surfaces. The three comprehensive fouling steps from the prepared membranes are shown in Figure 6.10(a) – (b). The mechanical deformation was due to more porous nature of the membrane surfaces. Due to the deposition or adsorption of the used protein molecules on the membranes surface pores, there is a drastic decrease in the permeability. In this analysis, the neat hollow fiber membranes (ALCA-0 and ALCAP-0) in three filtration stages showed lower permeability performance. The reduced permeability was witnessed because of the smaller pore size, hydrophobic and more fouling nature of the neat membranes. There is a substantial increase in permeability as increased nano-Al_2O_3 concentrations to the neat dope solution, since nano-Al_2O_3 contained membranes are more vulnerable to hydrophilic and have less fouling tendency. This is due to the presence of more hydrophilic groups (–COOH and –OH) on the membrane surface, which creates more affinities with water molecules, converting PPSU membrane hydrophobic surfaces into more hydrophilic adsorptive hollow fiber membrane surfaces. From Figure 6.10(c) – (d), the FRR parameters for pristine membranes ALCA-0 and ALCAP-0 were 72.03% and 77.49%

162

respectively. The improved FRR of the nano-Al_2O_3 concentrated membranes was observed to be 85.09% and 89.24% respectively, for ALCA-1.5 and ALCAP-1.5 hollow fiber membranes, which further suggested that the membranes were hydraulically cleaning and highly resistant to fouling. Other remaining increased antifouling-related parameters are R_r and decreased parameters of R_{ir} and R_t with increased nano-Al_2O_3 concentration showed better antifouling properties from modified hollow fiber membranes.
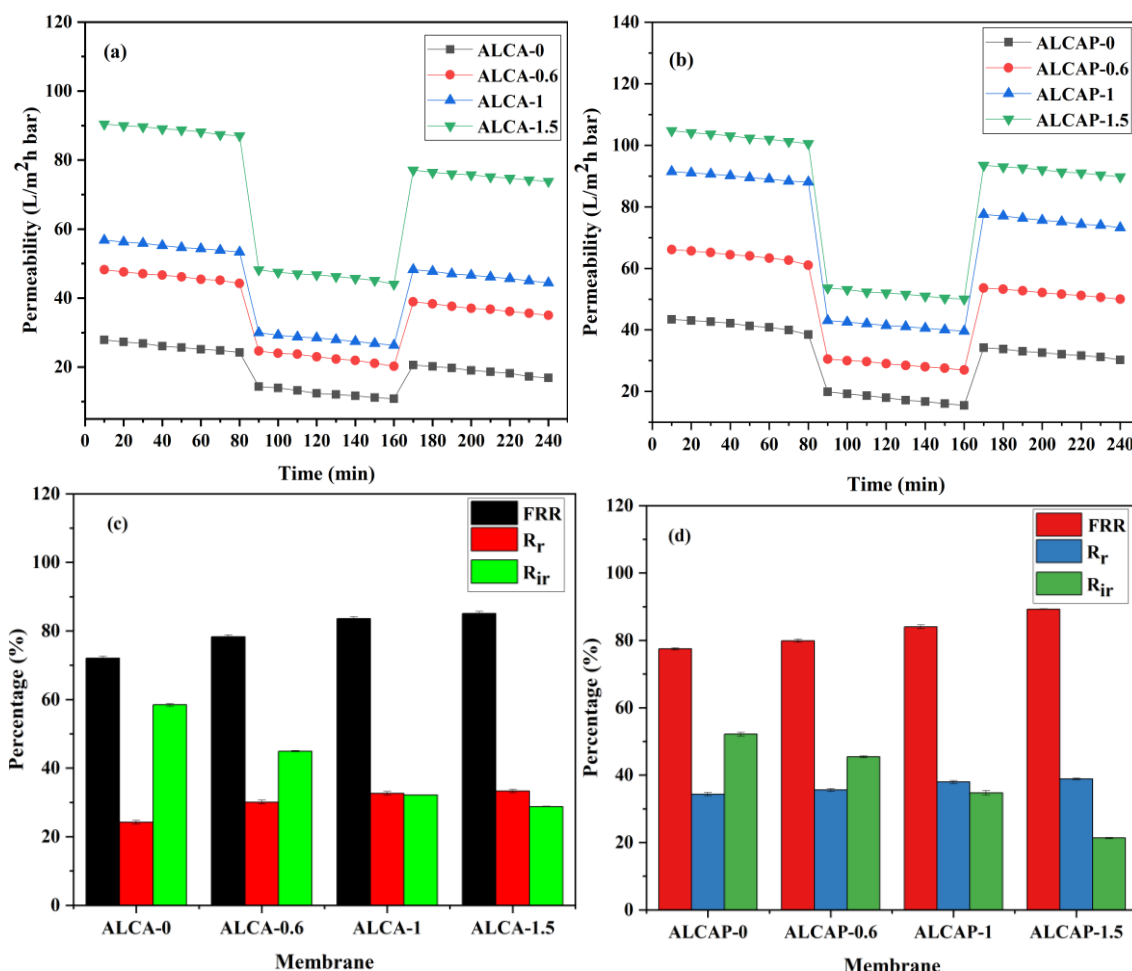
Figure 6.10 Antifouling permeability behaviours of the prepared membranes (a) nano-Al_2O_3/CA/PPSU (b) nano-Al_2O_3/CAP/PPSU membranes. Antifouling properties (FRR, R_r and R_{ir}) of (c) nano-Al_2O_3/CA/PPSU and (d) nano-Al_2O_3/CAP/PPSU membranes.

6.2.9 Atomic force microscopy (AFM) analysis of the hollow fiber membranes

Atomic force microscopy (AFM), three-dimensional topological pictures of the pristine and nano-Al_2O_3 incorporated hollow fiber membranes was shown in Figure 6.11. Generally, the surface roughness parameters (R_a) was interpreted for topological analysis. The roughness (R_a) parameters for neat membranes AlCA-0 and ALCAP-0 were 8.6 nm and 18.3 nm respectively from Table 6.2. The gradual dosages of nano-Al_2O_3 (0.6, 1 and 1.5 wt%) into the

neat polymeric dope solutions, such as ALCA-1.5 and ALCAP-1.5 were 32.5 nm and 43.9 nm respectively. There is an increase in surface roughness parameter. An enhanced R_a parameter indicated an improved surface pore on the membrane surfaces. This in turn promotes reduced fouling nature and increased hydrophilicity. Also, the enhanced concentrations of the nano-Al_2O_3 dosages, the mean square Z information related to roughness (R_q), peak difference between few maximum peaks and minimum peak (R_z) parameters were increased.

In addition, the presence of a small amount of nanoparticle segregation and distribution of small pores on the membrane surfaces was shown by bright side and darkest portion relative to the membrane surface. A high concentration (1.5 wt%) of nano-Al_2O_3 in CA/PPSU and CAP/PPSU showed increased peaks (bright surfaces) as the highest percentages of nano-Al_2O_3 were present in the corresponding dope solution, confirming the improvement of the membrane surface roughness. Previous studies have shown that rough membrane surfaces increase the overall effective surface area, thus increasing water permeability. This finding was favored by the increased porosity, water contact angle and measurement of pure water permeability shown in Figure 6.7, Figure 6.8 and Figure 6.9 respectively.

Table 6.2 Properties of roughness for fabricated hollow fiber membrane surfaces

Membranes code	R_a (nm)	R_q (nm)	R_{max} (nm)
ALCA-0	8.62	10.2	79
ALCA-0.6	10.3	13.5	105
ALCA-1	14.6	21.7	174
ALCA-1.5	32.5	43.8	315
ALCAP-0	18.3	23.4	125
ALCAP-0.6	22.8	30.4	194
ALCAP-1	25.6	37.3	333
ALCAP-1.5	43.9	61.8	612
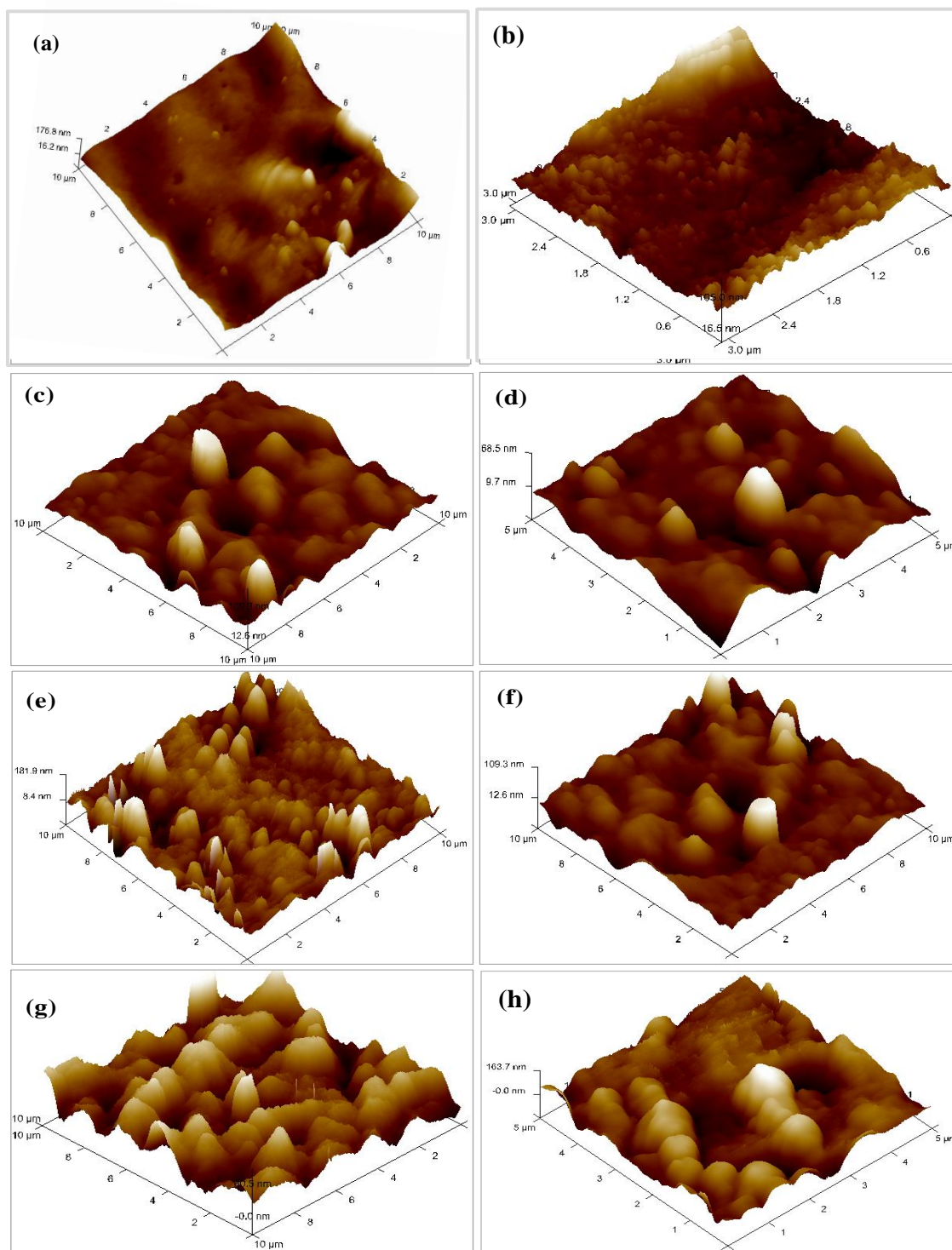
Figure 6.11 Atomic force microscopy (AFM) pictures of the fabricated pristine and nano-Al$_2$O$_3$ contained hollow fiber membranes.

6.2.10 Thermogravimetric analysis (TGA) of the prepared hollow fiber membranes

The temperature decomposition of the prepared pristine and nano-Al$_2$O$_3$ integrated CA/PPSU and CAP/PPSU hollow fiber membranes was demonstrated in Figure 6.12. For

each membrane, thermal degradation behavior can be represented in three different phases. It is clear from the TGA investigation that the membranes contained in nano-Al_2O_3 (ALCA-1.5 and ALCAP-1.5) have better thermal stability than the neat membranes (ALCA-0 and ALCAP-0). In the case of neat membranes, the initial temperature degradation of the ALCA-0 and ALCAP-0 starts at room temperature to 132.73 °C and for the ALCAP-0 membrane starts at 29.10 °C – 132.73 °C respectively. The initial thermal degradation is due to the volatilization of moisture content present on the membrane surfaces. The second level of thermal degradation for the ALCA-0 from 135.24 °C – 368.51 °C and ALCAP-0 from 139.5 °C to 293.84 °C respectively. This stage of thermal degradation is for the degradation of polymeric hydrophilic groups of the sulphuric acid group and cellulose acetate (Golpour and Pakizeh 2018b; Kumar et al. 2020b).

In the temperature range of 464.85 °C – 685.45 °C for the ALCA-0 membrane, the last thermal decomposition step is to disrupt all-polymer content and eventually form ash content. The final step of temperature decomposition for ALCA-0 and ALCAP-0 membrane was 505.02 °C – 706.6 °C respectively. The second degradation stage for ALCA-1.5 was 129.34 °C –276.42 °C and for the ALCAP-1.5 membrane was 130.64 °C –285.07 °C for the decomposition of the polymers on the membrane surfaces. The thermal degradation for the final stage for ALCA-1.5 and ALCAP-1.5 membrane was 467.02 °C –691.41 °C and 475.02 °C –715.30 °C respectively. The polymers were broken at that temperature and started to form ash. Increased nanoparticle concentrations to the neat membranes internally result in improved decomposition temperature and reduced weight loss from modified hollow fiber membranes. The figure noted that, because of the high surface area to volume ratio and increased porosity, the ALCAP-1.5 membrane demonstrated significantly increased weight loss relative to the ALCA-1.5 membrane (Kumar et al. 2020d). Also, from the ALCAP-0 membrane, the degradation of the phthalic anhydride. However, due to the improved thermal miscibility of the used cellulose acetate derivatives and increased nano-Al_2O_3 nanoparticle in the PPSU membranes. The nano-Al_2O_3 integrated membranes showed improved thermal stability as compared to pristine membranes (Prihatiningtyas et al. 2020).
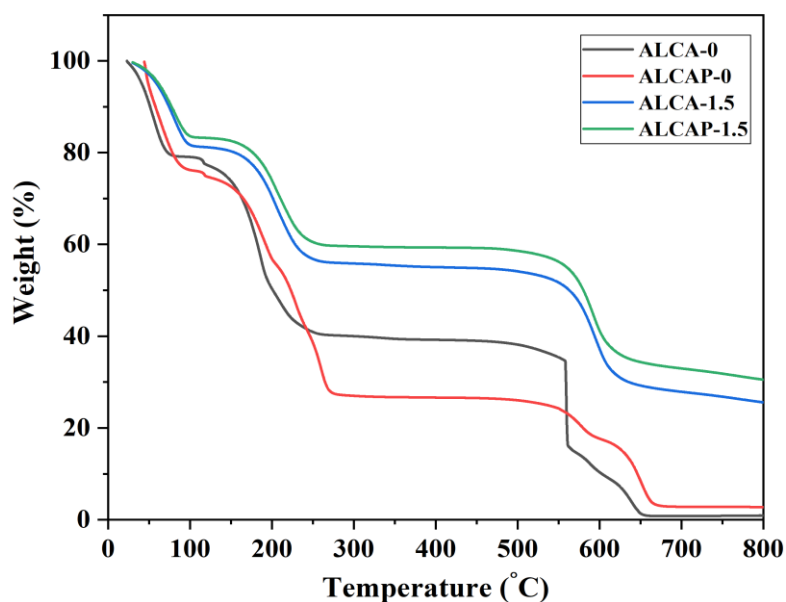
Figure 6.12 Thermogravimetric analysis (TGA) of the neat membrane (ALCA-0 and ALCAP-0) along with increased dosages membranes (ALCA-1.5 and ALCAP-1.5).

6.2.11 Molecular weight cut off study of the membrane

The best performing membrane (ALCA-1.5) molecular weight cut off was demonstrated in Figure 6.13. The molecular weight cut off of the best performing membrane was found to be 17403.1 Da. The PEG rejection percentage for ALCA-1.5 membrane was 61.23%, 70.81% and 94.52% with corresponding to molecular weight of PEG-4000, PEG-6000 and PEG-20000 respectively.
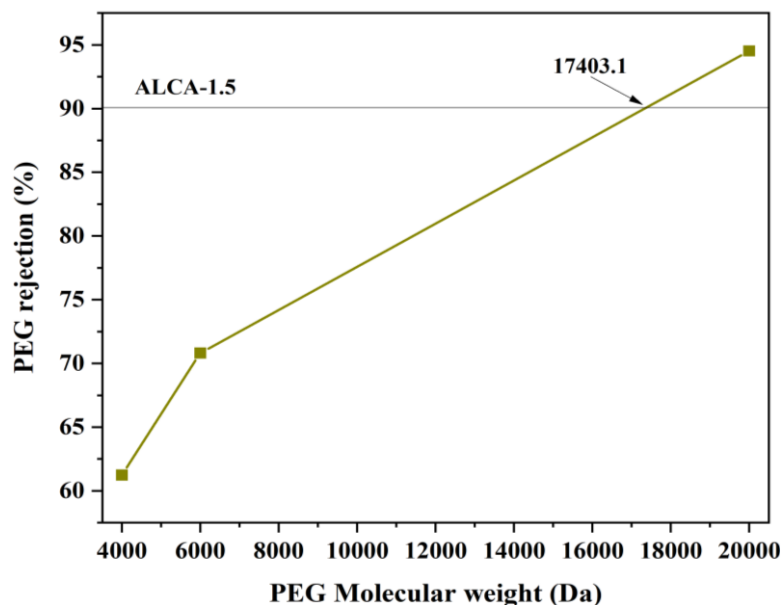
Figure 6.13 Molecular weight cut off study of the prepared hollow fiber membrane.

6.2.12 Surface potential (Zeta potential) of the best performing membrane

The measurement of the surface potential of the prepared best performing membrane (ALCA-1.5) was represented in Figure 6.14, by pH on the X-axis and zeta potential on the Y-axis respectively. At pH 1.05, which was 7.45 mV the ALCA-1.5 membrane was positively charged. The negative zeta potential was reported at different pH parameters of 3.10, 5.2, 7.3, 9.1 and 10.1 as -18.1 mV, -40.3 mV, -49.5 mV and -53.6 mV respectively. Typically, the enhanced negative charge was result of hydroxyl (–OH) and carboxylic (–COOH) groups accumulation (Kumar et al. 2020c). In addition, the deprotonation of the used hydrophilic functional groups on the membrane surfaces. The modified negatively charged membrane surfaces help to enhance rejection of the arsenate oxide (AsO_4^{3-}) by repulsion phenomenon. The negative surface potential helps increase the membrane's surface area, which appears to increase hydrophilicity and pure water permeability (Bai et al. 2020). At pH 1.39, a considerable isoelectric point (IEP) was also recorded. The membrane surface exhibited no surface charge at this pH, i.e., the surface potential parameter is zero.
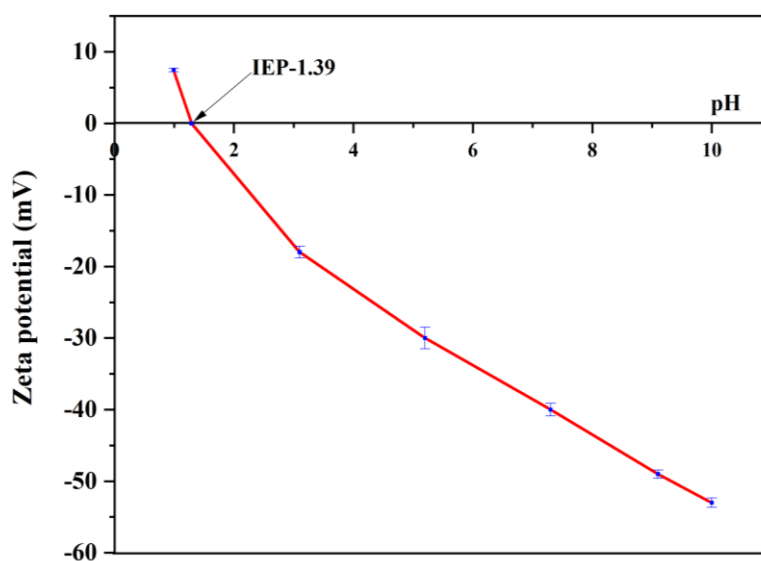
Figure 6.14 Zeta potential (surface potential) measurement of ALCA-1.5 membrane surface.

6.2.13 Attenuated total reflectance- Fourier transform infrared spectroscopy (ATR-FTIR) investigation of the prepared membranes

The ATR-FTIR spectra of prepared neat (ALCA-0 and ALCAP-0) along with increased dosaged of nano-Al_2O_3 nanoparticle in CA/PPSU and CAP/PPSU membranes (ALCA-1.5 and ALCAP-1.5) was represented in the Figure 6.15. From Figure 6.15(a), neat membrane ALCA-0, the peak 3324.85 cm^{-1} assigned to –OH (hydroxyl) group and 2833.95 cm^{-1} –

2932.67 cm^{-1} attributed to –CH$_2$ group respectively. The peak 1584.95-1654.82 cm^{-1} attributed to –C=O (carbonyl) group and 1481.85 cm^{-1} –O=C–OR functional group respectively. Peaks 869.54 cm^{-1} and 1233.99 cm^{-1} were attributed to –C–O– and –C–H– functional groups respectively (Kumar et al. 2019a, 2020b). From Figure 6.15(b), neat ALCAP-0 membrane 3358.93 cm^{-1} assigned to –OH group and 2834.85 cm^{-1} –2936.95 cm^{-1} was attributed to –CH$_2$ group of stretching group of methylene –C–H– group respectively. The peak at 1739.45 cm^{-1} attributed to –C=O– carbonyl functional group which was absent in ALCA-0 neat membrane. 1236.50 cm^{-1} peak was assigned to cyclic ether group –C–O– of cellulose acetate phthalate, 1035.85 cm^{-1} – 1104.85 cm^{-1} attributed to –C–O–C– vibrational stretching respectively. Peaks 867.85 cm^{-1} and 1600.95 cm^{-1} were assigned to –C–H– and –C=C– groups of vinyl aromatic conjugated ring (Garcia-Ivars et al. 2014b).

However, for ALCA-1.5 and ALCAP-1.5 membranes there is a shift was perceived in the FTIR spectra for –CH$_2$, –C–O– and –C–O–C– functional sites, due to the occurrence of hydrogen bonding in-between nano-Al$_2$O$_3$ nanoparticle and cellulose acetate constitutes. As such for ALCA-1.5 membrane, from Figure 6.15(c), the peak 3400 – 3300 cm^{-1} attributed to hydroxyl group (–OH), 1487 cm^{-1} and 1236 cm^{-1} attributed to –C–C bond stretching and –C–O stretching vibration respectively. Peaks 1039.01 cm^{-1} and 1647 cm^{-1} corresponds to –O=S=O– symmetry stretching and carbonyl stretching group, 1036 – 1000 cm^{-1} attributed to complex vibration of Al–O group respectively. The peak 1577 cm^{-1} assigned to benzene stretching group. Peak at 790.02 cm^{-1} – 1039.50 cm^{-1} stretching vibration and the symmetric ending modes of Al–O–Al bond respectively. Peak at 2350 cm^{-1} and 2959 cm^{-1} were attributed to –CH stretching vibration of the methyl group and asymmetric stretching vibration respectively (Garcia-Ivars et al. 2014b).

Similarly, in case of the ALCAP-1.5 membrane from Figure 6.15(d), the peak at 3100 cm^{-1} – 3400 cm^{-1} correspond to hydroxyl group (–OH), peak at 1483 cm^{-1} and 1236.50 cm^{-1} assigned to –C–C bond stretching and –C–O– stretching vibration respectively. Peaks 1038.16 cm^{-1} and 1647.82 cm^{-1} attributed to –O=S=O– and –O–C=O– carbonyl stretching group respectively. the peak 1582.82 cm^{-1} benzene stretching vibration. Peak at 1038.36 cm^{-1} to 1000.83 cm^{-1} assigned to complex vibration of Al–O. The peak at 780.12 – 1038.85 cm^{-1} corresponds to stretching vibration and the symmetric bending modes of the Al–O–Al bend respectively. The 2381.68 cm^{-1} and 2951.20 cm^{-1} peak attributed to –C–H stretching vibration of methyl group and –CH$_2$ asymmetric stretching vibration respectively (Garcia-Ivars et al. 2014b; Kumar et al. 2020c).
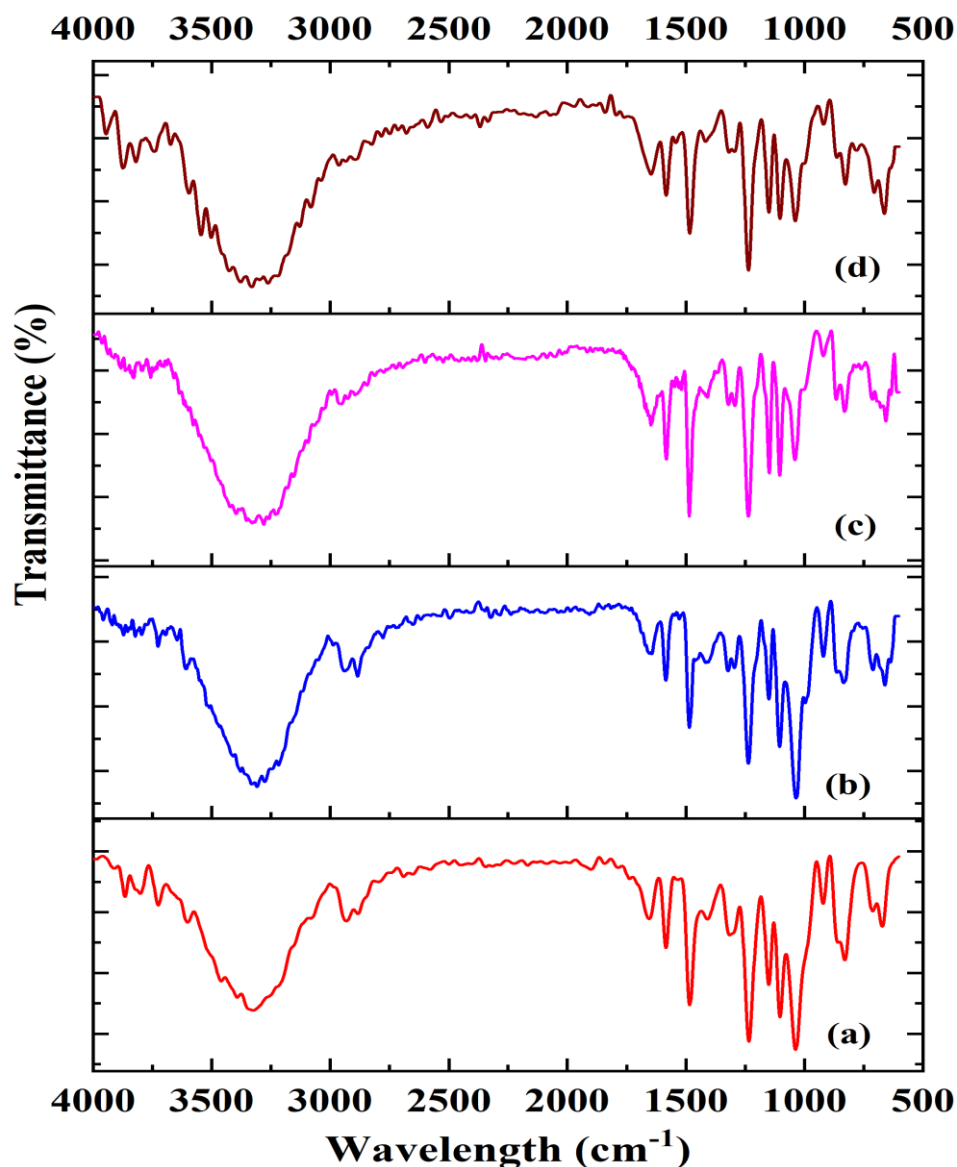
Figure 6.15 ATR-FTIR studies of the fabricated neat membranes (ALCA-0 and ALCAP-0) as (a and b) along with aluminum oxide contained membranes (ALCA-1.5 and ALCAP-1.5) as (c and d) respectively.

6.2.14 X-ray photoelectron spectroscopy (XPS) analysis of the membrane

The best performing x-ray photoelectron wide and narrow range of prepared ALCA-1.5 membrane was shown in Figure 6.16. The 283.9 eV, 530.5 eV and 166.4 eV binding energies respectively reported the existence of functional elements O1s, C1s and S2p respectively (Ibrahim et al. 2018c). the deconvoluted results of O1s, C1s and S2p were shown by Figure 6.16(b) – (d). the –C–H/–C–N, –C–C and –C=O and –O–C=O bonds were attributed to C1s binding energies of 283.6 eV, 284.5 eV, 286.9 eV and 289.5 eV respectively. The relatively weak of 282.2 eV was attributed to the presence of a carbon atom in the nano-Al_2O_3 lattice,

further confirming the replacement of a small amount of C^{4+} with Al^{4+} and the existence of C-Al-O bonds. The functional group $-CO_2H$, $-O=C-O$, $-C-OH$, $-C=O$ and $-C-O-C$ bonds attributed to the O1s binding energy peaks of 529.2 eV, 529.8 eV, 530.6 eV, 531.2 eV and 531.8 eV respectively (Barathi et al. 2014). The S2p binding energy peaks 165.2 eV, 165.7 eV, 166.5 eV and 166.7 eV are related to sulphite ($SO_3^{(2-)}$), $S2p_{(1/2)}$, sulphone (SO_2-C), oxidized sulphur (-So$_x$) and $S2p_{(3/2)}$ sulphate group $SO_4^{(2-)}$ respectively (Fantauzzi et al. 2015). The functional groups Al–O, Al(OH)$_3$, Al–O–C and nano-Al$_2$O$_3$ were assigned the Al2p binding energy peaks of 73.0 eV, 74.1 eV, 75.3 eV and 75.9 eV respectively (Hu et al. 2015). The homogeneous blend of the various additives and nanoparticle was verified by different binding energies on the membrane surfaces.
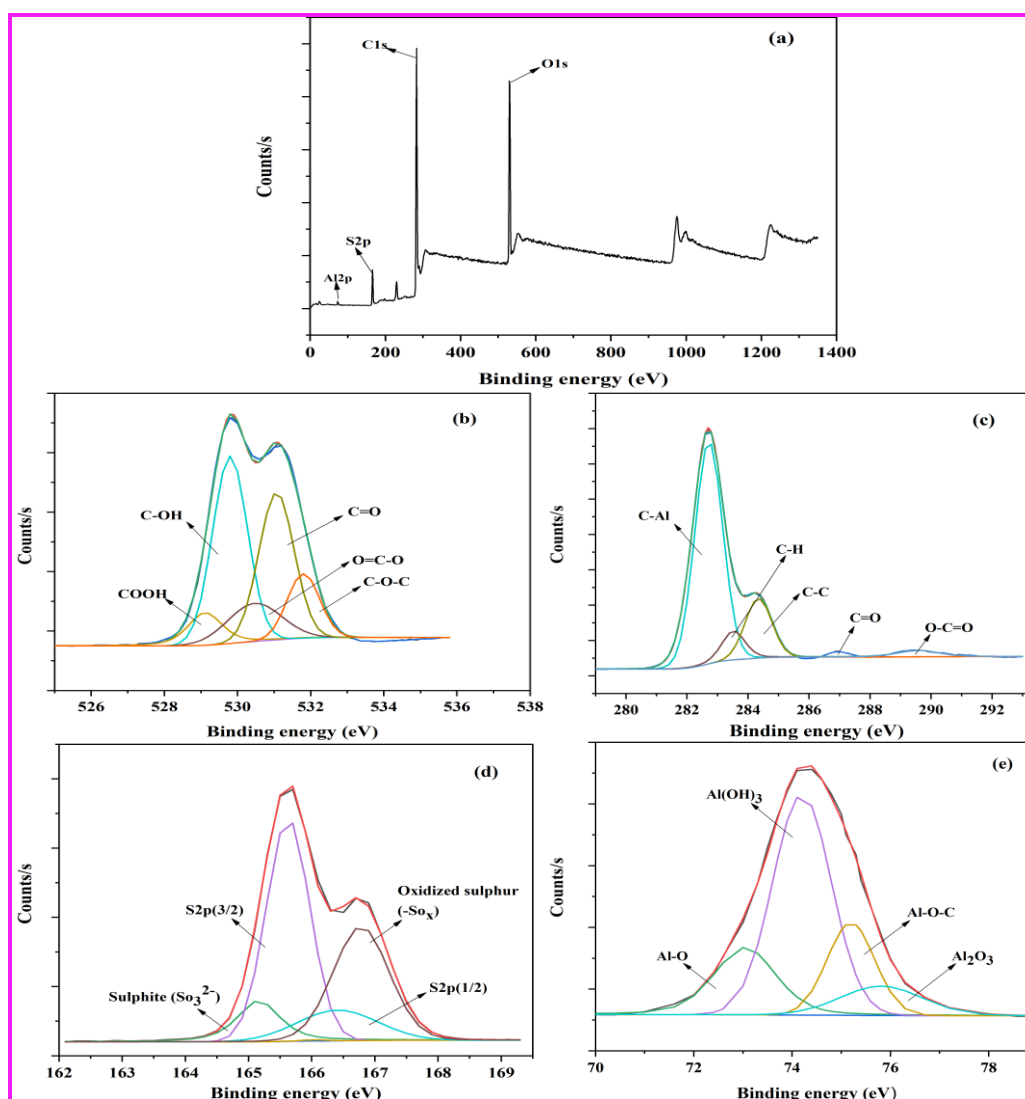
Figure 6.16 X-ray photoelectron spectra's (XPS) wide spectrum (a) and broadened images of (b), (c), (d) and (e) are narrow binding energies spectrum of O1s, C1s, S2p and nano-Al$_2$O$_3$ for best performing (ALCA-1.5) membrane.

6.2.15 Arsenic-V removal from fabricated hollow fiber membranes

The percentage arsenic-V removal from various concentrations (0.6, 1 and 1.5 wt%) of nano-Al_2O_3 in CA/PPSU and CAP/PPSU membranes and the pristine membrane was demonstrated in Figure 6.17. Initially, after ionizing with water (H_2O), neutral arsenate acid (H_3AsO_4) was reduced to arsenate oxide (AsO_4^{3-}) for fast decontamination of membrane surfaces, which can be shown in Equation 3.1. This is because uncharged arsenate ions in water are inconvenient in the pH range of 6 to 9 for the removal. In addition, due to the electrostatic repulsion, negatively charged arsenate ions can easily be repelled from negatively charged membrane surfaces (Zheng et al. 2012). The decreased arsenate oxide from the neat membrane surfaces was witnessed. The membrane ALCA-0 removes 17.12% and ALCAP-0 of 25.85% with the little negative surface charge hydrophilic sites shows negligible arsenic-V properties from aqueous solution. From Figure 6.18(a)-(b), the arsenic-V permeability properties for neat membranes ALCA-0 and ALCAP-0 were 23.06 L/m^{2}h bar and 39.89 L/m^{2}h bar respectively. The removal percentage of arsenic-V was considerably improved by adding the cumulative dosages of nano-Al_2O_3 to pristine CA/PPSU membranes. The ALCA-1.5 and ALCA-1 modified membranes extract 98.67% and 94.89% with the arsenic-V permeabilities as 88.41 L/m^{2}h bar and 53.42 L/m^{2}h bar respectively. The membrane removed increased arsenic-V, however, the active sites are saturated and the membrane needs to be regenerated. The significant improvement in decontamination of arsenic-V is due to the better distribution of the used nanoparticle (nano-Al_2O_3) and additives (CA and CAP) on membrane surfaces. The potential interaction between CA/PPSU and CAP/PPSU has been shown in Figure 6.19(a) – (b) respectively. The interaction of nano-Al_2O_3/PPSU was also observed; there is an interaction between Van der Waals and ionic dipole interaction. In the polymers, the hydrogen bonding interaction was absent.

The negative charge on the membrane surfaces was exerted by the presence of the carboxylic (–CO_2H) and amine (–NH_2) functional sites (Pérez-Sicairos et al. 2009b). In addition, the occurrence of negatively charged –SO_3H functional group on the membrane surface also influence negatively charge on the membrane surface (Abdullah et al. 2019). Increased negative charged membrane surfaces, which repels arsenic-V species that are negatively charged. The indecent of the negatively charged surfaces is also due to aqueous solution deprotonation by the acetate group (Kumar et al. 2020b). In this study, with improved dosages of nano-Al_2O_3 in CAP/PPSU dope solution, the percentage rejection of arsenic-V was increased and then reduced. As such the ALCAP-0.6 membrane shows 21.73% and small improvement in arsenic-V rejection of 34.02% from ALCAP-1 membrane, with

permeabilities as 61.35 L/m^{2}h bar and 86.71 L/m^{2}h bar respectively. A decrease in percentage arsenic-V removal with 1.5 wt% of nano-Al$_2$O$_3$ in CAP/PPSU (ALCAP-1.5) dope solution extracts 25.75% with the permeability 99.24 L/m^{2}h bar respectively. We fabricated in our previous work, hollow fiber membranes by 1 wt% of ZrO$_2$ in CA/PPSU (PZCA-1) and 0.6 wt% of ZrO$_2$ in CAP/PPSU (PZCAP-0.6) for the removal of arsenic-V from aqueous solution. Membranes PZCA-1 and PZCAP-0.6 removes 87.27% and 70.48% of arsenic-V with permeabilities of 89.94 L/m^{2}h bar and 70.59 L/m^{2}h bar respectively (Kumar et al. 2020b). In another chapter of this thesis, 1 wt% on zinc-magnesium oxide (ZnO-MgO) in CA/PPSU (ZMCA-1) and 0.6 wt% of ZnO-MgO in CAP/PPSU (ZMCAP-0.6) removes arsenic-V as 78.48% and 81.31% with permeabilities 198.47 L/m^{2}h bar and 69.58 L/m^{2}h bar respectively (Kumar et al. 2020c). In addition, with 44.01 L/m^{2}h bar permeability, the neat PPSU membrane removed 22% arsenic-V respectively (Kumar et al. 2019a). Additionally, the percentage of arsenic-V removal was reduced due to the concentration polarization from increased agglomeration on the membrane surfaces. Substantial dosages of the nano-Al$_2$O$_3$ do not affect the CAP/PPSU dope solutions with arsenic-V permeability. The concentration polarization for arsenic-V removal of the fabricated hollow fiber membranes was illustrated in Table 6.3.
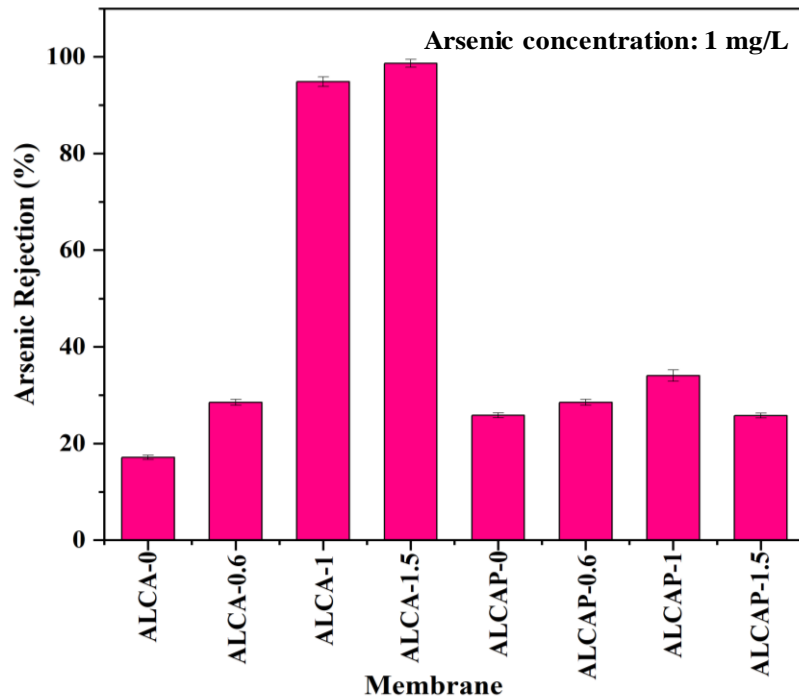
Figure 6.17 Arsenic-V removal properties from fabricated hollow fiber membranes.
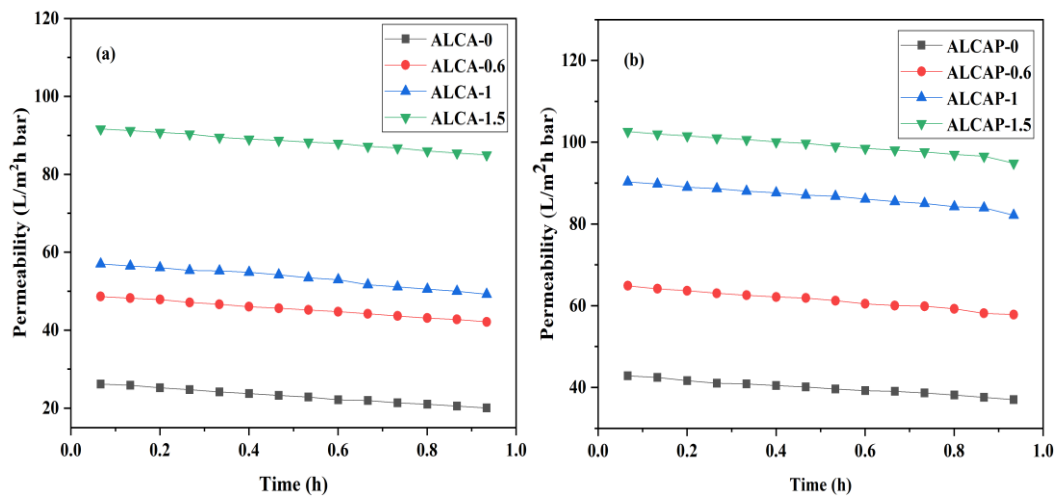
Figure 6.18 Arsenic-V permeabilities of (a) nano-Al_2O_3/CA/PPSU and (b) nano-Al_2O_3/CAP/PPSU from prepared membranes respectively.

(a)

(b)

R=H
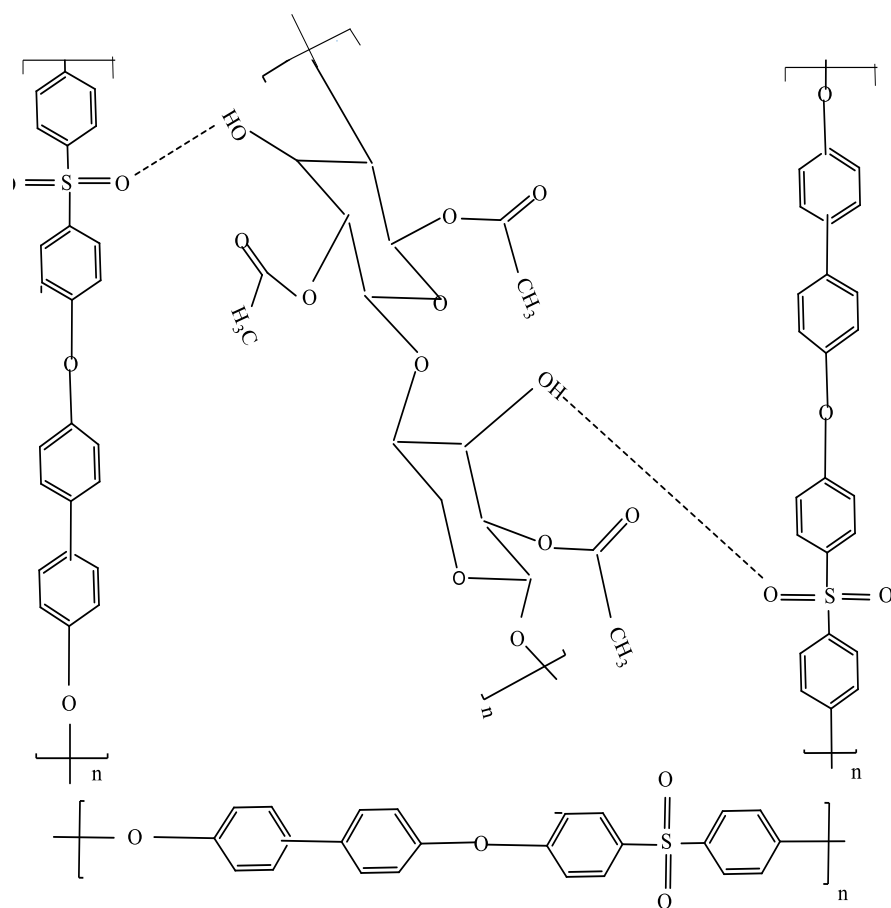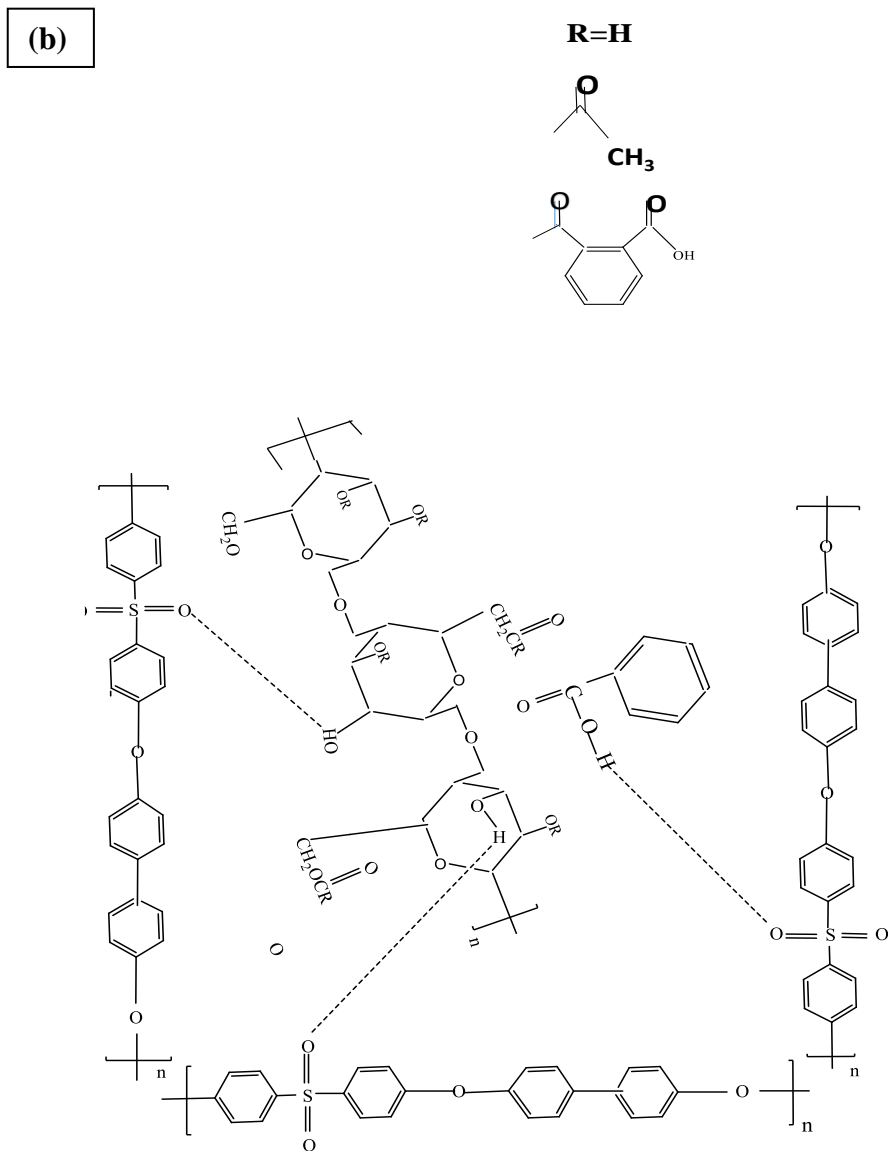
Figure 6.19 (a) Possible interaction of polyphenylsulfone and cellulose acetate, (b) Possible interaction of polyphenylsulfone and cellulose acetate phthalate.

Table 6.3 Concentration polarization for arsenic-V removal of the fabricated membrane

Membrane codes	Velocity (v) $\times 10^{-3}$ (m/s)	Mass transfer coefficient (K) $\times 10^{-5}$ (m/s)	Concentration polarization ($\frac{Cm}{Cb}$)
ALCA-0	3.26	1.425	1.066
ALCA-0.6	3.82	1.480	1.142
ALCA-1	6.23	1.777	2.164
ALCA-1.5	4.10	1.358	5.713
ALCAP-0	3.86	3.063	1.3
ALCAP-0.6	4.56	1.491	1.241
ALCAP-1	5.81	1.740	1.341
ALCAP-1.5	7.55	1.811	1.096

6.3 SUMMARY OF THE PRESENT WORK

The novel hollow fiber ultrafiltration membranes were successfully fabricated from aluminum oxide concentrated with cellulose acetate/polyphenylsulfone and cellulose acetate phthalate/polyphenylsulfone. The effect on the CA/PPSU and CAP/PPSU ultrafiltration membranes of increased aluminum oxide nanoparticles was well understood. The structure was interpreted as a crystalline morphological structure from TEM and XRD results. As the nano-Al_2O_3 concentrations increased, the finger-like and micropores were expanded. The introduction of nano-Al_2O_3 concentrations has improved surface roughness from atomic force microscopy (AFM) of the modified membranes. The temperature stability of the fabricated hollow fiber membranes has been improved by various dosages of nano-Al_2O_3 from TGA analysis. The doping of the various nano-Al_2O_3 concentrations improved hydrophilic properties such as pure water permeability, water uptake and porosity. With the results of nano-Al_2O_3 in the CA/PPSU and CAP/PPSU dope solution, the improved pure water permeabilities were 88.87 L/m^{2}h bar and 102.13 L/m^{2}h bar respectively for ALCA-1.5 and ALCAP-1.5 hollow fiber membranes. The increased antifouling efficacy was demonstrated by a high flux recovery ratio (FRR). The enhanced properties of arsenic-V removal were witnessed by improved electrostatic repulsion from the modified nano-Al_2O_3 membranes.

Due to the concentration polarization on the surfaces of the charged membranes, a decreased tendency to extract arsenic-V was observed from increased dosages of nano-Al_2O_3 and CAP additives on the polymeric (PPSU) dope solution. With the arsenic-V permeabilities of 88.41 L/m^{2}h bar and 99.24 L/m^{2}h bar, the improved arsenic-V removal properties from ALCA-1.5 and ALCA-1 were recorded as 98.67% and 94.64% respectively. The fabricated hollow fiber membranes are suitable for the efficient decontamination of arsenic-V from the arsenic-V-contaminated aqueous solution.

CHAPTER -7

HYDROPHILIC POLYDOPAMINE/POLYVINYLPYRROLIDONE BLENDED POLYPHENYLSULFONE HOLLOW FIBER MEMBRANES FOR THE REMOVAL OF ARSENIC (As-V) FROM WATER

Abstract

In this chapter, the polyphenylsulfone (PPSU) hollow fiber membranes were prepared using increased dosages of the polydopamine (PDA; 1, 2, 3 and 5 wt%) in the presence of pore-forming agent as polyvinylpyrrolidone (PVP) by non-solvent induced phase separation (NIPS) process as-fabricated membranes were tested for the morphologies and topological studies using filed emission scanning electron microscopy (FESEM) and atomic force microscopy (AFM) respectively. The used PDA nanoparticle was investigated using x-ray diffraction (XRD) to interpret the PDA crystallinity analysis. The hydrophilicity /hydrophobicity behavior of the hollow fiber membranes was confirmed using contact angle measurement, porosity/water uptake, pure water permeability and antifouling studies. Also, the fourier transform infrared spectroscopy (FTIR) and x-ray photoelectron spectroscopy (XPS) were also employed to interpret the different functional groups and binding energies. An attempt to investigate the arsenic-V removal from the hollow fiber membranes was also carried out. Also, increased arsenic-V rejection was observed from 3 wt% of PDA in PPSU/PVP (PDA-3) membrane as 87.15% with the flux of 31.80 L/m^2h, which was superior as compared to the neat membrane (PDA-0) as 67.70% with arsenic-V flux of 15.07 L/m^2h at a transmembrane pressure of 0.2 MPa with laboratory prepared 5 mL/L of arsenic-V solution.

7.1 INTRODUCTION

In recent decades, groundwater depletion and degradation has a significant impact on climate, poor resource management and environmental instability hampered the availability of clean drinking water (Vairavamoorthy et al. 2008). Freshwater is required for life-sustaining human activities including cooking, cleaning, farming, and drinking pure water. Modern activities, on the other hand, have thrown off the balance between use and purification, resulting in a scarcity of drinkable water. The demand for fresh drinking water is skyrocketing as the world's population and urbanization continue to grow (Cohen 2006). The world's total population is currently around 7.1 billion people and it is expected to exceed 9 billion people by 2050. As a result, annual water demand is expected to rise by 64 billion cubic meters. Untreated heavy industrial wastes, such as heavy metals and metalloids, are often the primary sources of metallic contaminants in aquatic environments. Heavy metals, which are needed for industrial production, have also been identified as an essential contaminant for wildlife, plants and humans (Hinrichsen and Tacio 2002). Scientists and researchers face a significant

challenge in extracting harmful waste pollutants from aqueous solution and reusing it for other purposes.

Due to its high toxicity and carcinogenicity, arsenic poses a severe threat to human health and the environment. Arsenic pollutes the atmosphere from various natural and anthropogenic causes, contaminating freshwater. Exposure due to long-term causes cancer of the kidney, bladder, lungs, liver and skin, and a variety of non-cancerous symptoms including black foot disease, keratosis pigmentation and nausea, among others (Saha et al. 1999). As a result, the Indian Agency of Research on Cancer (IARC) classified arsenic as a potent carcinogen (IARC, 2012). Arsenic is found mainly inorganic arsenic oxides, such as arsenite As(III), arsenate As(V) and methylated structures. Arsenic in its reduced form, arsenite As(III), is more toxic than arsenate. Due to its strong affinity for thiol-groups in arsenic (V). As(III) is 25-60 times more detrimental to human health than As(V) (Rasul et al. 2002). As a result, preoxidation of As(III) to As(V) is usually necessary prior to the arsenic removal process. Many research studies showed that various oxidizing agents converted As(III) to As(V). As a result, the most effective oxidizing agents were determined to be chlorine, ozone and permanganate. Chlorine dioxide and monocloramine are also commonly used for converting As(III) to As(V) (Katsoyiannis and Zouboulis 2006).

According to WHO documentation, arsenic is a leading cause of death for thousands of people worldwide. Because of the possible health risk posed by arsenic, the United States Environmental Protection Agency (USEPA) lowered the average toxicity level for distilled water from 50 µg/L to 10 µg/L in 2001 (Dambies 2005; Shao et al. 2021). To address the issue concerning arsenic toxicity, a cost-effective, environmentally sustainable technology for removing arsenic from contaminated water and safe for human health is essential. Several arsenic treatment methods have been investigated for removing arsenic from drinking water. Different arsenic treatment processes adsorption, biological treatment, chemical-sorption, filtration, ion exchange and membrane filtration are few to mention (Ng et al. 2004). Nonetheless, environmental and operational restrictions such as higher costs, complicated and time-consuming separation methods. Nevertheless, realistic implementations are hampered by technical and environmental limitations such as higher costs, complex and time-consuming separation methods. Compared to reverse osmosis and nanofiltration, the ultrafiltration membrane technology for extracting arsenic from arsenic-contaminated water has sparked a lot of interest because it is less costly, has a lower operating pressure and needs less energy, and has higher permeability with efficient arsenic rejection (Brandhuber and Amy 2001).

Various polymers have been used to fabricate and develop ultrafiltration membrane characteristics, according to the literature. One of the sulfone polymer families, the polyphenylsulfone (PPSU) has recently become an essential polymer for water filtration applications.

Polyphenylsulfone (PPSU) has a number of essential characteristics, such as enhanced stability, improved stress and chemical resistance and excellent mechanical properties. Although hydrophobic and reduced porous membrane morphologies restrict its use in membrane filtration applications due to increased fouling tendency (Gronwald et al. 2020). Various adsorbents are being utilized to change the membrane surface and strengthen the membrane's hydrophilic and rejection properties. Aluminum oxide (Al_2O_3), zirconium oxide (ZrO_2), zinc oxide (ZnO), titanium oxide (TiO_2) and graphene oxide are the adsorbents used for the membrane fabrication (Amy 2005). Nevertheless, certain restrictions in enhancing the membrane's properties are mentioned above. Polydopamine (PDA) has in turn constituting benzene, catechol, quinone and amine functional sites, improving efficiency membranes infiltration (Fang et al. 2017; Kallem et al. 2021). Recently,

Xi et al. (2009) hydrophobic polyethylene (PE), PVDF and PTFE porous membranes were modified to more hydrophilic by surface coating of poly(DOPA) layer, under mild conditions. The close interaction between poly(DOPA) and membrane materials maintained the poly(DOPA) layer containing carboxyl, hydroxyl and amino groups tightly adhered to the membranes. The water contact angle of the PDA modified membranes was slightly lower than that of the original membranes, implying that the membrane hydrophilicity was significantly improved.

Jiang et al. (2010) developed a novel and cost-effective method for inert polyethylene (PE) porous membranes by surface hydrophilization and heparinization. Dopamine tends to self-polymerize and cross-link on the surface of PE porous membranes in an aqueous solution. The hydrophilicity and water flux of the dopamine-coated and heparin-immobilized PE membrane surfaces was substantially higher than that of the pristine membrane.

Li et al. (2012) fabricated hydrophilic nanofiltration membranes by simply dipping in polysulfone (PSf) ultrafiltration substrate with increased self-polymerized and strongly adhered PDA concentrations. Water contact angle measurements were used to determine membrane surface hydrophilicity. Membrane hydrophilicity improved significantly after coating a polydopamine (PDA) substrate, especially after double coating. The composite

membranes had a positively charged characteristic and good stability in the water phase NF process.

Jiang et al. (2014) utilized PDA and polyvinylidene fluoride (PVDF) to fabricate ultrafiltration flat sheet membrane. By blending with PDA NPs, the hydrophilicity, strength, hydrodynamic permeability, antifouling properties and better thermal stability of PVDF membranes are improved significantly. Due to the strong interactions among PDA NPs and PVDF chains, PVDF/PDA blended membranes have good long-term stability and durability in aqueous environments.

Hebbar et al. (2016) developed polyethyleneimine (PEI) composite membranes along with different concentrations of PDA by immersion precipitation method for the removal of Pb^{2+} and Cd^{2+}. As per the outcomes, modified membranes have shown increased porosity, water absorption capability and hydrophilicity with increased PDA concentrations. The modified membrane exhibited superior antifouling behavior with 3 wt% modified halloysite nanotube (MHNT) dosage in the membrane matrix, with an FRR of 74.5% and a reversible fouling ratio of 60.7% respectively.

Fang et al. (2017) fabricated polyethersulfone (PES)/PDA mixed matrix membrane for other heavy metal removals such as lead (Pb^{2+}), copper (Cu^{2+}) and cadmium (Cd^{2+}) from contaminated aqueous solution. The improved rejection of heavy metals can be observed with the PDA dosages membranes than the pristine membrane. Consequently, the PDA dosage also showed significant improvement in the membrane morphologies and pure water flux studies.

Rao et al. (2017) fabricated mixed matrix membranes by MOF/graphene oxide (GO) onto polysulfone (PSf) coated PDA for the removal of copper (Cu-II) from the membrane surface. At a pressure of 0.7 MPa and pH of 5.0, the rejection of copper (II) approaches around 90% while maintaining a relatively high flux of about 31 $L/m^2/h$, as compared to other heavy metals such as lead (Pb^{2+}), nickel (Ni^{2+}), cobalt (Co^{2+}) and iron (Fe^{3+}) ions.

Ma et al. (2018) fabricated PDA/regenerated graphene oxide/cellulose acetate (CA) composite membranes with vacuum-assisted filtration. The Cu(II) removal ratio of up to 99.99% were achieved using PDA/RGO/CA membranes. Because of the thin sheet structure of PDA/RGO, it has a high adsorption capability. A PDA's amine and hydroxyl groups have binding sites for heavy metal ions to coordinate. PDA also served as an excellent crosslinking agent between the GO sheets, enhancing membrane stability.

He et al. (2020) developed thin-film nanocomposite membranes using polyacrylonitrile (PAN)/PDA/metal-organic framework (MOF) by interfacial polymerization. As fabricated, PDA-contained membranes showed enhanced cadmium (Cd^{2+}), nickel (Ni^{2+}) and lead (Pb^{2+}) removal from aqueous solution. The water flux of PDA/MOF-TFN membrane was increased by 30% compared to the traditional thin-film composite (TFC) membrane, while the reverse salt flux was decreased by 44%. The water flux of the polydopamine/metal-organic framework thin-film nanocomposite (PDA/MOF-TFN) membrane increased by 6% over that of the conventional MOF-TFN membrane, although the reverse salt flux reduced by 62%. Unfavorably, PDA nanoparticles clump together and form aggregation on the membrane surface separation layer, restricting the use of their functional groups and dramatically lowering the hydrophilic membrane properties. However, no research work using the polydopamine membrane filtration process to remove arsenic-V has been identified in the literature.

Therefore, we used a constant dose of polyvinylpyrrolidone (PVP), a hydrophilic pore-forming additive, to control the membrane morphological structure of the non-toxic PVP, which is miscible with a wide variety of polymeric membrane materials, to illustrate as an above-stated research gap. PVP has piqued the interest of many researchers due to its ability to dissolve in water and a variety of other organic solvents. Increased porous morphological structure resulted from the application of PVP to the membrane surface, which increases hydrophilicity and pure water permeation properties (Mansur et al. 2018; Tofighy et al. 2021).

The PVP's use as a pore former in PPSU/PDA hollow fiber membranes for membrane fabrication and arsenic rejection has yet to be reported in the literature. In the present study, hollow fiber membranes were fabricated using increased dosages of PDA in PPSU/PVP using non-solvent induced phase separation (NIPS). Contact angle analysis, porosity/water uptake interpretation and antifouling studies were conducted to validate the modified membrane surfaces hydrophilicity. The XRD analysis was also carried out for as used PDA additive. The morphological and topological structures and PDA's effect on PPSU/PVP have been well defined. Furthermore, using fabricated hollow fiber membranes, an arsenic-V removal tendency was evaluated by a laboratory-developed 5 mL/L of arsenic-V solution (pH 6.8± 0.2) at 2 bar transmembrane pressure.

7.2 RESULTS AND DISCUSSION

7.2.1 X-ray diffraction (XRD) of polydopamine

The crystallinity, x-ray diffraction (XRD) measurement of PDA was illustrated in Figure 7.1. The diffraction peaks were documented at an angle of $12.11°$, $20.07°$, $24.57°$, $34.02°$, $37.93°$, $54.54°$ and $62.58°$ with reference planes (0 0 1), (1 0 0), (0 0 2), (1 1 0), (0 0 3), (2 1 0) and (3 0 0) respectively. The polydopamine nanoparticle peaks were attributed to JCPDS card number 00-029-1487 and executed a crystalline structure.
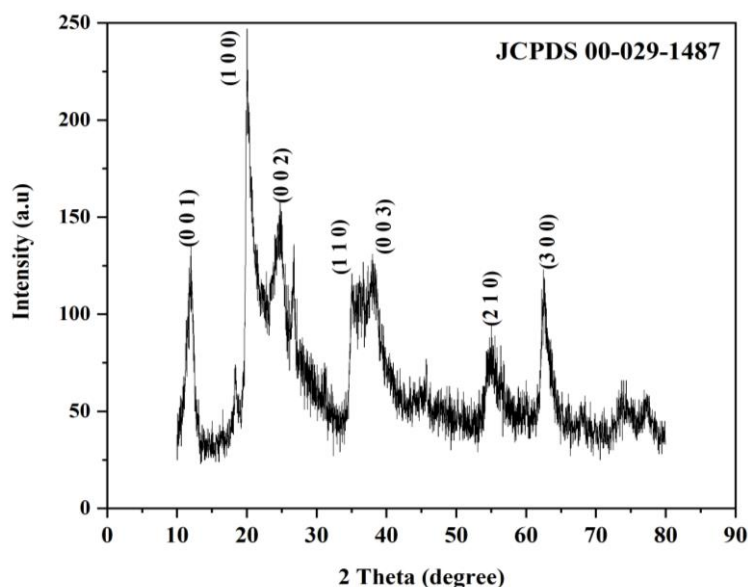
Figure 7.1 Illustration of x-ray diffraction for polydopamine.

7.2.2 Scanning electron microscope investigation of fabricated hollow fiber membranes

The scanning electron microscopy analysis of fabricated virgin and PDA dosaged hollow fiber membranes were illustrated in Figure 7.2(a) and (b). An asymmetric structure on both sides and finger-like morphologies sandwiched between a sponge-like structure can be seen in the morphological pictures. Because of the more hydrophobic behavior of the PPSU polymer, the neat membrane (PDA-0) had many macrovoids and less porous structure as shown in Figure 7.2(a). Increased concentrations of PDA to the virgin membrane in the membrane sublayer bulged or expanded the microvoids and finger-like morphologies. The addition of constant polyvinylpyrrolidone (PVP) into the neat dope solution increased the porous surface structure significantly. In addition, PVP is water-soluble polymer. When the membrane was immersed in water, some PVP leached out from the membrane matrix in the coagulation bath. The dosage of PVP to the dope solution can accelerate the membrane fabrication and migration of nanoparticles on the surfaces of the membrane, which in turn resulted in

enhanced pore interconnectivity (Kajekar et al. 2015a). The improved porous structure is also due to the reduced viscosity of the casting solution and decrease in water miscibility, increasing the ratio of water inflow to solvent outflow, resulted in an improved porous structure (Hebbar et al. 2017a). With increased PDA dosage to the neat dope solution, delayed demixing of the polymer and solvent (NMP) in nonsolvent (water) results in enhanced sponge-like structure, as seen in Figure 7.2(d) and (e). The scanning electron microscopy (SEM) cross sectional complete view was illustrated in Figure 7.3. The neat and increased dosages of PDA contained PPSU/PVP hollow fiber membrane's surface morphologies were illustrated in Figure 7.4. From the figure it is revealed that the neat membrane surface contains less porous structure. With the increased dosages of PDA in the membrane matrix results in enhancement of porous structure. The enhanced porosity on the membrane surfaces also better outcomes the hydrophilic, porosity/water uptake and antifouling properties. The inner/outer diameter (ID/ OD) and mean pore radius of the fabricated hollow fiber membranes were illustrated in Table 7.1.
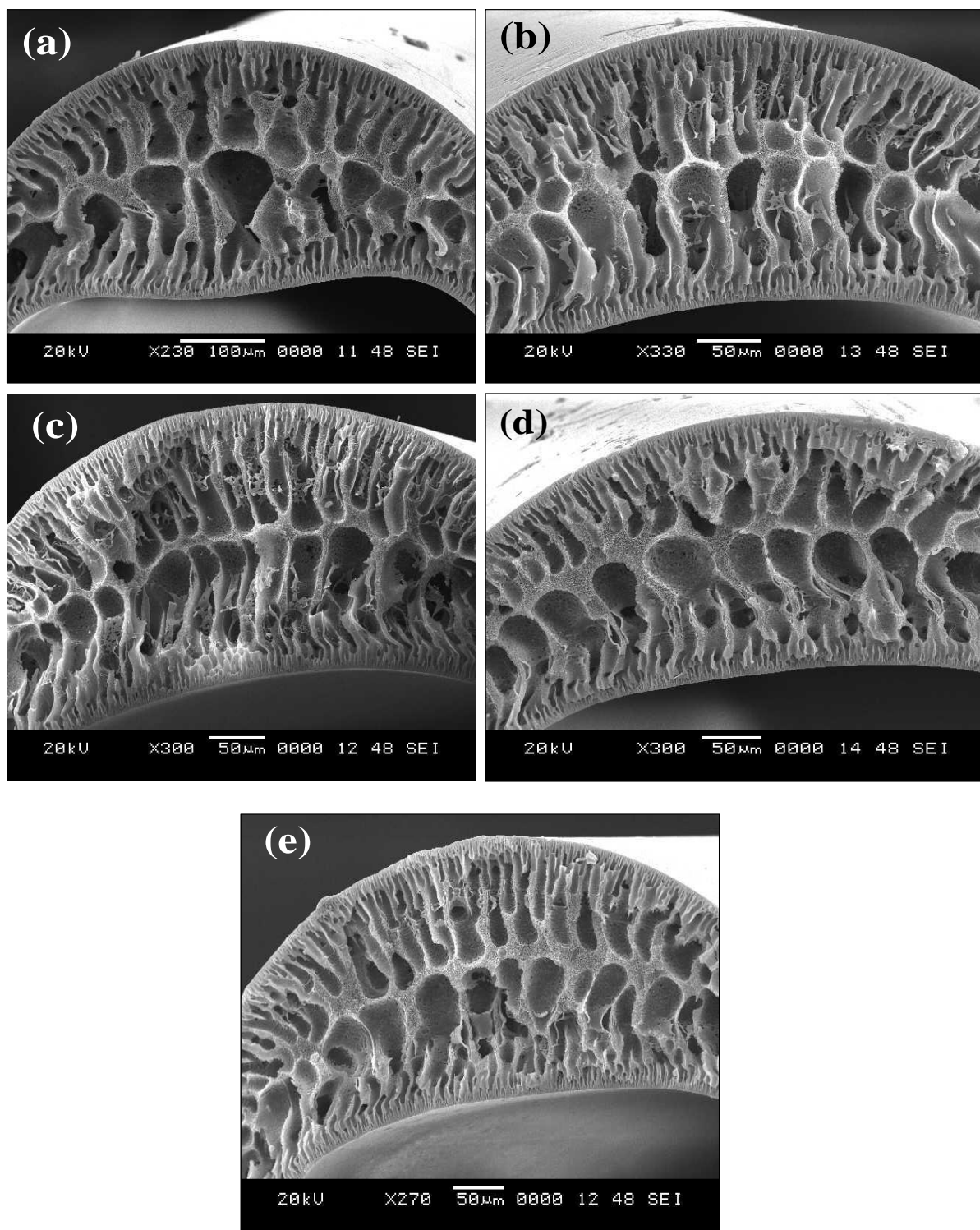
Figure 7.2 (a) cross sectional scanning electron microscopy (SEM) pictures of fabricated neat membrane (PDA-0), 1 wt% (PDA-1), 2 wt% (PDA-2), 3 wt% (PDA-3) and 5 wt% (PDA-5), of PDA in PPSU/PVP membranes represented as a, b, c, d and e respectively.
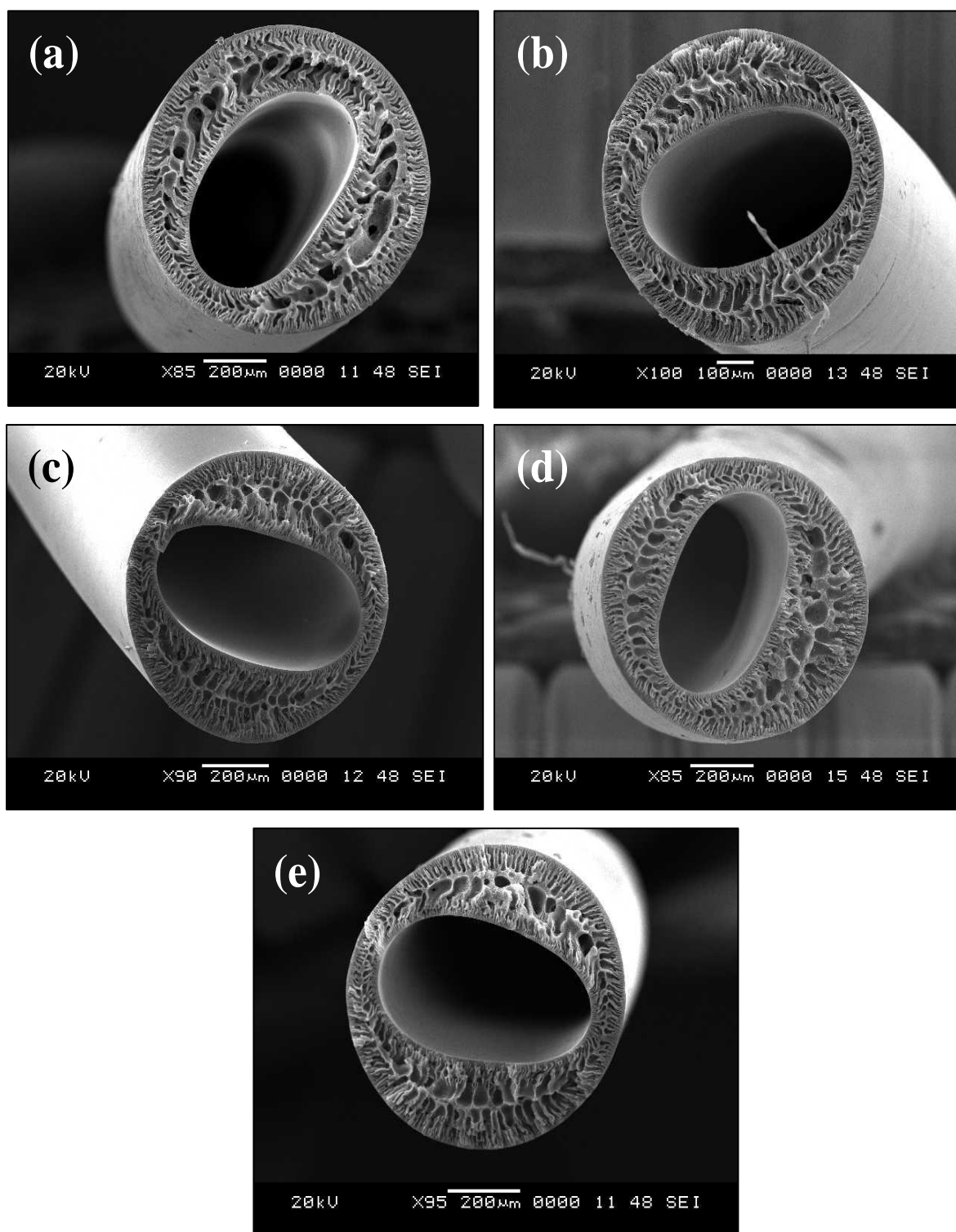
Figure 7.3 (a) cross sectional (complete view) scanning electron microscopy (SEM) pictures of fabricated neat membrane (PDA-0), 1 wt% (PDA-1), 2 wt% (PDA-2), 3 wt% (PDA-3) and 5 wt% (PDA-5), of PDA in PPSU/PVP membranes represented as a, b, c, d and e respectively.
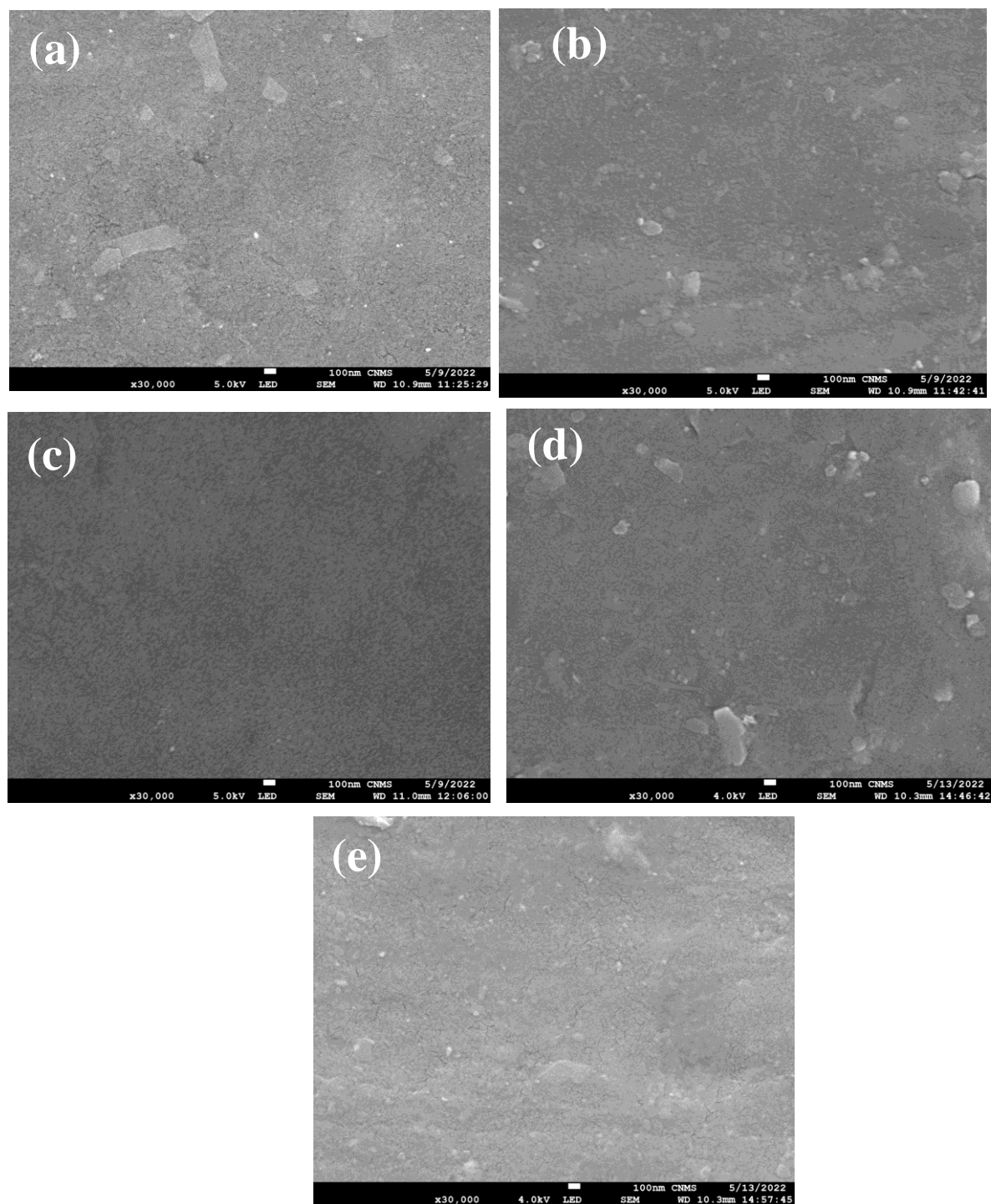
Figure 7.4 Scanning electron microscopy (SEM) surface morphological analysis of the prepared neat membrane (PDA -0) as 'a', increased polydopamine concentrations 1 wt%, 2 wt%, 3 wt% and 5 wt% in PPSU/PVP as PDA-1, PDA -2, PDA -3 and PDA -5 as 'b', 'c', 'd' and 'e' respectively.

Table 7.1 Outer/ inner (OD/ID) diameter and mean pore radius of the fabricated hollow fiber membranes

Hollow fiber membranes	Outer diameter (OD in µm)	Inner diameter (ID in µm)	Mean pore radius (m)
PDA-0	812	568	2.199×10^{-8}
PDA-1	758	533	1.852×10^{-8}
PDA-2	823	575	1.685×10^{-8}
PDA-3	859	531	2.294×10^{-8}
PDA-5	765	471	1.466×10^{-8}
Spinneret dimension, inner diameter: 550 µm, outer diameter:1100 µm			

7.2.3 Hydrophilicity/hydrophobicity characterization of membranes

The virgin and PDA dosage PPSU/PVP hollow fiber membranes hydrophobic/hydrophilic nature was illustrated in Figure 7.5. The virgin membrane (PDA-0) shows a contact angle of $75.96^{\circ} \pm 3.87^{\circ}$. However, incremental dosages of PDA to neat membrane exhibited increased hydrophilic properties. The PDA-5 and PDA-3 membranes showed $63.32^{\circ} \pm 5.38^{\circ}$ and $60.49^{\circ} \pm 4.30^{\circ}$ respectively. With slightly reduced PDA concentrated membrane PDA-1 and PDA-2 revealed $68.02^{\circ} \pm 2.86^{\circ}$ and $67.78^{\circ} \pm 1.38^{\circ}$ respectively. The increased contact angle parameter from the modified hollow fiber membrane is more hydrophobic and lower surface porous morphological structures. The hydrophobic membrane surface was internally modified to more hydrophilic as the incremental PDA is added to neat dope solution. The existence of amine and hydroxyl functional sites on the membrane surface leads to reducing the contact angle parameters (Jiang et al. 2014). A migrant behavior of the as used PDA on the membrane surface was also one reason for decreasing the values of contact angle. The catecholamine ($-NH_2$ and $-OH$) functional sites on the modified membrane surface played a vital role in enhancing membrane hydrophilicity (Mulyati et al. 2020b).
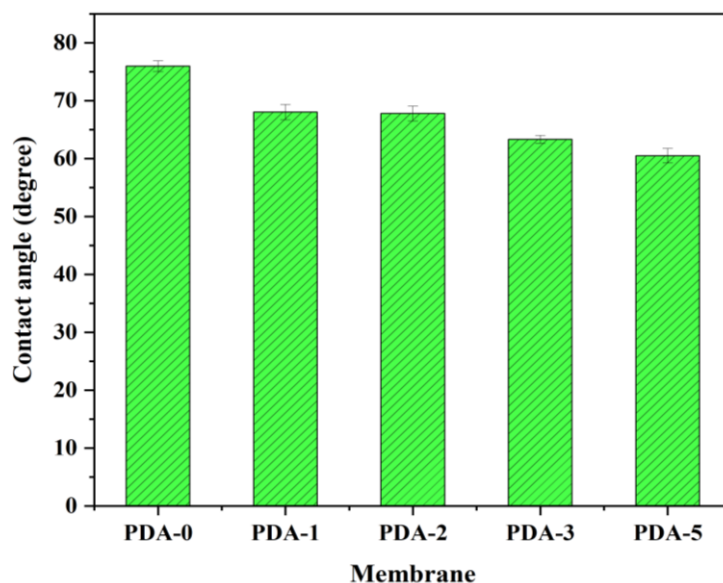
Figure 7.5 Contact angle measurement of the hollow fiber membranes.

7.2.4 Porosity/water uptake determination of prepared membranes

The water uptake and porosity investigation of the fabricated virgin and PDA containing hollow fiber membranes was demonstrated in Figure 7.6. The water absorption and porosity parameters for virgin membrane (PDA-0) were 24% and 10.93% respectively. Improved PDA concentrations (1, 2, 3 and 5 wt%) in the PPSU/PVP dope solution, there is a considerable enhancement of the hydrophilicity (porosity/water uptake) properties. With 1 and 2 wt% of PDA membrane (PDA-1 and PDA-2) revealed 26.43% and 23.88% respectively. Furthermore, the dosage of the PDA (3 and 5 wt%) membrane PDA-3 and PDA-5 were 29.78% and 50.50% respectively. The pristine hollow fiber membrane influenced the hydrophobicity behavior, with less porosity and water uptake properties. With the enhanced PDA dosage to pristine membrane, the SEM images indicated intensified porous and finger-like predictions, which helped to increase water holding ability.

Furthermore, the increased PDA nanoparticle was leached out during the phase inversion process. Increased additive leaching in the coagulation bath increased the membrane structure's porous morphologies (Ang et al. 2020). Furthermore, increased additive dosages in the PPSU dope solution resulted in thermal instability, strengthening the porous morphological structures by allowing rapid demixing in the coagulation bath (Guo et al. 2019).
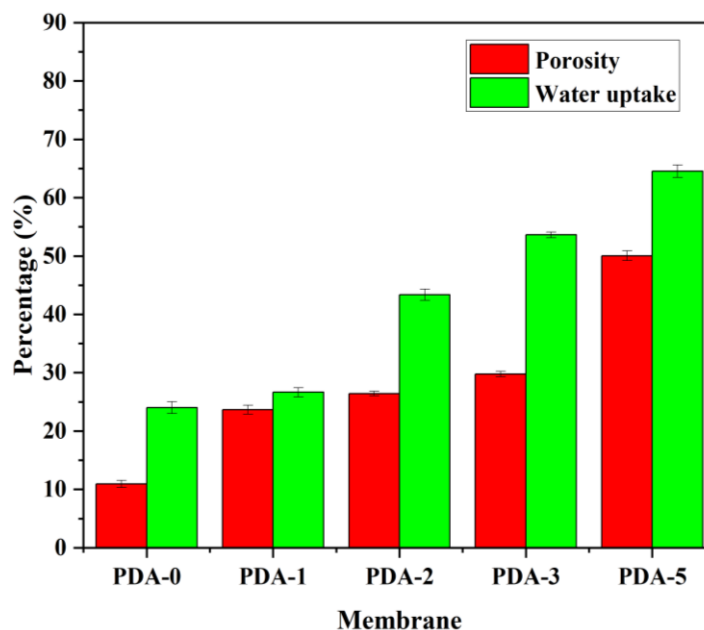
Figure 7.6 Porosity and water uptake measurement of the prepared hollow fiber membranes.

7.2.5 Pure water permeation of fabricated membranes

Pure water permeation at 0.2 MPa transmembrane pressure (TMP) of prepared pristine and PDA contained hollow fiber membranes was illustrated in Figure 7.7. Increased PDA dosaged PPSU hollow fiber membrane exhibited increased hydrophilicity and pure water permeability. According to figure, the enhanced pure water permeation for increased dosages of PDA concentrations by 5 wt%. Because of the increased hydrophilicity and water absorption capability, the PDA-5 hollow fiber membrane has a superior pure water flux of 37.44 L/m^{2}h respectively. The enhanced pure water permeation from the modified membranes is mainly due to the -NH$_2$ and -OH groups on the membrane surfaces, making them more hydrophilic (Ang et al. 2020). The high membrane surface area ensured superior hydrophilicity because of the homogeneous dispersion of the incorporated PDA nanoparticle into the membrane matrix. Additionally, the presence of a sulphuric acid (-SO$_2$) functional site on the membrane surfaces aids in the preservation of thick hydration layer which enhances the pure water permeation of the modified hollow fiber membranes. Nevertheless, due to the increased hydrophilicity and less porous behavior of the membrane morphological structures of the PPSU, pure water permeation of the neat membrane (PDA-0) as 15.07 L/m^{2}h, which was lower than PDA-5 membrane. The remaining PDA contained membranes PDA-1, PDA-2 and PDA-3 had pure water fluxes of 16.84, 22.66 and 31.80 L/m^{2}h respectively (Ayyaru and Ahn 2017).
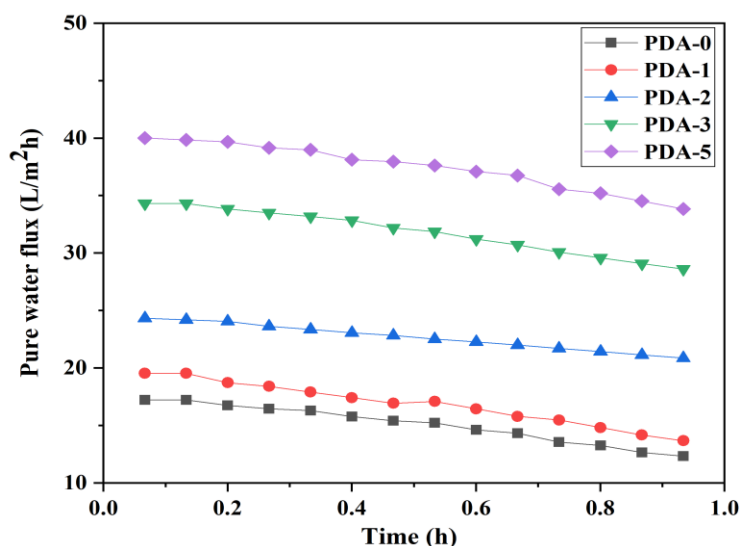
Figure 7.7 Pure water permeation study of the fabricated hollow fiber membranes.

7.2.6 Antifouling properties of prepared hollow fiber membranes

The antifouling properties of prepared neat and PDA hollow fiber membranes were presented in Figure 7.8. The antifouling research demonstrated that the hydrophilic and adsorptive properties of the membrane surfaces could be improved (Hebbar et al. 2016). The pristine hollow fiber membrane exposed more fouling propensity than PDA-contained membranes due to the more hydrophobic, less soluble and adsorptive sites on the membrane surface (Ayyaru and Ahn 2017). The pure water permeation (J_{w1}), BSA (J_p) and permeation after washing with water (J_{w2}) properties of the neat membrane were 18.50, 8.21 and 13.01 L/m^{2}h respectively as shown in Figure 7.8(a). The fouling phenomenon is believed to be caused by the aggregation of foulants molecules on the membrane active layer. The fouling has a significant impact on the membrane's separation efficiency and operating lifetime. Fouling creates a dense blocking layer that serves as a barrier to water permeation. Increased dosages of PDA nanoparticles (1, 2, 3 and 5 wt%) in the dope solution, on the other hand, resulted in improved parameters for pure water flux and BSA flux (Shao et al. 2014). The parameters of (J_{w1}), (J_p) and (J_{w2}) were 36.85, 24.21 and 19.85 L/m^{2}h respectively, as the dosage of 5 wt% PDA in PPSU/PVP dope solution was increased. The increased hydrophilic and absorptiveness of membrane surfaces are responsible for the improved flux properties in each filtration stage. More –OH and –NH$_2$ groups on the surface of modified membranes improved their hydrophilicity, antifouling nature and separation characteristics. From Figure 7.8(b) the neat PDA-0 membranes flux recovery ratio (FRR) and reversible fouling (R_r) were 70.32% and 25.94% respectively. For the PDA-5 membrane, the modified membrane with increased PDA dosage improved FRR and R_r properties by 92.83% and 38.96%, respectively.

The intensified FRR and R_r for more extended periods without significant flux decreases, suggesting that the modified hollow fiber membranes have a higher antifouling property. Similarly, the lower R_{ir} indicated a higher degree of fouling resistance. The results of using PDA as a nanoparticle to improve antifouling were consistent with past literature (Li et al. 2018c; Xi et al. 2009).
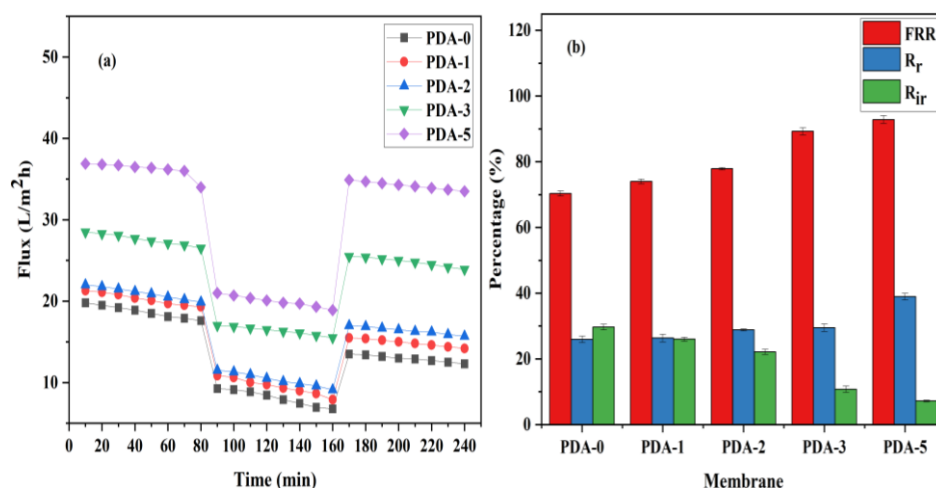
Figure 7.8 (a) Antifouling flux properties (b) antifouling properties of prepared neat and PDA contained hollow fiber membranes.

7.2.7 Surface roughness properties of hollow fiber membrane

Three-dimensional topological atomic force microscopy (AFM) images of the virgin and PDA- containing hollow fiber membranes were demonstrated in Figure 7.9. The surface roughness (R_a) value was used to illustrate the fabricated hollow fiber membranes (Kumar et al. 2019d). The 'R_a' of the pristine membrane (PDA-0) was 14.1 nm, gradually increasing as the progressive amounts of PDA were added to the neat membrane. The 'R_a' parameter was increased to 15.3, 17.1, 19.3 and 25.0 nm for membranes PDA-1, PDA-2, PDA-3 and PDA-5 respectively. It was noticeable from the increased R_a values that the percentage of PDA to the neat membrane has increased. Adhesion and the aggregation of nano-sized PDA on membrane surfaces can cause uneven peaks and valleys in modified membranes (Wang et al. 2017a). According to the Wengel theory, increased surface roughness is crucial in improving surface wettability modes of super hydrophilicity or super-hydrophobicity. Higher surface roughness of fabricated membranes was observed in the following literature with increased PDA nanoparticle dosages (Xiang et al. 2015; Zhu et al. 2018).
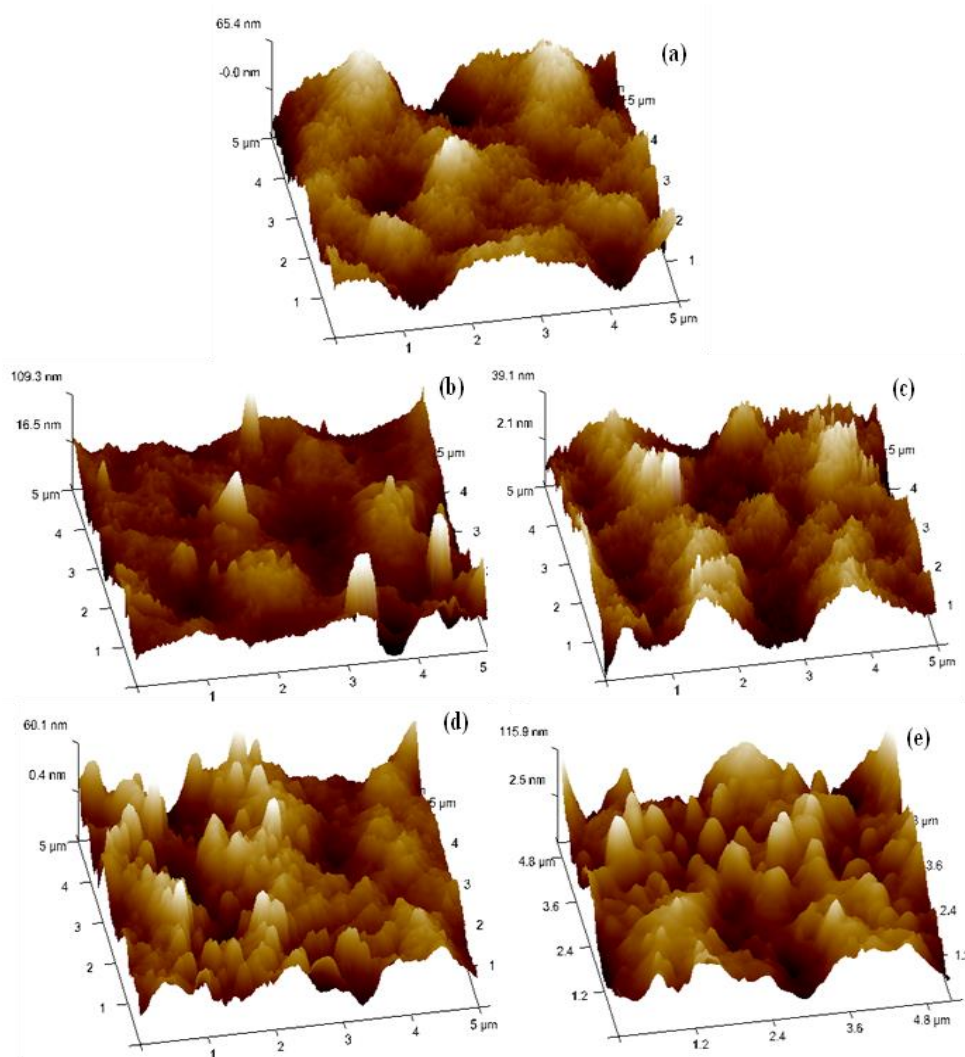
Figure 7.9 3-Dimensional atomic force microscopy (AFM) images of the fabricated neat membrane (PDA-0) as 'a' increased polydopamine concentrations 1 wt%, 2 wt%, 3 wt% and 5 wt% in PPSU/PVP as PDA-1, PDA-2, PDA -3 and PDA-5 as 'b', 'c', 'd' and 'e' respectively.

7.2.8 Attenuated total reflection–Fourier transform infrared spectroscopy (ATR-FTIR) analysis of the fabricated membranes

The interpretation of the best executed membrane (PDA-3) using attenuated total reflection–fourier transform infrared (ATR-FTIR) was demonstrated in Figure 7.10. The absorption peaks at 3082-3575.01 cm^{-1} was due to –OH group in FTIR of the PDA-3 membrane. The peaks at 2935.42 cm^{-1} and 2327.53 cm^{-1} are due to the –C–H group and –O=C=O stretching respectively. The –C=O, –C=N stretching and –C=C resonance vibration have peaks at 1735.96, 1658.44 and 1585.67 cm^{-1} respectively. The presence of polydopamine on the membrane surface due to self-polymerization was suggested by the –C=C resonance

196

vibration in the PDA/PPSU/PVP membrane. The –N–H rocking vibrations are illustrated by the peak at 1485 cm^{-1} (Wu et al. 2015). As a result, peaks at 1299.42, 1240.26 and 1148.58 cm^{-1} were assigned to the functional groups –C–O aromatic ester, –C–N amine stretching and –C–O ester stretching respectively. The functional group 630.33 cm^{-1} corresponded to the alkyne –C–H bending group. The presence of hydroxyl, imine and amine functional groups on the modified membrane indicates that polydopamine nanoparticles were blended into the PDA-3 hollow fiber membrane (Xiang et al. 2015).
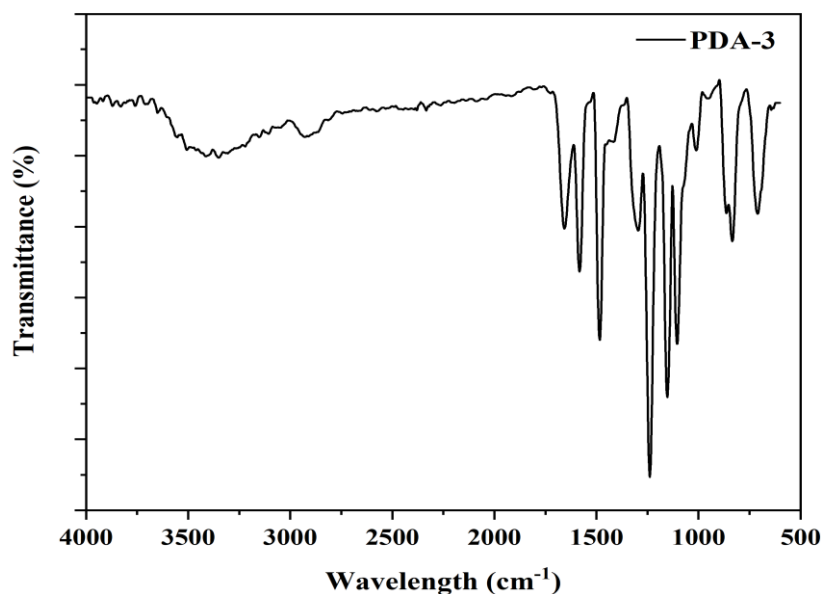
Figure 7.10 ATR-FTIR spectrum of the best performing hollow fiber membrane (PDA-3).

7.2.9 Surface potential measurement of hollow fiber membrane

Surface potential measurement of the as-prepared neat membrane (PDA-0) and PDA contained membrane (PDA-3) hollow fiber membranes was demonstrated in Figure 7.11. At pH 7, the surface charge of the neat membrane PDA-0 was -23.40 mV, while that of the modified membrane PDA-3 was -30.38 mV. As shown in the figure, hollow fiber membrane surface charge parameters are positive at an acidic pH (pH 2.5) and become negative as the pH rises to basic level (2.60 to 8). Furthermore, fabricated modified hollow fiber membranes (PPSU/PVP/PDA) primarily contain –OH, >NH and –NH$_2$ functional groups. A positive surface potential arises from the protonation of these groups in the membrane matrix. Nonetheless, deprotonation of these functional sites results in a more negatively surface potential membrane surface. As compared to the pristine membrane (IEP-2.90), the modified membrane (PDA-3) with the increased negative surface potential had a lower isoelectric point (IEP-2.60). The most important interpretation is that a higher PDA dosage in the membrane

197

resulted in high surface potential properties than a virgin membrane (Zhang et al. 2014). As a result of the increased PDA concentrations, the membrane's overall performance improved in hydrophilicity, permeability, antifouling properties and separation efficiency with the membrane's increased negative surface potential.
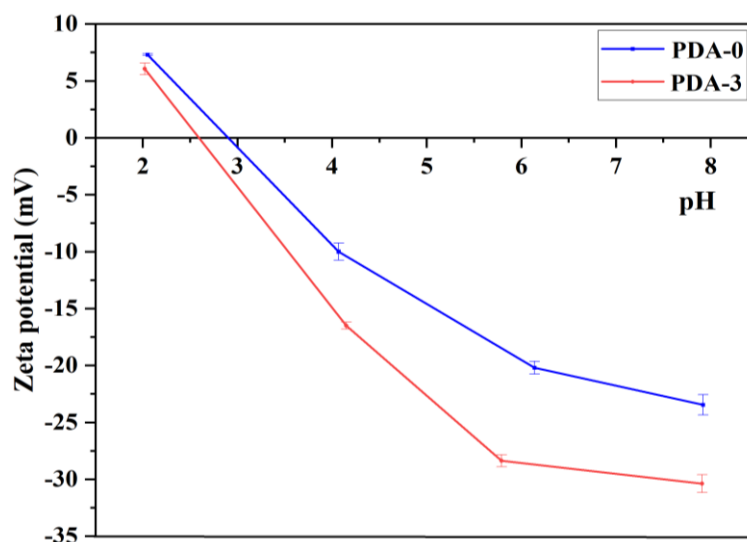
Figure 7.11 Zeta potential (surface potential) of fabricated neat membranes (PDA-0) and PDA-3 membranes.

7.2.10 Thermogravimetric analysis of the fabricated membrane

The thermogravimetric analysis (TGA) of a PDA incremental dosage membrane (PDA-3) was shown in Figure 7.12. The degradation behaviors of the tested membrane were interpreted using three-stage thermal degradation stages. The initial decomposition process started at room temperature and continued to 145.83 $^\circ$C, due to the volatilization of volatile matter and the removal of moisture from the membrane surface. The base polymer polyphenylsulfone (PPSU) and additive polyvinylpyrrolidone (PVP) chain groups are degraded in the second thermal degradation, ranging from 161.66 $^\circ$C to 453.24 $^\circ$C. The decomposition of used polydopamine (PDA) chain groups induced the third stage of thermal degradation, which ranged from 471.83 $^\circ$C to 685.05 $^\circ$C. Furthermore, at temperatures above 685.05 $^\circ$C, full polymeric chains degrade and gradually become ash material (Tiwari et al. 2019). According to the TGA tests, hollow fiber membranes containing a higher dosage (3 wt%) of polydopamine (PDA-3) in PPSU/PVP had high thermal stability.
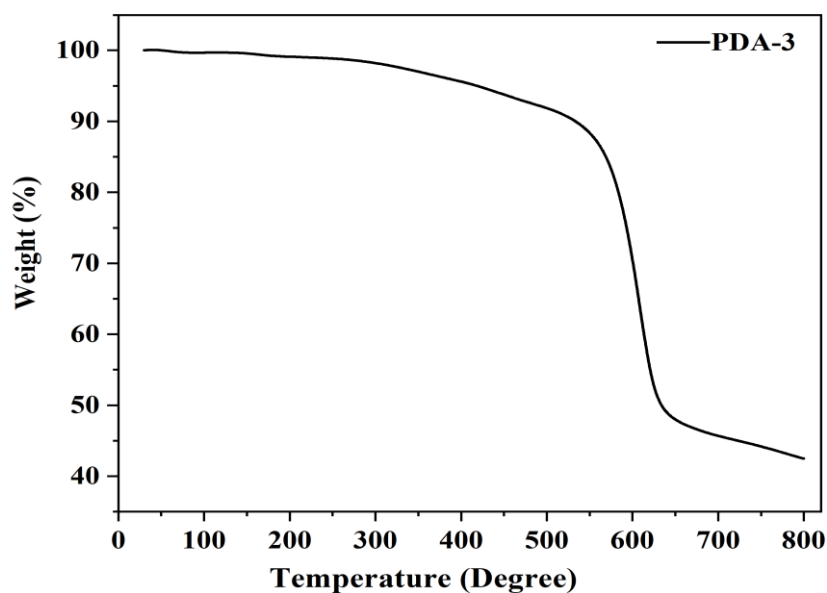
Figure 7.12 Thermogravimetric analysis of the fabricated hollow fiber membrane (PDA-3).

7.2.11 Molecular weight cut off study for hollow fiber membrane

The molecular weight cut-off for the best performing (PDA-3) membrane was found to be 18554.26 Da in Figure 7.13. The (PDA-3) membrane's MWCO results also demonstrated that the produced membrane was an ultrafiltration membrane. The percentage PEG rejection of PDA-3 was noted as 63.56%, 67.67% and 92.7% for PEG-4000, PEG-6000 and PEG-20000 respectively.
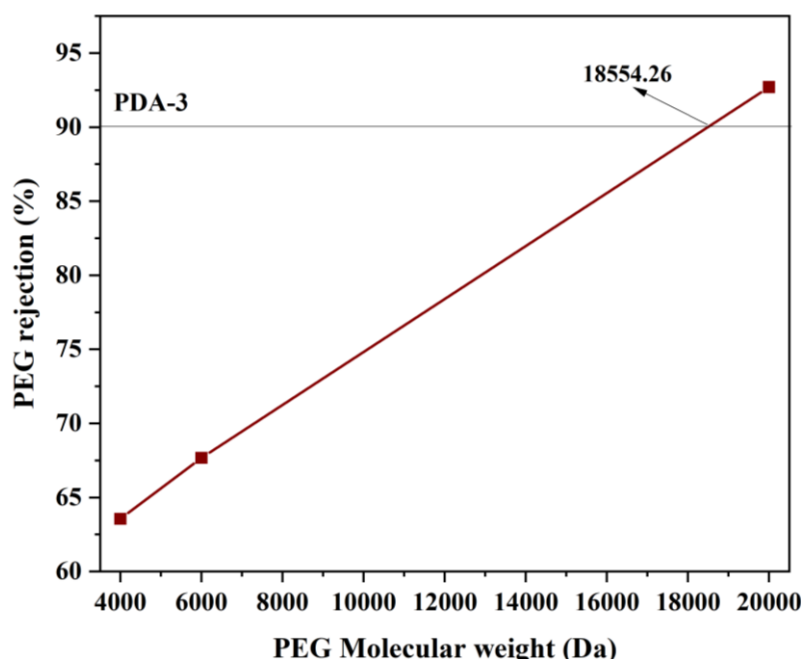
Figure 7.13 Molecular weight cut off study of the prepared membrane.

7.2.12 X-ray photoelectron spectroscopy (XPS) analysis of the fabricated membrane

The narrow and wide spectrum images of the best performing membrane PDA-3 was illustrated from X-ray photoelectron spectroscopy are shown in Figure 7.14(a) − (e). The existence of four major emission peaks at 284.79 eV, 532.10 eV, 167.90 eV and 399.6 eV is attributed to the occurrence of C1s, O1s, S2p and N1s respectively. In addition, deconvoluted C1s, O1s, S2p and N1s results were shown in Figure 7.14(b) − (d) respectively. As shown in Figure 7.14(b), the binding energy peaks for oxygen (O1s) functional groups are 531.8 eV, 532.7 eV and 533.5 eV for −C=O, −COH and −CO, respectively (Tsai et al. 2011; Yang et al. 2017). As shown in Figure 7.14(c), the carbon binding energy (C1s) peaks 284.22 eV, 284.78 eV, 285.41 eV, 286.47 eV and 288.19 eV were attributed to −C=C, −C−C, −C−O, −C−O−C and −O−C=O respectively (Huang et al. 2011). Sulphur binding energy peaks of 167.65 eV and 168.57 eV were assigned to S2p$_{(3/2)}$ and S2p$_{(1/2)}$ respectively as shown in Figure 7.14(d) (Noor et al. 2018). The binding energy peaks of nitrogen (N1s) are 399.64 eV and 400.30 eV for −N−C and −N−C=O, respectively as shown in Figure 7.13(e) (Chen et al. 2017). As a result, the XPS study confirmed the presence of the additives and nanoparticles on the hollow fiber membrane surfaces.
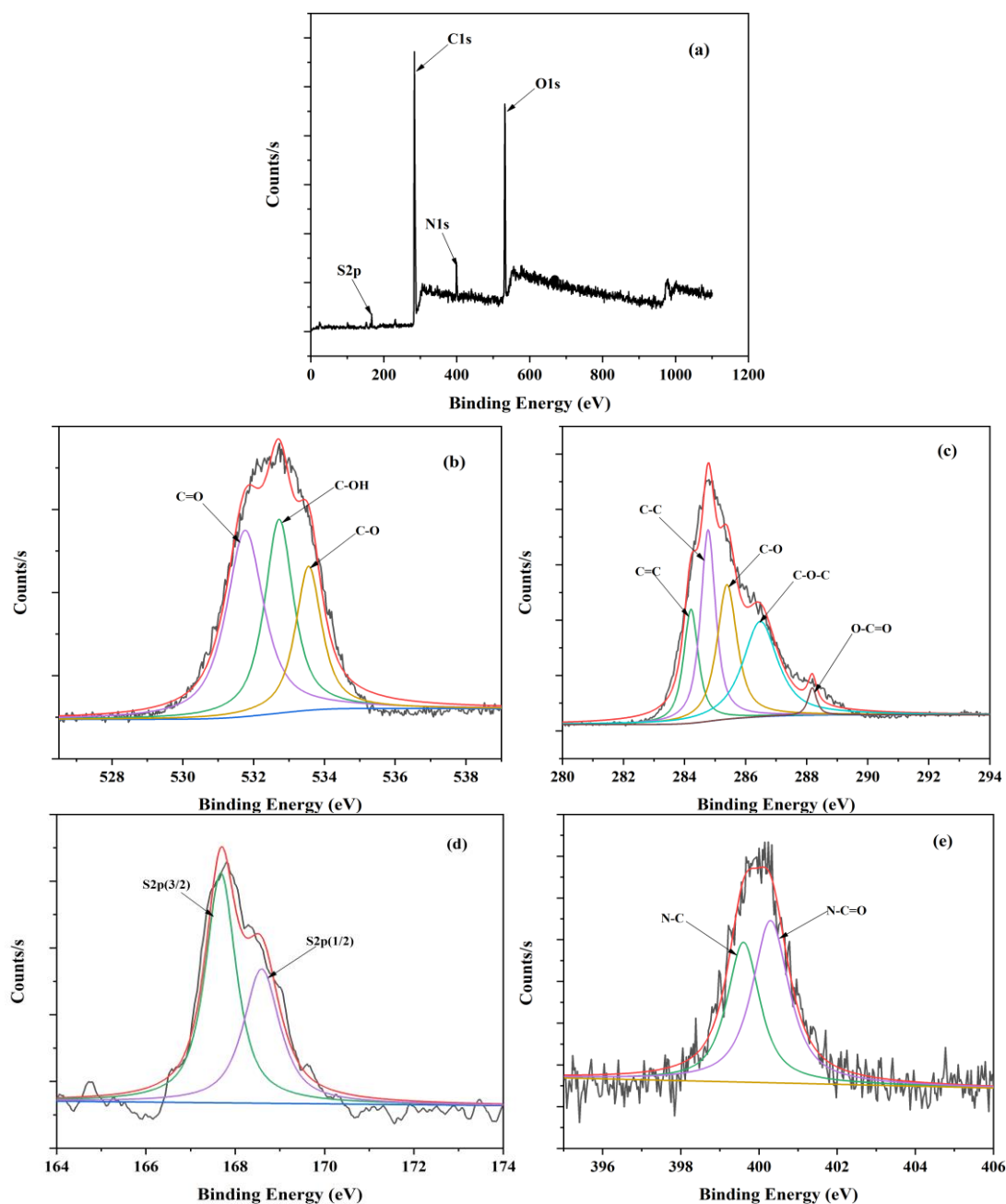
Figure 7.14 XPS analysis of the membrane (PDA-5) wide view spectrum (a) and narrow spectrum (b), (c), (d) and (e) for O1s, C1s, S2p and N1s binding energies, respectively.

7.2.13 Arsenic-V removal from prepared hollow fiber membranes

The arsenic-V extraction properties of pristine and PDA modified membranes were demonstrated in Figure 7.15. Initially, the arsenic (H_3AsO_4) was transformed to arsenate solution (AsO_4^{3-}) after ionizing with water (3 H_2O), which was illustrated in Equation 3.1 (Criscuoli and Figoli 2019). To perform arsenic-V extraction tests using fabricated hollow fiber membranes, the laboratory prepared 5000 PPM (5 mL/L) from standard arsenic stock

solution with a pH range of 6.8±0.2 and a transmembrane pressure (TMP) of 0.2 MPa was employed. The neat membrane exhibited lower arsenate oxide (AsO_4^{3-}) rejection properties due to the less hydrophilic and minimum number of negatively charged sites on the membrane surface. The pristine hollow fiber membrane (PDA-0) decontaminated 67.70% with the flux properties of 15.07 L/m^{2}h. With incremental concentrations (1, 2, 3 and 5 wt%) to the neat membrane, a massive improvement in extraction for arsenate oxide from the modified fabricated membranes was witnessed.

A PDA-3 membrane showed outstanding rejection of arsenate oxide as 87.15% with an arsenate oxide flux of 31.80 L/m^{2}h as shown in Figure 7.15(a) and (b) respectively. The PDA-1 and PDA-2 hollow fiber membranes extract 84.20 and 82.54% with the flux of 16.84 and 47.77 L/m^{2}h respectively. PDA concentrations increased the hydrophilic and negatively charged membrane surfaces. The electrostatic repulsion phenomenon removed more arsenate oxide (AsO_4^{3-}) with negatively charged membrane surfaces. Also, amine and hydroxyl sites on the PDA-contained membrane acted as binding sites, allowing more arsenic-V ions to be removed (Rao et al. 2017). Furthermore, PDA's functional groups interact strongly with various polymeric materials. The PDA benzene functional sites can form a greater Π- Π stacking with the PPSU benzene group, while the catechol and amine groups can form strong hydrogen bonding with the PPSU oxygen group (Ang et al. 2019). Moreover, a homogeneous blend of used PDA and additive PVP in the PPSU casting solution improves arsenate oxide removal (AsO_4^{3-}). Nevertheless, the PDA-5 membrane removed significantly reduced arsenite oxide by 82.77% with the flux properties of 37.44 L/m^{2}h respectively. The rate of removal of arsenate was slightly slowed down due to the increased concentration polarization on the membrane surfaces (Kumar et al. 2021). The concentration polarization for arsenic –V removal of the fabricated hollow fiber membranes was illustrated in Table 7.2.
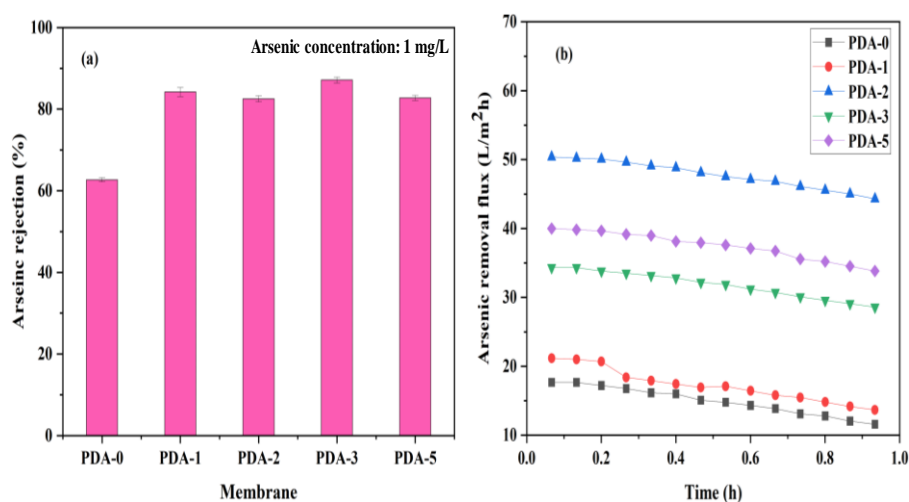
Figure 7.15 (a) Percentage arsenic-V removal properties (b) arsenic-V flux from the prepared hollow fiber membranes.

Table 7.2 Concentration polarization for arsenic –V removal of the fabricated hollow fiber membranes

Membrane codes	Velocity (v) $\times 10^{-3}$ (m/s)	Mass transfer coefficient (K) $\times 10^{-5}$ (m/s)	Concentration polarization ($\frac{Cm}{Cb}$)
PDA-0	1.186	0.928	1.291
PDA-1	1.762	1.09	1.42
PDA-2	1.726	1.083	2.686
PDA-3	1.628	0.596	1.393
PDA-5	2.267	1.088	1.277

7.2.14 Mechanical (tensile) strength of fabricated hollow fiber membranes

The prepared hollow fiber membranes mechanical (tensile) properties are clearly illustrated in Table 7.3. Also, the stress-strain properties of hollow fiber membranes are shown in Figure 7.16. The tensile strength and strain parameters of the pristine (PDA-0) hollow fiber membranes were 3.03 MPa and 5.24% respectively. As the PDA concentrations enhanced in the PPSU dope solutions, the decreased tensile stress and strain properties were

witnessed. The membrane PDA-5 had a lower tensile strength of 1.54 MPa and strain of 2.01% respectively. The presence of polydopamine in the membrane polymer matrix affects the mechanical properties of the modified membranes, particularly at high dopamine loadings. This shows that the membrane morphological parameters like pore size and structure affect the properties of polymer membrane as membrane strength decreases as the pore size increases (Kotsilkova et al. 2018).

Table 7.3 Mechanical properties of hollow fiber membranes

Membrane code	Tensile strength (MPa)	Standard Deviation	Strain at maximum load (mm/mm)	Standard Deviation	Elongation at break (%)	Standard Deviation	Load at break (N)	Standard Deviation	Maximum load (N)	Standard Deviation	Modulus (MPa)	Standard Deviation	Elongation at break (mm)	Standard Deviation
PDA-0	3.0	0.3	0.05	0.0004	5.3	0.014	0.82	0.006	0.85	0.006	100.2	1.758	1.60	0.05
PDA-1	2.2	0.4	0.03	0.0006	3.2	0.018	0.62	0.004	0.64	0.005	96.1	1.44	0.98	0.07
PDA-2	2.2	0.3	0.04	0.0008	4.6	0.105	0.51	0.012	0.64	0.004	80.9	1.89	1.40	0.005
PDA-3	1.9	0.1	0.02	0.001	2.9	0.01	0.37	0.006	0.54	0.007	90.5	0.94	0.87	0.011
PDA-5	1.5	0.1	0.02	0.0009	2.2	0.02	0.24	0.005	0.43	0.004	103.3	1.22	0.67	0.002

In addition, when 1 wt% of PDA was used in a PPSU/PVP (PDA-1) hollow fiber membrane, the mechanical strength i.e., tensile strength was 2.28 MPa and elongation at

break was 3.29%, when 5 wt% of PDA in PPSU/PVP (PDA-5) membrane, the mechanical strength was 1.54 MPa and elongation at break was 2.25%. The morphologies of the membranes were found to be closely related to the mechanical strength properties. When the PDA dosage is increased, an enhanced porous structure is observed. This is due to the membrane's tendency to store water, which reduces the membrane's mechanical stability (Kotsilkova et al. 2018; Mulyati et al. 2020a).
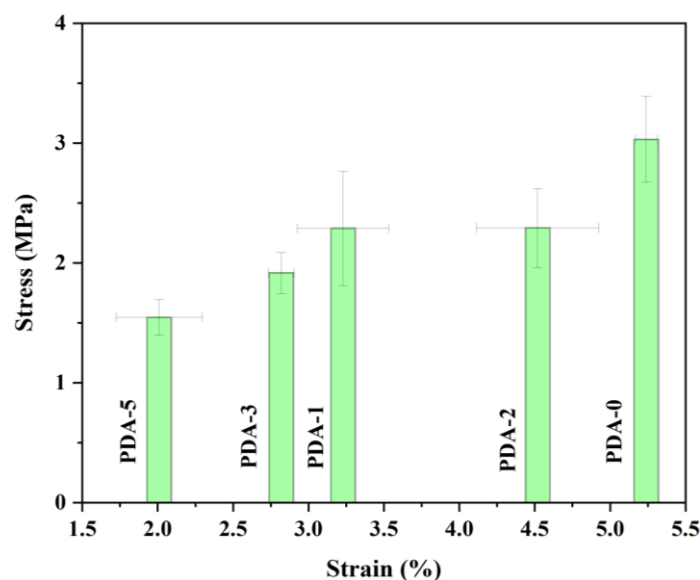
Figure 7.16 Mechanical properties (Stress vs strain) of the fabricated neat membrane (PDA-0) and incremental dosages (1 wt%, 2 wt%, 3 wt% and 5 wt%) hollow fiber membranes (PDA-1, PDA-2, PDA-3 and PDA-5) respectively.

7.3 SUMMARY OF THE PRESENT WORK

Polyphenylsulfone (PPSU) containing increased dosages of hydrophilic polydopamine (PDA; 1, 2, 3 and 5wt%) and pore-forming agent polyvinylpyrrolidone (PVP) hollow fiber membranes were successfully fabricated by non-solvent induced phase separation (NIPS) process. The effects of increased PDA dosages on PPSU/PVP hollow fiber membranes have been thoroughly investigated. The XRD analysis verified the crystalline structure of the PDA. The increased arsenic-V rejection can be seen due to the amine and hydroxyl groups effect on the PDA polymeric additive. The increased arsenic-V rejection can be seen due to the amine and hydroxyl groups effect on the PDA polymeric additive. The PDA-3 membrane showed an improved arsenic-V removal of 87.15% with an arsenic-V flux of 31.80 L/m^{2}h respectively. This is much higher than the neat membrane PDA-0, which has an arsenic-V rejection rate of 67.70% and flux of 15.07 L/m^{2}h. Increased PDA concentrations to PPSU/PVP hollow fiber

membranes resulted in major morphological and topological membrane structures improvements as seen by SEM and AFM. The finger-like structures were expanded and the membranes surface roughness was increased. Increased PDA concentrations to PPSU/PVP hollow fiber membranes resulted in improvements in significant morphological and topological membrane structures as seen by SEM and AFM. The finger-like structures were expanded and the membrane's surface roughness was increased. The improved surface roughness (R_a) for modified membrane PDA-5 was 25.0 nm and 14.1 nm for nascent hollow fiber membrane PDA-0 respectively.

Consequently, the incorporation of polydopamine on the membrane surfaces was confirmed by several functional groups and binding energies confirmed by FTIR and XPS interpretation. At pH 7, the negatively charged modified (PDA-3) membrane surface had a zeta potential of -29.48 mV, indicating an improvement in zeta potential. Because of the influence of hydrophilic catechol moieties, polydopamine increased hydrophilicity, which resulted in better antifouling behavior, as demonstrated by a flux recovery ratio (FRR) of 92.83% for charged PDA-5 membrane, which is higher than the FRR of 70.32% for nascent membrane (PDA-0). The modified membrane (PDA-5) shows higher pure water flux of 37.44 L/m^{2}h than the pristine membrane (PDA-0), 15.07 L/m^{2}h. However, because of the increased concentration polarization on the membrane surface, the PDA (5wt%) enhanced concentration to PPSU/PVP membranes resulted in a decreased arsenic-V removal tendency. These membranes may be used to remove arsenic-V from arsenic-V-contaminated drinking water effectively.

CHAPTER -8

IMPROVED SEPARATION OF DYES AND PROTEINS USING MEMBRANES MADE OF POLYPHENYLSULFONE/CELLULOSE ACETATE AND POLYPHENYLSULFONE/CELLULOSE ACETATE PHTHALATE

Abstract

In this contemporary work, asymmetric polyphenylsulfone hollow fiber membranes were fabricated using the non-solvent induced phase separation process with the intensified concentrations (1, 3 and 5 wt%) of cellulose acetate derivatives (cellulose acetate (CA) and cellulose acetate phthalate (CAP)). The prepared hollow fiber membrane's morphology and topographical structures were studied using field emission scanning electron microscopy (FE-SEM) and atomic force microscopy (AFM) respectively. Prepared membrane's antifouling analysis was performed using bovine serum albumin (BSA). The thermogravimetric analysis (TGA) was employed to interpret the thermal stability of the fabricated membranes. The hydrophilicity/hydrophobicity of the fabricated membranes was confirmed using porosity, water uptake and pure water permeability analysis. Furthermore, rejection of various toxic azo dyes, namely reactive orange-16 (RO-16) and reactive black-5 (RB-5), was carried out. Incremental concentrations of cellulose acetate and cellulose acetate phthalate in polyphenylsulfone enhanced the hydrophilic properties of fabricated membrane. A high percentage of separation of dyes and proteins were observed for cellulose acetate phthalate membranes compared to cellulose acetate membranes due to the higher adsorptive nature. The dye removal for hollow fiber membranes prepared using 5 wt% of cellulose acetate phthalate in polyphenylsulfone (PCAP-5) and 5 wt% of cellulose acetate in polyphenylsulfone (PCA-5) were 95.49% and 82.69%. The corresponding permeabilities were 83.45 L/m^{2}h bar and 80.02 L/m^{2}h bar respectively for bovine serum albumin protein. A higher rejection can be observed from RB-5 and bovine serum albumin due to increased molecular weight than other dyes and proteins. As additive content has been increased in the polyphenylsulfone dope solution, there is an improvement in pure water permeability. Pure water permeabilities for PCAP-5 and PCA-5 membranes were 64.49 L/m^{2}h bar and 72.60 L/m^{2}h bar respectively, higher than the neat membrane permeability 41.26 L/m^{2}h bar.

8.1 INTRODUCTION

Nowadays, due to the urbanization and endless growth of various industrial activities, water bodies are being polluted. However, wastewater disposal from multiple industries (textiles, printing, pulp and paper) is dominant. Several metal ions, toxic proteins and different types of reactive dyes are included in the wastewater. The composition of such hazardous materials can pose a severe risk to human health and to the environment (Ibrahim et al. 2018d; Mashkoor et al. 2018). In general, for coloring the cellulose fibers, various azo dyes were used (Burkinshaw and Salihu 2019). Skin inflammation, permanent blindness,

vomiting, gastric, vertigo, edema of tongue, ears, pharynx, larynx and respiratory distress are severe human health issues related to azo dyes (Ismail et al. 2018). To mitigate these environmental and health hazardous issues, there is an extreme need to remove various dyes and proteins from aqueous solutions. There are several rejection processes such as coagulation (Cheng et al. 2018; Wang et al. 2017b), flocculation (Lou et al. 2017), adsorption (Jin et al. 2019; Li et al. 2018b) and ion exchange (Sharma et al. 2016) that are in practice. The membrane filtration process is a promising technology, due to it's less toxicity, simplicity in handling, high rejection efficacy for the sustainable environment (Bet-Moushoul et al. 2016; Karim et al. 2014). Reverse osmosis, microfiltration, nanofiltration and ultrafiltration are the efficient processes for extracting various highly toxic dyes and proteins from aqueous solutions (Escobar et al. 2005; Othman et al. 2021). However, high transmembrane pressure limits and concentration polarization are significant limitations because of the small pore size on the membrane surfaces for nanofiltration and reverse osmosis. Because of the less energy consumption, increased rejection with high permeability, cost-effectiveness and with no phase change, the tangential flow ultrafiltration membrane process is effective compared to other filtration methods (Al-Ani et al. 2021; Vetrivel et al. 2018c).

In recent years, different polymers have been used to improve the properties of the membranes, such as polysulfone (PSf) (Kajekar et al. 2015b), polyethersulfone (PES) (Wang et al. 2015), cellulose acetate (CA) (Yang et al. 2019), polyvinylidene fluoride (PVDF) (Srivastava et al. 2011), polyethyleneimine (Dasgupta et al. 2015) and many others. Nevertheless, polymers showed some downsides as PSf membranes were less capable of absorbing and suffer from severe fouling because of the high hydrophobicity (Sharma and Purkait 2019). The PES membranes are less sensitive to transmembrane pressure, are toxic and prone to fouling (Farahani et al. 2019). Polymers such as cellulose acetate and cellulose acetate phthalate (Mukherjee and De 2014b; Rahimpour and Madaeni 2007c) provide significant hydrophilicity for membrane fabrication and enhance the rejection of the different dyes and proteins.

Sivakumar et al. (2006b) fabricated CA and PSf ultrafiltration-blended membranes for different protein rejection. Increased rejection rate relative to pepsin and egg albumin is because of the higher molecular weight of BSA protein. The pure water permeability in the presence of different additives was evaluated, the polyvinylpyrrolidone (PVP) with CA membranes exhibited enhanced permeation properties. The membrane's porosity and water uptake of modified blended membranes were improved significantly. The enlarged finger-like morphologies were evidenced with PVP dosage in the CA membrane.

Yu et al. (2010) prepared polyamides (PA) and CA blended membranes by non-solvent induced phase separation (NIPS) process. The modified membranes showed enhanced membrane properties such as hydrophilicity, surface roughness, porosity, pure water permeability with well rejection of the various dyes compared to the neat membrane.

Ali et al. (2014) prepared novel PSf and increased dosages of CAP membranes. The enhanced properties such as hydrophilicity, porosity, water uptake and pure water permeabilities were witnessed from the modified membranes. The dense morphologies on the top skin layer and porous like structure on the sublayer of the membrane were enhanced by adding gradual CAP dosages to the PSf polymer matrix (Mohammadi and Saljoughi 2009; Mukherjee and De 2014b). The existence in its configurations of different functional groups (–C=O and –OH) has proven to be essential for the hydrophilic nature of the additive (Chatterjee and De 2014b).

Mu et al. (2017) prepared ultrafiltration hollow fiber membranes using CA and L-dopa coated halloysite nanotube (HNT) by NIPS process. Higher hydrophilicity, porosity, water absorption, well rejection of egg albumin and superior thermal stability was observed from modified membranes. FTIR and XPS analysis confirmed various functional groups and binding energies present in the composite membrane surfaces. Significant improvement in antifouling properties of modified membranes was witnessed compared to pristine membranes.

Karmakar et al. (2017) fabricated ultrafiltration mixed matrix membranes using CAP and aluminum fumarate. The blended membranes provide improved hydrophilicity, porosity, pure water permeability and antifouling properties. The roughness on the membrane surface enhanced with aluminum fumarate in CAP hollow fiber membranes. The fluoride removal was witnessed from CAP membranes as the aluminum fumarate dosage was increased in the dope solution.

Silva et al. (2020) fabricated carbon nanotube (CNT) and cellulose acetate (CA) membrane using the nonsolvent induced phase separation (NIPS) process. Increased concentrated CA membranes exhibited enhanced thermal stability; an improved hydrophilicity was witnessed by verifying the improvement in porosity, water uptake and pure water flux of the membranes. Also, the antifouling properties of the membranes were enhanced by the increased flux recovery ratio of the modified membranes by incorporating cellulose acetate into the membrane matrix. Furthermore, the cellulose acetate dosaged mixed matrix membranes exhibited improved removal of methylene blue from aqueous dye solution.

Serbanescu et al. (2020) fabricated cellulose acetate incorporated membranes for the removal of Gadolinium-III (Gd-III)). The fabricated membranes morphological finger-like structures got expanded as the dosage of cellulose acetate in the dope solution increased. The enhanced thermal stability and hydrophilicity of CA-modified membranes can be witnessed as the increased dosages of CA into the neat PPSU dope solution. The presence of CA was confirmed by using FTIR and XPS analysis through different functional groups and binding energies respectively.

Polyphenylsulfone (PPSU) is also one of the sulfone polymer families and has recently been commonly used for applications in water purification. PPSU has fascinating characteristics such as significantly higher thermal stability, chemical compatibility, improved resistance to stress and high surface wettability (Shukla et al. 2017e). The addition of various hydrophilic additives to hydrophobic PPSU could improve the properties such as thermal stability, chemical/mechanical stability and membrane filtration (Nayak et al. 2017b).

Arockiasamy et al. (2017b) developed mixed matrix membranes from PPSU/PEG-600/TiO$_2$ using the NIPS technique. The results revealed improved hydrophilicity, surface roughness, water absorption, porosity, water permeability and improved membrane antifouling properties by incremental dosages of TiO$_2$ with PEG-600. However, due to its higher hydrophobic behavior and lower water permeability, PPSU is more prone to fouling. Thus limited work was documented using PPSU for the ultrafiltration membrane process (Golpour and Pakizeh 2018c). We proposed a new approach of blending PPSU with increased dosages of CA and CAP to overcome these disadvantages and improve different membrane properties and rejection of various dyes and proteins.

Nayak et al. (2018c) developed the PPSU hollow fiber ultrafiltration membranes with the incremental dosages of ZSM-5 by the non-solvent induced phase separation process. The membranes showed enhanced antifouling properties, water-holding capability, porosity and pure water permeability. Also, increased dosages of ZSM-5 expanded finger-like projections, which was witnessed from SEM analysis.

Shukla et al. (2020) fabricated hollow fiber ultrafiltration membranes by PPSU-zinc oxide using NIPS process. The prepared membranes were subjected to anionic dyes and antibacterial studies. Enhanced removal of methyl orange dye and improved antibacterial properties were witnessed from ZnO modified membranes than the pristine membrane. Also, as-fabricated membranes exhibited enhanced antifouling properties by increased flux recovery

ratio (FRR) and reversible fouling (R_r). The enhanced finger-like morphologies and porous structures were observed with the incremental dosages of ZnO to PPSU membranes.

The literature study indicated that no any research work was documented on polyphenylsulfone/cellulose acetate and polyphenylsulfone/cellulose acetate phthalate hollow fiber membranes from the aqueous wastewater solution for the rejection of various dyes/proteins. It was decided to prepare asymmetric hollow fiber membranes to decontaminate varieties of dyes and proteins from an aqueous solution to address the above requirements. This research work aims to prepare, characterize and perform the rejection properties of different dyes and proteins from fabricated hollow fiber membranes.

8.2 RESULTS AND DISCUSSIONS

8.2.1 Cross-section and surface morphologies of prepared membranes

The field-emission scanning electron microscopy (FE-SEM) images of the fabricated membranes are illustrated in Figure 8.1. By adding hydrophilic additives (CA and CAP) into the neat PPSU dope solution, there is a tremendous improvement in the morphological structures of the membranes. In addition, the modified hollow fiber membranes exhibited asymmetric structure, finger-like projections on either side, which was sandwiched by spongy morphologies. From Figure 8.1(a), the neat membranes have a more macroporous structure than the modified membranes. Also the gradual expansion in finger-like projections were witnessed as the concentrations of CA and CAP (1, 3 and 5 wt%) increased in neat membrane as shown in Figure 8.1(b) – (g). This enables the augmentation of modified membrane with hydrophilicity and better pure water permeability. From Table 8.2, there is an increase in pure water permeability, porosity and water uptake properties of the modified membranes because of the improved pore-forming nature of the CAP. Also, the complete SEM cross sectional view of the fabricated membranes was illustrated in Figure 8.2. Inner/outer diameter (ID and OD) and mean pore radius of the fabricated hollow fiber membranes are illustrated in Table 8.1.
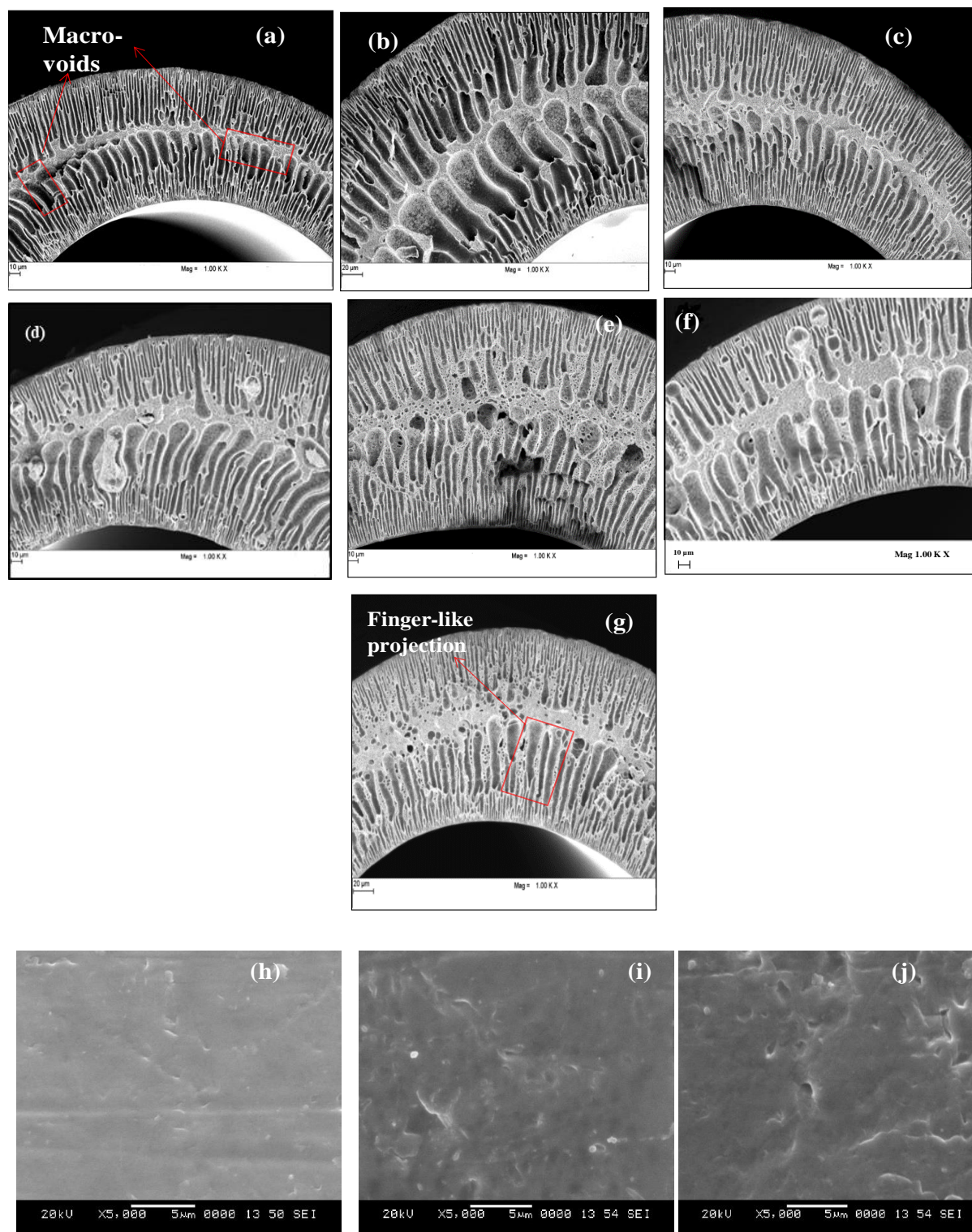
Figure 8.1 Cross sectional FE-SEM images of prepared membranes (a) neat membrane (b), (c) and (d) are 1 wt%, 3 wt% and 5 wt% of CA in PPSU hollow fiber membranes, (e), (f) and (g) are 1 wt%, 3 wt% and 5 wt% of CAP in PPSU hollow fiber membranes respectively. Surface morphological analysis of neat membrane (h), 5 wt% of CA in PPSU membrane (i) and 5 wt% of CA in PPSU membrane (j) respectively.
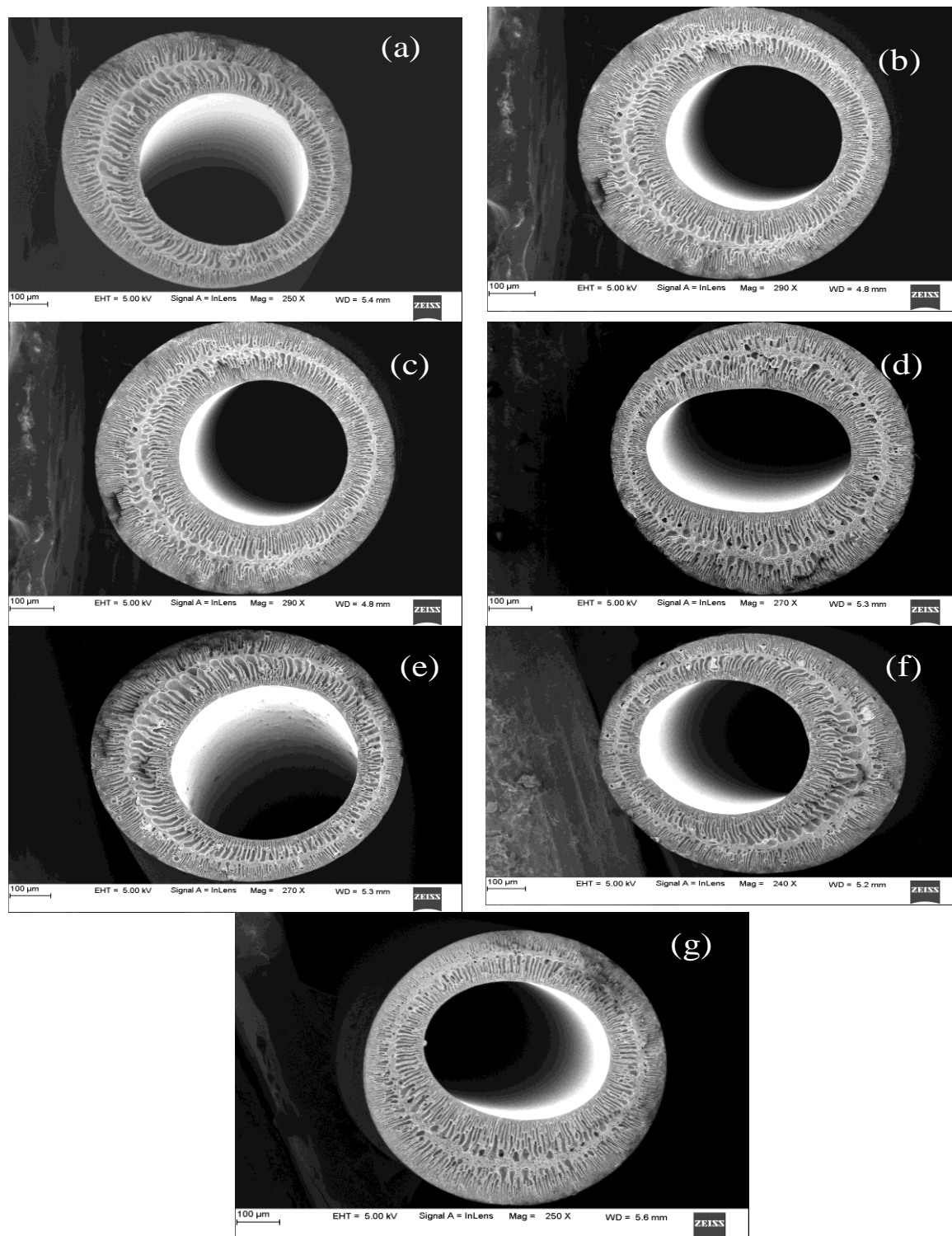
Figure 8.2 Cross sectional (complete view) FE-SEM images of prepared membranes (a) neat membrane (b), (c) and (d) are 1 wt%, 3 wt% and 5 wt% of CA in PPSU hollow fiber membranes, (e), (f) and (g) are 1 wt%, 3 wt% and 5 wt% of CAP in PPSU hollow fiber membranes respectively.

Table 8.1 Outer/ inner (OD/ID) diameter and mean pore radius of the fabricated hollow fiber membranes

Hollow fiber membranes	Outer diameter (OD in μm)	Inner diameter (ID in μm)	Mean pore radius (m)
NM	707	408.2	2.280×10^{-7}
PCA-1	760.5	448.8	1.170×10^{-7}
PCA-3	686	368.7	1.115×10^{-7}
PCA-5	808.1	449.2	1.088×10^{-7}
PCAP-1	715.1	340.7	1.751×10^{-7}
PCAP-3	768.2	447	1.076×10^{-7}
PCAP-5	704.3	377.3	1.285×10^{-7}
Spinneret dimension, inner diameter: 550 μm, outer diameter:1100 μm			

8.2.2 Hydrophilicity/hydrophobicity measurement of fabricated membranes

The hydrophilicity/hydrophobicity nature of the fabricated neat and modified hollow fiber membranes was demonstrated in Figure 8.3. From Figure 8.3, the decreased contact angle parameters were witnessed with the incremental dosages of hydrophilic additive (CA and CAP) to neat PPSU dope solution. The neat membrane revealed the contact angle as 79.07°. The dosage of 5 wt% of CA in PPSU (PCA-5) and 5 wt% of CAP in PPSU (PCAP-5) to neat dope solution exhibited contact angle of 57.31° and 49.47° respectively. There is an increased in water holding capacity because of increased hydrophilicity of the functional groups on the surfaces of the membrane (Rahimpour and Madaeni 2007c; Sivakumar et al. 2006b). The decreased contact angle values for cellulose acetate/polyphenylsulfone hollow fiber membranes PCA-5<PCA-3<PCA-1<PCA-0 and for cellulose acetate phthalate/polyphenylsulfone membranes PCAP-5<PCAP-3<PCAP-1<PCAP-0 respectively.
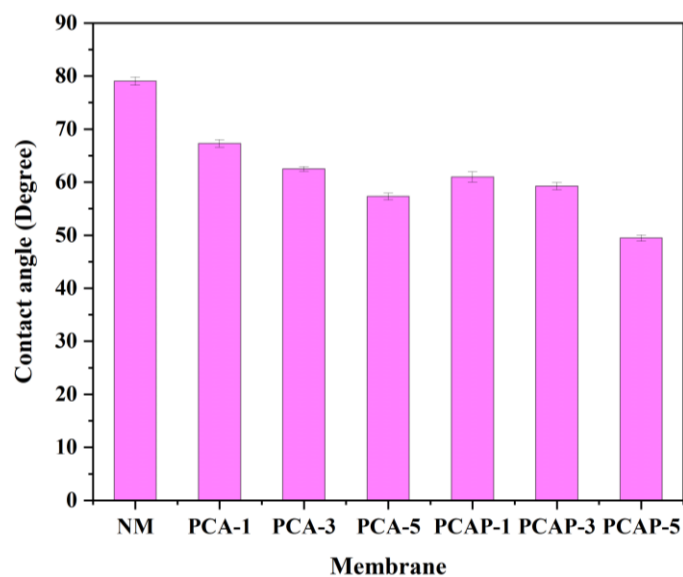
Figure 8.3 Contact angle measurement of prepared hollow fiber membranes.

8.2.3 Pure water permeability analysis of fabricated hollow fiber membranes

The fabricated neat and modified hollow fiber membrane's time-dependent pure water permeability was illustrated in Figure 8.4. Modified membranes exhibited higher pure water permeability compared to the neat membrane. From Figure 8.4(a) – (b), the permeability parameters for the neat membrane was 41.26 L/m^2h bar. With 5 wt% of CAP in PPSU (PCAP-5) and 5 wt% of CA in PPSU (PCA-5) exhibited permeability of 72.60 L/m^2h bar and 64.47 L/m^2h bar respectively. The CAP incorporated PPSU membranes exhibited more excellent water permeability, hydrophilicity and porosity than CA-incorporated PPSU membranes. Also, various hydrophilic functional groups such as –OH and –C=O facilitated enhanced water-absorption capacity and hydrophilicity from the modified hollow fiber membranes (de Moraes et al. 2015; Mukherjee and De 2014b).
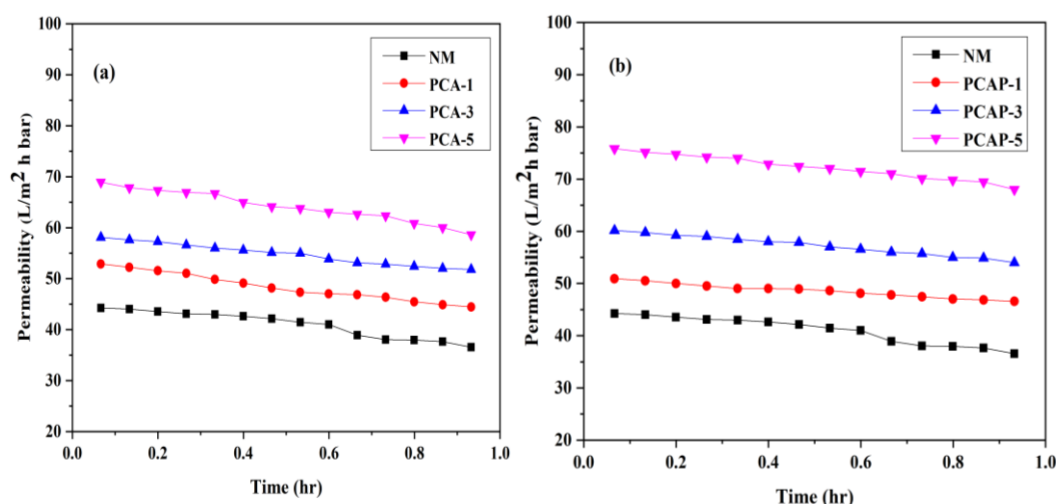
Figure 8.4 Time-dependent pure water permeability of prepared (a) neat membrane and increased dosage of CA (1, 3, and 5 wt%) in PPSU as PCA-1, PCA-3 and PCA-5 (b) neat membrane and increased dosage of CAP (1, 3, and 5 wt%) in PPSU as PCAP-1, PCAP-3 and PCAP-5 respectively.

8.2.4 Water uptake and porosity of fabricated hollow fiber membranes

The water uptake and porosity of the fabricated neat and CA incorporated PPSU and CAP incorporated PPSU modified membranes were illustrated in Figure 8.5. From Figure 8.5, the neat membrane exhibited the porosity parameter as 4.49%, also PCA-5 and PCAP-5 membranes showed 29.97% and 32.06% respectively. Neat membranes exhibited a water uptake capacity of 31.53%, PCA-5 and PCAP-5 membranes showed 31.53% and 68.81% respectively. There is improvement in water uptake and porosity parameters with the gradual increased dosages of hydrophilic CA and CAP additives to the PPSU dope solution. Productivity (filtration rate) along with membrane quality (permeate concentrations) of the fabricated hollow fiber membranes were dependent on the porosity of the membranes (Ma et al. 2012). Because of the leaching of CA and CAP additives in the PPSU dope solution in the phase inversion process, there is an enhancement of water absorption and porosity parameters (Dasgupta et al. 2014; Rahimpour and Madaeni 2007c). The order of water holding capacity and porosity values for prepared PPSU/CA membranes as PCA-5>PCA-3>PCA-1>NM and PPSU/CAP membranes as PCAP-5> PCAP-3>PCAP-1>NM.
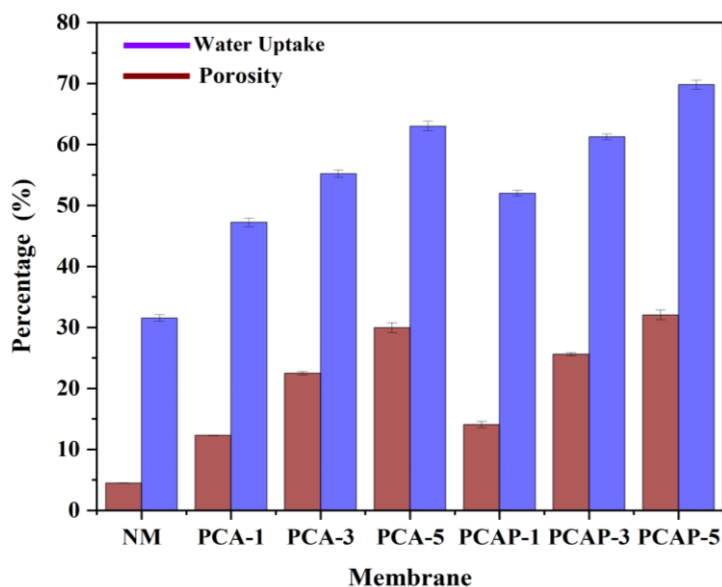
Figure 8.5 Porosity/water uptake measurement for prepared neat and increased dosage of CA (1, 3, and 5 wt%) in PPSU as PCA-1, PCA-3 and PCA-5, and increased dosage of CAP (1, 3, and 5 wt%) in PPSU as PCAP-1, PCAP-3 and PCAP-5 respectively.

8.2.5 Study of antifouling properties of the prepared hollow fiber membranes

The antifouling analysis of the fabricated neat and CA/CAP modified membranes was demonstrated in Figures 8.6(a) – (b). The time-dependent study of the prepared membranes using BSA protein was demonstrated. The CA and CAP additives demonstrated higher adsorption properties (Chatterjee and De 2014b; Lv et al. 2018). The hydrophilic and fouling properties of the neat membrane (NM) over the modified membranes were demonstrated in Table 8.2. From Figure 8.6(c), the neat membrane's flux recovery ratio (FRR) was 66.06% and the remaining parameters for were R_r, R_{ir} and R_t were 35.16%, 33.93% and 69.09% respectively. The FRR for PCA-5 and PCAP-5 membranes was reported as 80.70% and 84.08% with the increased dosages. The remaining parameters such as R_r, R_{ir} and R_t were 48.06, 19.26 and 67.27% respectively, for PCA-5 hollow fiber membrane and 60.34, 15.91 and 60.34% for PCAP-5 hollow fiber membrane respectively.

The presence of hydrophilic functional group such as amine and hydroxyl on the modified CA incorporated PPSU and CAP incorporated PPSU membrane surfaces resulted in a substantial increase in the behavior of fouling resistance (Rahimpour and Madaeni 2007c; Vinodhini et al. 2017). Due to the higher molecular weight and larger size of BSA molecules, the increased rejection of BSA protein from modified hollow fiber membranes was witnessed (Lv et al. 2018). With incremental parameters of FRR and R_r, the fabricated hollow fiber

membranes showed better antifouling character with reduced parameter of irreversible fouling (R_{ir}).

Table 8.2 Antifouling results of the prepared membranes

Membranes codes	J_P (L/m² h bar)	Standard deviation	J_{w1} (L/m² h bar)	Standard deviation	J_{w2} (L/m² h bar)	Standard deviation	FRR (%)	Standard deviation	R_r (%)	Standard deviation	R_{ir} (%)	Standard deviation	R_t (%)	Standard deviation
NM	12.7	0.3	42.2	0.4	27.2	0.3	66.0	0.5	35.1	0.5	33.9	0.5	69.0	0.6
PCA-1	14.8	0.1	45.0	0.5	32.5	0.3	72.2	0.3	39.2	0.5	27.7	0.5	66.9	0.7
PCA-3	18.9	0.3	54.6	0.7	42.7	0.3	78.2	0.3	43.5	0.08	21.7	0.08	65.2	0.6
PCA-5	21.0	0.5	64.4	0.2	52.0	0.3	80.7	0.4	48.0	1.5	19.2	1.5	67.3	0.8
PCAP-1	13.4	0.4	48.7	0.4	34.6	0.4	71.0	0.5	43.4	0.3	28.9	0.3	72.4	0.5
PCAP-3	15.2	0.4	56.6	0.3	45.6	0.5	80.5	0.5	53.6	0.6	19.4	0.6	73.1	0.7
PCAP-5	16.2	0.2	68.6	0.4	57.6	0.9	84.0	0.5	60.3	0.4	15.9	0.4	76.2	0.6
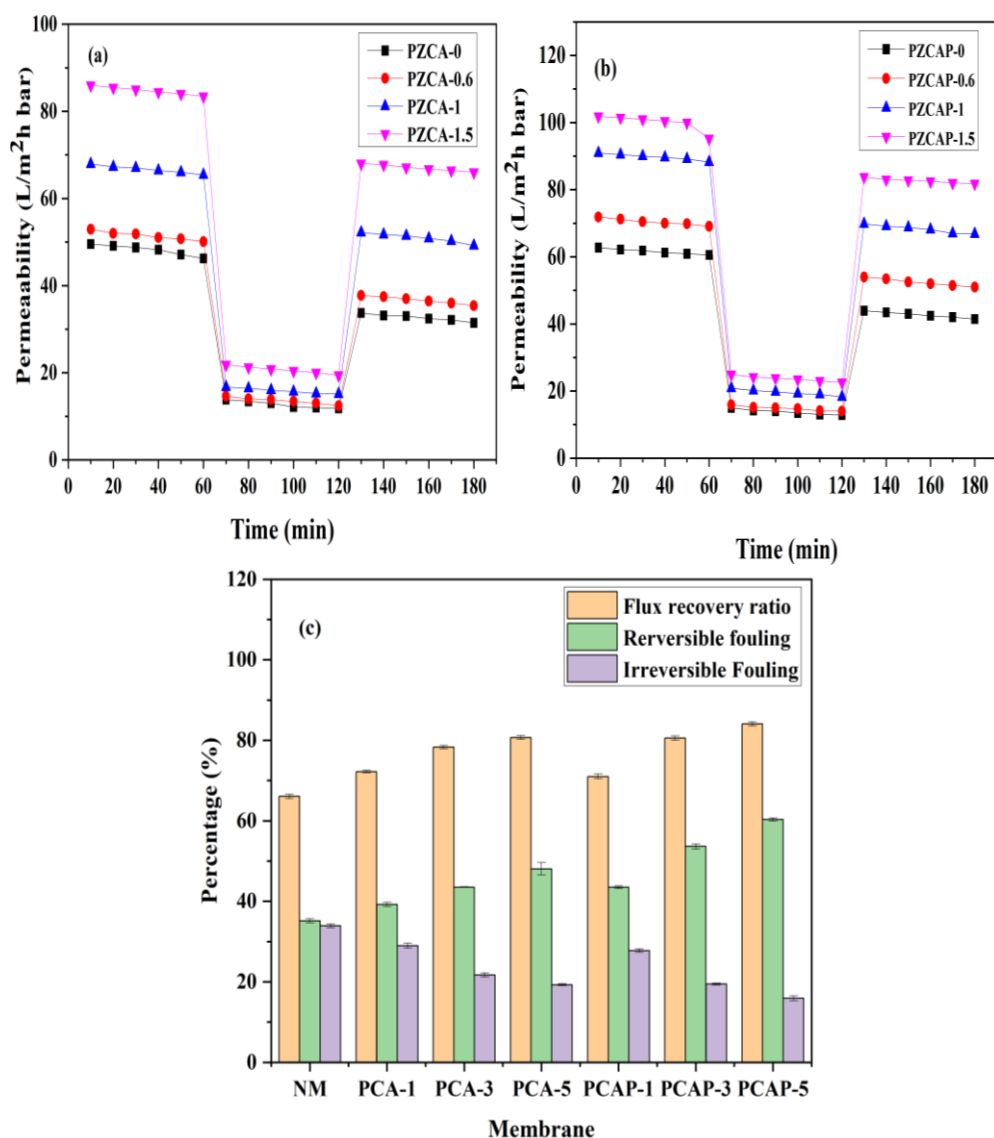
Figure 8.6 Comparison of time dependent pure water permeability, BSA permeability and succeeded by washing with water of (a) polyphenylsulfone/cellulose acetate, (b) polyphenylsulfone/cellulose acetate phthalate hollow fiber membranes and (c) protein removal properties from membranes.

8.2.6 Thermogravimetric analysis (TGA) of the prepared membranes

The thermogravimetric analysis (TGA) of the prepared neat, PCA-5 and PCAP-5 hollow fiber membranes were illustrated in Figure 8.7. Three phases of weight loss with respect to temperature were reported for describing the TGA thermographs. From room temperature to 180 $^{\circ}$C, the initial weight loss stage is due to the volatilization of volatile substances and adsorbed water evaporation. The second stage of weight loss is from 200 $^{\circ}$C to 520 $^{\circ}$C, which was due to the breakdown of SO_2 groups present in the polymer chains. Polymer chains were broken entirely in the third stage above 550 $^{\circ}$C and started to form ash (Arockiasamy et al. 2017b). Similarly, the first thermal degradation for PCA-5 and PCAP-5 membranes at room

221

temperature to 150 $^{\circ}$C for the evaporation of adsorbed water, the second thermal degradation begins at 190 $^{\circ}$C to 610 $^{\circ}$C and 180 $^{\circ}$C to 570 $^{\circ}$C for the decomposition of CA and CAP polymer chains and the third thermal degradation starts above 600 $^{\circ}$C. In this temperature range, the CA and CAP decompose fully into ash. Due to the addition of CA and CAP additives to the PPSU dopes solution, there is a significant thermal miscibility (Dehkordi et al. 2015b). The TGA study has shown that modified hollow fiber membranes have higher thermal stability.
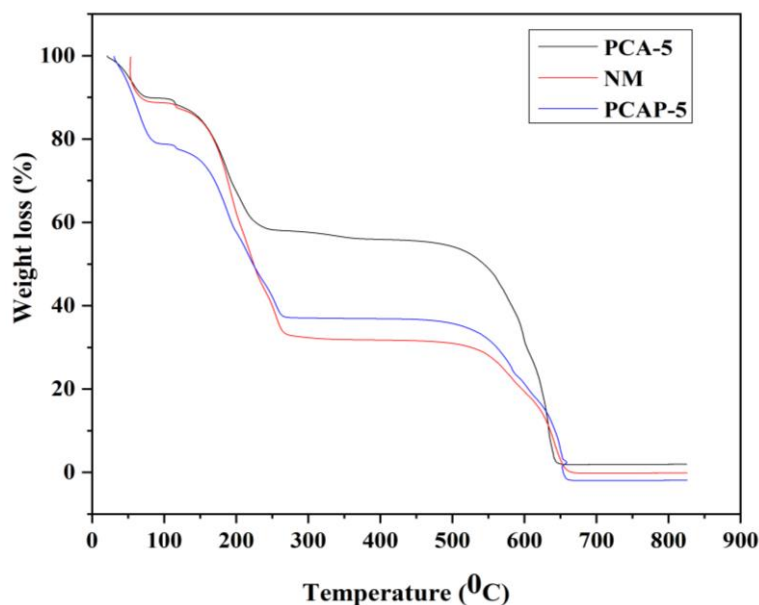
Figure 8.7 Thermogravimetric analysis of the neat membrane (NM), PCA-5 and PCAP-5 hollow fiber membranes.

8.2.7 Dyes and proteins rejection studies from fabricated membranes

8.2.7.1 Dyes rejection studies from prepared membranes

The reactive orange-16 (RO-16) and reactive black-5 (RB-5) removal with the help of hollow fiber membranes from aqueous solutions was demonstrated in Figure 8.8(a). The maximum rejection from membranes was witnessed from PCA-5 and PCAP-5 hollow fiber membranes. In the case of the neat membrane (NM), the dye rejection was 42.08% and 47.72% with corresponding permeability of 35.41 L/m^{2}h bar and 42.01 L/m^{2}h bar for RO-16 and RB-5 respectively. An incremental dosage of CA and CAP in the PPSU dope solution results in improved dye rejection efficiency. This is because of the enhancement of adsorptive properties due to the presence of CA and CAP additives (Chatterjee and De 2014b; Puspasari et al. 2018). From Table 8.3 and Figure 8.9(a) – (b), dye rejection properties of RO-16 for PCAP-5 membrane was 83.45% and for membrane, PCA-5 was 80.02% and corresponding permeabilities were 77.63 L/m^{2}h bar and 68.13 L/m^{2}h bar for PCAP-5 and PCA-5

respectively. The dye rejection properties of RB-5 reactive dye for the PCAP-5 membrane was 95.49% and PCA-5 was 82.69%. Corresponding permeabilities were 70.02 L/m^{2}h bar and 68.18 L/m^{2}h bar for PCAP-5 and PCA-5 membranes respectively. Due to the higher molecular weight of CAP membranes compared to CA membranes, the rejection was considerable in CAP membranes, which is also a cause for optimal dye rejection from CAP membranes. From the literature, the molecular weight of dye increases for RB-5 (991.78 g/mol) than for the RO-16 (617.52 g/mol). The rejection efficiency of the fabricated hollow fiber membranes also increases (Thong et al. 2018). Similarly, CAP incorporated PPSU hollow fiber membranes have superior adsorptive nature and are less susceptible to fouling and an improved hydrophilicity were dominating factors for the optimal rejection of dyes from the fabricated hollow fiber membranes (Nayak et al. 2017b). Concentration polarization of the fabricated membranes were illustrated in Table 8.4.

8.2.7.2 Proteins removal studies of hollow fiber membranes

The rejection of various proteins (BSA, egg albumin and pepsin) from fabricated pristine, CA/PPSU and CAP/PPSU hollow fiber membranes were demonstrated in Figure 8.8(b). From Table 8.3 and Figure 8.8, the neat membrane exhibited 39.85, 21.61 and 23.07% for BSA, egg albumin and pepsin proteins with permeabilities were 33.98, 41.46 and 48.58 L/m^{2}h bar respectively. From Table 8.3 and Figure 8.10, increased dosage of additives also revealed increased rejection parameters for PCA-5 membrane of 93.63, 92.30 and 83.13% respectively for BSA, egg albumin and pepsin with permeability were 49.89, 63.68 and 65.19 L/m^{2}h bar respectively. The PCAP-5 hollow fiber membrane exhibited 94.26, 95.37 and 94.92% with permeabilities of 52.61, 65.08 and 70.01 L/m^{2}h bar for BSA, egg albumin and pepsin respectively. From Figure 8.11, as filtration time increases, there is a decreased permeability due to fouling or deposition of the protein molecules (Vetrivel et al. 2018b).

Table 8.3 Dye/ protein rejection from fabricated hollow fiber membranes

Membranes Code	Dye rejection (%)				Protein rejection (%)					
	RB-5	Standard deviation	RO-16	Standard deviation	Bovine serum albumin	Standard deviation	Egg albumin	Standard deviation	Pepsin	Standard deviation
Neat membrane (NM)	42.7	1.0	42.2	1.1	39.8	2.7	21.6	0.5	23.0	0.5
PCA-1	62.7	0.9	55.6	1.1	58.2	2.5	61.9	0.5	71.2	0.8
PCA-3	77.1	1.3	65.6	0.9	85.5	1.1	88.2	0.6	76.8	1.1
PCA-5	82.6	0.7	80.0	1.5	93.6	0.8	92.3	0.4	83.1	0.6
PCAP-1	70.4	0.9	60.6	0.4	68.1	0.8	64.8	0.3	66.6	0.4
PCAP-3	79.7	1.1	72.1	1.3	90.7	1.05	90.6	0.5	75.4	0.4
PCAP-5	95.4	0.4	83.4	1.3	95.2	0.9	94.9	0.4	94.9	0.5

Also there is a considerable improvement in rejection percentage of proteins with gradual increase in the concentrations of (1, 3 and 5 wt%) CA and CAP hollow fiber membranes relative to the neat membrane due to high adsorptive properties of the additives used (Vinodhini et al. 2017). The higher rejection of BSA proteins from prepared hollow fiber membranes of PCA-5 and PCAP-5 compared to pepsin and egg albumin was observed due to

size exclusion and higher BSA proteins molecular weight (66.43 kDa) than the egg albumin (42.69 kDa) and pepsin (35 kDa) (Arockiasamy et al. 2017b).
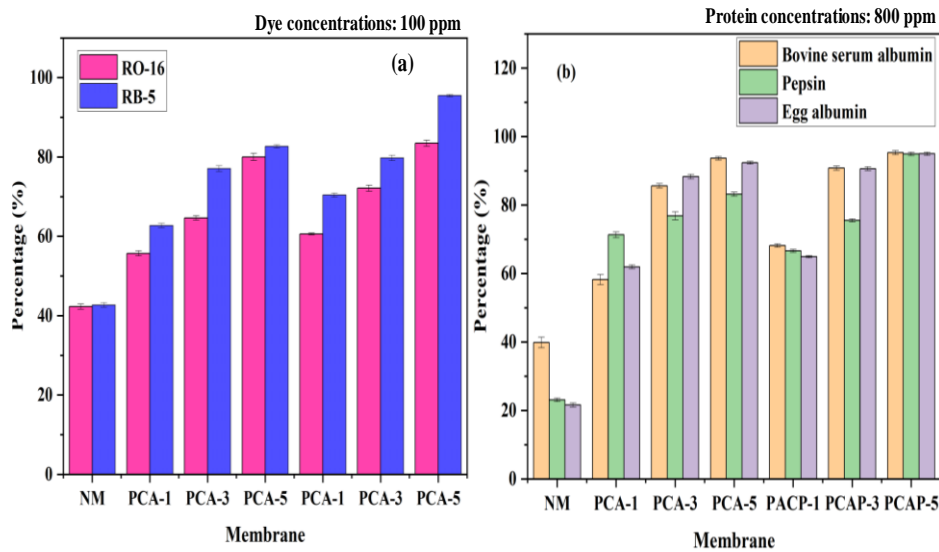
Figure 8.8 (a) Comparison of dyes rejection and (b) proteins rejection study from prepared hollow fiber membranes.
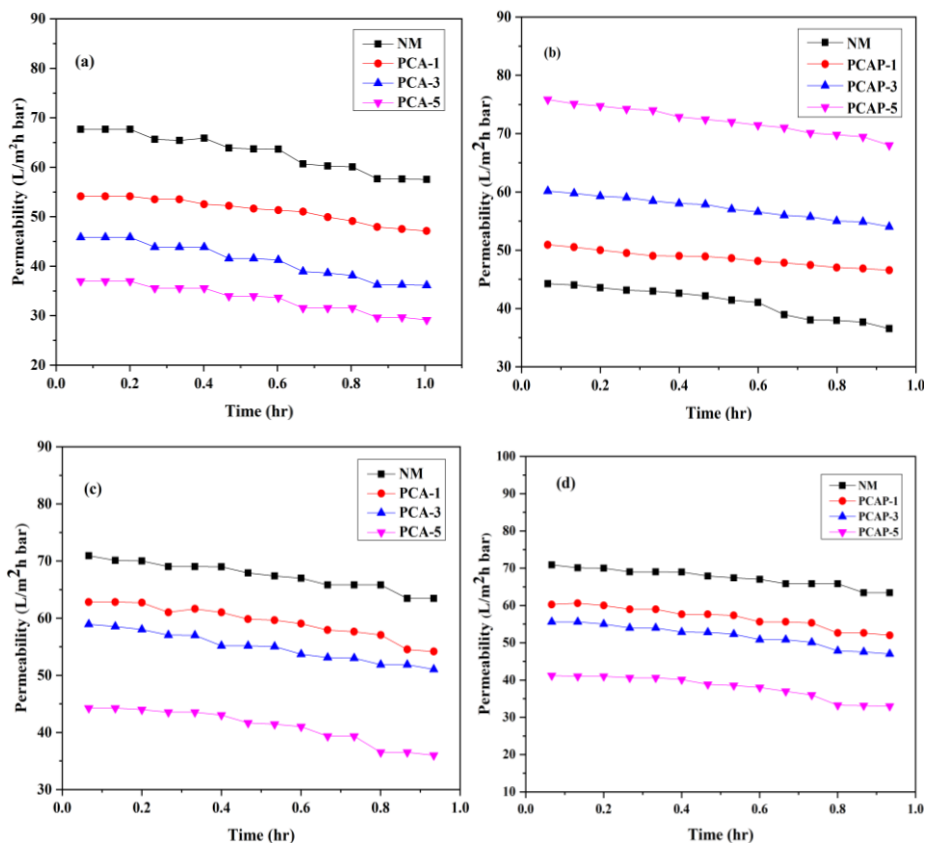
Figure 8.9 Dyes permeabilities of Reactive orange-16 (RO-16) of (a) and (b) CA/PPSU and CAP/PPSU along with Reactive black-5 (RB-5) of (c) and (d) are CA/PPSU and CAP/PPSU hollow fiber membranes respectively.
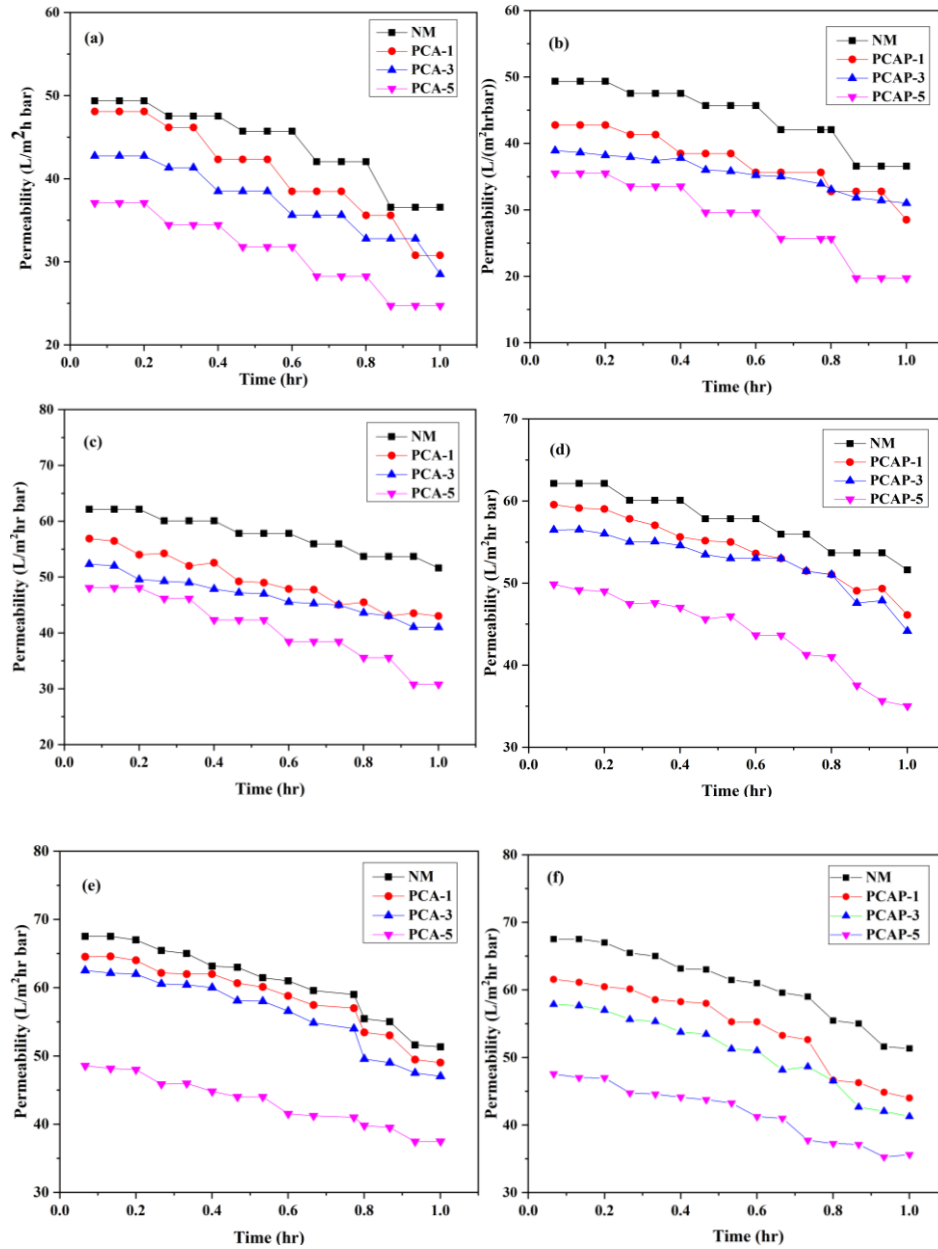
Figure 8.10 Proteins permeability (a and b) for BSA of CA/PPSU and CAP/PPSU hollow fiber membranes respectively. Similarly, for egg albumin is (c and d) and for pepsin is (e and f) respectively.

Table 8.4 Concentration polarization of the fabricated hollow fiber membranes

Membrane codes	Velocity (v) (m/s)	Mass transfer coefficient (K) (m/s)	Concentration polarization ($\frac{Cm}{Cb}$)
BOVINE SERUM ALBUMIN			
NM	0.0417	7.269×10^{-6}	1.138
PCA-1	0.00253	1.091×10^{-5}	1.648
PCA-3	0.00253	1.092×10^{-5}	2.056
PCA-5	0.00164	8.32×10^{-6}	2.540
PCAP-1	0.002237	9.611×10^{-6}	1.114
PCAP-3	0.002039	9.499×10^{-6}	2.411
PCAP-5	0.001805	9.596×10^{-6}	1.142
PEPSIN			
NM	0.00319	1.071×10^{-5}	1.217
PCA-1	0.0028	1.508×10^{-5}	2.227
PCA-3	0.003	1.064×10^{-5}	1.674
PCA-5	0.00241	1.031×10^{-5}	2.332
PCAP-1	0.00284	1.511×10^{-5}	2.009
PCAP-3	0.00272	1.155×10^{-5}	2.135
PCAP-5	0.00289	1.1402×10^{-5}	2.539
EGG ALBUMIN			
NM	0.00339	1.232×10^{-5}	1.178
PCA-1	0.00262	1.121×10^{-5}	1.770
PCA-3	0.00248	1.088×10^{-5}	2.584

PCA-5	0.001878	9.481×10^{-6}	2.804
PCAP-1	0.00242	1.018×10^{-5}	2.162
PCAP-3	0.00232	1.084×10^{-5}	3.118
PCAP-5	0.00248	7.764×10^{-5}	2.803
REACTIVE ORANGE -16 (RO-16)			
NM	0.106	3.87×10^{-5}	1.183
PCA-1	0.00819	1.425×10^{-5}	1.481
PCA-3	0.0721	1.556×10^{-5}	1.92
PCA-5	0.0055	1.37×10^{-5}	1.65
PCAP-1	0.0074	1.481×10^{-5}	1.556
PCAP-3	0.0071	1.537×10^{-5}	1.833
PCAP-5	0.0077	1.574×10^{-5}	1.702
REACTIVE BLACK -5 (RB-5)			
NM	0.1006	3.81×10^{-5}	1.199
PCA-1	0.00878	1.673×10^{-5}	1.646
PCA-3	0.00845	1.63×10^{-5}	1.882
PCA-5	0.00609	1.445×10^{-5}	1.821
PCAP-1	0.00702	1.447×10^{-5}	1.877
PCAP-3	0.00685	1.519×10^{-5}	1.954
PCAP-5	0.00748	1.545×10^{-5}	1.895

8.3 SUMMARY OF THE PRESENT WORK

Hollow fiber membranes of asymmetric polyphenylsulfone with the incremental concentrations 1, 3 and 5 wt% of cellulose acetate and cellulose acetate phthalate were fabricated successfully using a non-solvent induced phase separation process. The effect of concentrations of additives on the polyphenylsulfone matrix was well understood. The increased dosages of cellulose acetate and cellulose acetate phthalate in the PPSU dope solution attributed to improved hydrophilicity, porosity, water absorption and antifouling properties. The progressive dosages of additives enhanced the water permeability with 64.47 L/m²h bar for PCA-5, 72.60 L/m²h bar for PCAP-5, whereas neat membrane showed the permeability of 41.26 L/m²h bar.

From SEM pictures, expanded micro-pores, finger-like morphologies, dense structures on the membrane's skin layer, and porous–like structure on the supporting layer were ensured in fabricated hollow fiber membranes. There is an increased surface roughness from AFM images from neat membranes to gradual increased additive dosage membranes (PCA-5 and PCAP-5). The neat membrane showed rejection parameters as 42.72% for reactive black-5 and 42.28% for reactive orange-16 respectively. The modified PCA-5 and PCAP-5 hollow fiber membranes exhibited enhanced 82.69% and 95.49% of rejection for reactive black -5 and 80.02% and 83.45% for reactive orange-16 respectively. Because of the increased adsorptive property of PCA-5 and PCAP-5, there is an increase in the rejection of dyes and proteins. The protein rejection parameter from the neat membrane was 39.85%, 21.61%, and 23.07% respectively, for BSA, egg albumin, and pepsin. The modified PCA-5 and PCAP-5 hollow fiber membranes exhibited enhanced rejection properties for various dyes and proteins. Rejection of proteins for PCA-5 and PCAP-5 was 93.63 and 95.26% for BSA, 92.30 and 94.97% for egg albumin and 83.13% and 94.92% for pepsin respectively. In conclusion, the prepared ultrafiltration PPSU membranes with increased dosages of 1, 3 and 5 wt% of cellulose acetate and cellulose acetate phthalate were effective in retaining an aqueous solution containing ions of different dyes (reactive orange-16 and reactive black-5) along with proteins (BSA, pepsin and egg albumin).

CHAPTER -9
SUMMARY AND CONCLUSION

Abstract

This chapter briefly describes the overall work and compares the properties and efficacy of the laboratory-prepared hollow fiber membranes. It also includes a summary of the work's main findings.

9.1 Summary

- In the present study, 36 hollow fiber membranes were fabricated with different additives and nanoparticles using a non-solvent induced phase separation (NIPS) process.

- Hollow fiber membranes with various nanoparticles such as zirconium oxide (ZrO_2), zinc –magnesium oxide (ZnO-MgO), nano-aluminum oxide (nano-Al_2O_3) and polydopamine (PDA; polymer) are incorporated in the membrane matrix.

- Hollow fiber membranes were prepared using N-methyl-2 pyrrolidone (NMP) as a solvent and water as a non-solvent.

- Scanning electron microscopy (SEM) and atomic force microscopy (AFM) apparatus were utilized to interpret membrane surface morphologies and topographies respectively.

- The fabricated pristine and modified membranes surface wettability behavior was scrutinized by contact angle measurement.

- The dry-wet weigh principle was carried out for membrane porosity/water uptake measurements.

- Pure water permeability, an antifouling study using bovine serum albumin as model protein and rejection properties of arsenic-V and dye/protein removal, was conducted using a cross-flow filtration system.

- The fabricated membranes surface potential and thermal stability were determined by zeta potential analysis and thermogravimetric analysis, respectively.

- The crystallinity and morphologies of used nanoparticles were interpreted by x-ray diffraction (XRD) and transmission electron microscopy (TEM) analysis respectively.

- The fourier transform infrared (FTIR) and x-ray photoelectron spectroscopy (XPS) were implemented for the existence of various functional groups and binding energies respectively.

- The arsenic-V and dye/protein removal performance was determined using laboratory-prepared aqueous solutions.

Table 9.1 Hollow fiber membranes series

Membrane series	Membranes codes	Nano-additives	Nanoparticles
MS-1	Neat membrane (NM), CA-1, CA-3, CA-5 and CAP-1, CAP-3, CAP-5,	Cellulose acetate (CA) and cellulose acetate phthalate (CAP)	--
MS-2	PZCA-0, PZCA-0.6, PZCA-1, PZCA-1.5 and PZCAP-0, PZCAP-0.6, PZCAP-1, PZCAP-1.5	Cellulose acetate (CA) and cellulose acetate phthalate(CAP)	Zirconium oxide (ZrO_2)
MS-3	ZMCA-0, ZMCA-0.6, ZMCA-1, ZMCA-1.5 and ZMCAP-0, ZMCAP-0.6, ZMCAP-1, ZMCAP-1.5	Cellulose acetate (CA) and cellulose acetate phthalate (CAP)	Zinc–magnesium oxide (ZnO-MgO)
MS-4	ALCA-0, ALCA-0.6, ALCA-1, ALCA-1.5 and ALCAP-0, ALCAP-0.6, ALCAP-1, ALCAP-1.5	Cellulose acetate (CA) and cellulose acetate phthalate (CAP)	Aluminum oxide(Al_2O_3)
MS-5	PDA-0, PDA-1, PDA-2, PDA-3, PDA-5	Polyvinylpyrrolidone (PVP)	Polydopamine (PDA)
MS-6	Neat membrane (NM), PPSU/CA-1 wt%, PPSU/CA-3 wt%, PPSU/CA-5 wt% and PPSU/CAP-1 wt%, PPSU/CAP-3 wt%, PPSU/CAP-5 wt%	Cellulose acetate (CA) and cellulose acetate phthalate (CAP)	--

The important findings were observed from the experimental investigations they are:

i. In membrane series (MS-1) from Table 9.1, **Use of cellulose acetate/polyphenylsulfone derivatives to fabricate ultrafiltration hollow fiber membranes for the removal of arsenic-V from water**, best performed hollow fiber membrane containing 5 wt% of cellulose acetate phthalate/polyphenylsulphone (CAP-5) and 5 wt% of cellulose acetate/polyphenylsulphone (CA-5) exhibited enhanced permeability of 69.60 and 61.47 L/m^{2}h bar respectively. The arsenate oxide (AsO$_4^{3-}$) removal properties for CA-5 and CAP-5 membranes were 34% and 41% with permeabilities of 44.42 and 40.11 L/m^{2}h bar respectively. The best performing CAP-5 membrane showed enhanced negative surface potential of -18.75 mV which was recorded at the pH 9.7. The enhanced flux recovery ratio (FRR) of 91.95% for CAP-5 membrane, implies enhanced antifouling properties.

ii. In membrane series (MS-2), **Removal of toxic arsenic-V from aqueous media using polyphenylsulfone/cellulose acetate and polyphenylsulfone/cellulose acetate phthalate hollow fiber membranes containing zirconium oxide,** best performing PZCA-1 hollow fiber membrane with increased surface potential of -28.19 mV at pH 7 was noticed. Hollow fiber membranes fabricated using 1 wt% of ZrO$_2$ in PPSU/CA (PZCA-1) and 0.6 wt% of ZrO$_2$ in PPSU/CAP (PZCAP-0.6) showed increased arsenate oxide (AsO$_4^{3-}$) removal as 87.24% and 70.48% with the permeabilities of 89.94 and 70.59 L/m^{2}h bar respectively with laboratory prepared 1 ppm arsenic-V solution (pH 6.8$\pm$0.2) at 1 bar transmembrane pressure. Also ZrO$_2$ modified membranes PZCA-1.5 and PZCAP-1.5 were exhibiting improved pure water permeability as 84.05 L/m^{2}h bar and 100.96 L/m^{2}h bar respectively. Because of the increased hydrophilicity of the membrane surface, the ZrO$_2$-containing hollow fiber membranes exhibited remarkable antifouling properties compared to the pristine membrane. As an outcome, the flux recovery ratio of PZCA-1.5 and PZCAP-1.5 were 79.01% and 81.94% respectively compared to neat membrane PZCA-0 and PZCAP-0 as 67.49% and 70.02% respectively.

iii. In membrane series (MS-3), **Effect of binary zinc-magnesium oxides on polyphenylsulfone/cellulose acetate derivatives hollow fiber membranes for the decontamination of arsenic-V from water,** the effect of binary zinc-magnesium oxide (ZnO-MgO) on PPSU/CA and PPSU/CAP hollow fiber membrane was well interpretated. The decreased contact angle parameter was noted for the modified membrane with 1wt% of zinc-magnesium oxide in PPSU/CA (ZMCA-1) and 1wt% of zinc-magnesium oxide in PPSU/CAP (ZMCAP-1) as 60.81° and 57.32° compared to neat

membrane ZMCA-0 and ZMCAP-0 as 71.56° and 68.85° respectively. The good performing hollow fiber membranes 0.6 wt% of zinc-magnesium oxide in PPSU/CAP (ZMCAP-0.6) and ZMCA-1 exhibited enhanced arsenic-V removal compared to pristine membrane. The enhanced arsenic-V removal from ZMCAP-0.6 and ZMCA-1 were 81.31% and 78.48% with permeability as 69.58 L/m^{2}h bar and 198.47 L/m^{2}h bar respectively from laboratory prepared 1 ppm arsenic-V solution (pH 6.8$\pm$0.2) at 1 bar transmembrane pressure. The enhanced flux recovery ratio (FRR) from membranes, 1.5 wt% of zinc-magnesium oxide in PPSU/CA (ZMCA-1.5) and 1.5 wt% of zinc-magnesium oxide in PPSU/CAP (ZMCAP-1.5) were 91.08% and 90.11% respectively than the neat membrane ZMCA-0 and ZMCAP-0 as 65.42% and 69.95% respectively. The increased FRR parameter from the modified membrane also revealed increased antifouling properties.

iv. In membrane series (MS-4), **Nano-aluminum oxide embedded cellulose acetate/ polyphenylsulfone derivatives hollow fiber membranes: Fabrication, characterization and arsenic-V removal from water,** the influences of nano-aluminum oxide (nano-Al$_2$O$_3$) on PPSU/CA and PPSU/CAP hollow fiber membranes was discussed in detail. The best performing membrane, 1.5 wt% of nano-Al$_2$O$_3$ in PPSU/CA (ALCA-1.5) showed increased negative potential of -49.5 mV at pH 7.3 respectively. The increased arsenic-V removal performance was witnessed from membranes ALCA-1.5 and 1 wt% of nano-Al$_2$O$_3$ in PPSU/CA (ALCA-1) removed 98.67% and 94.89% with permeability were 88.41 L/m^{2}h bar and 53.42 L/m^{2}h bar respectively. Nano–Al$_2$O$_3$ modified hollow fiber membranes with enhanced hydrophilicity showed improved pure water permeabilities as 88.87 L/m^{2}h bar and 102.13 L/m^{2}h bar respectively. The increased flux recovery ratio of the modified membranes for ALCA-1.5 and ALCAP-1.5 as 85.09% and 89.24% respectively ensures the enhancement of antifouling properties.

v. In membrane series (MS-5), **Hydrophilic polydopamine/polyvinylpyrrolidone embedded polyphenylsulfone hollow fiber membranes for the removal of arsenic (As-V) from water,** the best performing membrane 3 wt% of polydopamine (PDA) in polyphenylsulfone (PPSU)/polyvinylpyrrolidone (PVP) (PDA-3) hollow fiber membrane unveiled enhanced arsenate oxide removal as 87.15% with the permeability of 15.90 L/m^{2}h bar as compared to neat membrane. The neat membrane (PDA-0) exhibited lower arsenate oxide removal performance as 67.70% with the permeability rate of 7.46 L/m^{2}h bar. Also the PDA-3 membrane showed increased negative potential of -30.38 mV at pH

7 and enhanced thermal stability and surface roughness. The modified 5 wt% of PDA in PPSU/PVP hollow fiber membrane (PDA-5) showed increased pure water permeability as 18.72 L/m^{2}h bar as compared to neat membrane (PDA-0) as 7.53 L/m^{2}h bar respectively. Furthermore, dosage of 5 wt% of PDA in PPSU/PVP membranes, the arsenic-V oxide rejection properties from the membrane decreased due to the concentration polarization.

vi. In membrane series (MS-6), **Improved separation of dyes and proteins using membranes made of polyphenylsulfone/cellulose acetate and polyphenylsulfone/cellulose acetate phthalate,** the best performing membrane 5 wt% of cellulose acetate phthalate (CAP) in PPSU (PCAP-5) showed 83.45% and 95.49% for reactive orange-16 (RO-16) and reactive black-5 (RB-5) with the permeability of 77.63 L/m^{2}h bar and 70.02 L/m^{2}h bar respectively. The neat membrane (NM) removed 42.08 % with the permeability of 35.41 L/m^{2}h bar. Similarly, for high molecular weight bovine serum albumin protein (BSA), the rejection of PCAP-5 membrane was 94.26% with the permeability of 52.61 L/m^{2}h bar. The lower rejection was recorded for pepsin and egg albumin compared to BSA protein. Also, increased dosages of CA and CAP incorporated PPSU membranes exhibited enhanced hydrophilicity, porosity/water uptake, pure water permeability, antifouling properties and thermal stability as compared to neat membrane. The pure water permeability for PCA-5 and PCAP-5 membrane was 64.47 L/m^{2}h bar and 72.60 L/m^{2}h bar which was more significant than the neat membrane 41.26 L/m^{2}h bar. The pure water permeability, contact angle, water uptake/porosity and arsenic-V removal abilities of all prepared hollow fiber membranes are compared as follows.

Figure 9.1 illustrated the contact angle of all fabricated hollow fiber membranes. Membrane contact angle assessment is critical for analyzing the permeability and performance in water treatment applications. The introduction of hydrophilic additives and nanoparticles into the PPSU hydrophobic dope solution in turn considerably enhances the hydrophilicity of the modified hollow fiber membranes. In the current investigation, the 5 wt% cellulose acetate phthalate in PPSU hollow fiber membranes in MS-1 exhibited a lower contact angle than other membranes.
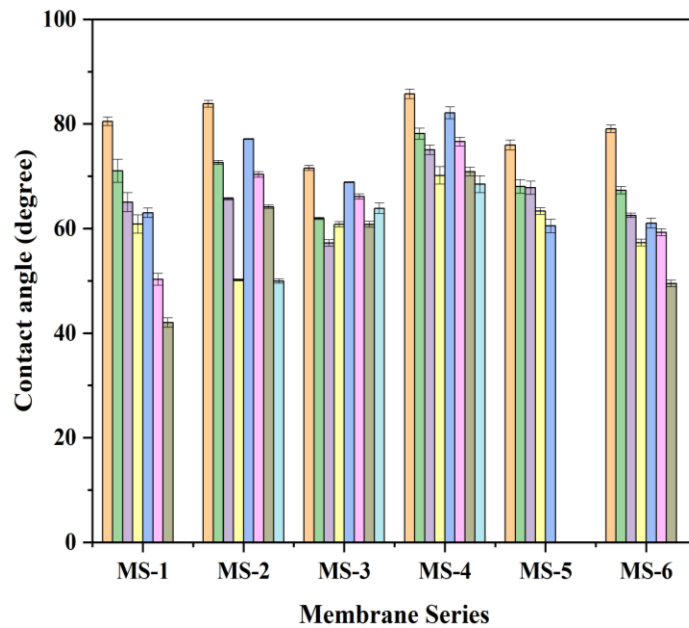
Figure 9.1 Contact angle outcome of the fabricated hollow fiber membranes.

Figure 9.2 shows the water uptake ability of the fabricated hollow fiber membranes. As the hydrophilicity of the additives and nanoparticles incorporated in modified hollow fiber membranes increases, the water-absorbing capacity also increases. As the membrane prepared by 1.5 wt% of the Al_2O_3 incorporated PPSU/CAP (ALCAP-1.5) hollow fiber membrane unveiled enhanced water uptake. Membrane ALCAP-1.5 (in MS-4) showed 84.26% of water uptake parameters than the other membranes.
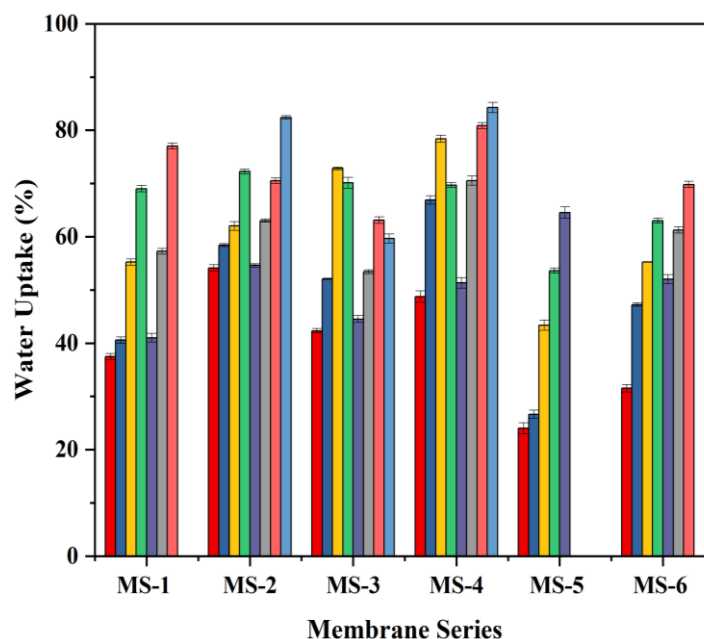
Figure 9.2 Water uptake measurement of the fabricated hollow fiber membranes.

Figure 9.3 unveiled the pure water permeability study of the fabricated hollow fiber membrane series (MS-1 to MS-6). According to the results, the membrane containing 1 wt% of zinc-magnesium oxide (ZnO-MgO) in polyphenylsulfone (PPSU)/cellulose acetate (MS-3) hollow fiber membrane exhibited higher pure water permeability than the other membranes. This is because of the enhanced finger-like structure and surface roughness in binary ZnO-MgO modified membranes. In addition, the ZnO-MgO binary oxide nanoparticle act as an excellent adsorbing agent and increases the water-holding capability. As a result, the permeability properties of membranes increased continuously as the percentage of ZnO-MgO in membranes increased. Also, the increased hydrophilic properties of bio-sorbents cellulose derivatives help to improve the permeability of modified membranes.
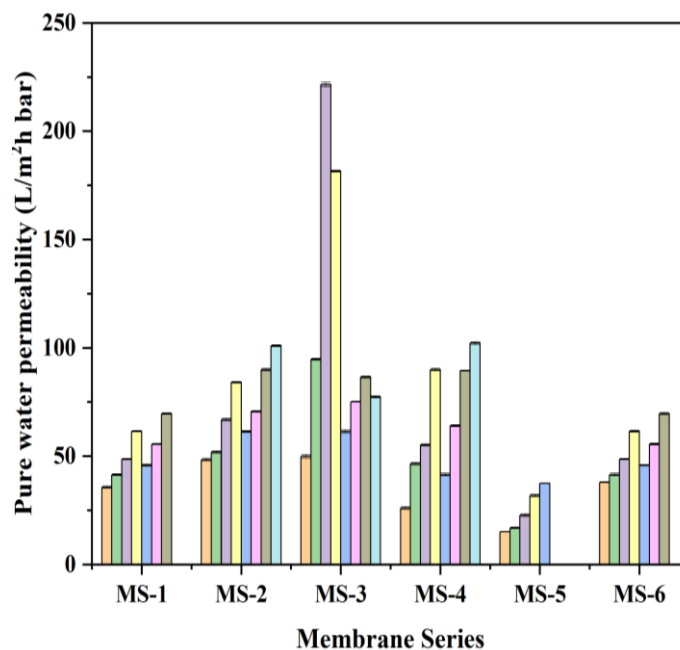
Figure 9.3 Pure water permeation study of fabricated hollow fiber membranes.

Figure 9.4 illustrated the antifouling capability of all fabricated pristine and modified hollow fiber membranes in terms of flux recovery ratio (FRR in %). The antifouling ability of the fabricated membranes was analyzed by FRR, as the FRR of the modified membranes increased with the dosages of hydrophilic cellulose derivatives and various dosages of nanoparticles into the PPSU hydrophobic dope solution. In our proposed research work, the enhanced flux recovery ratio was witnessed from the membrane prepared by 1.5 wt% of zinc-magnesium oxide (ZnO-MgO) in PPSU/CAP (ZMCAP-1.5) from membrane series MS-3. The enhanced flux recovery ratio in turn revealed enhanced membrane durability than the other membranes.
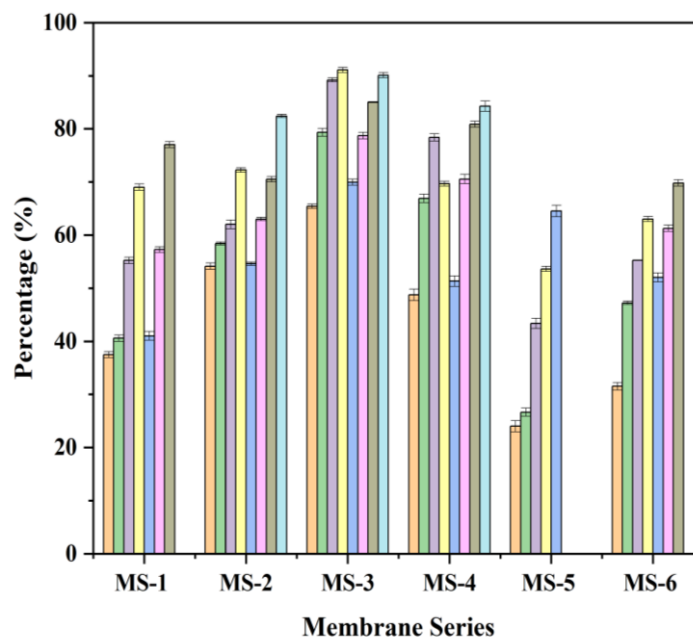
Figure 9.4 Flux recovery ratio (FRR) parameter of fabricated hollow fiber membranes.

Figure 9.5 the comparison of percentage AsO_4^{3-} removal of all prepared hollow fiber membranes. As such, the membrane prepared with 1.5 wt% of nano-Al_2O_3 in PPSU/CA (ALCA-1.5) and 1 wt% of nano-Al_2O_3 in PPSU/CA (ALCA-1) from membrane series MS-4 exhibited increased arsenic-V removal ability as compared to other membrane series, because of the electrostatic repulsion between the membrane surface and the arsenate oxide (AsO_4^{3-}). The ALCA-1.5 membrane exhibited increased surface charge, which further repels more arsenate oxide than other membrane series from laboratory prepared arsenic-V aqueous solution at pH 6.8±0.2.
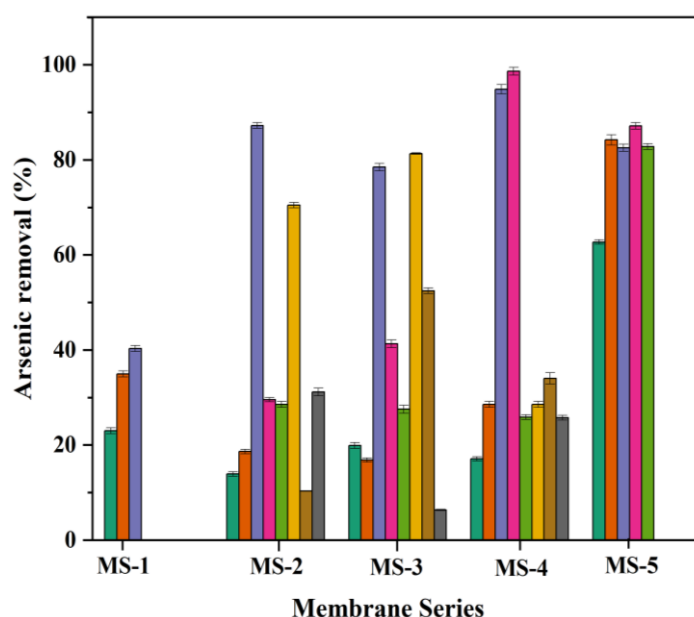
Figure 9.5 Percentage arsenic-V removal properties of the fabricated hollow fiber membranes.

9.2 Conclusions

The hydrophobic polyphenylsulfone (PPSU) hollow fiber membranes were modified with cellulose derivatives as additives such as cellulose acetate and cellulose acetate phthalate, along with different nanoparticles, zirconium oxide (ZrO_2), zinc-magnesium oxide (ZnO-MgO), aluminum oxide (Al_2O_3) and polydopamine (PDA). The quality and performance of the modified hollow fiber membranes was confirmed by analyzing membrane hydrophilicity/hydrophobicity, porosity/water uptake, pure water permeation, antifouling and arsenic-V separation.

The key findings of the proposed investigation are:

- The addition of cellulose derivatives along with various nanoparticles such as zirconium oxide (ZrO_2), zinc-magnesium oxide (ZnO-MgO), aluminum oxide (Al_2O_3) and polyvinylpyrrolidone (PVP)/polydopamine (PDA) considerably enhances the membranes hydrophilicity, pure water permeability, antifouling and rejection of arsenate oxide (AsO_4^{3-}).

- Adding increased concentrations of hydrophilic inorganic nanoparticles into the PPSU hydrophobic dope in turn enhances modified membrane surface morphology, topological structures and performances.

- Due to the effect of binary zinc-magnesium oxide (ZnO-MgO) on the PPSU and cellulose derivative (cellulose acetate phthalate), there is enhanced pure water permeability (MS-3) antifouling properties compared to other membranes.

- Due to the modifications, induced surface charge on the membrane surfaces may lead to increased selectivity since the solutes and charged membrane surface have an electrostatic interaction.

- As such, the membranes prepared using aluminum oxide (Al_2O_3) in PPSU and cellulose derivative (cellulose acetate) ($PPSU/CA/Al_2O_3$) membranes (in MS-4) exhibited an enhanced surface charge of -40.3 mV at pH 7.0. This is because of the increased repulsion between the negatively charged membrane surface and negatively charged arsenate oxide (AsO_4^{3-}) present in the arsenic-V aqueous solution (pH 6.8 ± 0.2) at 1 bar transmembrane pressure (TMP).

- The good performed membranes used in this study can be utilized to separate arsenic-V from aqueous solution under standard conditions with better results.

- Also, the modified, well-performed membranes (MS-6) utilized in this study can be employed to retain different dyes and proteins from aqueous solutions under standard conditions with better outcomes.

In the future, as fabricated additives and nanoparticles embedded polyphenylsulfone (PPSU) hollow fiber membranes can be used selectively for the arsenic-V rejection from the drinking water and other metals impurities. However, the primary objective of this research study is focused on the removal of arsenic-V. As the interactions of the membrane surface with the other heavy metals are different, the rejections properties of those heavy metals were different from that of arsenic-V.

REFERENCES

Abdel-Fatah, M. A. (2018). "Nanofiltration systems and applications in wastewater treatment." Ain Shams Engineering Journal, 9(4), 3077–3092.

Abd Elkodous, M., Hassaan, A., Ghoneim, A. I., & Abdeen, Z. (2018). "C-dots dispersed macro-mesoporous TiO2 phtocatalyst for effective waste water treatment." Characterization and Application of Nanomaterials, 1(2).

Abdul, K. S. M., Jayasinghe, S. S., Chandana, E. P., Jayasumana, C., and De Silva, P. M. C. (2015). "Arsenic and human health effects: A review." Environmental toxicology and pharmacology, 40(3), 828–846.

Abdullah, N., Yusof, N., Lau, W. J., Jaafar, J., and Ismail, A. F. (2019). "Recent trends of heavy metal removal from water/wastewater by membrane technologies." Journal of Industrial and Engineering Chemistry, 76, 17–38.

Abejón, A., Garea, A., and Irabien, A. (2015). "Arsenic removal from drinking water by reverse osmosis: Minimization of costs and energy consumption." Separation and Purification Technology, 144, 46–53.

Aerts, P., Kuypers, S., Genne, I., Leysen, R., Mewis, J., Vankelecom, I. F. J., and Jacobs, P. A. (2006). "Polysulfone- ZrO2 Surface Interactions. The Influence on Formation, Morphology and Properties of Zirfon-Membranes." The Journal of Physical Chemistry B, 110(14), 7425–7430.

Al-Ani, D. M., Al-Ani, F. H., Alsalhy, Q. F., and Ibrahim, S. S. (2021). "Preparation and characterization of ultrafiltration membranes from PPSU-PES polymer blend for dye removal." Chemical Engineering Communications, 208(1), 41–59.

Ali, A., Yunus, R. M., Awang, M., Johari, A., and Mat, R. (2014). "Effect of Cellulose Acetate Phthalate (CAP) on Characteristics and Morphology of polysulfone/cellulose acetate phthalate (PSf/CAP) blend membranes." Applied Mechanics and Materials, Trans Tech Publ, 640–644.

Amy, G. L. (2005). "Adsorbent treatment technologies for arsenic removal." American Water Works Association.

Ang, M. B. M. Y., Macni, C. R. M., Caparanga, A. R., Huang, S.-H., Tsai, H.-A., Lee, K.-R., and Lai, J.-Y. (2020). "Mitigating the fouling of mixed-matrix cellulose acetate membranes

for oil–water separation through modification with polydopamine particles." Chemical Engineering Research and Design, 159, 195–204.

Araújo, T., Bernardo, G., and Mendes, A. (2020). "Cellulose-Based Carbon Molecular Sieve Membranes for Gas Separation: A Review." Molecules, 25(15), 3532.

Arockiasamy, D. L., Alhoshan, M., Alam, J., Muthumareeswaran, M. R., Figoli, A., and Kumar, S. A. (2017). "Separation of proteins and antifouling properties of polyphenylsulfone based mixed matrix hollow fiber membranes." Separation and Purification Technology, 174, 529–543.

Arockiasamy, D. Lawrence; Nagendran, A.; Shobana, K. H.; Mohan, D. (2009). "Preparation and Characterization of Cellulose Acetate/Aminated Polysulfone Blend Ultrafiltration Membranes and their Application Studies." Separation Science and Technology, 44(2), 398–421.

Ayyaru, S., Dinh, T. T. L., & Ahn, Y. H. (2020). "Enhanced antifouling performance of PVDF ultrafiltration membrane by blending zinc oxide with support of graphene oxide nanoparticle." Chemosphere, 241, 125068.

Ayyaru, S., and Ahn, Y.-H. (2017). "Application of sulfonic acid group functionalized graphene oxide to improve hydrophilicity, permeability, and antifouling of PVDF nanocomposite ultrafiltration membranes." Journal of membrane science, 525, 210–219.

Back, J. O., Stadlmayr, W., Jabornig, S., Winkler, F., Winkler, K., and Rupprich, M. (2018). "Removal of arsenic from water with non-thermal plasma (NTP), coagulation and membrane filtration." Water, 10(10), 1385.

Bai, L., Wu, H., Ding, J., Ding, A., Zhang, X., Ren, N., Li, G., and Liang, H. (2020). "Cellulose nanocrystal-blended polyethersulfone membranes for enhanced removal of natural organic matter and alleviation of membrane fouling." Chemical Engineering Journal, 382, 122919.

Baker, B. A., Cassano, V. A., and Murray, C. (2018). "Arsenic exposure, assessment, toxicity, diagnosis, and management: guidance for occupational and environmental physicians." Journal of occupational and environmental medicine, 60(12), e634–e639.

Balasubramanian, N., Kojima, T., and Srinivasakannan, C. (2009). "Arsenic removal through electrocoagulation: kinetic and statistical modeling." Chemical Engineering Journal, 155(1–2), 76–82.

Banerjee, P., & De, S. (2010). "Coupled concentration polarization and pore flow modeling of nanofiltration of an industrial textile effluent." Separation and purification technology, 73(3), 355-362.

Barathi, M., Kumar, A. S. K., Kumar, C. U., and Rajesh, N. (2014). "Graphene oxide–aluminium oxyhydroxide interaction and its application for the effective adsorption of fluoride." Rsc Advances, 4(96), 53711–53721.

Bet-Moushoul, E., Mansourpanah, Y., Farhadi, K., and Tabatabaei, M. (2016). "TiO2 nanocomposite based polymeric membranes: a review on performance improvement for various applications in chemical engineering processes." Chemical Engineering Journal, 283, 29–46.

Böddeker, K. W. (2008). "Tracing membrane science, an historical account." Liquid Separations with Membranes: An introduction to barrier interference, 113–119.

Boddu, V. M., Abburi, K., Talbott, J. L., Smith, E. D., and Haasch, R. (2008). "Removal of arsenic (III) and arsenic (V) from aqueous medium using chitosan-coated biosorbent." Water research, 42(3), 633–642.

Bottino, A., Capannelli, G., and Comite, A. (2002). "Preparation and characterization of novel porous PVDF-ZrO2 composite membranes." Desalination, 146(1–3), 35–40.

Brandhuber, P., and Amy, G. (2001). "Arsenic removal by a charged ultrafiltration membrane—influences of membrane operating conditions and water quality on arsenic rejection." Desalination, 140(1), 1–14.

Burkinshaw, S. M., and Salihu, G. (2019). "The role of auxiliaries in the immersion dyeing of textile fibres part 2: Analysis of conventional models that describe the manner by which inorganic electrolytes promote direct dye uptake on cellulosic fibres." Dyes and Pigments, 161, 531–545.

Campling, P., Joris, I., Calliera, M., Capri, E., Marchis, A., Kuczyńska, A., Vereijken, T., Majewska, Z., Belmans, E., and Borremans, L. (2021). "A multi-actor, participatory approach

to identify policy and technical barriers to better farming practices that protect our drinking water sources." Science of The Total Environment, 755, 142971.

Castner, D. G., Hinds, K., and Grainger, D. W. (1996). "X-ray photoelectron spectroscopy sulfur 2p study of organic thiol and disulfide binding interactions with gold surfaces." Langmuir, 12(21), 5083–5086.

Chatterjee, S., and De, S. (2014). "Adsorptive removal of fluoride by activated alumina doped cellulose acetate phthalate (CAP) mixed matrix membrane." Separation and Purification Technology, 125, 223–238.

Chen, T., Duan, M., Shi, P., and Fang, S. (2017). "Ultrathin nanoporous membranes derived from protein-based nanospheres for high-performance smart molecular filtration." Journal of Materials Chemistry A, 5(38), 20208–20216.

Cheng, Z., Yang, B., Chen, Q., Ji, W., and Shen, Z. (2018). "Characteristics and difference of oxidation and coagulation mechanisms for the removal of organic compounds by quantum parameter analysis." Chemical Engineering Journal, 332, 351–360.

Chong, K. C., Lai, S. O., Lau, W. J., San Thiam, H., Ismail, A. F., and Zulhairun, A. K. (2017). "Fabrication and characterization of polysulfone membranes coated with polydimethysiloxane for oxygen enrichment." Aerosol and Air Quality Research, 17(11), 2735–2742.

Choong, T. S., Chuah, T. G., Robiah, Y., Koay, F. G., and Azni, I. (2007). "Arsenic toxicity, health hazards and removal techniques from water: an overview." Desalination, 217(1–3), 139–166.

Chung, Y. T., Mahmoudi, E., Mohammad, A. W., Benamor, A., Johnson, D., and Hilal, N. (2017). "Development of polysulfone-nanohybrid membranes using ZnO-GO composite for enhanced antifouling and antibacterial control." Desalination, 402, 123–132.

Cohen, B. (2006). "Urbanization in developing countries: Current trends, future projections, and key challenges for sustainability." Technology in society, 28(1–2), 63–80.

Crini, G., and Lichtfouse, E. (2019). "Advantages and disadvantages of techniques used for wastewater treatment." Environmental Chemistry Letters, 17(1), 145–155.

Criscuoli, A., and Figoli, A. (2019). "Pressure-driven and thermally-driven membrane operations for the treatment of arsenic-contaminated waters: A comparison." Journal of hazardous materials, 370, 147–155.

Dai, J., Li, S., Liu, J., He, J., Li, J., Wang, L., and Lei, J. (2019). "Fabrication and characterization of a defect-free mixed matrix membrane by facile mixing PPSU with ZIF-8 core–shell microspheres for solvent-resistant nanofiltration." Journal of Membrane Science, 589, 117261.

Dambies, L. (2005). "Existing and prospective sorption technologies for the removal of arsenic in water." Separation Science and Technology, 39(3), 603–627.

Darvishmanesh, S., Jansen, J. C., Tasselli, F., Tocci, E., Luis, P., Degrève, J., Drioli, E., and Van der Bruggen, B. (2011). "Novel polyphenylsulfone membrane for potential use in solvent nanofiltration." Journal of Membrane Science, 379(1–2), 60–68.

Dasgupta, J., Chakraborty, S., Sikder, J., Kumar, R., Pal, D., Curcio, S., and Drioli, E. (2014). "The effects of thermally stable titanium silicon oxide nanoparticles on structure and performance of cellulose acetate ultrafiltration membranes." Separation and Purification Technology, 133, 55–68.

DeFriend, K. A., Wiesner, M. R., and Barron, A. R. (2003). "Alumina and aluminate ultrafiltration membranes derived from alumina nanoparticles." Journal of membrane science, 224(1–2), 11–28.

Dehkordi, F. S., Pakizeh, M., and Namvar-Mahboub, M. (2015). "Properties and ultrafiltration efficiency of cellulose acetate/organically modified Mt (CA/OMMt) nanocomposite membrane for humic acid removal." Applied Clay Science, 105, 178–185.

Díez-Pascual, A. M., and Díez-Vicente, A. L. (2014). "Effect of TiO2 nanoparticles on the performance of polyphenylsulfone biomaterial for orthopaedic implants." Journal of Materials Chemistry B, 2(43), 7502–7514.

Dilshad, M. R., Islam, A., Hamidullah, U., Jamshaid, F., Ahmad, A., Butt, M. T. Z., and Ijaz, A. (2019). "Effect of alumina on the performance and characterization of cross-linked PVA/PEG 600 blended membranes for CO2/N2 separation." Separation and Purification Technology, 210, 627–635.

Dorra, G., Ines, K., Imen, B. S., Laurent, C., Sana, A., Olfa, T., Pascal, C., Thierry, J., and Ferid, L. (2018). "Purification and characterization of a novel high molecular weight alkaline protease produced by an endophytic Bacillus halotolerans strain CT2." International journal of biological macromolecules, 111, 342–351.

Dos Santos, V., Silveira, N. P. da, and Bergmann, C. P. (2014). "In-situ evaluation of particle size distribution of ZrO2-nanoparticles obtained by sol–gel." Powder technology, 267, 392–397.

Doyen, W., Leysen, R., Mottar, J., and Waes, G. (1991). "Zirconium oxide based composite tubular membranes for ultrafiltration." Effective Industrial Membrane Processes: Benefits and Opportunities, Springer, 199–216.

Durthi, C. P., Rajulapati, S. B., Palliparambi, A. A., Kola, A. K., and Sonawane, S. H. (2018). "Studies on removal of arsenic using cellulose acetate–zinc oxide nanoparticle mixed matrix membrane." International Nano Letters, 8(3), 201–211.

Ekambaram, K., & Doraisamy, M. (2017). "Surface modification of PVDF nanofiltration membrane using Carboxymethylchitosan-Zinc oxide bionanocomposite for the removal of inorganic salts and humic acid." Colloids and Surfaces A: Physicochemical and Engineering Aspects, 525, 49-63.

Eftekhari, M., Schwarzenberger, K., Javadi, A., and Eckert, K. (2020). "The influence of negatively charged silica nanoparticles on the surface properties of anionic surfactants: electrostatic repulsion or the effect of ionic strength?" Physical Chemistry Chemical Physics.

Escobar, I. C., Hoek, E. M., Gabelich, C. J., and DiGiano, F. A. (2005). "Committee report: recent advances and research needs in membrane fouling." American Water Works Association. Journal, 97(8), 79.

Estay, H., Troncoso, E., Ruby-Figueroa, R., & Romero, J. (2018). "Performance evaluation of mass transfer correlations in the GFMA process: A review with perspectives to the design." Journal of Membrane Science, *554*, 140-155.

Evans, R. D. (1955). "The Atomic Nucleus. McGraw-Hill." New York, 19552, 785–793.

Fakhri, A., and Behrouz, S. (2015). "Comparison studies of adsorption properties of MgO nanoparticles and ZnO–MgO nanocomposites for linezolid antibiotic removal from aqueous

solution using response surface methodology." Process Safety and Environmental Protection, 94, 37–43.

Fang, X., Li, J., Li, X., Pan, S., Zhang, X., Sun, X., Shen, J., Han, W., and Wang, L. (2017). "Internal pore decoration with polydopamine nanoparticle on polymeric ultrafiltration membrane for enhanced heavy metal removal." Chemical Engineering Journal, 314, 38–49.

Fantauzzi, M., Elsener, B., Atzei, D., Rigoldi, A., and Rossi, A. (2015). "Exploiting XPS for the identification of sulfides and polysulfides." RSC advances, 5(93), 75953–75963.

Farahani, M. H. D. A., Rabiee, H., and Vatanpour, V. (2019). "Comparing the effect of incorporation of various nanoparticulate on the performance and antifouling properties of polyethersulfone nanocomposite membranes." Journal of water process engineering, 27, 47–57.

Fausey, C. L., Zucker, I., Shaulsky, E., Zimmerman, J. B., and Elimelech, M. (2019). "Removal of arsenic with reduced graphene oxide-TiO2-enabled nanofibrous mats." Chemical Engineering Journal, 375, 122040.

Ferjani, E., Lajimi, R. H., Deratani, A., and Roudesli, M. S. (2002). "Bulk and surface modification of cellulose diacetate based RO/NF membranes by polymethylhydrosiloxane preparation and characterization." Desalination, 146(1–3), 325–330.

Fields, K. A., Chen, A. H., & Wang, L. (2000). "Arsenic removal from drinking water by coagulation/filtration and lime softening plants. Washington: National Risk Management Research Laboratory, Office of Research and Development" US Environmental Protection Agency.

Freger, V., Gilron, J., and Belfer, S. (2002). "TFC polyamide membranes modified by grafting of hydrophilic polymers: an FT-IR/AFM/TEM study." Journal of Membrane Science, 209(1), 283–292.

Garcia-Costa, A. L., Sarabia, A., Zazo, J. A., and Casas, J. A. (2021). "UV-assisted Catalytic Wet Peroxide Oxidation and adsorption as efficient process for arsenic removal in groundwater." Catalysis Today, 361, 176–182.

Garcia-Ivars, J., Alcaina-Miranda, M.-I., Iborra-Clar, M.-I., Mendoza-Roca, J.-A., and Pastor-Alcañiz, L. (2014). "Enhancement in hydrophilicity of different polymer phase-inversion

ultrafiltration membranes by introducing PEG/Al2O3 nanoparticles." Separation and Purification Technology, 128, 45–57.

Genne, I., Kuypers, S., and Leysen, R. (1996). "Effect of the addition of ZrO2 to polysulfone based UF membranes." Journal of Membrane Science, 113(2), 343–350.

Ghaemi, N., and Daraei, P. (2016). "Enhancement in copper ion removal by PPy@ Al2O3 polymeric nanocomposite membrane." Journal of industrial and engineering chemistry, 40, 26–33.

Ghaemi, N., Madaeni, S. S., Alizadeh, A., Daraei, P., Zinatizadeh, A. A., and Rahimpour, F. (2012). "Separation of nitrophenols using cellulose acetate nanofiltration membrane: Influence of surfactant additives." Separation and purification technology, 85, 147–156.

Gholami, A., Moghadassi, A. R., Hosseini, S. M., Shabani, S., and Gholami, F. (2014). "Preparation and characterization of polyvinyl chloride based nanocomposite nanofiltration-membrane modified by iron oxide nanoparticles for lead removal from water." Journal of Industrial and Engineering Chemistry, 20(4), 1517–1522.

Ghosh, S., Debsarkar, A., Dutta, A., Bhandary, S., and Chopra, D. (2021). "Delivering Arsenic-free Drinking Water-Made Practically Possible: Continuous Scale Electrochemical Arsenic Remediation Process Furnished, based on Experimental Studies and ANN Simulation." Environment, Development and Sustainability, 1–26.

Ghurye, G. L., Clifford, D. A., and Tripp, A. R. (1999). "Combined arsenic and nitrate removal by ion exchange." Journal-American Water Works Association, 91(10), 85–96.

Golpour, M., and Pakizeh, M. (2018). "Preparation and characterization of new PA-MOF/PPSU-GO membrane for the separation of KHI from water." Chemical Engineering Journal, 345, 221–232.

Graham, T. (1861). "X. liquid diffusion applied to analysis." Philosophical transactions of the Royal Society of London, (151), 183–224.

Greish, Y. E., Meetani, M. A., Al Matroushi, E. A., and Al Shamsi, B. (2010). "Effects of thermal and chemical treatments on the structural stability of cellulose acetate nanofibers." Carbohydrate Polymers, 82(3), 569–577.

Gronwald, O., Frost, I., Ulbricht, M., Shalmani, A. K., Panglisch, S., Grünig, L., Handge, U. A., Abetz, V., Heijnen, M., and Weber, M. (2020). "Hydrophilic poly (phenylene sulfone) membranes for ultrafiltration." Separation and Purification Technology, 250, 117107.

Guha, R., Xiong, B., Geitner, M., Moore, T., Wood, T. K., Velegol, D., and Kumar, M. (2017). "Reactive micromixing eliminates fouling and concentration polarization in reverse osmosis membranes." Journal of Membrane Science, 542, 8–17.

Guo, X., Fan, S., Hu, Y., Fu, X., Shao, H., and Zhou, Q. (2019). "A novel membrane biofouling mitigation strategy of D-amino acid supported by polydopamine and halloysite nanotube." Journal of Membrane Science, 579, 131–140.

Gupta, S. K., and Chen, K. Y. (1978). "Arsenic removal by adsorption." Journal (Water Pollution Control Federation), 493–506.

Gupta, V. K., Pathania, D., Singh, P., Rathore, B. S., and Chauhan, P. (2013). "Cellulose acetate–zirconium (IV) phosphate nano-composite with enhanced photo-catalytic activity." Carbohydrate polymers, 95(1), 434–440.

Gurunathan, P., Hari, S., Suseela, S. B., Sankararajan, R., and Mukannan, A. (2019). "Production, characterization and effectiveness of cellulose acetate functionalized ZnO nanocomposite adsorbent for the removal of Se (VI) ions from aqueous media." Environmental Science and Pollution Research, 26(1), 528–543.

Han, B., Zhang, D., Shao, Z., Kong, L., and Lv, S. (2013). "Preparation and characterization of cellulose acetate/carboxymethyl cellulose acetate blend ultrafiltration membranes." Desalination, 311, 80–89.

Han, S., Mao, L., Wu, T., and Wang, H. (2016). "Homogeneous polyethersulfone hybrid membranes prepared with in-suit synthesized magnesium hydroxide nanoparticles by phase inversion method." Journal of Membrane Science, 516, 47–55.

Hao, L., Liu, M., Wang, N., and Li, G. (2018a). "A critical review on arsenic removal from water using iron-based adsorbents." RSC advances, 8(69), 39545–39560.

Hao, L., Wang, N., Wang, C., and Li, G. (2018b). "Arsenic removal from water and river water by the combined adsorption-UF membrane process." Chemosphere, 202, 768–776.

Harper, T. R., and Kingham, N. W. (1992). "Removal of arsenic from wastewater using chemical precipitation methods." Water Environment Research, 64(3), 200–203.

He, J., Matsuura, T., and Chen, J. P. (2014). "A novel Zr-based nanoparticle-embedded PSF blend hollow fiber membrane for treatment of arsenate contaminated water: material development, adsorption and filtration studies, and characterization." Journal of membrane science, 452, 433–445.

He, M., Wang, L., Lv, Y., Wang, X., Zhu, J., Zhang, Y., and Liu, T. (2020). "Novel polydopamine/metal organic framework thin film nanocomposite forward osmosis membrane for salt rejection and heavy metal removal." Chemical Engineering Journal, 389, 124452.

He, Y., Liu, J., Han, G., and Chung, T.-S. (2018). "Novel thin-film composite nanofiltration membranes consisting of a zwitterionic co-polymer for selenium and arsenic removal." Journal of membrane science, 555, 299–306.

He, Y., Tang, Y. P., Ma, D., and Chung, T.-S. (2017). "UiO-66 incorporated thin-film nanocomposite membranes for efficient selenium and arsenic removal." Journal of Membrane Science, 541, 262–270.

Hebbar, R. S., Isloor, A. M., Ananda, K., Abdullah, M. S., and Ismail, A. F. (2017a). "Fabrication of a novel hollow fiber membrane decorated with functionalized Fe2O3 nanoparticles: towards sustainable water treatment and biofouling control." New Journal of Chemistry, 41(10), 4197–4211.

Hebbar, R. S., Isloor, A. M., Ananda, K., and Ismail, A. F. (2016). "Fabrication of polydopamine functionalized halloysite nanotube/polyetherimide membranes for heavy metal removal." Journal of materials chemistry A, 4(3), 764–774.

Hebbar, R. S., Isloor, A. M., and Ismail, A. F. (2014). "Preparation of antifouling polyetherimide/hydrolysed PIAM blend nanofiltration membranes for salt rejection applications." RSC Advances, 4(99), 55773–55780.

Hebbar, R. S., Isloor, A. M., Ismail, A. F., Shilton, S. J., Obaid, A., and Fun, H.-K. (2015). "Probing the morphology and anti-organic fouling behaviour of a polyetherimide membrane modified with hydrophilic organic acids as additives." New Journal of Chemistry, 39(8), 6141–6150.

Hebbar, R. S., Isloor, A. M., Prabhu, B., Asiri, A. M., and Ismail, A. F. (2018). "Removal of metal ions and humic acids through polyetherimide membrane with grafted bentonite clay." Scientific reports, 8(1), 4665 (16pp).

Hebbar, R. S., Isloor, A. M., Zulhairun, A. K., Abdullah, M. S., and Ismail, A. F. (2017b). "Efficient treatment of hazardous reactive dye effluents through antifouling polyetherimide hollow fiber membrane embedded with functionalized halloysite nanotubes." Journal of the Taiwan Institute of Chemical Engineers, 72, 244–252.

Hinrichsen, D., and Tacio, H. (2002). "The coming freshwater crisis is already here." The linkages between population and water. Washington, DC: Woodrow Wilson International Center for Scholars, 1–26.

Homaeigohar, S., & Elbahri, M. (2014). "Nanocomposite electrospun nanofiber membranes for environmental remediation". *Materials*, *7*(2), 1017-1045.

Hong, J., & He, Y. (2012). "Effects of nano sized zinc oxide on the performance of PVDF microfiltration membranes". Desalination, *302*, 71-79.

Hu, J., Chen, G., and Lo, I. M. (2005). "Removal and recovery of Cr (VI) from wastewater by maghemite nanoparticles." Water research, 39(18), 4528–4536.

Hu, X., Yu, Y., Zhou, J., Wang, Y., Liang, J., Zhang, X., Chang, Q., and Song, L. (2015). "The improved oil/water separation performance of graphene oxide modified Al2O3 microfiltration membrane." Journal of Membrane Science, 476, 200–204.

Hu, Y., Tsen, W.-C., Chuang, F.-S., Jang, S.-C., Zhang, B., Zheng, G., Wen, S., Liu, H., Qin, C., and Gong, C. (2019). "Glycine betaine intercalated layered double hydroxide modified quaternized chitosan/polyvinyl alcohol composite membranes for alkaline direct methanol fuel cells." Carbohydrate polymers, 213, 320–328.

Huang, X., Mutlu, H., and Theato, P. (2020). "A CO2-gated anodic aluminum oxide based nanocomposite membrane for de-emulsification." Nanoscale, 12(41), 21316–21324.

Huang, Y.-L., Tien, H.-W., Ma, C.-C. M., Yang, S.-Y., Wu, S.-Y., Liu, H.-Y., and Mai, Y.-W. (2011). "Effect of extended polymer chains on properties of transparent graphene nanosheets conductive film." Journal of Materials Chemistry, 21(45), 18236–18241.

Huisman, I. H., Prádanos, P., and Hernández, A. (2000). "The effect of protein–protein and protein–membrane interactions on membrane fouling in ultrafiltration." Journal of membrane science, 179(1–2), 79–90.

Hwang, L.-L., Tseng, H.-H., and Chen, J.-C. (2011). "Fabrication of polyphenylsulfone/polyetherimide blend membranes for ultrafiltration applications: The

effects of blending ratio on membrane properties and humic acid removal performance." Journal of membrane science, 384(1–2), 72–81.

Ibrahim, G. S., Isloor, A. M., Asiri, A. M., Ismail, A. F., Kumar, R., and Ahamed, M. I. (2018). "Performance intensification of the polysulfone ultrafiltration membrane by blending with copolymer encompassing novel derivative of poly (styrene-co-maleic anhydride) for heavy metal removal from wastewater." Chemical Engineering Journal, 353, 425–435.

Ibrahim, G. S., Isloor, A. M., Asiri, A. M., Ismail, N., Ismail, A. F., and Ashraf, G. M. (2017a). "Novel, one-step synthesis of zwitterionic polymer nanoparticles via distillation-precipitation polymerization and its application for dye removal membrane." Scientific reports, 7(1), 15889 (16pp).

Ibrahim, G. S., Isloor, A. M., Moslehyani, A., and Ismail, A. F. (2017b). "Bio-inspired, fouling resistant, tannic acid functionalized halloysite nanotube reinforced polysulfone loose nanofiltration hollow fiber membranes for efficient dye and salt separation." Journal of water process engineering, 20, 138–148.

Islam, M. A., Morton, D. W., Johnson, B. B., Pramanik, B. K., Mainali, B., and Angove, M. J. (2018). "Metal ion and contaminant sorption onto aluminium oxide-based materials: A review and future research." Journal of environmental chemical engineering, 6(6), 6853–6869.

Isloor, A. M., Nayak, M. C., Prabhu, B., Ismail, N., Ismail, A. F., and Asiri, A. M. (2019). "Novel polyphenylsulfone (PPSU)/nano tin oxide (SnO2) mixed matrix ultrafiltration hollow fiber membranes: Fabrication, characterization and toxic dyes removal from aqueous solutions." Reactive and Functional Polymers, 139, 170–180.

Ismail, M., Khan, M. I., Khan, S. B., Akhtar, K., Khan, M. A., and Asiri, A. M. (2018). "Catalytic reduction of picric acid, nitrophenols and organic azo dyes via green synthesized plant supported Ag nanoparticles." Journal of Molecular Liquids, 268, 87–101.

Jarma, Y. A., Karaoğlu, A., Tekin, Ö., Baba, A., Ökten, H. E., Tomaszewska, B., Bostancı, K., Arda, M., and Kabay, N. (2021). "Assessment of different nanofiltration and reverse osmosis membranes for simultaneous removal of arsenic and boron from spent geothermal water." Journal of Hazardous Materials, 405, 124129.

Jiang, J.-H., Zhu, L.-P., Li, X.-L., Xu, Y.-Y., and Zhu, B.-K. (2010). "Surface modification of PE porous membranes based on the strong adhesion of polydopamine and covalent immobilization of heparin." Journal of Membrane Science, 364(1–2), 194–202.

Jiang, J.-H., Zhu, L.-P., Zhang, H.-T., Zhu, B.-K., and Xu, Y.-Y. (2014). "Improved hydrodynamic permeability and antifouling properties of poly (vinylidene fluoride) membranes using polydopamine nanoparticles as additives." Journal of membrane science, 457, 73–81.

Jin, Y., Zeng, C., Lü, Q.-F., and Yu, Y. (2019). "Efficient adsorption of methylene blue and lead ions in aqueous solutions by 5-sulfosalicylic acid modified lignin." International journal of biological macromolecules, 123, 50–58.

Jung, B. K., Jun, J. W., Hasan, Z., and Jhung, S. H. (2015). "Adsorptive removal of p-arsanilic acid from water using mesoporous zeolitic imidazolate framework-8." Chemical Engineering Journal, 267, 9–15.

Kajekar, A. J., Dodamani, B. M., Isloor, A. M., Karim, Z. A., Cheer, N. B., Ismail, A. F., and Shilton, S. J. (2015). "Preparation and characterization of novel PSf/PVP/PANI-nanofiber nanocomposite hollow fiber ultrafiltration membranes and their possible applications for hazardous dye rejection." Desalination, 365, 117–125.

Kallem, P., Ibrahim, Y., Hasan, S. W., Show, P. L., and Banat, F. (2021). "Fabrication of novel polyethersulfone (PES) hybrid ultrafiltration membranes with superior permeability and antifouling properties using environmentally friendly sulfonated functionalized polydopamine nanofillers." Separation and Purification Technology, 261, 118311.

Kanagaraj, P., Nagendran, A., Rana, D., and Matsuura, T. (2016). "Separation of macromolecular proteins and removal of humic acid by cellulose acetate modified UF membranes." International journal of biological macromolecules, 89, 81–88.

Karim, Z., Mathew, A. P., Grahn, M., Mouzon, J., and Oksman, K. (2014). "Nanoporous membranes with cellulose nanocrystals as functional entity in chitosan: removal of dyes from water." Carbohydrate polymers, 112, 668–676.

Karimipour, H., Shahbazi, A., & Vatanpour, V. (2021). "Fouling decline and retention increase of polyethersulfone membrane by incorporating melamine-based dendrimer amine functionalized graphene oxide nanosheets (GO/MDA)". Journal of Environmental Chemical Engineering, 9(1), 104849.

Karmakar, S., Bhattacharjee, S., and De, S. (2017). "Experimental and modeling of fluoride removal using aluminum fumarate (AlFu) metal organic framework incorporated cellulose

acetate phthalate mixed matrix membrane." Journal of environmental chemical engineering, 5(6), 6087–6097.

Kasi, G., and Seo, J. (2019). "Influence of Mg doping on the structural, morphological, optical, thermal, and visible-light responsive antibacterial properties of ZnO nanoparticles synthesized via co-precipitation." Materials Science and Engineering: C, 98, 717–725.

Katsoyiannis, I. A., and Zouboulis, A. I. (2006). "Comparative evaluation of conventional and alternative methods for the removal of arsenic from contaminated groundwaters." Reviews on environmental health, 21(1), 25.

Khandaker, N. R., Brady, P. V., Teter, D. M., and Krumhansl, J. L. (2004). "Arsenic removal in conjunction with lime softening" Google Patents. US Patent 6802980B1.

Kiani, S., Mousavi, S. M., Shahtahmassebi, N., and Saljoughi, E. (2015). "Hydrophilicity improvement in polyphenylsulfone nanofibrous filtration membranes through addition of polyethylene glycol." Applied Surface Science, 359, 252–258.

Kolangare, I. M., Isloor, A. M., Karim, Z. A., Kulal, A., Ismail, A. F., and Asiri, A. M. (2019). "Antibiofouling hollow-fiber membranes for dye rejection by embedding chitosan and silver-loaded chitosan nanoparticles." Environmental Chemistry Letters, 17(1), 581–587.

Kolbasov, A., Sinha-Ray, S., Yarin, A. L., and Pourdeyhimi, B. (2017). "Heavy metal adsorption on solution-blown biopolymer nanofiber membranes." Journal of Membrane Science, 530, 250–263.

Kotsilkova, R., Borovanska, I., Todorov, P., Ivanov, E., Menseidov, D., Chakraborty, S., and Bhattacharjee, C. (2018). "Tensile and surface mechanical properties of polyethersulphone (pes) and polyvinylidene fluoride (PVDF) membranes." Journal of Theoretical and Applied Mechanics, 48(3), 85–99.

Krause, B., Meyer, T., Sieg, H., Kästner, C., Reichardt, P., Tentschert, J., Jungnickel, H., Estrela-Lopis, I., Burel, A., and Chevance, S. (2018). "Characterization of aluminum, aluminum oxide and titanium dioxide nanomaterials using a combination of methods for particle surface and size analysis." RSC advances, 8(26), 14377–14388.

Kumar, E., Bhatnagar, A., Kumar, U., and Sillanpää, M. (2011). "Defluoridation from aqueous solutions by nano-alumina: characterization and sorption studies." Journal of Hazardous Materials, 186(2–3), 1042–1049.

Kumar, M., Isloor, A. M., Rao, T. S., Ismail, A. F., Farnood, R., and Nambissan, P. M. G. (2020a). "Removal of toxic arsenic from aqueous media using polyphenylsulfone/cellulose acetate hollow fiber membranes containing zirconium oxide." Chemical Engineering Journal, 393, 124367.

Kumar, M., Isloor, A. M., Somasekhara, R. T., Hosakoppa, N., Ismail, A. F., and Susanti, R. (2021). "Effect of binary zinc-magnesium oxides on polyphenylsulfone/cellulose acetate derivatives hollow fiber membranes for the decontamination of arsenic from drinking water." Chemical Engineering Journal, 405, 126809.

Kumar, M., Isloor, A. M., Todeti, S. R., Ibrahim, G. S., Ismail, A. F., and Asiri, A. M. (2020b). "Improved separation of dyes and proteins using membranes made of polyphenylsulfone/cellulose acetate or acetate phthalate." Environmental Chemistry Letters, 18, 1–7.

Kumar, M., RaoT, S., Isloor, A. M., Ibrahim, G. S., Ismail, N., Ismail, A. F., and Asiri, A. M. (2019). "Use of cellulose acetate/polyphenylsulfone derivatives to fabricate ultrafiltration hollow fiber membranes for the removal of arsenic from drinking water." International journal of biological macromolecules, 129, 715–727.

Kumar, R., Isloor, A. M., and Ismail, A. F. (2014). "Preparation and evaluation of heavy metal rejection properties of polysulfone/chitosan, polysulfone/N-succinyl chitosan and polysulfone/N-propylphosphonyl chitosan blend ultrafiltration membranes." Desalination, 350, 102–108.

Kumar, R., Isloor, A. M., Ismail, A. F., Rashid, S. A., and Matsuura, T. (2013). "Polysulfone–Chitosan blend ultrafiltration membranes: preparation, characterization, permeation and antifouling properties." Rsc Advances, 3(21), 7855–7861.

Li, B., Gu, B., Yang, Z., and Zhang, T. (2018). "The role of submerged macrophytes in phytoremediation of arsenic from contaminated water: A case study on Vallisneria natans (Lour.) Hara." Ecotoxicology and environmental safety, 165, 224–231.

Li, C., Lou, T., Yan, X., Long, Y., Cui, G., and Wang, X. (2018). "Fabrication of pure chitosan nanofibrous membranes as effective absorbent for dye removal." International journal of biological macromolecules, 106, 768–774.

Li, H.-J., Cao, Y.-M., Qin, J.-J., Jie, X.-M., Wang, T.-H., Liu, J.-H., and Yuan, Q. (2006). "Development and characterization of anti-fouling cellulose hollow fiber UF membranes for oil–water separation." Journal of Membrane science, 279(1–2), 328–335.

Li, R., Wu, Y., Shen, L., Chen, J., and Lin, H. (2018). "A novel strategy to develop antifouling and antibacterial conductive Cu/polydopamine/polyvinylidene fluoride membranes for water treatment." Journal of colloid and interface science, 531, 493–501.

Li, X., Liu, Y., Zhang, C., Wen, T., Zhuang, L., Wang, X., Song, G., Chen, D., Ai, Y., and Hayat, T. (2018). "Porous Fe2O3 microcubes derived from metal organic frameworks for efficient elimination of organic pollutants and heavy metal ions." Chemical Engineering Journal, 336, 241–252.

Li, X., Zhu, L., Jiang, J., Yi, Z., Zhu, B., and Xu, Y. (2012). "Hydrophilic nanofiltration membranes with self-polymerized and strongly-adhered polydopamine as separating layer." Chinese Journal of Polymer Science, 30(2), 152–163.

Li, Y., Zhang, D., Li, W., Lan, Y., and Li, Y. (2020a). "Efficient removal of As (III) from aqueous solution by S-doped copper-lanthanum bimetallic oxides: Simultaneous oxidation and adsorption." Chemical Engineering Journal, 384, 123274.

Li, Y., Zhu, X., Qi, X., Shu, B., Zhang, X., Li, K., Wei, Y., and Wang, H. (2020b). "Removal and Immobilization of Arsenic from Copper Smelting Wastewater using Copper Slag by in Situ Encapsulation with Silica Gel." Chemical Engineering Journal, 394, 124833.

Liao, Y., Loh, C. H., Tian, M., Wang, R., & Fane, A. G. (2018). "Progress in electrospun polymeric nanofibrous membranes for water treatment: Fabrication, modification and applications." Progress in Polymer Science, 77, 69-94.

Liu, J., Zhong, Z., Ma, R., Zhang, W., and Li, J. (2016). "Development of High-Antifouling PPSU Ultrafiltration Membrane by Using Compound Additives: Preparation, Morphologies, and Filtration Resistant Properties." Membranes, 6(2), 35.

Liu, L., Tan, W., Suib, S. L., Qiu, G., Zheng, L., and Su, S. (2019). "Enhanced adsorption removal of arsenic from mining wastewater using birnessite under electrochemical redox reactions." Chemical Engineering Journal, 375, 122051.

Liu, Y., Huang, H., Huo, P., and Gu, J. (2017). "Exploration of zwitterionic cellulose acetate antifouling ultrafiltration membrane for bovine serum albumin (BSA) separation." Carbohydrate polymers, 165, 266–275.

Liu, Y., Zhang, S., Zhou, Z., Ren, J., Geng, Z., Luan, J., and Wang, G. (2012). "Novel sulfonated thin-film composite nanofiltration membranes with improved water flux for treatment of dye solutions." Journal of membrane science, 394, 218–229.

Lohokare, H. R., Muthu, M. R., Agarwal, G. P., and Kharul, U. K. (2008). "Effective arsenic removal using polyacrylonitrile-based ultrafiltration (UF) membrane." Journal of Membrane Science, 320(1–2), 159–166.

Lops, C., Ancona, A., Di Cesare, K., Dumontel, B., Garino, N., Canavese, G., Hérnandez, S., and Cauda, V. (2019). "Sonophotocatalytic degradation mechanisms of Rhodamine B dye via radicals generation by micro-and nano-particles of ZnO." Applied Catalysis B: Environmental, 243, 629–640.

Lou, T., Wang, X., Song, G., and Cui, G. (2017). "Synthesis and flocculation performance of a chitosan-acrylamide-fulvic acid ternary copolymer." Carbohydrate polymers, 170, 182–189.

Luo, X., Wang, C., Wang, L., Deng, F., Luo, S., Tu, X., and Au, C. (2013). "Nanocomposites of graphene oxide-hydrated zirconium oxide for simultaneous removal of As (III) and As (V) from water." Chemical engineering journal, 220, 98–106.

Luo, J., Cao, W., Ding, L., Zhu, Z., Wan, Y., & Jaffrin, M. Y. (2012). "Treatment of dairy effluent by shear-enhanced membrane filtration: The role of foulants." Separation and Purification Technology, 96, 194-203.

Lv, J., Zhang, G., Zhang, H., and Yang, F. (2017). "Exploration of permeability and antifouling performance on modified cellulose acetate ultrafiltration membrane with cellulose nanocrystals." Carbohydrate polymers, 174, 190–199.

Lv, J., Zhang, G., Zhang, H., Zhao, C., and Yang, F. (2018). "Improvement of antifouling performances for modified PVDF ultrafiltration membrane with hydrophilic cellulose nanocrystal." Applied Surface Science, 440, 1091–1100.

Ma, B., Xue, W., Hu, C., Liu, H., Qu, J., and Li, L. (2019). "Characteristics of microplastic removal via coagulation and ultrafiltration during drinking water treatment." Chemical Engineering Journal, 359, 159–167.

Ma, J., He, Y., Zeng, G., Li, F., Li, Y., Xiao, J., and Yang, S. (2018). "Bio-inspired method to fabricate poly-dopamine/reduced graphene oxide composite membranes for dyes and heavy metal ion removal." Polymers for Advanced Technologies, 29(2), 941–950.

Ma, Y., Shi, F., Wang, Z., Wu, M., Ma, J., and Gao, C. (2012). "Preparation and characterization of PSf/clay nanocomposite membranes with PEG 400 as a pore forming additive." Desalination, 286, 131–137.

Mahendran, R., Malaisamy, R., Arthanareeswaran, G., and Mohan, D. (2004). "Cellulose acetate–poly (ether sulfone) blend ultrafiltration membranes. II. Application studies." Journal of applied polymer science, 92(6), 3659–3665.

Mahlangu, O. T., Nackaerts, R., Thwala, J. M., Mamba, B. B., and Verliefde, A. R. D. (2017). "Hydrophilic fouling-resistant GO-ZnO/PES membranes for wastewater reclamation." Journal of membrane science, 524, 43–55.

Manjunath, L., and Sailaja, R. R. N. (2014). "PMMA–cellulose acetate phthalate nanocomposites reinforced with silane-treated nanoclay." Cellulose, 21(3), 1793–1802.

Mansur, S., Othman, M. H. D., Ismail, A. F., Abidin, M. N. Z., Said, N., Goh, P. S., Hasbullah, H., Kadir, S., and Kamal, F. (2018). "Study on the effect of PVP additive on the performance of PSf/PVP ultrafiltration hollow fiber membrane." Mal. J. Fund. Appl. Sci, 14, 343–347.

Marcus, Y. (2014). "The molar volumes of ions in solution, Part 7. Electrostriction and hydration numbers of aqueous polyatomic anions at 25° C." The Journal of Physical Chemistry B, 118(8), 2172-2175.

Mulder, M., & Mulder, J. (1996). "Basic principles of membrane technology." Springer science & business media.

Mashkoor, F., Nasar, A., and Asiri, A. M. (2018). "Exploring the reusability of synthetically contaminated wastewater containing crystal violet dye using Tectona grandis sawdust as a very low-cost adsorbent." Scientific reports, 8(1), 8314 (16pp).

Maximous, N., Nakhla, G., Wan, W., and Wong, K. (2009). "Preparation, characterization and performance of Al2O3/PES membrane for wastewater filtration." Journal of Membrane Science, 341(1–2), 67–75.

Maximous, N., Nakhla, G., Wan, W., and Wong, K. (2010). "Performance of a novel ZrO2/PES membrane for wastewater filtration." Journal of Membrane Science, 352(1–2), 222–230.

Mazumder, M. A. J., Raja, P. H., Isloor, A. M., Usman, M., Chowdhury, S. H., Ali, S. A., and Al-Ahmed, A. (2020). "Assessment of sulfonated homo and co-polyimides incorporated polysulfone ultrafiltration blend membranes for effective removal of heavy metals and proteins." Scientific Reports, 10(1), 7049 (13pp).

Meharg, A. A., and Meharg, C. (2021). "The Pedosphere as a Sink, Source, and Record of Anthropogenic and Natural Arsenic Atmospheric Deposition." Environmental Science & Technology 55(12), 7757-7769.

Mohammadi, T., and Saljoughi, E. (2009). "Effect of production conditions on morphology and permeability of asymmetric cellulose acetate membranes." Desalination, 243(1–3), 1–7.

Moideen K, I., Isloor, A. M., Ismail, A. F., Obaid, A., and Fun, H.-K. (2016). "Fabrication and characterization of new PSF/PPSU UF blend membrane for heavy metal rejection." Desalination and Water Treatment, 57(42), 19810–19819.

Mondal, M., and De, S. (2015). "Characterization and antifouling properties of polyethylene glycol doped PAN–CAP blend membrane." RSC Advances, 5(49), 38948–38963.

Mondal, M., Bhattacharjee, S., & De, S. (2020). "Prediction of long term filtration by coupled gel layer and pore transport model for salt removal using mixed matrix hollow fiber ultrafiltration membrane." Separation and Purification Technology, 250, 117213.

Mondal, P., Majumder, C. B., and Mohanty, B. (2006). "Laboratory based approaches for arsenic remediation from contaminated water: recent developments." Journal of Hazardous materials, 137(1), 464–479.

Moradihamedani, P., and Abdullah, A. H. (2017). "High-performance cellulose acetate/polysulfone blend ultrafiltration membranes for removal of heavy metals from water." Water Science and Technology, 75(10), 2422–2433.

Moraes, A. C. M. de, Andrade, P. F., Faria, A. F. de, Simões, M. B., Salomão, F. C. C. S., Barros, E. B., Carmo Gonçalves, M. do, and Alves, O. L. (2015). "Fabrication of transparent and ultraviolet shielding composite films based on graphene oxide and cellulose acetate." Carbohydrate polymers, 123, 217–227.

Mu, K., Zhang, D., Shao, Z., Qin, D., Wang, Y., and Wang, S. (2017). "Enhanced permeability and antifouling performance of cellulose acetate ultrafiltration membrane assisted by L-DOPA functionalized halloysite nanotubes." Carbohydrate Polymers, 174, 688–696.

Muhamad, M. S., Salim, M. R., and Lau, W.-J. (2015). "Surface modification of SiO2 nanoparticles and its impact on the properties of PES-based hollow fiber membrane." RSC advances, 5(72), 58644–58654.

Mukherjee, R., and De, S. (2014). "Adsorptive removal of phenolic compounds using cellulose acetate phthalate–alumina nanoparticle mixed matrix membrane." Journal of hazardous materials, 265, 8–19.

Muleja, A. A., and Mamba, B. B. (2018). "Development of calcined catalytic membrane for potential photodegradation of Congo red in aqueous solution." Journal of environmental chemical engineering, 6(4), 4850–4863.

Mulyati, S., Muchtar, S., Arahman, N., Meirisa, F., Syamsuddin, Y., Zuhra, Z., Rosnelly, C. M., Shamsuddin, N., Mat Nawi, N. I., and Wirzal, M. D. H. (2020a). "One-Pot Polymerization of Dopamine as an Additive to Enhance Permeability and Antifouling Properties of Polyethersulfone Membrane." Polymers, 12(8), 1807.

Mulyati, S., Muchtar, S., Arahman, N., Syamsuddin, Y., Mat Nawi, N. I., Yub Harun, N., Bilad, M. R., Firdaus, Y., Takagi, R., and Matsuyama, H. (2020b). "Two-step dopamine-to-polydopamine modification of polyethersulfone ultrafiltration membrane for enhancing anti-fouling and ultraviolet resistant properties." Polymers, 12(9), 2051.

Nayak, M. C., Isloor, A. M., Lakshmi, B., Marwani, H. M., and Khan, I. (2020). "Polyphenylsulfone/multiwalled carbon nanotubes mixed ultrafiltration membranes: Fabrication, characterization and removal of heavy metals Pb2+, Hg2+, and Cd2+ from aqueous solutions." Arabian Journal of Chemistry, 13(3), 4661–4672.

Nayak, M. C., Isloor, A. M., Moslehyani, A., and Ismail, A. F. (2017). "Preparation and characterization of PPSU membranes with BiOCl nanowafers loaded on activated charcoal for oil in water separation." Journal of the Taiwan Institute of Chemical Engineers, 77, 293–301.

Nayak, M. C., Isloor, A. M., Moslehyani, A., Ismail, N., and Ismail, A. F. (2018). "Fabrication of novel PPSU/ZSM-5 ultrafiltration hollow fiber membranes for separation of

proteins and hazardous reactive dyes." Journal of the Taiwan Institute of Chemical Engineers, 82, 342–350.

Nevárez, L. M., Casarrubias, L. B., Canto, O. S., Celzard, A., Fierro, V., Gómez, R. I., and Sánchez, G. G. (2011). "Biopolymers-based nanocomposites: Membranes from propionated lignin and cellulose for water purification." Carbohydrate polymers, 86(2), 732–741.

Ng, K.-S., Ujang, Z., and Le-Clech, P. (2004). "Arsenic removal technologies for drinking water treatment." Reviews in Environmental Science and Biotechnology, 3(1), 43–53.

Noor, N., Koll, J., Scharnagl, N., Abetz, C., and Abetz, V. (2018). "Hollow fiber membranes of blends of polyethersulfone and sulfonated polymers." Membranes, 8(3), 54.

Noori, A. J., and Kareem, F. A. (2019). "The effect of magnesium oxide nanoparticles on the antibacterial and antibiofilm properties of glass-ionomer cement." Heliyon, 5(10), e02568.

Obaid, M., Ghaffour, N., Wang, S., Yoon, M.-H., and Kim, I. S. (2020). "Zirconia nanofibers incorporated polysulfone nanocomposite membrane: Towards overcoming the permeance-selectivity trade-off." Separation and Purification Technology, 236, 116236.

Ociński, D., Jacukowicz-Sobala, I., Mazur, P., Raczyk, J., and Kocio\lek-Balawejder, E. (2016). "Water treatment residuals containing iron and manganese oxides for arsenic removal from water–Characterization of physicochemical properties and adsorption studies." Chemical Engineering Journal, 294, 210–221.

Ortega-Requena, S., and Rebouillat, S. (2015). "Retracted Article: Bigger data open innovation: potential applications of value-added products from milk and sustainable valorization of by-products from the dairy industry." Green Chemistry, 17(12), 5100–5113.

Othman, M. H. D., Adam, M. R., Kamaludin, R., Ismail, N. J., Rahman, M. A., and Jaafar, J. (2021). "Advanced Membrane Technology for Textile Wastewater Treatment." Membrane Technology Enhancement for Environmental Protection and Sustainable Industrial Growth, Springer, 91–108.

Pakrashi, S., Dalai, S., Sneha, B., Chandrasekaran, N., and Mukherjee, A. (2012). "A temporal study on fate of Al2O3 nanoparticles in a fresh water microcosm at environmentally relevant low concentrations." Ecotoxicology and environmental safety, 84, 70–77.

Pallier, V., Feuillade-Cathalifaud, G., Serpaud, B., and Bollinger, J.-C. (2010). "Effect of organic matter on arsenic removal during coagulation/flocculation treatment." Journal of Colloid and Interface Science, 342(1), 26–32.

Pandas, H. M., and Fazli, M. (2018). "Fabrication of MgO and ZnO nanoparticles by the aid of eggshell bioactive membrane and exploring their catalytic activities on thermal decomposition of ammonium perchlorate." Journal of Thermal Analysis and Calorimetry, 131(3), 2913–2924.

Parani, S., & Oluwafemi, O. S. (2021). "Membrane Distillation: Recent Configurations, Membrane Surface Engineering, and Applications." Membranes, 11(12), 934.

Parcero, E., Herrera, R., and Nunes, S. P. (2006). "Phosphonated and sulfonated polyhphenylsulfone membranes for fuel cell application." Journal of membrane science, 285(1–2), 206–213.

Pereira, V. R., Isloor, A. M., Bhat, U. K., and Ismail, A. F. (2014). "Preparation and antifouling properties of PVDF ultrafiltration membranes with polyaniline (PANI) nanofibers and hydrolysed PSMA (H-PSMA) as additives." Desalination, 351, 220–227.

Peretyazhko, T. S., Zhang, Q., and Colvin, V. L. (2014). "Size-controlled dissolution of silver nanoparticles at neutral and acidic pH conditions: kinetics and size changes." Environmental science & technology, 48(20), 11954–11961.

Pérez-Sicairos, S., Lin, S. W., Félix-Navarro, R. M., and Espinoza-Gómez, H. (2009). "Rejection of As (III) and As (V) from arsenic contaminated water via electro-cross-flow negatively charged nanofiltration membrane system." Desalination, 249(2), 458–465.

Pessoa-Lopes, M., Crespo, J. G., and Velizarov, S. (2016). "Arsenate removal from sulphate-containing water streams by an ion-exchange membrane process." Separation and Purification Technology, 166, 125–134.

Prihatiningtyas, I., Gebreslase, G. A., and Van der Bruggen, B. (2020). "Incorporation of Al2O3 into cellulose triacetate membranes to enhance the performance of pervaporation for desalination of hypersaline solutions." Desalination, 474, 114198.

Puspasari, T., Huang, T., Sutisna, B., and Peinemann, K.-V. (2018). "Cellulose-polyethyleneimine blend membranes with anomalous nanofiltration performance." Journal of Membrane Science, 564, 97–105.

Qin, J.-J., Oo, M. H., Cao, Y.-M., and Lee, L.-S. (2005). "Development of a LCST membrane forming system for cellulose acetate ultrafiltration hollow fiber." Separation and purification technology, 42(3), 291–295.

Qiu, Z., Shi, S., Qiu, F., Xu, X., Yang, D., and Zhang, T. (2020). "Enhanced As (Ⅲ) removal from aqueous solutions by recyclable Cu@ MNM composite membranes via synergistic oxidation and absorption." Water research, 168, 115147.

Quilaqueo, M., Seriche, G., Valetto, S., Barros, L., Díaz-Quezada, S., Ruby-Figueroa, R., ... & Estay, H. (2020). An experimental study of membrane contactor modules for recovering cyanide through a gas membrane process. *Membranes*, *10*(5), 105.

Rabiee, H., Vatanpour, V., Farahani, M. H. D. A., and Zarrabi, H. (2015). "Improvement in flux and antifouling properties of PVC ultrafiltration membranes by incorporation of zinc oxide (ZnO) nanoparticles." Separation and purification technology, 156, 299–310.

Rahimpour, A., and Madaeni, S. S. (2007). "Polyethersulfone (PES)/cellulose acetate phthalate (CAP) blend ultrafiltration membranes: preparation, morphology, performance and antifouling properties." Journal of Membrane Science, 305(1–2), 299–312.

Rahman, A., Persson, L.-\AAke, Nermell, B., Arifeen, S. E., Ekström, E.-C., Smith, A. H., and Vahter, M. (2010). "Arsenic exposure and risk of spontaneous abortion, stillbirth, and infant mortality." Epidemiology, 21(6), 797–804.

Rajesh, S., Shobana, K. H., Anitharaj, S., and Mohan, D. R. (2011). "Preparation, morphology, performance, and hydrophilicity studies of poly (amide-imide) incorporated cellulose acetate ultrafiltration membranes." Industrial & Engineering Chemistry Research, 50(9), 5550–5564.

Raliya, R., and Tarafdar, J. C. (2014). "Biosynthesis and characterization of zinc, magnesium and titanium nanoparticles: an eco-friendly approach." International Nano Letters, 4(1), 93.

Ramos, M. L. P., González, J. A., Albornoz, S. G., Pérez, C. J., Villanueva, M. E., Giorgieri, S. A., and Copello, G. J. (2016). "Chitin hydrogel reinforced with TiO2 nanoparticles as an arsenic sorbent." Chemical Engineering Journal, 285, 581–587.

Rao, L. S., Rao, T. V., Naheed, S., and Rao, P. V. (2018). "Structural and optical properties of zinc magnesium oxide nanoparticles synthesized by chemical co-precipitation." Materials Chemistry and Physics, 203, 133–140.

Rao, Z., Feng, K., Tang, B., and Wu, P. (2017). "Surface decoration of amino-functionalized metal–organic framework/graphene oxide composite onto polydopamine-coated membrane substrate for highly efficient heavy metal removal." ACS applied materials & interfaces, 9(3), 2594–2605.

Rasul, S. B., Munir, A. K. M., Hossain, Z. A., Khan, A. H., Alauddin, M., and Hussam, A. (2002). "Electrochemical measurement and speciation of inorganic arsenic in groundwater of Bangladesh." Talanta, 58(1), 33–43.

Ravenscroft, P., Brammer, H., and Richards, K. (2011). Arsenic pollution: a global synthesis. John Wiley & Sons.

Ravikumar, R., Ganesh, M., Ubaidulla, U., Choi, E. Y., and Jang, H. T. (2017). "Preparation, characterization, and in vitro diffusion study of nonwoven electrospun nanofiber of curcumin-loaded cellulose acetate phthalate polymer." Saudi pharmaceutical journal, 25(6), 921–926.

Ray, P. G., Biswas, S., Roy, T., Ghosh, S., Majumder, D., Basak, P., Roy, S., and Dhara, S. (2019). "Sonication Assisted Hierarchical Decoration of Ag-NP on Zinc Oxide Nanoflower Impregnated Eggshell Membrane: Evaluation of Antibacterial Activity and in Vitro Cytocompatibility." ACS Sustainable Chemistry & Engineering, 7(16), 13717–13733.

Razzaghi, M. H., Safekordi, A., Tavakolmoghadam, M., Rekabdar, F., and Hemmati, M. (2014). "Morphological and separation performance study of PVDF/CA blend membranes." Journal of membrane science, 470, 547–557.

Rajabi, H., Ghaemi, N., Madaeni, S. S., Daraei, P., Astinchap, B., Zinadini, S., & Razavizadeh, S. H. (2015). Nano-ZnO embedded mixed matrix polyethersulfone (PES) membrane: Influence of nanofiller shape on characterization and fouling resistance. *Applied Surface Science*, *349*, 66-77.

Ren, Z., Zhang, G., and Chen, J. P. (2011). "Adsorptive removal of arsenic from water by an iron–zirconium binary oxide adsorbent." Journal of colloid and interface science, 358(1), 230–237.

Riaz, T., Ahmad, A., Saleemi, S., Adrees, M., Jamshed, F., Hai, A. M., and Jamil, T. (2016). "Synthesis and characterization of polyurethane-cellulose acetate blend membrane for chromium (VI) removal." Carbohydrate polymers, 153, 582–591.

Rodrigues-Filho, U. P., Gushikem, Y., Gonçalves, M. do C., Cachichi, R. C., and Castro, S. C. de. (1996). "Composite membranes of cellulose acetate and zirconium dioxide: preparation and study of physicochemical characteristics." Chemistry of materials, 8(7), 1375–1379.

Ronco, C., Ghezzi, P. M., and Bowry, S. K. (2004). "Membranes for hemodialysis." Replacement of Renal Function by Dialysis, Springer, 301–323.

Ruiz-García, A., Melián-Martel, N., & Nuez, I. (2017). "Short review on predicting fouling in RO desalination." Membranes, 7(4), 62.

Sadeghfam, S., Abdi, M., Khatibi, R., and Nadiri, A. A. (2021). "An investigation into uncertainties within Human Health Risk Assessment to gain an insight into plans to mitigate impacts of arsenic contamination." Journal of Cleaner Production, 311, 127667.

Saha, J. C., Dikshit, A. K., Bandyopadhyay, M., and Saha, K. C. (1999). "A review of arsenic poisoning and its effects on human health." Critical reviews in environmental science and technology, 29(3), 281–313.

Saha, N., and Rahman, M. S. (2020). "Groundwater hydrogeochemistry and probabilistic health risk assessment through exposure to arsenic-contaminated groundwater of Meghna floodplain, central-east Bangladesh." Ecotoxicology and Environmental Safety, 206, 111349.

Sajitha, C. J., and Mohan, D. (2005). "Studies on cellulose acetate-carboxylated polysulfone blend ultrafiltration membranes. III." Journal of applied polymer science, 97(3), 976–988.

Salama, A., Alyan, A., El Amin, M., Sun, S., Zhang, T., and Zoubeik, M. (2021). "The Effect of the Oleophobicity Deterioration of a Membrane Surface on Its Rejection Capacity: A Computational Fluid Dynamics Study." Membranes, 11(4), 253.

Sánchez, J., and Rivas, B. L. (2010). "Arsenic extraction from aqueous solution: electrochemical oxidation combined with ultrafiltration membranes and water-soluble polymers." Chemical Engineering Journal, 165(2), 625–632.

Sani, N. A. A., Lau, W. J., and Ismail, A. F. (2014). "Influence of polymer concentration in casting solution and solvent-solute-membrane interactions on performance of polyphenylsulfone (PPSU) nanofiltration membrane in alcohol solvents." Journal of Polymer Engineering, 34(6), 489–500.

Serbanescu, O. S., Pandele, A. M., Miculescu, F., and Voicu, S. I. (2020). "Synthesis and characterization of cellulose acetate membranes with self-indicating properties by changing the membrane surface color for separation of Gd (III)." Coatings, 10(5), 468.

Shan, C., Dong, H., Huang, P., Hua, M., Liu, Y., Gao, G., Zhang, W., Lv, L., and Pan, B. (2019). "Dual-functional millisphere of anion-exchanger-supported nanoceria for synergistic As (III) removal with stoichiometric H_2O_2: Catalytic oxidation and sorption." Chemical Engineering Journal, 360, 982–989.

Shao, K., Zhou, Z., Xun, P., and Cohen, S. M. (2021). "Bayesian benchmark dose analysis for inorganic arsenic in drinking water associated with bladder and lung cancer using epidemiological data." Toxicology, 455, 152752.

Shao, L., Wang, Z. X., Zhang, Y. L., Jiang, Z. X., and Liu, Y. Y. (2014). "A facile strategy to enhance PVDF ultrafiltration membrane performance via self-polymerized polydopamine followed by hydrolysis of ammonium fluotitanate." Journal of Membrane Science, 461, 10–21.

Sharma, G., Kumar, A., Naushad, M., Pathania, D., and Sillanpää, M. (2016). "Polyacrylamide@ Zr (IV) vanadophosphate nanocomposite: ion exchange properties, antibacterial activity, and photocatalytic behavior." Journal of Industrial and Engineering Chemistry, 33, 201–208.

Sharma, N., and Purkait, M. K. (2019). "Improving the Hydrophilicity of Polysulfone Membrane by the Addition of Imidazol with Polyvinyl Pyrrolidone for Crystal Violet Dye Removal." Advances in Waste Management, Springer, 395–407.

Shenvi, S., Ismail, A. F., and Isloor, A. M. (2014). "Enhanced permeation performance of cellulose acetate ultrafiltration membranes by incorporation of sulfonated poly (1, 4-phenylene ether ether sulfone) and poly (styrene-co-maleic anhydride)." Industrial & Engineering Chemistry Research, 53(35), 13820–13827.

Sherugar, P., Naik, N. S., Padaki, M., Nayak, V., Gangadharan, A., Nadig, A. R., and Déon, S. (2021). "Fabrication of zinc doped aluminium oxide/polysulfone mixed matrix membranes for enhanced antifouling property and heavy metal removal." Chemosphere, 275, 130024.

Shibutani, T., Kitaura, T., Ohmukai, Y., Maruyama, T., Nakatsuka, S., Watabe, T., and Matsuyama, H. (2011). "Membrane fouling properties of hollow fiber membranes prepared from cellulose acetate derivatives." Journal of Membrane Science, 376(1–2), 102–109.

Shih, M.-C. (2005). "An overview of arsenic removal by pressure-drivenmembrane processes." Desalination, 172(1), 85–97.

Shukla, A. K., Alam, J., Alhoshan, M., Dass, L. A., Ali, F. A. A., Mishra, U., and Ansari, M. A. (2018). "Removal of heavy metal ions using a carboxylated graphene oxide-incorporated polyphenylsulfone nanofiltration membrane." Environmental Science: Water Research & Technology, 4(3), 438–448.

Shukla, A. K., Alam, J., Alhoshan, M., Dass, L. A., and Muthumareeswaran, M. R. (2017). "Development of a nanocomposite ultrafiltration membrane based on polyphenylsulfone blended with graphene oxide." Scientific Reports, 7(1), 41976 (12).

Shukla, A. K., Alam, J., Ali, F. A. A., and Alhoshan, M. (2020). "Efficient soluble anionic dye removal and antimicrobial properties of ZnO embedded-Polyphenylsulfone membrane." Water and Environment Journal, 35(2), 670-684.

Siddique, T. A., Dutta, N. K., and Roy Choudhury, N. (2020). "Nanofiltration for Arsenic Removal: Challenges, Recent Developments, and Perspectives." Nanomaterials, 10(7), 1323.

Sigwadi, R., Dhlamini, M. S., Mokrani, T., and Nemavhola, F. (2019). "Enhancing the mechanical properties of zirconia/Nafion® nanocomposite membrane through carbon nanotubes for fuel cell application." Heliyon, 5(7), e02112.

Silva, M. A., Hilliou, L., and Amorim, M. P. de. (2020). "Fabrication of pristine-multiwalled carbon nanotubes/cellulose acetate composites for removal of methylene blue." Polymer Bulletin, 77(2), 623–653.

Singh, R. (2014). Membrane technology and engineering for water purification: application, systems design and operation. Butterworth-Heinemann.

Siow, K. S., Britcher, L., Kumar, S., and Griesser, H. J. (2018). "XPS study of sulfur and phosphorus compounds with different oxidation states." Sains Malays, 47, 1913–1922.

Sivakumar, M., Mohan, D. R., and Rangarajan, R. (2006). "Studies on cellulose acetate-polysulfone ultrafiltration membranes: II. Effect of additive concentration." Journal of Membrane Science, 268(2), 208–219.

Sivakumar, M., Mohan, D. R., Rangarajan, R., and Tsujita, Y. (2005). "Studies on cellulose acetate–polysulfone ultrafiltration membranes: I. Effect of polymer composition." Polymer international, 54(6), 956–962.

Song, J., Zhang, M., Figoli, A., Yin, Y., Zhao, B., Li, X.-M., and He, T. (2015). "Arsenic removal using a sulfonated poly (ether ether ketone) coated hollow fiber nanofiltration membrane." Environmental Science: Water Research & Technology, 1(6), 839–845.

Song, P., Yang, Z., Zeng, G., Yang, X., Xu, H., Wang, L., Xu, R., Xiong, W., and Ahmad, K. (2017). "Electrocoagulation treatment of arsenic in wastewaters: a comprehensive review." Chemical Engineering Journal, 317, 707–725.

Sotoma, S., Akagi, K., Hosokawa, S., Igarashi, R., Tochio, H., Harada, Y., and Shirakawa, M. (2015). "Comprehensive and quantitative analysis for controlling the physical/chemical states and particle properties of nanodiamonds for biological applications." RSC Advances, 5(18), 13818–13827.

Srivastava, H. P., Arthanareeswaran, G., Anantharaman, N., and Starov, V. M. (2011). "Performance of modified poly (vinylidene fluoride) membrane for textile wastewater ultrafiltration." Desalination, 282, 87–94.

Strathmann, H., Scheible, P., and Baker, R. W. (1971). "A rationale for the preparation of Loeb-Sourirajan-type cellulose acetate membranes." Journal of Applied Polymer Science, 15(4), 811–828.

Sun, H., Sur, G. S., and Mark, J. E. (2002). "Microcellular foams from polyethersulfone and polyphenylsulfone: Preparation and mechanical properties." European Polymer Journal, 38(12), 2373–2381.

Sun, Z., and Chen, F. (2016). "Hydrophilicity and antifouling property of membrane materials from cellulose acetate/polyethersulfone in DMAc." International journal of biological macromolecules, 91, 143–150.

Tan, Y. H., Goh, P. S., Ismail, A. F., Ng, B. C., and Lai, G. S. (2017). "Decolourization of aerobically treated palm oil mill effluent (AT-POME) using polyvinylidene fluoride (PVDF) ultrafiltration membrane incorporated with coupled zinc-iron oxide nanoparticles." Chemical Engineering Journal, 308, 359–369.

Tavangar, T., Ashtiani, F. Z., and Karimi, M. (2020). "Morphological and performance evaluation of highly sulfonated polyethersulfone/polyethersulfone membrane for oil/water separation." Journal of Polymer Research, 27(9), 1–12.

Terrazas-Bandala, L. P., Gonzalez-Sanchez, G., Garcia-Valls, R., Gumi, T., Beurroies, I., Denoyel, R., Torras, C., and Ballinas-Casarrubias, L. (2014). "Influence of humidity,

temperature, and the addition of activated carbon on the preparation of cellulose acetate membranes and their ability to remove arsenic from water." Journal of Applied Polymer Science, 131(8).

Thanigaivelan, A., Noel Jacob, K., and Rajkumar, K. (2015). "Development of nano hybrid polyphenylsulfone (PPSU) ultrafiltration membranes: preparation, characterization and antifouling studies." International Journal of ChemTech Research, 8(5), 77–84.

Thirukumaran, P., Atchudan, R., Parveen, A. S., Kalaiarasan, K., Lee, Y. R., and Kim, S.-C. (2019). "Fabrication of ZnO nanoparticles adorned nitrogen-doped carbon balls and their application in photodegradation of organic dyes." Scientific reports, 9(1), 1–13.

Thong, Z., Gao, J., Lim, J. X. Z., Wang, K.-Y., and Chung, T.-S. (2018). "Fabrication of loose outer-selective nanofiltration (NF) polyethersulfone (PES) hollow fibers via single-step spinning process for dye removal." Separation and Purification Technology, 192, 483–490.

Thuyavan, Y. L., Anantharaman, N., Arthanareeswaran, G., and Ismail, A. F. (2014). "Adsorptive removal of humic acid by zirconia embedded in a poly (ether sulfone) membrane." Industrial & Engineering Chemistry Research, 53(28), 11355–11364.

Tiwari, A. P., Bhattarai, D. P., Maharjan, B., Ko, S. W., Kim, H. Y., Park, C. H., and Kim, C. S. (2019). "Polydopamine-based implantable multifunctional nanocarpet for highly efficient photothermal-chemo therapy." Scientific reports, 9(1), 1–13.

Tofighy, M. A., Mohammadi, T., and Sadeghi, M. H. (2021). "High-flux PVDF/PVP nanocomposite ultrafiltration membrane incorporated with graphene oxide nanoribbones with improved antifouling properties." Journal of Applied Polymer Science, 138(4), 49718.

Trzaskus, K. W., Vos, W. M. de, Kemperman, A., and Nijmeijer, K. (2015). "Towards controlled fouling and rejection in dead-end microfiltration of nanoparticles–Role of electrostatic interactions." Journal of membrane science, 496, 174–184.

Tsai, C.-Y., Chang, Y.-C., and Huang, C. (2011). "Surface Hydrophilization of Polysulfone Membrane by Cyclonic Atmospheric Pressure Plasma." Osaka University.

Vairavamoorthy, K., Gorantiwar, S. D., and Pathirana, A. (2008). "Managing urban water supplies in developing countries–Climate change and water scarcity scenarios." Physics and Chemistry of the Earth, Parts A/B/C, 33(5), 330–339.

Verliefde, A. R., Cornelissen, E. R., Heijman, S. G. J., Verberk, J., Amy, G. L., Van der Bruggen, B., and Van Dijk, J. C. (2008). "The role of electrostatic interactions on the rejection of organic solutes in aqueous solutions with nanofiltration." Journal of Membrane Science, 322(1), 52–66.

Vetrivel, S., Saraswathi, M. S. A., Rana, D., Divya, K., and Nagendran, A. (2018a). "Cellulose acetate composite membranes tailored with exfoliated tungsten disulfide nanosheets: permeation characteristics and antifouling ability." International journal of biological macromolecules, 115, 540–546.

Vetrivel, S., Saraswathi, M. S. A., Rana, D., and Nagendran, A. (2018b). "Fabrication of cellulose acetate nanocomposite membranes using 2D layered nanomaterials for macromolecular separation." International journal of biological macromolecules, 107, 1607–1612.

Villaescusa, I., and Bollinger, J.-C. (2008). "Arsenic in drinking water: sources, occurrence and health effects (a review)." Reviews in Environmental Science and Bio/Technology, 7(4), 307–323.

Vinodhini, P. A., Sangeetha, K., Thandapani, G., Sudha, P. N., Jayachandran, V., and Sukumaran, A. (2017). "FTIR, XRD and DSC studies of nanochitosan, cellulose acetate and polyethylene glycol blend ultrafiltration membranes." International journal of biological macromolecules, 104, 1721–1729.

Vörösmarty, C. J., McIntyre, P. B., Gessner, M. O., Dudgeon, D., Prusevich, A., Green, P., Glidden, S., Bunn, S. E., Sullivan, C. A., and Liermann, C. R. (2010). "Global threats to human water security and river biodiversity." nature, 467(7315), 555–561.

Wan, P., Yuan, M., Yu, X., Zhang, Z., and Deng, B. (2020). "Arsenate removal by reactive mixed matrix PVDF hollow fiber membranes with UIO-66 metal organic frameworks." Chemical Engineering Journal, 382, 122921.

Wang, J., Xu, W., Chen, L., Huang, X., and Liu, J. (2014). "Preparation and evaluation of magnetic nanoparticles impregnated chitosan beads for arsenic removal from water." Chemical Engineering Journal, 251, 25–34.

Wang, J., Zhu, J., Tsehaye, M. T., Li, J., Dong, G., Yuan, S., Li, X., Zhang, Y., Liu, J., and Van der Bruggen, B. (2017). "High flux electroneutral loose nanofiltration membranes based

on rapid deposition of polydopamine/polyethyleneimine." Journal of Materials Chemistry A, 5(28), 14847–14857.

Wang, S.-X., Maimaiti, H., Xu, B., Awati, A., Zhou, G.-B., and Cui, Y. (2019). "Synthesis and visible-light photocatalytic N2/H2O to ammonia of ZnS nanoparticles supported by petroleum pitch-based graphene oxide." Applied Surface Science, 493, 514–524.

Wang, W., Yue, Q., Li, R., Song, W., Gao, B., and Shen, X. (2017). "Investigating coagulation behavior of chitosan with different Al species dual-coagulants in dye wastewater treatment." Journal of the Taiwan Institute of Chemical Engineers, 78, 423–430.

Wang, Y., Zhu, J., Dong, G., Zhang, Y., Guo, N., and Liu, J. (2015). "Sulfonated halloysite nanotubes/polyethersulfone nanocomposite membrane for efficient dye purification." Separation and Purification Technology, 150, 243–251.

Watson, J. H. P., Cressey, B. A., Roberts, A. P., Ellwood, D. C., Charnock, J. M., and Soper, A. K. (2000). "Structural and magnetic studies on heavy-metal-adsorbing iron sulphide nanoparticles produced by sulphate-reducing bacteria." Journal of magnetism and magnetic materials, 214(1–2), 13–30.

Weng, T.-H., Tseng, H.-H., and Wey, M.-Y. (2008). "Preparation and characterization of PPSU/PBNPI blend membrane for hydrogen separation." international journal of hydrogen energy, 33(15), 4178–4182.

Worou, C. N., Kang, J., Alamou, E. A., Degan, A., Yan, P., Gong, Y., Guene, R. L., and Chen, Z. (2021). "High flux membrane based on in-situ formation of zirconia layer coated the polyethersulfone substrate for ions separation." Water Supply.

Wu, C., Wang, H., Wei, Z., Li, C., and Luo, Z. (2015). "Polydopamine-mediated surface functionalization of electrospun nanofibrous membranes: preparation, characterization and their adsorption properties towards heavy metal ions." Applied Surface Science, 346, 207–215.

Wu, H., Ang, J. M., Kong, J., Zhao, C., Du, Y., & Lu, X. (2016). One-pot synthesis of polydopamine–Zn complex antifouling coatings on membranes for ultrafiltration under harsh conditions. *RSC advances*, *6*(105), 103390-103398.

Wu, L.-K., Wu, H., Zhang, H.-B., Cao, H.-Z., Hou, G.-Y., Tang, Y.-P., and Zheng, G.-Q. (2018). "Graphene oxide/CuFe2O4 foam as an efficient absorbent for arsenic removal from water." Chemical Engineering Journal, 334, 1808–1819.

Xi, Z.-Y., Xu, Y.-Y., Zhu, L.-P., Wang, Y., and Zhu, B.-K. (2009). "A facile method of surface modification for hydrophobic polymer membranes based on the adhesive behavior of poly (DOPA) and poly (dopamine)." Journal of Membrane Science, 327(1–2), 244–253.

Xiang, Y., Liu, F., and Xue, L. (2015). "Under seawater superoleophobic PVDF membrane inspired by polydopamine for efficient oil/seawater separation." Journal of Membrane Science, 476, 321–329.

Yadav, M. K., Saidulu, D., Gupta, A. K., Ghosal, P. S., and Mukherjee, A. (2021). "Status and management of arsenic pollution in groundwater: A comprehensive appraisal of recent global scenario, human health impacts, sustainable field-scale treatment technologies." Journal of Environmental Chemical Engineering, 105203.

Yang, S., Zou, Q., Wang, T., and Zhang, L. (2019). "Effects of GO and MOF@ GO on the permeation and antifouling properties of cellulose acetate ultrafiltration membrane." Journal of membrane science, 569, 48–59.

Yang, X., Duan, L., and Ran, X. (2017). "Effect of polydopamine coating on improving photostability of polyphenylene sulfide fiber." Polymer Bulletin, 74(3), 641–656.

Youngran, J., Maohong, F. A. N., Van Leeuwen, J., and Belczyk, J. F. (2007). "Effect of competing solutes on arsenic (V) adsorption using iron and aluminum oxides." Journal of Environmental Sciences, 19(8), 910–919.

Yu, J., Huang, T., Jiang, Z., Sun, M., and Tang, C. (2018). "Synthesis and characterizations of zinc oxide on reduced graphene oxide for high performance electrocatalytic reduction of oxygen." Molecules, 23(12), 3227.

Yu, M., Jia, J., Liu, X., Cui, J., Xi, B., He, X., and Mao, X. (2019). "p-Arsanilic acid degradation and arsenic immobilization by a disilicate-assisted iron/aluminum electrolysis process." Chemical Engineering Journal, 368, 428–437.

Yu, S., Liu, M., Ma, M., Qi, M., Lü, Z., and Gao, C. (2010). "Impacts of membrane properties on reactive dye removal from dye/salt mixtures by asymmetric cellulose acetate and composite polyamide nanofiltration membranes." Journal of Membrane Science, 350(1–2), 83–91.

Yurekli, Y. (2016). "Removal of heavy metals in wastewater by using zeolite nano-particles impregnated polysulfone membranes." Journal of hazardous materials, 309, 53–64.

Zaid, O. F., El-Said, W. A., Yousif, A. M., Galhoum, A. A., Elshehy, E. A., Ibrahim, I. A., and Guibal, E. (2020). "Synthesis of microporous nano-composite (hollow spheres) for fast detection and removal of As (V) from contaminated water." Chemical Engineering Journal, 390, 124439.

Zaw, M., and Emett, M. T. (2002). "Arsenic removal from water using advanced oxidation processes." Toxicology letters, 133(1), 113–118.

Zhang, R., Su, Y., Zhao, X., Li, Y., Zhao, J., and Jiang, Z. (2014). "A novel positively charged composite nanofiltration membrane prepared by bio-inspired adhesion of polydopamine and surface grafting of poly (ethylene imine)." Journal of membrane science, 470, 9–17.

Zhang, Y., Li, H., Lin, J., Li, R., and Liang, X. (2006). "Preparation and characterization of zirconium oxide particles filled acrylonitrile-methyl acrylate-sodium sulfonate acrylate copolymer hybrid membranes." Desalination, 192(1–3), 198–206.

Zhao, D., Yu, Y., Wang, C., and Chen, J. P. (2016). "Zirconium/PVA modified flat-sheet PVDF membrane as a cost-effective adsorptive and filtration material: A case study on decontamination of organic arsenic in aqueous solutions." Journal of colloid and interface science, 477, 191–200.

Zhao, S., Wang, Z., Wei, X., Zhao, B., Wang, J., Yang, S., and Wang, S. (2012). "Performance improvement of polysulfone ultrafiltration membrane using well-dispersed polyaniline–poly (vinylpyrrolidone) nanocomposite as the additive." Industrial & engineering chemistry research, 51(12), 4661–4672.

Zheng, Y.-M., Yu, L., Wu, D., and Chen, J. P. (2012). "Removal of arsenite from aqueous solution by a zirconia nanoparticle." Chemical engineering journal, 188, 15–22.

Zheng, Y.-M., Zou, S.-W., Nanayakkara, K. N., Matsuura, T., and Chen, J. P. (2011). "Adsorptive removal of arsenic from aqueous solution by a PVDF/zirconia blend flat sheet membrane." Journal of membrane science, 374(1–2), 1–11.

Zheng, Y., Zhang, W., Tang, B., Ding, J., & Zhang, Z. (2018). Membrane fouling mechanism of biofilm-membrane bioreactor (BF-MBR): Pore blocking model and membrane cleaning. Bioresource technology, 250, 398-405.

Zeng, J., Qi, P., Shi, J., Pichler, T., Wang, F., Wang, Y., and Sui, K. (2020). "Chitosan functionalized iron nanosheet for enhanced removal of As (III) and Sb (III): Synergistic effect and mechanism." Chemical Engineering Journal, 382, 122999.

Zhou, Z., Liu, Y., Liu, S., Liu, H., Zeng, G., Tan, X., Yang, C., Ding, Y., Yan, Z., and Cai, X. (2017). "Sorption performance and mechanisms of arsenic (V) removal by magnetic gelatin-modified biochar." Chemical Engineering Journal, 314, 223–231.

Zhu, J., Yuan, S., Uliana, A., Hou, J., Li, J., Li, X., Tian, M., Chen, Y., Volodin, A., and Van der Bruggen, B. (2018). "High-flux thin film composite membranes for nanofiltration mediated by a rapid co-deposition of polydopamine/piperazine." Journal of Membrane Science, 554, 97–108.

List of Publication

Details of Publication:

PATENT (INDIAN)

1. **Mithun Kumar**[a], Arun M. Isloor[b,c*], Somasekhara Rao T.[a*], (2021) Nano-aluminum oxide embedded cellulose acetate/ polyphenylsulfone derivatives hollow fiber membranes: Fabrication, characterization and arsenic removal from drinking water **(Indian patent: communicated the first graft).**

2. Arun M. Isloor[a,b*], **Mithun Kumar**[c], Somasekhara Rao T.[a*], M. Chandrashekhar Nayak (2021) Hydrophilic polydopamine/polyvinylpyrrolidone embedded polyphenylsulfone hollow fiber membranes for the removal of arsenic (As-V) from drinking water **(Indian Patent: Preparing prior art search).**

International/National Journals

Sl. No.	Title of Paper	Authors (in the same order as in the paper. Underline the Research Scholar's name)	Name of the Journal/ Conference/ Symposium, Vol., No., Pages	Month & Year of Publication	Category *
1	Use of cellulose acetate/polyphenylsulfone derivatives to fabricate ultrafiltration hollow fiber membranes for the removal of arsenic from drinking water	**Mithun Kumar**[a], Somasekhara Rao T.[a], Arun M. Isloor[b], G.P. Syed Ibrahim[b], Inamuddin[def], Norafiqah Ismail[c], Ahmed Fauzi Ismail[c], Abdullah M. Asiri[de]	International Journal of biological macromolecules, Volume 129, Pages 715-727. (Elsevier)	3rd February 2019	Science Citation Index Expanded <u>Impact Factor (8.02)</u>

Sl. No.	Title of Paper	Authors (in the same order as in the paper. Underline the Research Scholar's name)	Name of the Journal/ Conference/ Symposium, Vol., No., Pages	Month & Year of Publication	Category *
2	Improved separation of dyes and proteins using membranes made of polyphenylsulfone/cellulose acetate or acetate phthalate	**Mithun Kumar**[1] · Arun M. Isloor[2] · Somasekhara Rao Todeti[1] · G. P. Syed Ibrahim[2] · Inamuddin[3,4,5] · Ahmed Fauzi Ismail[6] · Abdullah M. Asiri[3,4]	Environmental Chemistry Letters, 18, 1-7. (Springer)	4th January 2020	Science Citation Index (SCI) / Science Citation Index Expanded (SCIE), Impact Factor (13.61)
3	Removal of toxic arsenic from aqueous media using polyphenylsulfone/cellulose acetate hollow fiber membranes containing zirconium oxide	**Mithun Kumar[a],** Arun M. Isloor[bc], T. Somasekhara Rao[a], Ahmed Fauzi Ismail[d], Ramin Farnood[e], P.M.G. Nambissan[f]	Chemical Engineering Journal, 393 (2020) 124367. (Elsevier)	1 August 2020	Science Citation Index Expanded Impact Factor (16.74)
4	Effect of binary zinc-magnesium oxides on polyphenylsulfone /cellulose acetate derivatives hollow fiber membranes for the decontamination of arsenic from drinking water.	**Mithun Kumar**[a], Arun M. Isloor[bc], Somasekhara Rao Todeti[a], Nagaraja H.S.[d] Ahmad Fauzi Ismail[e] Rini Susanti[f]	Chemical Engineering Journal, 405 (2021) 126809. (Elsevier)	1 February 2021	Science Citation Index Expanded Impact Factor (16.74)
5	Hydrophilic nano-aluminum oxide	**Mithun Kumar**, Arun M. Isloor,	Journal of Water	29th	Science

Sl. No.	Title of Paper	Authors (in the same order as in the paper. Underline the Research Scholar's name)	Name of the Journal/ Conference/ Symposium, Vol., No., Pages	Month & Year of Publication	Category *
	containing polyphenylsulfone hollow fiber membranes for the extraction of arsenic	Somasekhara Rao Todeti., Ahmad Fauzi Ismail, Ramin Farnood	Processing Engineering, (Elsevier)	September 2021	Citation Index Expanded (SCIE) Impact Factor (7.34)
6	Polysulfone nanocomposite membranes containing nanostructured TiO_2, SiO_2 and 3-Aminopropyltriethoxysilane (APTES) modified nano-TiO_2 and nano-SiO_2 nanocomposites: Fabrication, characterization and removal of cadmium (Cd^{2+}) ions from aqueous solution	Valeen Rashmi Pereira; Arun Mohan Isloor; **Mithun Kumar**; Ahmad Fauzi Ismail	Environmental Science and Pollution Research (Springer)	Accepted on 27th May 2022	Science Citation Index Expanded (SCIE) Impact Factor (4.22)

International/National Conferences

Sl. No.	Title of Paper	Name of Authors	Name of the Conference, Year, Place, Date	Published in Journal (Yes/No)
1.	Preparation and characterization of multilayer composites from nanocellulose and epoxy for packaging applications.	**Mithun Kumar**, Somasekhara Rao T. and Arun M. Isloor	9th international Bengaluru India Nano conference -2017, in Ashoka Hotel, Bengaluru	NO (Poster presentation)
2.	Development of multi-layer bio-composites from nanocellulose using chitosan and gluteraldehyde as a crosslinking agent for packaging applications.	**Mithun Kumar**, Somasekhara Rao T. and Arun M. Isloor	International conference on systems and processes in physics, chemistry, and biology (icsppcb 2018) In Assam university, Silchar, Assam	NO (Poster presentation)
3.	Preparation and characterization of nanocellulose and epoxy multilayer composites for packaging application.	**Mithun Kumar**, Somasekhara Rao T. and Arun M. Isloor	Indian Nano electronics users program center for Nano science and engineering –inup, iisc, bangalore-2018	NO (Poster presentation)
4.	Preparation and evaluation of dye /protein rejection properties from polyphenylsulfone /cellulose acetate and polyphenylsulfone /cellulose acetate phthalate hollow fiber membranes.	**Mithun Kumar**, Somasekhara Rao T. and Arun M. Isloor	National conference on advances in chemical sciences 2 – 3, November 2018 in Manipal	NO (Poster presentation)

List of Publications

Sl. No.	Title of Paper	Name of Authors	Name of the Conference, Year, Place, Date	Published in Journal (Yes/No)
5.	Removal of toxic arsenic from aqueous media using polyphenylsulfone /cellulose acetate hollow fiber membranes containing zirconium oxide	**Mithun Kumar**, Arun M. Isloor, Somasekhara Rao T. and Ahmed Fauzi Ismail.	11th International Bengaluru India Nano conference -2020	NO (Poster presentation)

(Mithun Kumar)
Name and Signature of Research Scholar

(Dr. T. Somasekhara Rao)
Name and Signature of Research Guide

03/10/2022

(Prof. Arun M. Isloor)
Name and Signature of Research Guide

285

BIODATA

MITHUN KUMAR

Phone: +91-7624846576

Email: mithunkumar.patil@gmail.com, mtnkmr.ptl@gmail.com

OBJECTIVES
A skilled and hardworking researcher aiming to pursue career in the research and development of novel membranes

RESEARCH INTEREST
• Polymer Science • Membrane Technology • Arsenic Removal

EXPERIENCE

Organization	Description	Year
University of Toronto, Toronto- Canada.	Research internship student under the guidance of Prof. Ramin Farnood in university of Toronto. Canada for 2 months.	2019
Advanced membrane technology in University of Teknologi Malaysia (UTM) Malaysia	Research attachment (collaboration) program under the guidance of Prof. Ahmed Fouzi Ismail for 4 months.	2018-2019

EDUCATION

Degree	Institution	Year
Ph.D. (Mechanical Engineering)	National Institute of Technology, Karnataka	2016-2022

M.Tech. in Machine Design	Adichunchanagiri Institute of Technology (AIT) Chikmangaluru, Karnataka	2013-2015
B.E. in (Mechanical Engineering)	Rao Bahadur Y Mahabaleswarappa Engineering College (RYMEC) Bellary, Karnataka	2010-2013
Diploma in (Mechanical Engineering)	V.V. Sangha's polytechnic cantonment, Bellary, Karnataka	2007-2010

SKILLS

- Fabrication of hollow fiber Membranes
- Instrumental analysis

PATENTS

- **Mithun Kumar**, Arun M. Isloor, Somasekhara Rao T., (2021) Nano-aluminum oxide embedded cellulose acetate/ polyphenylsulfone derivatives hollow fiber membranes: Fabrication, characterization and arsenic removal from drinking water **(Indian Patent: Patent filed)**.

- Arun M. Isloor, **Mithun Kumar**, Somasekhara Rao T., M. Chandrashekhar Nayak (2021) Hydrophilic polydopamine/polyvinylpyrrolidone embedded polyphenylsulfone hollow fiber membranes for the removal of arsenic (As-V) from drinking water **(Indian Patent: Patent filed)**.

PUBLICATIONS (INTERNATIONAL JOURNALS)

- **Kumar, M.,** Isloor, A. M., Todeti, S. R., Nagaraja, H. S., Ismail, A. F., & Susanti, R. (2021). Effect of binary zinc-magnesium oxides on polyphenylsulfone/cellulose acetate derivatives hollow fiber membranes for the decontamination of arsenic from drinking water. *Chemical Engineering Journal*, *405*, 126809.

- **Kumar, M.,** Isloor, A. M., Rao, T. S., Ismail, A. F., Farnood, R., & Nambissan, P. M. G. (2020). Removal of toxic arsenic from aqueous media using polyphenylsulfone/cellulose acetate hollow fiber membranes containing zirconium oxide. *Chemical Engineering Journal*, *393*, 124367.

- **Kumar, M.,** RaoT, S., Isloor, A. M., Ibrahim, G. S., Ismail, N., Ismail, A. F., & Asiri, A. M. (2019). Use of cellulose acetate/polyphenylsulfone derivatives to fabricate ultrafiltration hollow fiber membranes for the removal of arsenic from drinking water. *International journal of biological macromolecules*, *129*, 715-727.

- **Kumar, M.,** Isloor, A. M., Todeti, S. R., Ibrahim, G. S., Ismail, A. F., & Asiri, A. M. (2020). Improved separation of dyes and proteins using membranes made of polyphenylsulfone/cellulose acetate or acetate phthalate. *Environmental Chemistry Letters*, 1-7.

- **Mithun Kumar**, Arun M. Isloor, Somasekhara Rao Todeti., Ahmad Fauzi Ismail, Ramin Farnood (2021) Hydrophilic nano-aluminum oxide containing polyphenylsulfone hollow fiber membranes for the extraction of arsenic, *Journal of Water Processing Engineering,* 44, 102357.

- **Mithun Kumar**, Arun M. Isloor, M.C.S Nayak, Somasekhara Rao Todeti. Mahesh Padaki, Ahmad Fauzi Ismail, (2022) Hydrophilic polydopamine/polyvinylpyrrolidone blended polyphenylsulfone hollow fiber membranes for the removal of arsenic from drinking water, *ACS Omega* (ACS Publication, Came for Major Revision).

- Arun Mohan Isloor; Valeen Rashmi Pereira; **Mithun Kumar**; Ahmad Fauzi Ismail (2022) Polysulfone nanocomposite membranes containing nanostructured TiO_2, SiO_2 and 3-Aminopropyltriethoxysilane (APTES) modified nano-TiO_2 and nano-SiO_2 nanocomposites: Fabrication, characterization and removal of cadmium (Cd^{2+}) ions from aqueous solution, *Environmental Science and Pollution Research* (Springer, Came for Major Revision).

- Mrutyunjay Swamy D, Arun M. Isloor, **Mithun Kumar,** Sooraj Nayak, Ahmad Fauzi Ismail, (2022) Polydopamine functionalized Halloysite

Nanotubes incorporated Polyethersulfone Hollow Fiber Membranes for removal of arsenic (As-V) from water, *Environmental Science and Pollution Research* (Springer, Under Review).

INTERNATIONAL/NATIONAL CONFERENCES

- Mithun Kumar, Somasekhara Rao T. and Arun M. Isloor, Preparation and characterization of multilayer composites from nanocellulose and epoxy for packaging applications. 9th international Bengaluru India Nano conference -2017, in Ashoka Hotel, Bengaluru **(Poster presentation).**

- Mithun Kumar, Somasekhara Rao T. and Arun M. Isloor, Development of multi-layer bio-composites from nanocellulose using chitosan and gluteraldehyde as a crosslinking agent for packaging applications. International conference on systems and processes in physics, chemistry, and biology (icsppcb 2018) In Assam university, Silchar, Assam **(Poster presentation).**

- Mithun Kumar, Somasekhara Rao T. and Arun M. Isloor, Preparation and characterization of nanocellulose and epoxy multilayer composites for packaging application. Indian Nano electronics users program center for Nano science and engineering –inup 2018, iisc, Bengaluru, Karnataka **(Poster presentation).**

- Mithun Kumar, Somasekhara Rao T. and Arun M. Isloor, Preparation and evaluation of dye /protein rejection properties from polyphenylsulfone /cellulose acetate and polyphenylsulfone /cellulose acetate phthalate hollow fiber membranes. National conference on advances in chemical sciences 2 – 3, November 2018 in Manipal **(oral presentation).**

- Mithun Kumar, Arun M. Isloor, Somasekhara Rao T. and Ahmed Fauzi Ismail. Removal of toxic arsenic from aqueous media using polyphenylsulfone /cellulose acetate hollow fiber membranes containing zirconium oxide, 11th International Bengaluru India Nano conference -2020, Bengaluru, Karnataka **(Poster presentation).**

PERSONAL DETAILS

Address for correspondence	#05, Anjaneya Nilaya, 2nd cross Shastrinagar, near S.P. Circle. Ballari, Karnataka -583101.
Date of Birth	25-12-1991
Sex	Male
Nationality	Indian
Marital Status	Single
Languages Known	Kannada, English, Hindi and Telugu

REFERENCES

Prof. Arun M. Isloor	*Dr. Somasekhara Rao T.*	*Prof. (Dr.) A. F. Ismail*
Professor Department of Chemistry NITK- Surathkal, Mangaluru, Karnataka. Phone no: +91-9448523990 Email: isloor@yahoo.com	**Assistant Professor** Department of Mechanical Engineering NITK- Surathkal, Mangaluru, Karnataka. Phone no: +91-9611057598 Email: ssrao@nitk.edu.in	**Vice-Chancellor (Research and Innovation)** Advanced Membrane Technology Centre (AMTEC) Universiti Teknologi, Malaysia Phone no: +60-97775545 Email: afauzi@utm.my